

# Constraining chondrule formation conditions in ordinary, enstatite and Kakangari chondrites

Inaugural-Dissertation

zur

Erlangung des Doktorgrades

der Mathematisch-Naturwissenschaftlichen Fakultät

der Universität zu Köln

vorgelegt von

Jens Barosch

aus Heidelberg

Köln, 2019

Berichterstatter: PD. Dr. Dominik C. Hezel  
Prof. Dr. Sandro Jahn

Tag der mündlichen Prüfung: 10.01.2020

## Abstract

Chondrites are primitive meteorites made from two major components: *chondrules*, small rocky spherules, embedded within fine-grained *matrix*. Both components formed in the protoplanetary disk, however, their formation mechanisms are not well understood. There are two fundamental questions that have not yet been answered: what process(es) formed chondrules, and what is the genetic relationship between chondrules and matrix? The purpose of my thesis is to constrain the conditions of chondrule and matrix formation. To do so, I obtained a comprehensive dataset, containing petrographic and chemical data of chondrules and matrix in ordinary (OC), enstatite (EC) and Kakangari (K) chondrites.

I used this dataset to examine the textural characteristics and bulk chemistries of chondrules. A large fraction of chondrules in all chondrites are mineralogically zoned. These chondrules have olivine cores, surrounded by low-Ca pyroxene rims. Average 2D fractions are high in carbonaceous chondrites (CC; 78%), intermediate in Rumuruti (R; 41%) and OC (39%), and rather low in EC (28%) and K chondrites (19%). Due to 2D sectioning effects, 3D zoned chondrule fractions are systematically higher by factor 1.24 in CC, 1.29 in OC and 1.62 in EC. These results show that mineralogically zoned chondrules are the dominant chondrule type in most chondrites. They formed when chondrule melts interacted with surrounding nebula gas, and material from the gas was added to the chondrules. By comparing the bulk compositions of chondrules that are mineralogically zoned with those that are not, I show that gas-melt interaction was a ubiquitous process during chondrule formation in all chondrites. This process explains the origin of chondrule textures and the large variability observed in chondrule bulk compositions.

Recent studies identified chondrule-matrix complementarities as key characteristics of CC and R chondrites. Various element and isotope ratios are different in chondrules and matrix, but, at the same time, solar in the bulk meteorite. This requires joint formation of chondrules and matrix from a single solar reservoir. In this thesis, the study of complementarity was expanded to Kakangari chondrites. Chondrules, matrix and bulk Kakangari have identical (solar) Mg/Si ratios as a likely result of chondrule-gas interaction, as well as element exchange between chondrules and matrix during parent body metamorphism. While not strictly complementary, I show that Kakangari chondrules and matrix are genetically linked, thereby supporting the concept of complementarity.

Another chapter of this thesis examines a unique compound object found in an ordinary chondrite. It consists of a barred olivine chondrule trapped within a large, Ca,Al-rich host object. The results indicate that this object could represent a macrochondrule that formed from collisions and merging of normal-sized chondrules. It might, therefore, provide first direct evidence for a genetic link between compound chondrules and macrochondrules.

Major constraints for chondrule formation conditions were specified in this thesis: chondrules were open systems and interacted with their environment, and each other. Furthermore, chondrules and matrix are genetically linked and formed in a common reservoir. Any proposed model of chondrule formation must meet these constraints.

## Zusammenfassung

Chondrite sind primitive Steinmeteorite. Sie bestehen hauptsächlich aus *Chondren*, kleinen Silikatkügelchen, die in einer feinkörnigen *Matrix* eingebettet sind. Beide Komponenten bildeten sich im frühen Sonnensystem, aber ihre Entstehungsprozesse sind noch weitgehend unbekannt. Zwei grundlegende Fragen konnten bisher nicht beantwortet werden: Welcher Prozess bildete Chondren und in welcher genetischen Verbindung stehen sie zur Matrix? Die vorliegende Arbeit untersucht insbesondere Petrographie und chemische Zusammensetzung beider Komponenten in Gewöhnlichen (OC), Enstatit (EC) und Kakangari (K) Chondriten. Auf Grundlage der Ergebnisse sollen die Bildungsbedingungen von Chondren und Matrix eingegrenzt werden.

Ein großer Teil der Chondren in allen Chondriten ist mineralogisch zониert. Olivin befindet sich im Kern zонierter Chondren und wird von einem Pyroxenrand umschlossen. Zониerte Chondren (in 2D) kommen besonders häufig in kohligen Chondriten vor (CC; 78%), sind relativ verbreitet in Rumuruti (R; 41%) und OC (39%), und etwas seltener in EC (28%) und K Chondriten (19%). Aufgrund von Schnitteffekten in 2D Untersuchungen zeigte sich, dass zониerte Chondren deutlich häufiger sind, wenn Chondren in 3D untersucht werden. In 3D sind zониerte Chondren um den Faktor 1.24 häufiger in CC, um den Faktor 1.29 häufiger in OC und um den Faktor 1.62 häufiger in EC. Damit sind zониerte Chondren der dominante Chondren-Typ in Chondriten. Die mineralogische Zонierung bildete sich als aufgeschmolzene Chondren mit ihrer gasreichen Umgebung interagierten und dabei Material aus dem Gas aufnahmen. Beim Vergleich der Gesamtzusammensetzungen mineralogisch zонierter und unzонierter Chondren wird deutlich, dass die Interaktion von Chondren mit Gas ein wichtiger Prozess während der Chondrenbildung war. Die Entstehung verschiedener Chondren-Texturen und die große Bandbreite ihrer Gesamtzusammensetzungen lassen sich auf diesen Prozess zurückführen.

In kohligen Chondriten sind viele Element- und Isotopenverhältnisse von Chondren und Matrix komplementär. Beide Komponenten sind jeweils unterschiedlich zusammengesetzt, jedoch solar im Gesamtmeteorit. Dies spricht dafür, dass sich Chondren und Matrix aus einem gemeinsamen Reservoir mit solarer Zusammensetzung bildeten. In dieser Arbeit wurde Komplementarität in Kakangari Chondriten untersucht. Chondren, Matrix und die Gesamtzusammensetzung von Kakangari sind identisch und solar in Mg/Si. Dies lässt sich auf die Interaktion von Chondren mit Gas, sowie den Elementaustausch zwischen Chondren und Matrix während niedriggradiger Metamorphose auf dem Mutterkörper zurückführen. Obwohl

Kakangari keine eindeutige Komplementarität besitzt, ist es dennoch wahrscheinlich, dass auch in diesem Meteorit ein genetischer Zusammenhang zwischen Chondren und Matrix besteht.

Ein weiteres Kapitel dieser Arbeit beschäftigt sich mit einem bislang einzigartigen Objekt in einem Gewöhnlichen Chondrit. Das Objekt ist ungewöhnlich groß, Ca,Al-reich und enthält eine eingeschlossene Chondre. Es könnte sich um eine Makrochondre handeln, die sich durch Kollision und Verschmelzung kleinerer Chondren bildete.

Die Ergebnisse dieser Arbeit zeigen, dass Chondren während ihrer Entstehung offene Systeme waren und sowohl untereinander, als auch mit ihrer Umgebung interagierten. Zudem stehen die Chondren in genetischem Zusammenhang mit der Matrix. Beide Komponenten bildeten sich in einem gemeinsamen Reservoir. Diese Erkenntnisse grenzen Chondren Bildungsmodelle und Mechanismen signifikant ein.

# Table of contents

<b>ABSTRACT .....</b>	<b>.....</b>
<b>ZUSAMMENFASSUNG .....</b>	<b>.....</b>
<b>TABLE OF CONTENTS.....</b>	<b>.....</b>
<b>1. INTRODUCTION .....</b>	<b>1</b>
1.1. FORMATION OF THE SOLAR SYSTEM.....	1
1.2. CLASSIFICATION AND COMPOSITION OF METEORITES .....	2
1.3. CHONDRITE COMPONENTS .....	4
1.4. CONSTRAINTS FOR CHONDRITE COMPONENT FORMATION .....	6
1.4.1. <i>Chondrule open vs. closed system behaviour</i> .....	7
1.4.2. <i>Single vs. multiple reservoirs: the chondrule-matrix complementarity</i> .....	9
1.5. OBJECTIVES OF THIS THESIS.....	10
<b>2. MINERALOGICALLY ZONED CHONDRULES IN ORDINARY CHONDRITES AS EVIDENCE FOR CHONDRULE OPEN SYSTEM BEHAVIOUR .....</b>	<b>12</b>
ABSTRACT .....	12
2.1. INTRODUCTION.....	13
2.2. METHODS .....	15
2.3. RESULTS.....	16
2.3.1. <i>Chondrule petrography and petrology</i> .....	18
2.3.2. <i>Unzoned chondrules</i> .....	23
2.3.3. <i>Bulk chondrule compositions</i> .....	23
2.4. DISCUSSION .....	27
2.4.1. <i>2D sectioning effects</i> .....	27
2.4.2. <i>Phase map techniques (IM vs. LAM)</i> .....	28
2.4.3. <i>Variation in type I/II fractions of porphyritic chondrules</i> .....	29
2.4.4. <i>Formation of low-Ca pyroxene rims</i> .....	29
2.4.5. <i>Formation of unzoned chondrules</i> .....	32
2.5. CONCLUSIONS .....	34
ACKNOWLEDGEMENTS.....	35
REFERENCES .....	36
APPENDIX .....	43
<b>3. SECTIONING EFFECTS OF PORPHYRITIC CHONDRULES: IMPLICATIONS FOR THE PP/POP/PO CLASSIFICATION AND CORRECTING MODAL ABUNDANCES OF MINERALOGICALLY ZONED CHONDRULES.....</b>	<b>50</b>
ABSTRACT .....	50
3.1. INTRODUCTION.....	51
3.2. METHODS .....	52
3.2.1. <i>Microtomography (<math>\mu</math>-CT)</i> .....	52
3.2.2. <i>3D serial sectioning</i> .....	55
3.3. RESULTS.....	56
3.3.1. <i>Sectioning effects when classifying chondrules</i> .....	56
3.3.2. <i>Sectioning effects when determining the fraction of mineralogically zoned chondrules</i> .....	57
3.4. DISCUSSION AND SUMMARY .....	58
ACKNOWLEDGEMENTS.....	60
REFERENCES .....	60

<b>4. AN UNUSUAL COMPOUND OBJECT IN YAMATO 793408 (H3.2-AN): THE MISSING LINK BETWEEN COMPOUND CHONDRULES AND MACROCHONDRULES? .....</b>	<b>64</b>
ABSTRACT .....	64
4.4. INTRODUCTION .....	65
4.4. METHODS .....	67
4.4. RESULTS.....	68
4.3.1. Petrography.....	68
4.3.2. Element compositions of the minerals in the compound object .....	69
4.3.3. Silica is quartz in the BO mesostasis and cristobalite in the host object's mesostasis.....	71
4.3.4. Mineral O-isotope compositions .....	72
4.4. DISCUSSION .....	75
4.4.1. Mineralogy, structure and petrography of the Y-793408 compound object.....	75
4.4.2. O-isotope composition of the compound object .....	78
4.4.3. Origin of Ca,Al-rich olivine cores.....	79
4.5. CONCLUSIONS .....	79
ACKNOWLEDGEMENTS.....	80
REFERENCES .....	81
<b>5. FORMATION OF CHONDRULES AND MATRIX IN KAKANGARI CHONDRITES .....</b>	<b>87</b>
ABSTRACT .....	87
5.1. INTRODUCTION.....	88
5.2. METHODS .....	90
5.3. RESULTS.....	93
5.3.1. Abundances and characteristics of components in K chondrites .....	93
5.3.2. Bulk chondrule and matrix compositions .....	97
5.4. DISCUSSION .....	99
5.4.1. Why are zoned chondrules rare in Kakangari, but not in LEW 87232? .....	99
5.4.2. The likely origin and formation of agglomeratic chondrules in Kakangari .....	103
5.4.3. Mg/Si ratios of Kakangari chondrules and matrix.....	103
5.4.4. Chondrule and matrix relationships in LEW 87232 .....	106
5.5. CONCLUSIONS .....	107
ACKNOWLEDGEMENTS.....	108
REFERENCES .....	109
APPENDIX .....	115
<b>6. DISCUSSION .....</b>	<b>118</b>
6.1. CONSTRAINTS FOR CHONDRULE FORMATION CONDITIONS .....	118
6.1.1. Chondrules behaved as open systems.....	118
6.1.2. Chondrules interacted with each other through collisions.....	122
6.1.3. Chondrules and matrix likely formed in common reservoirs .....	124
6.2. FORMATION OF CHONDRITES AND THEIR COMPONENTS .....	126
6.2.1. Characteristics of chondrite forming reservoirs .....	126
6.2.2. Origin of K chondrites.....	127
6.2.3. Processes during chondrite component formation .....	130
6.3. CONCLUSIONS .....	131
<b>REFERENCES FOR CHAPTERS 1 AND 6 .....</b>	<b>133</b>
<b>DANKSAGUNG .....</b>	<b>142</b>
<b>ERKLÄRUNG ZUM EIGENANTEIL AN DEN PUBLIKATIONEN .....</b>	<b>143</b>
<b>ERKLÄRUNG GEMÄß §4, ABS. 9 PROMOTIONSORDNUNG MNF.....</b>	<b>144</b>

# Chapter 1

## Introduction

Extraterrestrial rocks hold information about the conditions and processes in the early solar system. This information can be deciphered by investigating their mineralogy, petrology and geochemistry. The most common extraterrestrial rocks available for study are meteorites that impacted on Earth. To understand the significance of meteorites, and the information stored within, it is necessary to learn about their origin and characteristics. The following chapter gives a brief introduction into meteoritics.

### 1.1. Formation of the solar system

Our solar system was born from a collapsing molecular cloud  $\sim 4.6$  Ga ago (Bouvier and Wadha, 2010). A molecular cloud is a domain of increased gas and dust densities amidst the interstellar medium. About 95% of its material formed in-situ through evaporation and re-condensation of presolar material. Only 5% of the presolar grains were unaffected by these processes (Zinner, 2014). The interstellar cloud became unstable and collapsed once a critical mass was exceeded (Jeans instability). The gravitational collapse could have been triggered by statistical noise effects, the shockwave of a nearby supernova explosion or by the increased density in the spiral arms of the galaxy. After the collapse, a swirling protoplanetary disk – also called the ‘solar nebula’ – remained, surrounding the protosun in its gravitational centre (Fig. 1.1). The ensuing episode of solar system formation was characterized by the growth of solid particles, governed by the processes and conditions in the protoplanetary disk. Constraining these conditions is the main objective of meteoritics.

Solid particles condensed during cooling of the solar nebula. Agglomeration of  $\mu\text{m}$ - to mm-sized grains, over time, formed meter- to kilometre-sized planetesimals. The onset of the sun’s T-Tauri stage (commencement of hydrogen fusion) cleared the gas from the protoplanetary disk and a debris disk remained. Planetesimals continued to grow through collisions (accretionary growth) and formed the planets of the solar system. However, a few million planetesimals survived until today as asteroids (e.g., Fig. 1.1). They are primordial building blocks of planets – left-overs from the protoplanetary disk. Some asteroids are highly pristine and never experienced large-scale element redistribution through differentiation. Their

chemistry still represents the solar photosphere (without volatile elements). Studying these asteroids allows us to unravel timing and origin of the solar system, the source and evolution of its chemical components and the processes they experienced.

Asteroids orbit the sun and vary greatly in size (from 1 m to >100 km). Most of them are located in the asteroid belt between Mars and Jupiter. Some asteroids have already been visited by spacecrafts to image their surface or to determine their mass by their gravitational effects on the passing probe. NEAR Shoemaker landed on Eros in 2001, but did not return to Earth with sample material. This task was carried out by Hayabusa in 2005 and is also planned for the Hayabusa 2 and OSIRIS-REx missions, which are currently in progress. There is also an easier and less expensive way to study asteroids: meteorites originate (mostly) from the asteroid belt. They were exposed and dislodged when their parent bodies collided and fragmented, which then started their journey to Earth. After falling through the atmosphere, they finally came to rest on the planet's surface. Tons of meteoritic material rain down on Earth every day but most material are  $\mu\text{m}$ -sized particles. Larger meteorite falls are much rarer. Typically, meteorites are recovered from hot and cold deserts as the dry climate allows their preservation.

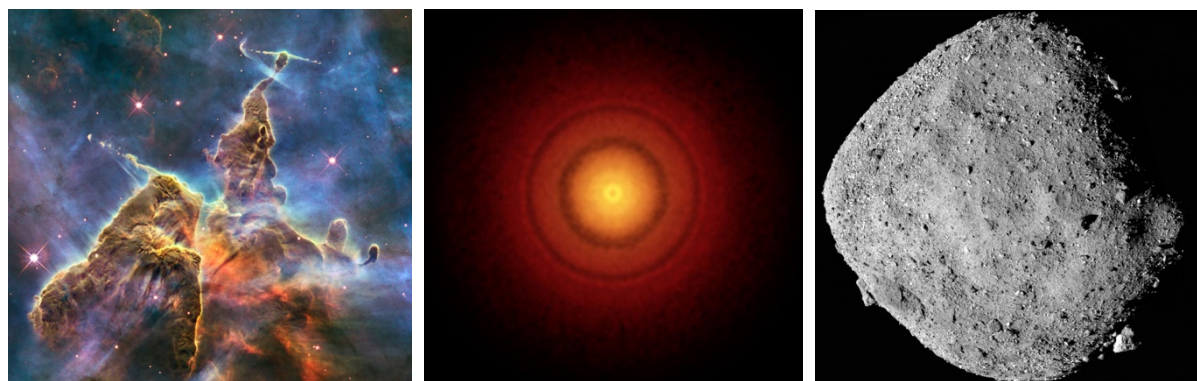


**Fig. 1.1:** Different steps of solar system evolution: stars were born from collapsing molecular clouds. A swirling protoplanetary disk formed around the star in its centre. Then, solid particles formed and grew to the size of planetesimal and/or planets. Left: Hubble image of the Carina Nebula (NGC 3372), a site of ongoing star formation (NASA, 2017). Centre: A protoplanetary disk around the young star TW Hydrae (Andrews et al., 2016, modified). Right: Asteroid Bennu is currently studied by the OSIRIS-REx spacecraft (NASA, 2018).

## 1.2. Classification and composition of meteorites

About  $\pm 60,000$  meteorites were discovered (The Meteoritical Society, 2019). They are broadly divided into two categories: differentiated and undifferentiated meteorites. Differentiated meteorites ( $\sim 8\%$ ) have been affected by melting and recrystallization. They originate from differentiated parent asteroids, but may represent different regions on that body. Iron meteorites were part of the metallic core. Stony-iron meteorites were located at the boundary between

core and silicate mantle. Achondrites are stony meteorites that were part of the outer layers of the parent body, and represent the solid residue after partial melts have been extracted. Martian and lunar meteorites also fall into this category.

The majority of meteorites discovered (~92%) are undifferentiated and have never been melted. These are called chondrites and can be classified into three major classes, which are further subdivided into several groups (listed in Table 1.1). Chondrites of the same group share many of the same characteristics, i.e., similar O-isotope composition, bulk chemistry and petrology. Ordinary chondrites (OC) are most abundant and can be further distinguished by their metal contents: there are high metal (H), low metal (L) and low metal + low iron (LL) ordinary chondrites. Enstatite chondrites (EC) are highly reduced and also distinguished by their high (EH) or low (EL) metal contents. Carbonaceous chondrites (CC) are subdivided into several chemical groups, each named after their type meteorite (for example CI = Ivuna; except CH). These groups are, however, not closely related to each other and reflect a wide variety of compositions, oxidation states and petrography. Other chondrites, such as Rumuruti (R) and Kakangari (K), are rare and have very distinct characteristics that do not allow assigning these to any of the other chondrite groups. Technically, K chondrites form a ‘grouplet’ as only four meteorites of this type have been recovered so far (Weisberg et al., 1996).

**Table 1.1:** Chondrite groups and component abundances (vol%; Scott and Krot, 2014, and references therein)

Class	Carbonaceous								Ordinary			Enstatite		Other	
	CI	CM	CO	CR	CH	CB	<b>CV</b>	CK	<b>H</b>	<b>L</b>	<b>LL</b>	<b>EH</b>	<b>EL</b>	<b>K</b>	R
Matrix	95	70	30	30-50	5	<5	40	75	10-15	10-15	10-15	<10	<10	70	35
Chondrules	<5	20	40	50-60	70	30-40	45	15	60-80	60-80	60-80	60-80	60-80	20-30	40
Metal	<0.1	0.1	<5	5-8	20	60-70	<5	<0.1	8	3	2	8	15	6-9	<0.1

Meteorites from groups printed **bold** were investigated in this thesis.

Secondary processes can significantly modify the primary characteristics of meteorites. Chondrites are therefore classified into several petrological types based on their degree of thermal metamorphism and/or aqueous alteration (Van Schmus and Wood, 1967; Huss et al., 2006; Brearley, 2014). Petrologic type 1 and 2 reflect increasing aqueous alteration and type 4–7 represent increasing thermal metamorphism. The most primitive chondrites are of petrologic type 3.

CI chondrites are highly aqueously altered and, therefore, classified as petrologic type 1. The alteration did, however, not change the bulk chemistry of these meteorites and they best match the solar elemental abundances for non-highly-volatile elements (i.e., not for H, He, N, O). The

composition of CI chondrites – also called the ‘chondritic’ or ‘solar’ composition – therefore represent the composition of the sun and can be used as a reference for various materials. Other chondrite groups may show chemical variations in their bulk compositions, such as element enrichment or depletion patterns relative to CI. The ratios of many refractory (e.g., Al, Ca, Ti) and major elements (e.g., Si, Mg, Fe) are, however, largely unfractionated among many bulk chondrites (e.g., CC) and approximately solar. If specific element ratios in chondrites or their components differ from the solar ratio of the same two elements, they are referred to as ‘super-chondritic’, if  $\frac{ratio}{CI-ratio} > 1$ , or as ‘sub-chondritic’, if  $\frac{ratio}{CI-ratio} < 1$ .

### 1.3. Chondrite components

Chondritic meteorites are mainly composed of chondrules and matrix (Fig. 1.2). These constitute up to 95 vol% of chondrites and are complemented by a number of minor or rare components such as opaque phases (Fe,Ni-metals and sulphides), Ca-Al-rich inclusions (CAI), amoeboid olivine aggregates (AOA) and presolar grains (‘stardust’). The different chondrite groups contain varying proportions of these components. Main component abundances are listed in Table 1.1.

*Chondrules:* chondrules are  $\mu\text{m}$ - to  $\text{mm}$ -sized spherules and primarily consist of silicate minerals and some opaque phases. Most chondrules have a porphyritic texture: large olivine and pyroxene crystals are set in a fine-grained or glassy background, which is called mesostasis. Depending on the modal abundances of olivine and pyroxene, chondrule textures are classified as porphyritic olivine (PO; with  $ol/px \geq 0.9$ ), porphyritic pyroxene (PP; with  $ol/px \leq 0.1$ ), or porphyritic olivine-pyroxene (POP) chondrules (Fig. 1.3; Gooding and Keil, 1981). Non-porphyritic chondrules are barred-, granular-, skeletal-olivine chondrules (BO, GO, SO), radial pyroxene chondrules (RP) or cryptocrystalline chondrules. Chondrules can also be distinguished by their mineral compositions: type I chondrule silicates contain little FeO ( $Mg\# > 90$ ) and type II chondrule silicates have high FeO contents ( $Mg\# < 90$ ).

*Matrix:* matrix material fills the space between the other components (e.g., chondrules, metal grains, CAIs). It is highly abundant in most CC, but less present in OC and EC (Table 1.1). Matrix is composed of a mixture of mainly silicates (mostly olivine and pyroxene), oxides, sulfides, metals, phyllosilicates and carbonates. Studying matrix material is challenging, as it is extremely fine-grained ( $< 100 \text{ nm} - 10 \mu\text{m}$ ). Matrix material is also more susceptible to alteration through aqueous fluids and/or metamorphism on asteroids than the other chondrite

components, e.g., due to its fine-grained nature, higher porosity and permeability. Mineralogy and chemical composition of matrix material is, therefore, highly variable in different chondrites (e.g., Scott and Krot, 2014, and references therein).

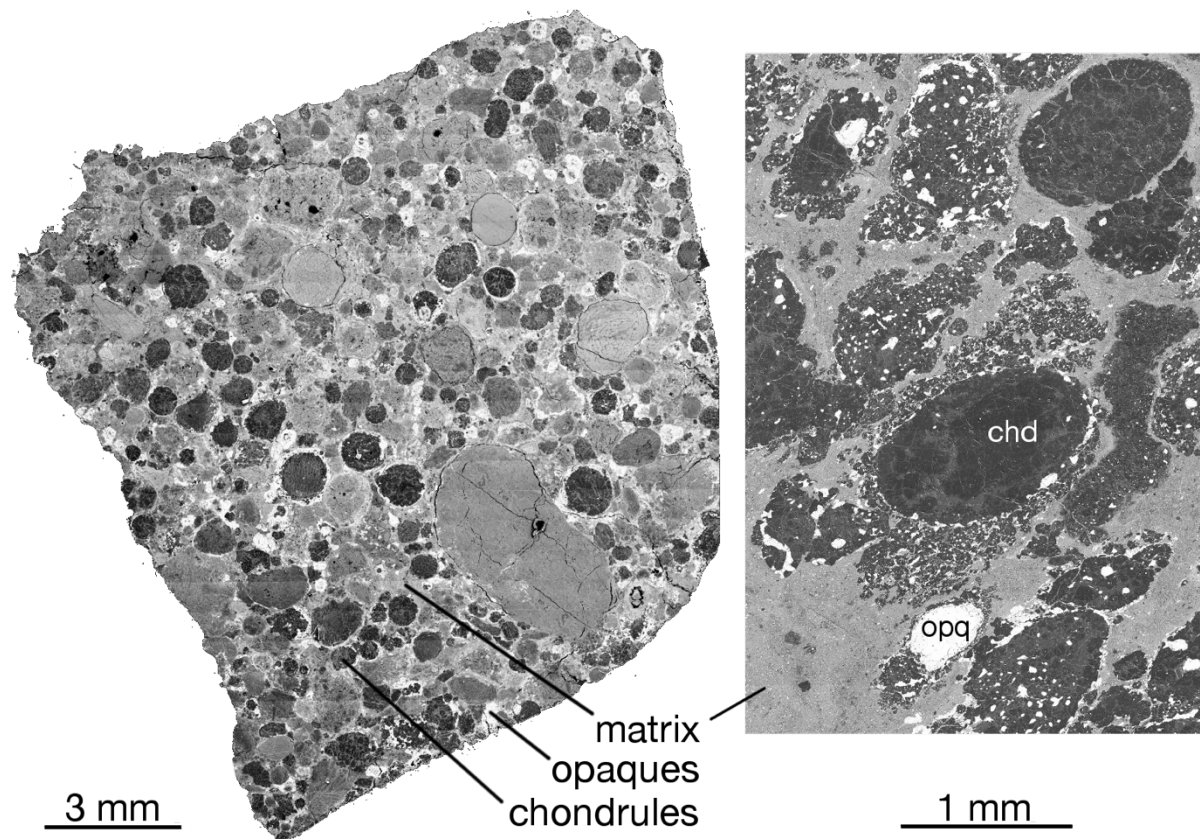


**Fig. 1.2:** Backscattered electrons (BSE) images of the ordinary chondrite NWA8276 (L3.00; left) and the carbonaceous chondrite Efremovka (CV3; right). Chondrites are mainly composed of chondrules (chd), fine-grained matrix and opaque phases (opq).

*Other components (opaques, CAIs):* minor components are opaque phases (metals and sulphides) and CAIs. Metal appears as grains of iron-nickel-cobalt (kamacite/taenite) inside chondrules or in the matrix. Sulphides (e.g., Troilit, FeS) are also present in chondrules and matrix. Ca-Al-rich inclusions mainly occur in CC with 0–3 vol% (Hezel et al., 2008). They consist of refractory (Ca, Al, Ti-rich) mineral phases and represent the first solids that condensed in the cooling solar nebula. The age of the solar system can be estimated by determining CAI formation ages with long-lived isotope chronometers (e.g.,  $^{207}\text{Pb}$ - $^{206}\text{Pb}$ ; Amelin et al., 2002; Bouvier and Wadhwa, 2010).

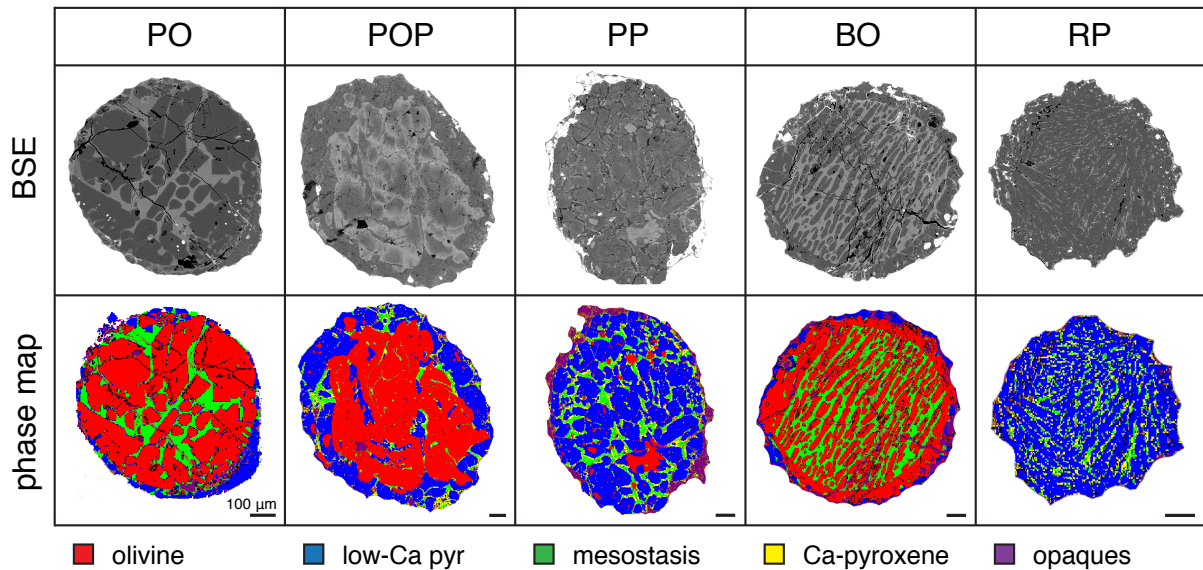


**Fig. 1.3:** BSE-images and phase maps showing the textural classification of chondrules after Gooding and Keil (1981). Phase maps show every mineral phase in false-colour. Most chondrules have porphyritic textures (PO: porphyritic olivine, POP: porphyritic olivine-pyroxene, PP: porphyritic pyroxene). Other chondrule textures are barred olivine (BO) and radial pyroxene (RP). The displayed examples for PO, POP and BO chondrules are mineralogically zoned: their olivine cores (red) are surrounded by low-Ca pyroxene rims (blue).

#### 1.4. Constraints for chondrite component formation

How chondrites and their components formed is a fundamental and long-standing question in meteoritics. A particularly challenging problem is the origin and formation mechanism of chondrules. The general consensus among meteoriticists is that chondrules formed in the protoplanetary disk within a time interval of about 2–3 Ma after or in part contemporaneously with CAIs (Amelin et al., 2002; Bizzarro et al., 2004; Becker et al., 2015). Their precursor material was melted in a flash-heating event and then rapidly cooled and crystallized in only minutes to hours. Still, the exact mechanics of chondrule formation, especially what caused the flash-heating event, are yet unknown and are highly debated. There is no limit of ideas, hypotheses and models (cf. Russell et al., 2018, and references therein). Popular explanations for the temperature spike are shockwaves that propagated through the protoplanetary disk (Wood, 1996; Desch and Connolly, 2002; Morris et al., 2012) or impact heating on planetesimals (Asphaug et al., 2011; Sanders and Scott, 2012, 2018; Johnson et al., 2015, 2018). These models require very different formation environments, i.e., chondrule formation in a ‘nebular’ or a ‘planetary’ setting.

Our present understanding of chondrule formation is limited by insufficient and, at times, contradicting constraints. Two of the most critical questions currently discussed are: (i) did chondrules behave as closed or open systems during their formation? And (ii) is there a genetic

relationship between chondrules and matrix – the main components of chondrites, i.e., did they form in the same, or in spatially separated locations? The following paragraphs briefly address these questions.

#### 1.4.1. Chondrule open vs. closed system behaviour

Chondrules were either open systems during their formation and interacted with their environment and/or each other to unknown extents. Or, no interaction took place and chondrules essentially behaved as closed systems. This is a pivotal constraint for chondrule formation models as various chondrule petrographic and petrologic characteristics must be explained very differently with respect to these scenarios.

Chondrules in all chondrites show a large range of bulk element and isotope compositions (e.g., Clayton, 1993; Jones et al., 2005; Jones and Schilk, 2009; Scott and Krot, 2014; Hezel et al., 2018a). These variations are displayed in Fig. 1.4 for Mg, a main element in CR chondrite chondrules. In a closed system, chondrules would have inherited their compositional variety entirely from heterogeneous chondrule precursor material (Grossman and Wasson, 1983; Alexander, 1994; Hezel et al., 2006, 2007, and references therein). In the open system scenario, chondrules could have altered their compositions by interacting with the surrounding nebular gas (e.g., Ebel et al., 2018, and references therein).

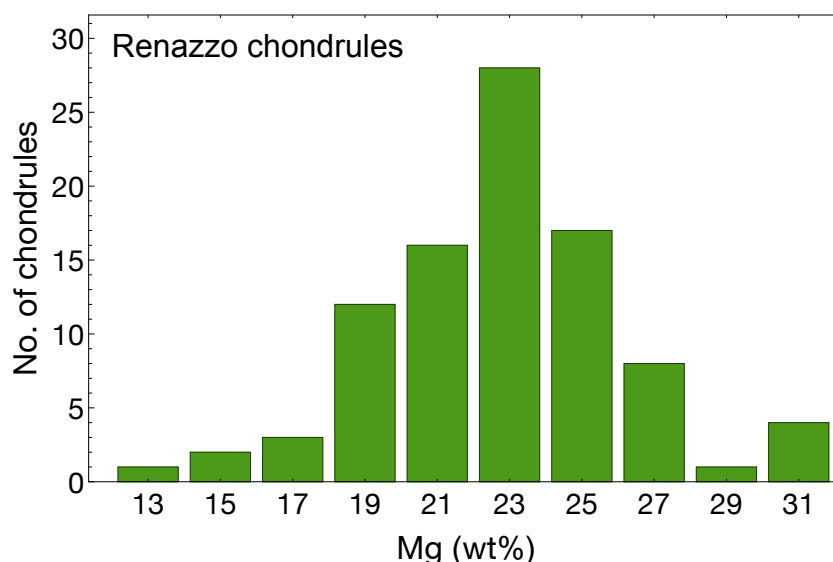


**Fig. 1.4:** The bar chart shows the large variations of Renazzo (CR) bulk chondrule Mg contents (data from Klerner 2001; Ebel et al., 2008; Hezel and Palme, 2010).

Recently, the open system scenario received much support from studies investigating chondrule compositions and textures (e.g., Tissandier et al., 2002; Hezel et al., 2003; Krot et al., 2004; Libourel et al., 2006; Jacquet et al., 2012; Friend et al., 2016; Soulié et al., 2017). Friend et al. (2016) recognized that the majority of chondrules in CC and R chondrites are mineralogically zoned. The cores of these chondrules are dominated by olivine. These are then surrounded by low-Ca pyroxene rims. Examples of mineralogically zoned chondrules are displayed Fig. 1.5 (also displayed in Fig. 1.3: PO, POP and BO chondrules). Mineralogical zonation likely results from the reaction of chondrule olivine ( $\text{Mg}_2\text{SiO}_4$ ) and SiO from the surrounding nebular gas, forming low-Ca pyroxene rims ( $\text{Mg}_2\text{Si}_2\text{O}_6$ ). Therefore, mineralogical zonation is attributed to open system interaction of chondrules and surrounding gas by the aforementioned authors.

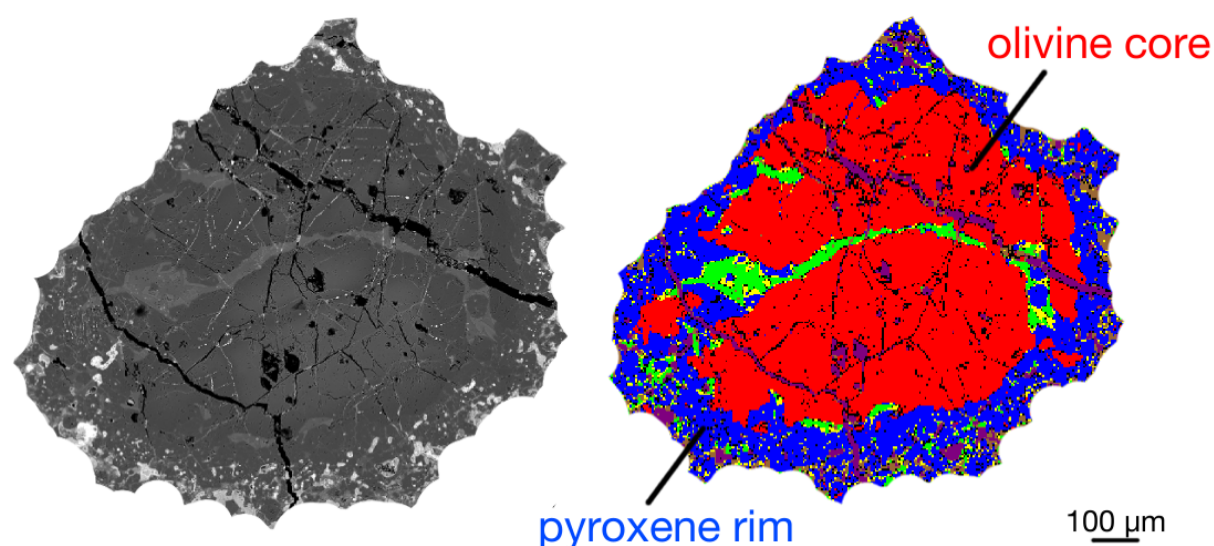


**Fig. 1.5:** BSE image (left) and phase map (right) of a mineralogically zoned POP chondrule. Zoned chondrules have olivine cores surrounded by pyroxene rims. False-color phase maps created with the PHAPS program (Hezel, 2010) are necessary to identify mineralogically zoned chondrules.

The occurrence of mineralogically zoned chondrules has so far only been quantified in CC and R chondrites (Friend et al., 2016). In other chondrites, the extent of interaction between chondrules and gas is not well known. Furthermore, only a limited number of bulk chondrule compositions have been reported in the literature (ChondriteDB; Hezel et al., 2018a). These are necessary to further investigate compositional variations in the chondrule populations of meteorites.

#### *1.4.2. Single vs. multiple reservoirs: the chondrule-matrix complementarity*

Chondrules and matrix might either originate from the same, or from multiple, spatially separated reservoirs. The first scenario suggests a genetic relationship between both components, while the second scenario implies separate origins, and subsequent transport and mixing of chondrules and matrix. Answering this question would provide crucial constraints for all chondrite formation models. The concept of ‘complementarity’ might be the decisive argument in this discussion.

The bulk chemistry of chondrites is largely defined by their two major components – chondrules and matrix. Studies that examined the isotope or element compositions of both components in CC and R chondrites report a chemical complementarity between them (e.g., Wood, 1985; Klerner, 2001; Bland et al., 2005; Hezel and Palme 2008, 2010; Becker et al. 2015, Palme et al. 2015; Budde et al. 2016a,b; Ebel et al., 2016; Friend et al., 2017, 2018; Hezel et al., 2018b, and references therein). Chondrules and matrix have different compositions from each other for various element or isotope ratios, e.g., chondrules in CC have super-chondritic Mg/Si ratios and matrix has sub-chondritic Mg/Si ratios (Fig. 1.6). Both components together add up to the CI-chondritic (solar) ratio of the same elements and/or isotopes. It is highly unlikely that both components formed in different reservoirs, but then mixed in exactly the right proportions to yield a solar bulk chondrite composition. The aforementioned authors conclude that both components must have formed from a single CI-chondritic parental reservoir. They furthermore conclude that chondrule-matrix complementarity was established in the solar nebula before parent body accretion, therefore excluding all chondrule formation models that require a planetary setting.

The complementarity argument is, however, not yet canonically accepted. Some authors attribute the aforementioned observations to element redistribution on chondrite parent bodies or analytical artefacts (Zanda et al., 2018). Other authors interpret their findings as evidence for multiple parental reservoirs, and mixing of components between them (e.g., Olson et al., 2016), which would be in conflict with complementarity. Lastly, complementarities have only been studied in CC and R chondrites. Wasson (2008) proposed that complementarities might be limited to these classes as other chondrites have distinct bulk chemistries, e.g., bulk OC and EC are sub-chondritic in Mg/Si. It is yet unknown if complementarities exist for chondrites other than CC and R.

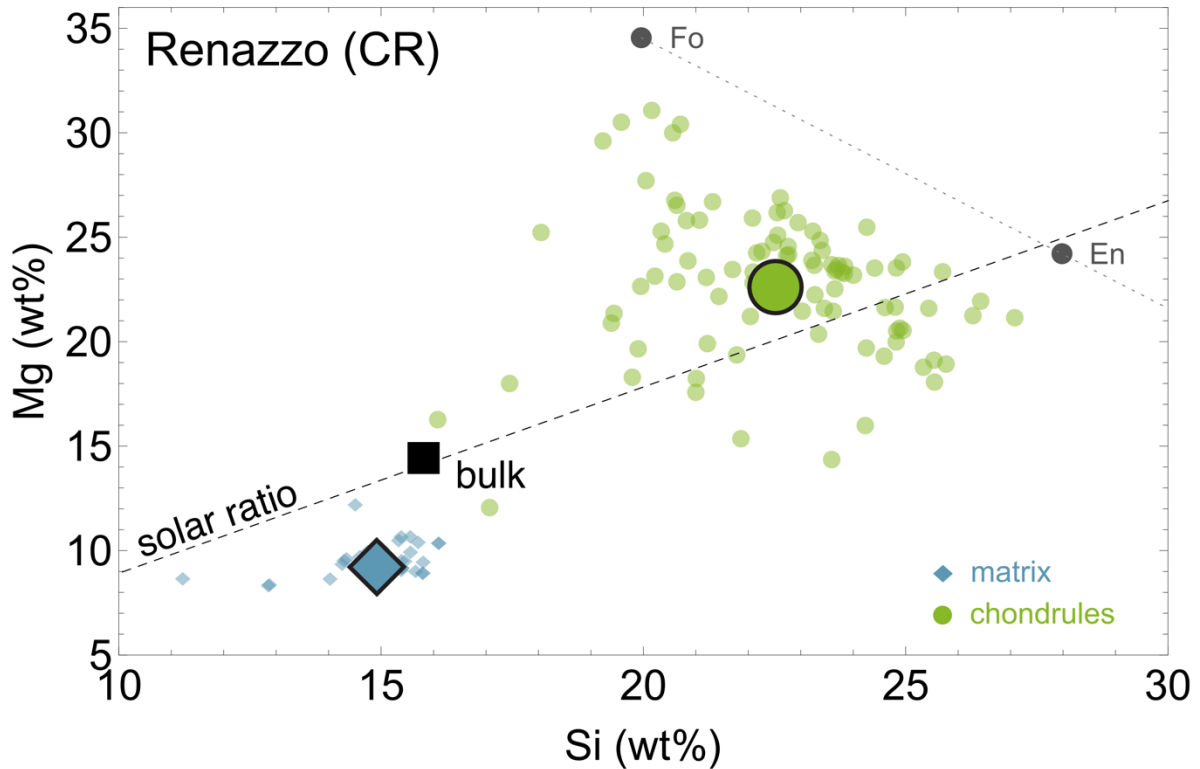


**Fig. 1.6:** The average compositions of chondrules and matrix in Renazzo (CR) are different (sub-, and super-chondritic) but complementary to each other. They add up to a solar bulk meteorite composition (Fo: forsterite, En: enstatite; CR data from Klemmer 2001; Ebel et al., 2008; Hezel and Palme, 2010; bulk Renazzo: Mason and Wiik, 1962; CI data: Palme et al., 2014).

## 1.5. Objectives of this thesis

I outlined two fundamental questions of chondrule formation in Section 1.4: the open vs. closed system case, and single vs. multiple reservoirs. Studying these scenarios would provide pivotal constraints for chondrule formation and significantly enhance our understanding of the processes and conditions in the early solar system. Many recent studies focused on CC and R chondrites and investigated mineralogically zoned chondrules (e.g., Friend et al., 2016, and references therein), bulk chondrule compositions (e.g., Hezel et al. 2018a, and references therein) and chondrule-matrix complementarities (e.g., Hezel et al., 2018b, and references therein). To obtain a more comprehensive picture of chondrule formation, I aim to expand these studies to OC, EC and K chondrites. These chondrites have very distinct characteristics and compositions from CC, and might originate from different regions in the protoplanetary disk (e.g., Warren, 2011; Gerber et al., 2017). Thus, they could have experienced very different processes and conditions during their formation. Ordinary chondrites might be particularly important as these are the most abundant chondrites found on Earth.

In the following chapters, I will in detail investigate the extent of chondrule interactions with their environment and with each other. For this purpose, I will quantify the abundance of mineralogically zoned chondrules in OC, EC and K chondrites, thereby completing the work started by Friend et al. (2016). Chondrule textures will be studied with 2D and 3D techniques. Furthermore, I will present a comprehensive dataset of bulk chondrule compositions in these chondrites, which will allow a detailed study of bulk chondrule compositional variations. Lastly, I will investigate the genetic relationship between chondrules and matrix in the rare and unusual K chondrite grouplet, thereby extending the study of chondrule-matrix complementarities beyond CC and R chondrites. A wide range of analytical tools are required for this study, and detailed descriptions of the methods used can be found in every chapter.

# Chapter 2

## Mineralogically zoned chondrules in ordinary chondrites as evidence for open system chondrule behaviour

Jens Barosch, Dominik C. Hezel, Denton S. Ebel, Pia Friend

*Geochimica et Cosmochimica Acta* 249 (2019), 1–16.

<https://doi.org/10.1016/j.gca.2019.01.018>

### **Abstract**

Chondrules are a major component of chondritic meteorites. Understanding their formation conditions provides fundamental insights about how the early solar system formed and evolved. We studied the textures of ~650 chondrules from all three groups (H, L, LL) of ordinary chondrites, in 2-dimensional (2D) sections through the meteorites. About 40% of the chondrules are mineralogically zoned. They consist of an olivine-rich core, which is surrounded by a low-Ca pyroxene-rich rim. Chondrules sectioned through their low-Ca pyroxene rim do not appear as zoned chondrules, hence, considering such sectioning effects, their true fraction might be as high as ~50%. Mineralogical zonation is, therefore, a typical chondrule texture in basically all ordinary chondrites, and records a fundamental process during chondrule formation. Chondrules were open systems, and initially olivine-rich chondrules reacted with their surrounding gas to form low-Ca pyroxene rims. Zoned and unzoned chondrules have the same range of bulk compositions, thus ordinary chondrite chondrules were likely affected by two sequential episodes: in the first episode, gaseous SiO<sub>2</sub> was added to all chondrules, thereby forming low-Ca pyroxene rims around all chondrules. In the second episode, only a portion of the chondrules were reheated, thereby remelting and homogenizing their initial pyroxene rims, but retaining their bulk compositions. It is therefore likely that all chondrules in ordinary chondrites were affected by gas-melt interactions during their formation. Open system exchange is consistent with previous studies of chondrule formation and can explain many chondrule textures and bulk chondrule compositional variations in single meteorites. Hence, the open system behaviour recorded in zoned chondrules provides a pivotal constraint on chondrule formation conditions.

## 2.1. Introduction

Chondrules are near-spherical, igneous-textured objects which are a main component in all chondritic meteorites except CI chondrites. Chondrules formed in brief high temperature events reaching peak-T of up to 2000°C, during which chondrule precursors were molten and rapidly crystallised afterwards (e.g. Scott et al., 1996; Desch and Connolly, 2002; Hewins et al., 2005). Olivine and low-Ca pyroxene are the major chondrule minerals, usually set in a glassy or microcrystalline mesostasis, which itself represents the residual melt. In a chondrite, chondrules are embedded in the matrix, a fine-grained mixture of mineral grains including presolar grains and organic matter. Despite many advances in understanding chondrule formation, critical details such as the source of the heating events or the interaction of the chondrule melt with the surrounding gas remain insufficiently understood.

Chondrules of all chondrite groups show large variations in their chemical and isotopic compositions (e.g. Clayton, 2005; Jones et al., 2005; Hezel et al., 2006, 2018a). The two major hypotheses explaining these variations are: (i) chondrules inherited the variations from heterogeneous precursor grains. This is known as the *closed system* case (e.g. Sears et al., 1996; Hezel and Palme, 2007, and references therein); and (ii) chondrules exchanged material with the surrounding gas, thereby also changing their bulk compositions, including isotopes. This is the *open system* case (e.g. Sears et al., 1996; Grossman et al., 2002; Tissandier et al., 2002; Hezel et al., 2003; Krot et al., 2004; Libourel et al., 2006; Chaussidon et al., 2008; Hezel and Palme, 2010; Kita et al., 2010; Jacquet et al., 2012; Harju et al., 2014; Di Rocco and Pack, 2015; Friend et al., 2016; Soulié et al., 2017). In a hybrid scenario, the compositional range of chondrules would not only be controlled by the composition of the precursor assemblage, but also by material exchange during chondrule formation.

A number of studies have provided direct evidence for the open system case: (i) Tissandier et al. (2002) experimentally allowed melt to react with gaseous SiO during crystallisation and reproduced textures similar to those of naturally zoned chondrules. This similarity supports the idea that chondrules experienced gas-melt interaction. (ii) Libourel et al. (2006) showed that chondrule glasses are not located on the subtraction lines of olivine or low-Ca pyroxene in appropriate phase diagrams, indicating that type I chondrules do not obey closed-system crystallization and gained material from the surrounding gas. (iii) Chaussidon et al. (2008) studied the oxygen isotope systematics of olivine and pyroxene in CR and CV chondrites. They found that the oxygen isotopic composition of low-Ca pyroxene at the chondrule rims

represents a mixture of dissolved precursor olivine (2/3 of the oxygen) and the addition of SiO from the surrounding nebula gas (1/3 of the oxygen). Although several subsequent studies have found O-isotopic agreement between coexisting chondrule olivine and pyroxene (Kita et al., 2010; Rudraswami et al., 2011; Weisberg et al., 2011; Ushikubo et al., 2012; Tenner et al., 2013, 2015, 2017; Nagashima et al., 2015; Miller et al., 2017; Schrader et al., 2017; Hertwig et al., 2018; Chaumard et al., 2018), these researchers nevertheless argue for open system behaviour of chondrules (e.g. Kita et al., 2010; Ushikubo et al., 2012; Schrader et al., 2014). Tenner et al. (2017) furthermore provides mechanisms that explain both the Si enrichment of chondrule rims and O-isotope homogeneity among chondrule olivine and pyroxene. (iv) Jacquet et al. (2012) measured trace elements in chondrule minerals of carbonaceous chondrites. While olivines have an igneous origin, trace element patterns of pyroxenes, particularly in the rim regions of the chondrules, suggest an interaction with the surrounding gas, presumably the addition of silica to the chondrule melt. The authors concluded that the formation of chondrule core olivine and their pyroxene-rich rims were distinct events. (v) Harju et al. (2014) measured the Si isotopic composition of Allende chondrule olivine and pyroxene. The difference between these minerals was on average  $\sim 0.3\text{‰}$  ( $\delta^{29}\text{Si}_{\text{px}} < \delta^{29}\text{Si}_{\text{ol}}$ ), while at equilibrium pyroxene would be only  $\sim 0.01\text{‰}$  lighter than olivine. Hence, these differences cannot result from an equilibrium fractionation between both phases. They are best explained by the condensation of isotopically lighter Si (as  $\text{SiO}_{(\text{g})}$ ) into the melt from which the pyroxene formed. In summary, various strands of evidence support the process of late addition of SiO to chondrules at high temperature, thereby forming low-Ca pyroxene rims on olivine-rich core material.

In a recent paper on chondrule open system behaviour, Friend et al. (2016) showed that the majority of chondrules in carbonaceous (CC) and Rumuruti (R) chondrites are mineralogically zoned, with olivine in the core surrounded by a rim dominated by low-Ca pyroxene. In agreement with the aforementioned studies, Friend et al. (2016) also explained the formation of low-Ca pyroxene rims by the reaction of chondrule olivine with SiO from the surrounding gas. They found that possibly up to  $>90\%$  of the chondrules in C and R chondrites have low-Ca pyroxene rims, and, hence, interpreted that the majority of chondrules acted as open systems when they formed. The authors further studied the appearance, abundance and general characteristics of zoned chondrules and estimated that about 3–15 wt.% of  $\text{SiO}_2$  was added to the chondrules during this process. The high portion of mineralogically zoned chondrules make them the dominant type of chondrules in C and R chondrites.

Mineralogical zonation in chondrules was recognised very early by Scott and Taylor (1983). Since then it has been frequently, if briefly, mentioned (e.g. Grossman, 1996; Grossman et al., 2002; Tissandier et al., 2002; Hezel et al., 2003, 2006; Krot et al., 2004; Hewins et al., 2005; Berlin et al., 2006; Lauretta et al., 2006; Chaussidon et al., 2008; Jones, 2012; Hewins and Zanda, 2012; Harju et al., 2014; Jacquet et al., 2012; Scott and Krot, 2014; Jacquet and Marrocchi, 2017; Soulié et al., 2017). Friend et al. (2016) presented the first systematic study of mineralogical chondrule zonation, restricted, however, to C and R chondrites. No similar study exists for ordinary chondrites (OC). OC generally have high chondrule modal abundances (60–80 vol.%) and correspondingly small matrix abundances (<20 vol.%; Lobo et al., 2014; Scott and Krot, 2014). Bulk OC have sub-chondritic Mg/Si ratios ( $\sim 0.9 \times CI$ ) and are slightly depleted in refractory elements (Scott and Krot, 2014; Hezel et al., 2018b, and references therein). It has been speculated that ordinary and carbonaceous chondrites formed in different formation regions in the protoplanetary disk (e.g. Walsh et al., 2011; Warren, 2011; Burkhardt et al., 2017).

Mineralogical zonation as a result of chondrule open system behaviour is an important constraint for chondrule formation. Here we study the appearance, abundance and distribution of mineralogically zoned, but also unzoned chondrules in all three groups (H, L, LL) of ordinary chondrites. We compare our results to the reported mineralogically zoned chondrules in C and R chondrites of Friend et al. (2016) and discuss the formation conditions of zoned and unzoned chondrule textures and bulk chondrule compositional variations. This includes similarities and differences that may have existed among chondrule-forming environments from different chondrite groups, and constraints on astrophysical theories that attempt to describe chondrule as well as chondrite formation.

## **2.2. Methods**

All analyses were performed with an electron microprobe (EPMA, JEOL JXA-8900RL Superprobe) and/or a scanning electron microscope (SEM, Zeiss Sigma 300 VP), both located at the Institute of Geology and Mineralogy, Cologne. Mineral compositions were determined by EPMA spot analyses with a focused beam of 1  $\mu\text{m}$  diameter and a beam current of 20 nA. The accelerating voltage was set to 20 kV. Well characterised reference materials were used for calibration and ZAF corrections were applied (Bence and Albee, 1968). Detection limits for minor elements were 100 wt.-ppm for CaO, TiO<sub>2</sub>, NiO and Na<sub>2</sub>O; 200 wt.-ppm for Cr<sub>2</sub>O<sub>3</sub>; and 250 wt.-ppm for MnO and FeO. Element x-ray maps of individual chondrules were

obtained with EPMA by moving the stage under the stationary electron beam. The chondrules for these individual map (IM) analyses were randomly chosen by hand from the entire area of the meteorite section. Every element map was recorded with a 1  $\mu\text{m}$  focused beam, a 20 nA beam current, a 4  $\mu\text{m}$  step size and a dwell time of 250 ms. Element maps were recorded before spot analyses.

The SEM was only used for chondrule imaging and compiling large area maps (LAM) of chondrite sections. For both tasks, the electron beam rastered the sample surface over small areas ( $\sim 800 \times 800 \mu\text{m}$ , pixel size  $\sim 2 \mu\text{m}$ ) at a working distance of 8.5 mm and a dwell time of 100 ms per pixel. The sample was then moved to a new centre and the next map was obtained. The aperture diameter was set to 60  $\mu\text{m}$  and the accelerating voltage to 20 kV, resulting in an output count rate of  $\sim 45,000$  cps. Individual maps constituting the LAM were recorded in random sequence to avoid local charge build-up. To test the robustness of IM and LAM analyses, we measured and compared the L3.00 chondrite sample NWA8276 with both methods.

The chondrule element maps and LAMs were used to create phase maps using the phase map program PHAPS (Hezel, 2010). The resulting false-colour images allow instant visual identification of the different mineral phases and quantification of rim abundances. Modal recombination of the phase maps and element analyses allowed determination of bulk chondrule compositions. In 2D chondrule sections, metal and sulphide contents cannot be determined reliably, as has been demonstrated by e.g. Hezel (2007), Ebel et al. (2009) and Hezel and Kießwetter (2010). Thus, chondrule metals and sulphides were not analysed and not included in the bulk chondrule data. Hezel and Kießwetter (2010, and references therein) furthermore noted that 2D bulk compositions are not necessarily representative of the true 3D chondrule bulk compositions and provided a tool to calculate the error of 2D bulk compositions relative to the true 3D bulk composition. The relative errors between 2D and 3D bulk compositions of porphyritic chondrules are typically between  $\pm 1\text{--}30$  rel.%.

### **2.3. Results**

We studied a total of  $\sim 650$  chondrules from 8 ordinary chondrites of all three subgroups (Table 2.1). Of these, we studied 227 chondrules in detail to determine their petrographic and petrologic characteristics. We further included 20 chondrules reported by Berlin (2009).

Most samples studied are of low petrologic type and experienced neither extensive thermal metamorphism, nor extensive aqueous alteration. Thermal metamorphism affected the samples of petrologic type 3.6 and 3.8, disturbing their primary chondrule mineral chemistry. However, chondrule textures in these chondrites remained unchanged and can thus be used for this study (see also Section 2.4.3).

In chondrites of petrologic type  $\leq 3.4$ , we classify porphyritic chondrules into type I ( $Fo \geq 90$ ) and type II ( $Fo < 90$ ) based on the abundance of their forsterite component in olivine. In petrologic type 3.6 chondrites, the onset of Mg-Fe equilibration prohibits this approach. Chondrule olivines frequently have FeO-rich rims and if we would classify the chondrules based on their average forsterite component, almost all chondrules would be type II. To our knowledge, no definite protocol exists for type I/II discrimination in samples of higher petrologic type. Diffusion coefficients in pyroxene are significantly lower than in olivine, thus equilibration occurs less rapidly (Jones, 1996a). Pyroxene equilibration is not completed until petrologic type 5 (Huss et al., 2006, and references therein). It is likely that chondrules retain primary pyroxene compositions until petrologic type  $> 3.8$ . Therefore, to classify chondrules in petrologic type 3.6 and 3.8 chondrites, as well as chondrules lacking olivine, we use low-Ca pyroxene compositions (type I:  $En \geq 90$  and type II:  $En < 90$ ).

A mineralogically zoned chondrule is characterised by olivine and mesostasis in its core and a rim of low-Ca pyroxene (Fig. 2.1). All chondrules with different textures are designated as unzoned (Section 2.3.2).

**Table 2.1:** Host meteorites of the ~650 chondrules studied.

Meteorite Group	Meteorite Name	Abbreviation	Petrologic type	Technique	Chondrules studied	Zoned Chondrules
LL	Huacachina	Hua	3	IM	34	13 = 38%
LL	Parnallee	Parn	3.60	IM	39	14 = 36%
LL	Semarkona	Sem	3.00	LAM	167	52 = 31%
L	NWA8276	N8276	3.00	IM	65	34 = 52%
L	NWA8276	N8276	3.00	LAM	165	71 = 43%
L	Moorabie	Moor	3.80-an	LAM	107	50 = 47%
H	Suwahib (Buwah)	Suw	3.80-an	IM	49	21 = 43%
H	Willard (b)	Will	3.60	IM	40	12 = 30%
L(LL)*	Meteorite Hills 00526	M0526	3.05	IM	20	6 = 30%

IM: Individual chondrule maps, LAM: Large area mapping. Petrographic details and mineral compositions were only studied on IM chondrules.

\* Data from Berlin (2009)

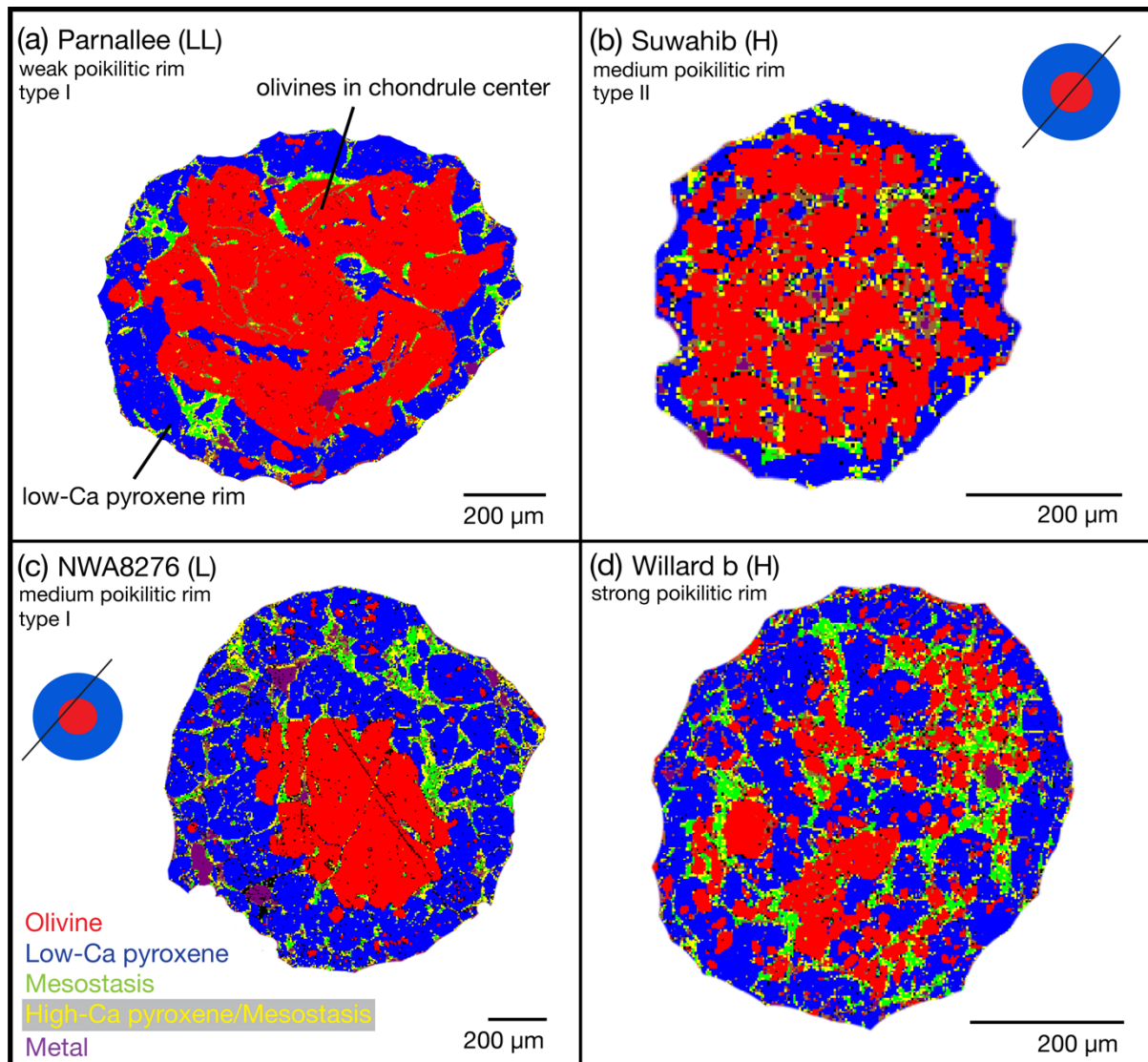


**Fig. 2.1:** Typical appearances of zoned chondrules in various ordinary chondrites. In these phase maps from the PHAPS program (Hezel, 2010), olivine (red) dominates the core and is surrounded by low-Ca pyroxene rims (blue) of variable thicknesses.

### 2.3.1. Chondrule petrography and petrology

The average fraction of zoned chondrules in all ordinary chondrites studied here is ~40% (Fig. 2.2). The fractions in individual chondrites vary from 30% to 52% (Table 2.1). In the H chondrites, the fraction of zoned chondrules is 30% in Willard b (H3.6) and 43% in Suwahib (Buwah, H3.8-an). In the LL chondrites, zoned chondrule fractions are quite similar, with 31% in Semarkona (LL3.00), 36% in Huacachina (LL3) and 38% in Parnallee (LL3.6). The chondrite MET 00526 (L/LL3.05) contains 30% zoned chondrules (Berlin, 2009) and Moorabie (L3.8-an) contains 47% zoned chondrules. In the second L chondrite, NWA8276 (L3.00), the fraction of zoned chondrules was determined with two different techniques (IM & LAM): Using IM, a fraction of 52% zoned chondrules was identified, whereas using LAM, a

lower fraction of 43% zoned chondrules was identified. This difference will be discussed in Section 2.4.2.

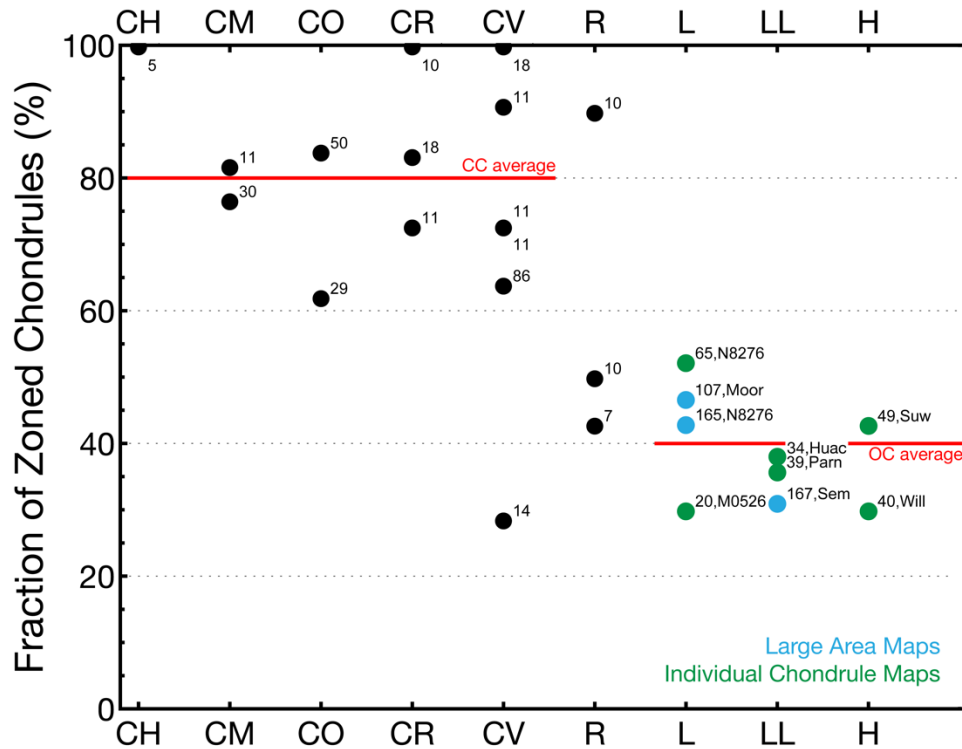


**Fig. 2.2:** Fraction of zoned chondrules in different groups of ordinary (this study), carbonaceous and Rumuruti chondrites (Friend et al., 2016). On average, 40% of all chondrules in ordinary chondrites are mineralogically zoned. The numbers indicate the amount of chondrules studied. Meteorite abbreviations are listed in Table 2.1.

The detailed petrographic chondrule characteristics presented in the following are based on the 227 high-resolution individual chondrule (IM) phase maps, as the LAM provide insufficient resolution to be used for such detailed petrographic studies. Almost all chondrules studied have a porphyritic texture. From these, 57% are porphyritic olivine-pyroxene chondrules (POP), 20% are porphyritic olivine chondrules (PO; containing <10 vol.% pyroxene) and 23% are porphyritic pyroxene chondrules (PP; containing <10 vol.% olivine). Most zoned porphyritic chondrules are POP (66%), with fewer being PO (20%) and PP (14%). Furthermore, five zoned chondrules are barred olivine (BO) chondrules.

The abundance of type I chondrules is lowest in Huacachina (LL3, 40%), intermediate in Willard b (H3.6, 46%), M0526 (L/LL3.05, 47%) and Suwahib (B) (H3.8-an, 53%), and high in Parnallee (LL3.6, 69%) and NWA8276 (L3.00, 82%; Fig. 2.3a). Most of the mineralogically zoned chondrules are type I. In NWA8276 ~94% of zoned chondrules are type I, in Parnallee 86%, M0526 75%, Suwahib 70%, Huacachina 60%, and in Willard b ~56% (Fig. 2.3b).

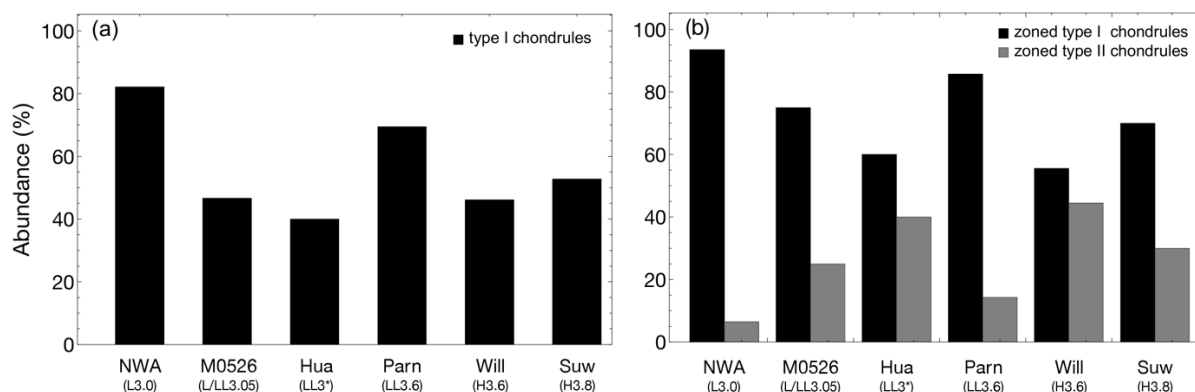


**Fig. 2.3:** (A) Fractions of type I porphyritic chondrules in the various ordinary chondrites. (B) Type I/II fractions of mineralogically zoned chondrules. The majority of zoned chondrules are type I. \*Huacachina is classified as petrologic type 3. Olivine Fa and Cr<sub>2</sub>O<sub>3</sub> mean values might indicate an increased petrologic type (possibly 3.4; Bouvier et al., 2017). From the Cr<sub>2</sub>O<sub>3</sub> contents determined in this study (~0.10 wt.% on average) we propose that Huacachina is at least petrologic type  $\geq 3.2$  following the classification by Grossman and Brearley (2005).

The relative abundances of zoned chondrules among the type I and II chondrules are markedly different (Table 2.2). In NWA8276, 29 out of 46 type I chondrules are zoned (63%), while only 2 out of 10 type II chondrules are zoned (20%). In addition to this difference among type I/II chondrules, 7 chondrules have non-porphyritic textures and 3 of them are zoned. No chondrule types were determined for 2 other chondrites, which are both unzoned. This totals 52% zoned chondrules in NWA8276 (Fig. 2.2). The abundances of type I chondrules which are also zoned are lowest in Willard b (42%), M0526 (43%) and Parnallee (48%), while their abundances are high in NWA8276 (63%), Suwahib (74%) and Huacachina (75%). Abundances of zoned chondrules which are type II chondrules are again very variable: only ~13% are zoned in M0526, 18% in Parnallee and 20% in NWA8276. Higher abundances of zoned type II chondrules are observed in Willard b (29%), Huacachina (33%) and Suwahib (35%).

**Table 2.2:** Chondrule types, (their respective zoned chondrule abundances), [and % zoned chondrule fractions].

Chondrules	NWA8276 (L)	MET0526 (L/LL)	Huacachina (LL)	Parnallee (LL)	Willard b (H)	Suwahib (H)
Type I (zoned) [%]	46 (29) [63]	7 (3) [43]	8 (6) [75]	25 (12) [48]	12 (5) [42]	19 (14) [74]
Type II (zoned) [%]	10 (2) [20]	8 (1) [13]	12 (4) [33]	11 (2) [18]	14 (4) [29]	17 (6) [35]
n.d.* (zoned) [%]	9 (3) [33]	5 (2) [40]	14 (3) [21]	3 (0) [0]	14 (3) [21]	13 (1) [8]
Total (zoned) [%]	65 (34) [52]	20 (6) [30]	34 (13) [38]	39 (14) [36]	40 (12) [30]	49 (21) [43]

\*n.d.: type not determined – this includes non-porphyritic chondrules.

The olivines in type I chondrules in Huacachina (LL3), Willard b (H3.6) and Parnallee (LL3.6) are typically compositionally zoned, presumably due to metamorphism. Their cores contain average fayalite of Fa<sub>8</sub> in Willard b and Fa<sub>7.5</sub> in Huacachina and Parnallee. At their rims, most olivines are significantly enriched in FeO, showing average fayalite of Fa<sub>18</sub> in Willard b, and

up to  $Fa_{26}$  in Huacachina. Olivines in Suwahib (H3.8-an) are mostly equilibrated in Fe-Mg and contain on average  $Fa_{13}$ . In the few remaining forsteritic olivine cores, the average is  $Fa_{4.5}$ . NWA8276 (L3.00) olivines usually do not show Fe-zoning. On average, they contain  $Fa_{3.75}$ , however, some olivines are almost entirely iron-free, with only 0.3 wt.% FeO. Type II chondrule olivines contain on average  $Fa_{13.5}$  in Suwahib (equilibrated in Fe-Mg),  $Fa_{17}$  in NWA8276,  $Fa_{19}$  in Willard b,  $Fa_{21}$  in Huacachina and  $Fa_{22}$  in Parnallee. Low-Ca pyroxene average compositions are less FeO-rich in Huacachina ( $Fs_8$ ), while higher FeO contents are observed in the other samples ( $Fs_{\sim 16}$ ).

Similarly, low-Ca pyroxenes in type I NWA8276 chondrules are poor in ferrosilite ( $Fs_4$  on average). The low-Ca pyroxenes have higher FeO contents in Huacachina ( $Fs_6$ ), Parnallee ( $Fs_{6.5}$ ) and are highest in Suwahib and Willard b ( $Fs_{7.5}$ ). High-Ca pyroxene is rare in most chondrules and usually appears as overgrowth on low-Ca pyroxene crystals. When present, it contains on average 14.7 wt.% CaO, 19.3 wt.% MgO and 5.3 wt.% FeO, translating to augite with average  $Fs_{17.7}$ ,  $Wo_{39.1}$ .

Only small differences are observed between mesostases in type I and II chondrules, e.g. the mesostasis in type I chondrules is usually slightly enriched in refractory elements (Al, Ti, Ca), compared to type II. In both chondrule types, the glassy/recrystallised mesostasis is normatively feldspathic with the highest CaO concentrations (7–12 wt.%) and simultaneously the lowest  $Na_2O$  contents (3–4 wt.%) in NWA8276 mesostasis, while the opposite is true for mesostasis in Huacachina (2–6 wt.% CaO and  $\sim 7$  wt.%  $Na_2O$ ). Average chondrule phase compositions are given in Table 2.3a for type I chondrules and Table 2.3b for type II chondrules.

The thickness of low-Ca pyroxene rims within zoned chondrules varies from very thin rims of only a few  $\mu m$  to comparatively thick rims that occupy large portions of the chondrules (cf. rim thicknesses displayed in Fig. 2.1 plate b compared to plate c). The average rim fraction is about 30% of a single chondrule, but varies from 6 to 70%. Some chondrules have non-uniform rim thicknesses or their olivine cores are only partially enclosed by low-Ca pyroxene. In chondrules with a large low-Ca pyroxene rim fraction, low-Ca pyroxene often also appears scattered throughout the entire chondrule, usually mixed with olivine and mesostasis (Fig. 2.1 d).

## 2. Mineralogically zoned chondrules in OC

**Table 2.3:** Average compositions of type I and II chondrule phases in OC samples (wt.%). Sample abbreviations are taken from Table 2.1.

<b>Type II chondrules</b>										
Mineral	<b>Olivine</b>					<b>Mesostasis</b>				
Sample	Suw (H)	Will (H)	NWA (L)	Parn (LL)	Hua (LL)	Suw (H)	Will (H)	NWA (L)	Parn (LL)	Hua (LL)
SiO <sub>2</sub>	40.42	38.97	39.74	38.67	38.98	64.88	61.65	61.27	63.07	58.77
TiO <sub>2</sub>	0.01	0.04	0.02	0.01	0.02	0.44	0.23	0.45	0.41	0.42
Al <sub>2</sub> O <sub>3</sub>	0.02	0.14	0.05	0.02	0.11	14.75	15.79	15.42	15.41	16.87
Cr <sub>2</sub> O <sub>3</sub>	0.03	0.08	0.44	0.07	0.14	0.18	0.27	0.12	0.22	0.36
FeO	12.99	17.63	15.95	20.35	19.52	3.55	4.51	7.01	3.97	3.39
MnO	0.47	0.47	0.41	0.44	0.35	0.19	0.08	0.23	0.16	0.24
NiO	0.02	0.02	0.02	0.02	0.13	0.06	0.09	0.02	0.03	0.25
MgO	46.96	42.77	43.87	39.86	41.20	4.90	4.35	2.25	3.61	6.75
CaO	0.03	0.09	0.19	0.05	0.11	4.73	5.25	7.38	5.22	7.93
Na <sub>2</sub> O	0.03	0.02	0.04	0.02	0.05	7.16	7.22	4.12	7.18	5.18
Total	100.99	100.21	100.72	99.49	100.61	100.83	99.45	98.28	99.28	100.17

Mineral	<b>low-Ca pyroxene</b>					<b>high-Ca pyroxene</b>				
Sample	Suw (H)	Will (H)	NWA (L)	Parn (LL)	Hua (LL)	Suw (H)	Will (H)	NWA (L)	Parn (LL)	Hua (LL)
SiO <sub>2</sub>	56.85	55.56	55.81	56.30	57.87	53.55	52.65	52.84	53.16	52.94
TiO <sub>2</sub>	0.04	0.16	0.11	0.03	0.08	0.24	0.35	0.46	0.31	0.49
Al <sub>2</sub> O <sub>3</sub>	0.40	0.70	0.96	0.39	0.52	1.37	1.77	3.16	2.31	3.72
Cr <sub>2</sub> O <sub>3</sub>	0.55	0.34	0.85	0.64	0.55	1.65	1.22	1.43	1.65	1.77
FeO	10.14	10.88	10.20	9.96	5.46	10.54	8.56	8.23	8.90	6.08
MnO	0.51	0.45	0.40	0.50	0.33	0.79	0.35	0.40	0.80	1.01
NiO	0.06	0.03	0.04	0.01	0.06	0.07	0.12	0.02	0.02	0.21
MgO	31.39	30.76	30.41	30.68	35.05	19.82	17.85	16.85	17.89	19.27
CaO	0.72	0.68	1.87	0.70	0.64	11.15	15.37	16.57	13.58	13.71
Na <sub>2</sub> O	0.18	0.18	0.06	0.07	0.11	0.70	1.00	0.52	0.66	0.68
Total	100.83	99.75	100.72	99.29	100.66	99.86	99.24	100.49	99.30	99.90

<b>Type I chondrules</b>										
Mineral	<b>Olivine*</b>					<b>Mesostasis</b>				
Sample	Suw (H)	Will (H)	NWA (L)	Parn (LL)	Hua (LL)	Suw (H)	Will (H)	NWA (L)	Parn (LL)	Hua (LL)
SiO <sub>2</sub>	41.11	40.79	41.76	40.80	41.10	58.00	63.73	55.05	59.80	62.61
TiO <sub>2</sub>	0.03	0.01	0.02	0.01	0.03	0.37	0.50	0.56	0.49	0.49
Al <sub>2</sub> O <sub>3</sub>	0.14	0.08	0.10	0.04	0.13	20.21	16.37	19.84	17.78	20.06
Cr <sub>2</sub> O <sub>3</sub>	0.08	0.07	0.39	0.05	0.09	0.33	0.32	0.37	0.43	0.39
FeO	4.52	7.76	3.75	7.61	8.77	2.44	4.83	3.02	2.86	3.84
MnO	0.07	0.28	0.21	0.29	0.23	0.20	0.25	0.34	0.36	0.06
NiO	0.01	0.02	0.03	0.01	0.06	0.05	0.05	0.18	0.05	0.21
MgO	53.90	51.04	54.25	50.16	50.12	4.63	3.34	4.94	4.33	2.87
CaO	0.34	0.12	0.21	0.11	0.23	8.86	3.20	11.73	6.65	2.24
Na <sub>2</sub> O	0.01	0.01	0.03	0.01	0.03	5.61	7.17	3.60	6.91	7.40
Total	100.23	100.18	100.77	99.09	100.75	100.71	99.76	99.64	99.65	100.17

Mineral	<b>low-Ca pyroxene</b>					<b>high-Ca pyroxene</b>				
Sample	Suw (H)	Will (H)	NWA (L)	Parn (LL)	Hua (LL)	Suw (H)	Will (H)	NWA (L)	Parn (LL)	Hua (LL)
SiO <sub>2</sub>	57.86	56.84	58.50	57.85	57.77	52.97	53.10	52.51	51.59	52.07
TiO <sub>2</sub>	0.09	0.10	0.10	0.05	0.13	0.55	0.37	0.79	0.72	0.87
Al <sub>2</sub> O <sub>3</sub>	0.72	0.80	0.68	0.46	0.97	3.64	3.10	4.87	5.65	9.88
Cr <sub>2</sub> O <sub>3</sub>	0.45	0.59	0.63	0.46	0.57	1.88	1.56	1.75	1.69	0.70
FeO	5.25	5.17	2.83	4.42	4.41	4.88	5.86	3.03	3.45	3.59
MnO	0.27	0.32	0.29	0.30	0.26	1.04	1.15	0.78	0.92	0.22
NiO	0.04	0.02	0.05	0.02	0.08	0.10	0.02	0.07	0.06	0.16
MgO	35.37	34.96	37.02	34.85	35.67	20.22	18.53	19.90	18.28	15.79
CaO	0.42	0.67	0.59	0.42	0.59	14.15	14.54	16.36	16.66	15.95
Na <sub>2</sub> O	0.12	0.11	0.05	0.10	0.14	0.58	0.64	0.25	0.46	1.31
Total	100.61	99.59	100.72	98.92	100.58	100.00	98.87	100.30	99.48	100.55

\*For type I chondrule olivines only average core compositions are tabulated. Olivines are often compositionally zoned and can contain up to 25 wt.% FeO at their rims.

In most of the zoned chondrules, the low-Ca pyroxenes of the rim poikilitically enclose olivine grains. We use a 4-step qualitative scheme to discriminate non-poikilitic rims versus weakly (Fig. 2.1a), medium (Fig. 2.1b, c) and strongly poikilitic rims (Fig. 2.1d). In total, about 5% of the zoned chondrules have non-poikilitic rims; 20% have weakly poikilitic rims; 47% have medium and 28% have strongly poikilitic rims. This distribution is similar to the distribution of poikilitic rims in carbonaceous and Rumuruti chondrites reported by Friend et al. (2016).

### 2.3.2. *Unzoned chondrules*

Unzoned chondrules lack mineralogical zonation by definition and have large variations of textural appearance (Fig. 2.4). The low-Ca pyroxene minerals in unzoned chondrules are not restricted to the chondrule borders, but can be randomly distributed in the whole chondrule, often intermingled with olivine and mesostasis. As shown in Table 2.2 and Fig. 2.3b, unzoned chondrules are predominantly, but not only, type II chondrules. In Fig. 2.4a, the chondrule contains skeletal olivine. The olivine appears in the chondrule centre, but also rims the entire chondrule. This texture, as well as inverse chondrule zonation with pyroxene in the core and olivine at the rim, was found in only five chondrules. The chondrules in Fig. 2.4b & c are composed of mesostasis with almost only olivine or only low-Ca pyroxene. The type I PP chondrule in Fig. 2.4d shows tiny amounts of poikilitically enclosed olivine in its centre. Abundant matrix material and some metal grains fill the space between individual low-Ca pyroxene crystals.

Apart from their textures and with a few exceptions, unzoned chondrules also share many characteristics with zoned chondrules, e.g. their average sizes and mineralogy. Chondrules that are exceptionally larger than the average chondrule in a meteorite section (e.g. macrochondrules) are, however, always unzoned.

### 2.3.3. *Bulk chondrule compositions*

We determined the silicate-only bulk compositions of 127 chondrules in H (35), L (50) and LL (42) chondrites. Major element (Mg, Si, Fe) and minor refractory element (Ca, Al, Ti) contents are highly variable in chondrules of all ordinary chondrite groups (Fig. 2.5). The chondrule Mg concentrations range from 13 to 23 wt.% in H and 12 to 26 wt.% in LL chondrites, while Fe varies between 2 and 13 wt.% in H and LL chondrites. Magnesium concentrations of L chondrite chondrules are higher than in the other groups and range from 14 up to 32 wt.%. The Fe concentrations are significantly lower in the L chondrite, with a peak below 1 wt.%, but

then spread to 12 wt.%. Bulk chondrule Si concentrations range from 20 to 27 wt.% in all ordinary chondrite groups. Bulk chondrule concentrations of the refractory minor elements Ca, Al and Ti are displayed in Fig. 2.5 (d, e, f). The average Ca concentration is controlled by the abundance of high-Ca pyroxene and mesostasis and ranges from 0.3 to 3.5 wt.%, but can in some cases be as high as 5.0 wt.%. The average Al concentrations depend on the abundance of mesostasis and vary from 0.3 to 1.5 wt.%. However, some chondrules contain up to 4.8 wt.% Al. Titanium contents are generally low, between 200 and 1000 wt.-ppm, with a few outliers of up to 1800 wt.-ppm. We note, that Fig. 2.5 contains samples of different petrologic types. The bulk chondrule elemental variance decreases with increasing petrologic type, but never increases. Thus, including chondrites of different petrologic types does not change our conclusion that bulk chondrule element contents are highly variable in OC. The average bulk compositions of porphyritic chondrules (type I/II) are listed in Table 2.4. Type II chondrules have higher Fe and lower (covariant) Mg contents.

**Table 2.4:** Average bulk chondrule compositions (wt.%) of the various ordinary chondrites.

Sample	Type I*					Type II				
	Suw (H3.8)	Will (H3.6)	NWA (L3.0)	Parn (LL3.6)	Hua (LL3)	Suw (H3.8)	Will (H3.6)	NWA (L3.0)	Parn (LL3.6)	Hua (LL3)
SiO <sub>2</sub>	54.64	52.87	50.40	52.87	46.40	51.92	50.36	48.23	50.94	52.73
TiO <sub>2</sub>	0.12	0.13	0.13	0.11	0.12	0.09	0.14	0.10	0.09	0.10
Al <sub>2</sub> O <sub>3</sub>	2.55	2.39	1.92	2.01	2.08	2.12	2.80	1.27	2.27	1.67
Cr <sub>2</sub> O <sub>3</sub>	0.43	0.53	0.56	0.43	0.23	0.37	0.31	0.58	0.48	0.51
FeO	6.17	7.07	3.20	8.04	11.16	10.45	11.73	11.90	12.93	8.22
MnO	0.35	0.46	0.26	0.37	0.22	0.48	0.39	0.29	0.47	0.37
NiO	0.05	0.02	0.05	0.03	0.08	0.06	0.03	0.03	0.02	0.09
MgO	33.82	32.68	41.89	32.82	38.85	32.79	30.06	36.35	29.31	34.57
CaO	1.72	2.37	1.91	1.75	1.09	1.61	2.68	1.52	2.02	1.85
Na <sub>2</sub> O	0.95	0.96	0.31	0.74	0.68	1.07	1.37	0.33	0.95	0.59
Total	100.79	99.46	100.62	99.16	100.91	100.94	99.86	100.61	99.50	100.71

Only the silicate portion of the chondrules were used to determine the bulk chondrule compositions. \*Type I chondrules: Average bulk chondrule compositions containing olivine forsteritic cores, as well as fayalite-rich rims.

The large range of chondrule Mg and Si concentrations is shown in Fig. 2.6. The bulk chondrule compositions (excluding metal and sulphides) fall between the Mg-rich endmembers of olivine and pyroxene. It is striking that bulk chondrule compositions of zoned and unzoned chondrules are basically identical in the Mg-Si plot. The NWA8276 (L) bulk chondrule compositions plot slightly off the LL and H chondrite chondrule compositions due to their higher Mg concentrations. NWA8276 is the lowest petrologic grade chondrite in this study. The bulk chondrule compositions taken from petrologic type 3.6 and 3.8 samples were affected by Fe-Mg exchange during thermal metamorphism. This shifts chondrules along the solid solution lines towards Fe-rich endmembers (Fig. 2.6). In consequence, this might have reduced the

initial spread in the Mg-Si plot but could not have enhanced it. Thus, the initial compositional spread of these chondrules could have only been larger.

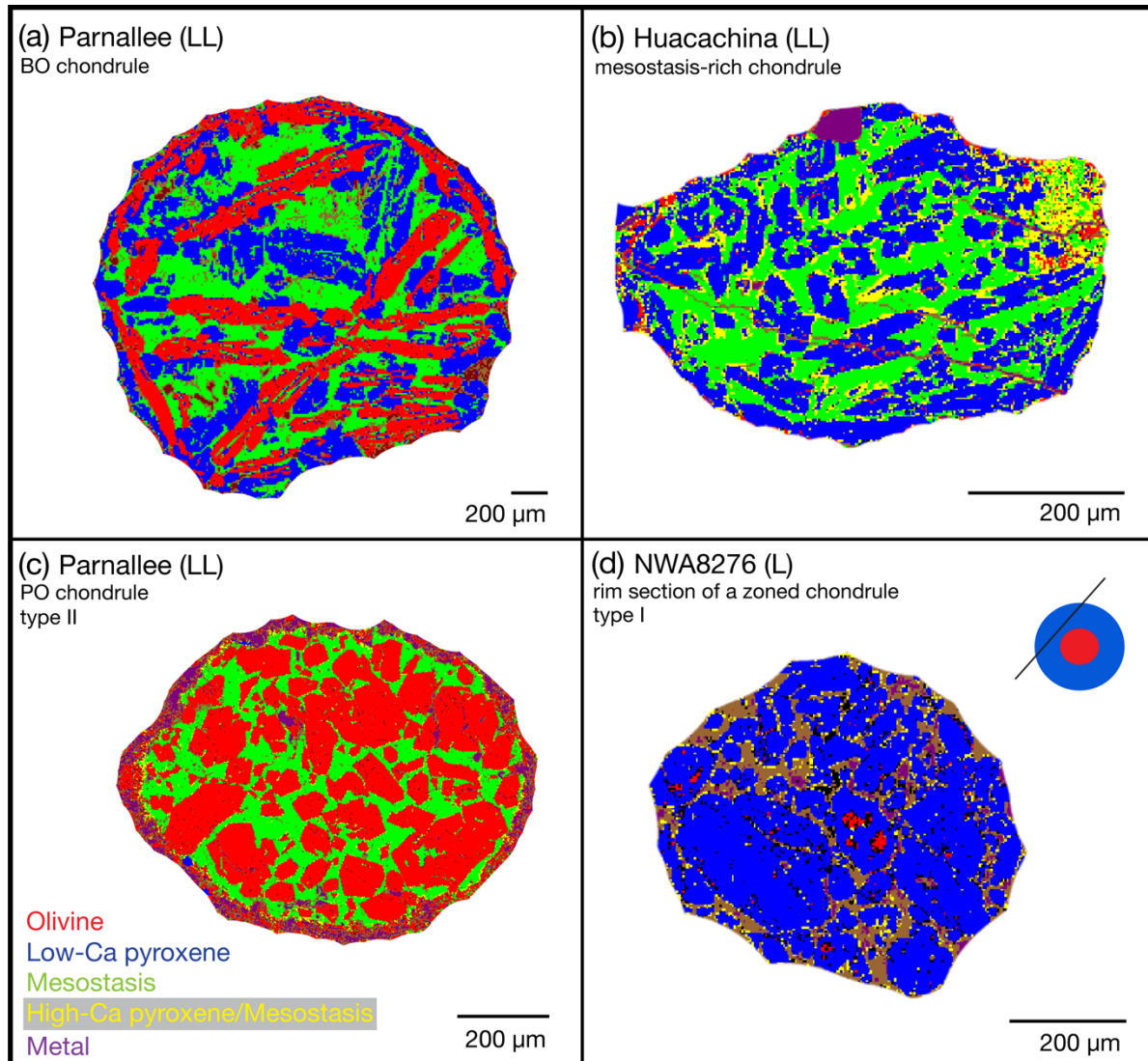


**Fig. 2.4:** Examples of typical unzoned chondrule types in the various ordinary chondrites. Phase maps from the PHAPS program show: (a) Unzoned chondrule with an olivine-rich rim. The mineral phases have a skeletal or elongated morphology and are randomly distributed in the chondrule. (b) A mesostasis-rich, unzoned chondrule with a very low abundance of olivine. (c) PO chondrule that is missing low-Ca pyroxene. (d) The appearance of tiny olivine grains in the centre of this PP chondrule and the high abundance of matrix material in it indicates that this is most likely a rim section of a zoned chondrule. As indicated in Section 2.4.1, this chondrule, as well as similar chondrule rim sections, are not included in the conservative count of zoned chondrules.

Literature data for ordinary chondrite bulk chondrule compositions taken from ChondriteDB (Hezel et al., 2018a) are provided for comparison. All chondrules studied are slightly shifted to higher Mg- and Si-concentrations than bulk OC chondrule compositions from the ChondriteDB database. Most bulk chondrule data in the ChondriteDB were obtained including all chondrule phases, i.e., silicates as well as the opaque phases metal and sulphides. In this

study, however, we used only the chondrule silicates to calculate the bulk chondrule compositions. If opaque phases were included in the bulk chondrule composition, their Mg- and Si- concentrations would be relatively lower. To test this, we calculated bulk chondrule compositions with their respective opaque phase abundances taken from the phase maps. Then, more than 90% of the chondrules studied plot in the field of the ChondriteDB data. Hence, the bulk chondrule compositions studied are in excellent agreement with the bulk chondrule compositions from the literature.

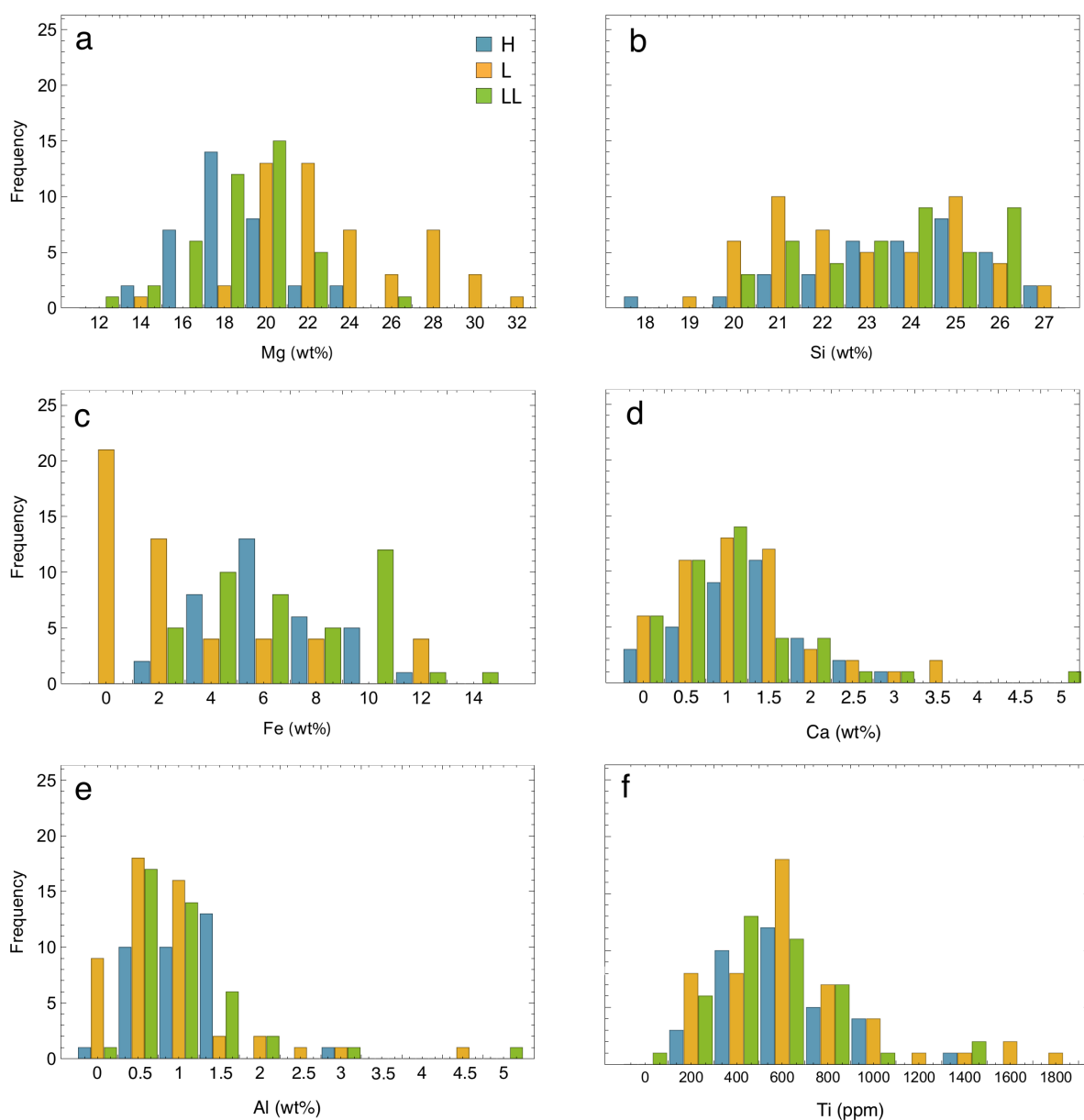


**Fig. 2.5:** Distributions of (silicate-only) bulk chondrule element concentrations in H, L, and LL chondrites.

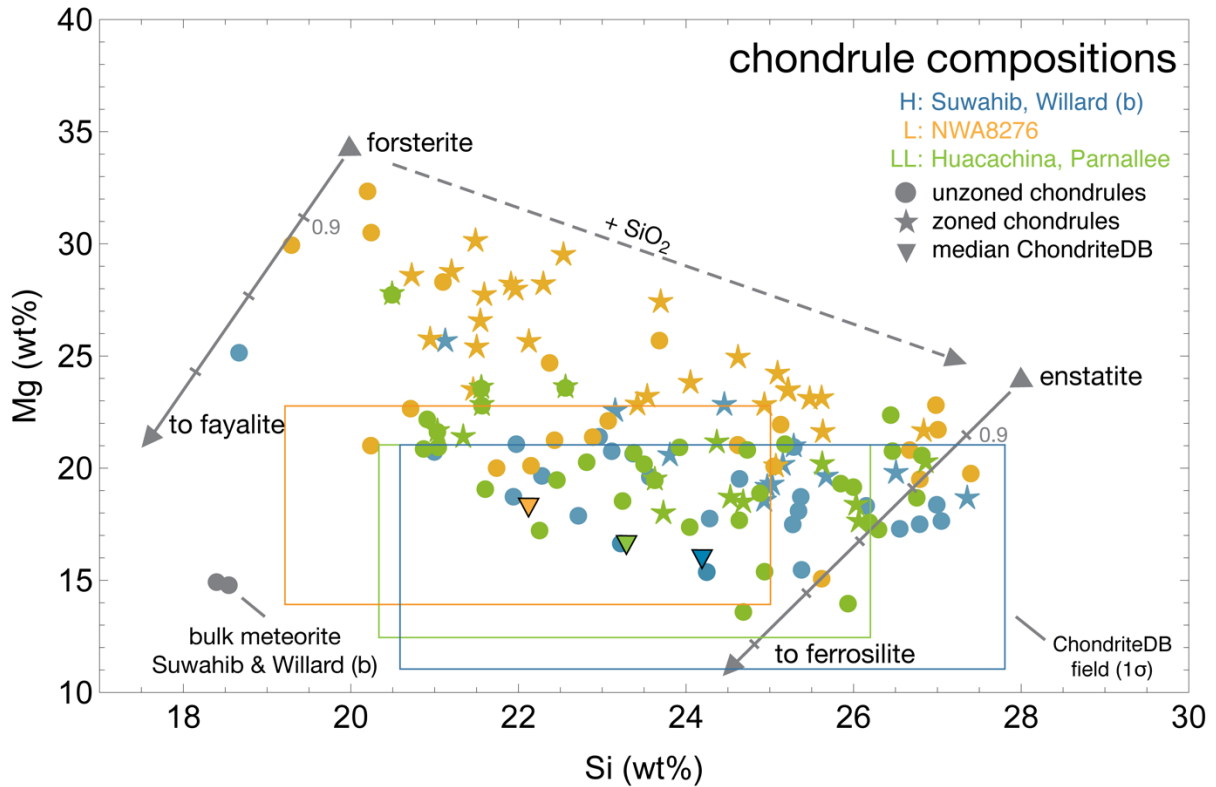


**Fig. 2.6:** Silicate-only bulk chondrule Mg and Si concentrations in H, L and LL chondrites, compared to bulk chondrule compositions obtained from the ChondriteDB database (Hezel et al., 2018a). Almost all chondrules would plot within the field of the literature bulk chondrule data, if chondrule metal was included when determining the bulk chondrule compositions of this study.

## 2.4. Discussion

### 2.4.1. 2D sectioning effects

A 2D section of a meteorite sample sections all chondrules randomly. The fraction of zoned chondrules might depend on whether the chondrules were sectioned close to their rims or close to their equators. Each section would produce a different 2D appearance of a zoned chondrule, but also of every other chondrule type. For example, the chondrule in Fig. 2.1c has a much thicker rim compared to the chondrules in Figs. 2.1a & b. The simplest explanation is that the apparent 2D rim thickness gradually increases towards the chondrule border and that chondrule c was sectioned closer to its border. In Fig. 2.1d, low-Ca pyroxene appears at the border, but also scattered throughout the entire chondrule, and is in all cases strongly poikilitic. This appearance could indicate a section similar to chondrule c, or even closer to its border. The low-Ca pyroxene at the centre of the chondrule in Fig. 2.1d would then also be rim pyroxene. A more extreme case of a potential rim section is the PP chondrule displayed in Fig. 2.4d. This chondrule contains olivine grains in the centre, but also substantial matrix material in-between the grains (brown parts in Fig. 2.4d). The matrix material intermingled with the low-Ca

pyroxenes could indicate that this chondrule was indeed sectioned very close to its border. Therefore, it is likely a zoned chondrule, but was sectioned through its low-Ca pyroxene rim. Up to 11% of all chondrules in LL chondrites and approximately 9% in L as well as H chondrites display this type of potential rim sectioning. All these were not included in the initial count of zoned chondrules. If these chondrules were indeed zoned chondrules, it would increase the total portion of zoned chondrules in ordinary chondrites to ~50%. Although this estimate is very reasonable, we will hereafter only refer to the conservative count of ~40% zoned chondrules.

It is further possible that some chondrules are only partially rimmed by low-Ca pyroxene. Not all sections of a partially rimmed chondrule would then display a low-Ca pyroxene rim. This might particularly be the case for large chondrules.

### *2.4.2. Phase map techniques (IM vs LAM)*

Chondrule phase maps were produced from either individual chondrules maps (IM), or large area maps (LAM; cf. Section 2.2). In NWA8276, the fraction of zoned chondrules was determined with both techniques, each producing a slightly but significantly different result: The fraction of zoned chondrules was lower when determined using LAM (43%), compared to when using IM (52%). The difference between the IM and LAM method is that LAM includes all chondrules in a meteorite section, whereas IM represents a random chondrule selection from the sample. Using IM, the fraction of zoned chondrules might be overestimated (by max. 10 percentage points, as demonstrated above), because particular chondrule appearances may have been inadvertently preferred. On the other hand, the fraction of zoned chondrules might be underestimated using LAM, since the lower resolution of the phase maps prevents the identification of chondrules with only a thin low-Ca pyroxene rim. The true fraction of zoned chondrules most likely lies between the IM and LAM results.

The different results when using IM or LAM might also explain why we determined small differences in zoned chondrule abundances among chondrites from of the same group. In Semarkona (LL), we determined a zoned chondrule abundance of 31% using LAM, but in Huacachina (LL) and Parnallee (LL) we determined abundances of 36% and 38%, respectively, using IM. It is reasonable to assume that in this case these differences more likely represent variations among the various chondrites, as similar variations are observed in H chondrites.

#### 2.4.3. Variation in type I/II fractions of porphyritic chondrules

Type I and II chondrules were classified according to the protocol given in Section 2.3. Our determined type I/II chondrule fractions of 46% type I chondrules in Willard b and 53% in Suwahib (H, petrologic types 3.6 and 3.8) are similar to literature data of Zanda et al. (2006), who reported a similar fraction of ~55% type I chondrules in unequilibrated H chondrites. However, in LL chondrites, Zanda et al. (2006) observed significantly fewer type I chondrules (25%), compared to the 70% we determined in Parnallee (LL3.6) and the 40% in Huacachina (LL3). According to McCoy et al. (1991) and Jones (1996a), minor effects of metamorphism can be observed in Parnallee pyroxenes. If pyroxene compositions in Parnallee were affected significantly by Fe-Mg equilibration, the pyroxene Fe contents would have increased. Then, we would have wrongfully classified type I chondrules as type II. This is clearly not the case as we determined a much higher type I fraction in Parnallee than Zanda et al. (2006) and, furthermore, a higher type I fraction compared to the lower petrologic type sample Huacachina. In addition, the high abundance of mineralogically zoned type I chondrules in Huacachina and Parnallee might indicate that type I chondrules are indeed very abundant in both samples.

It is important to note that neither increasing petrologic type, nor any other known parent body process, produces (see Section 2.4.4) or erases mineralogical chondrule zonation below the onset of textural equilibration due to thermal metamorphism at petrologic type ~3.6. Only minor textural changes occur until petrologic type 5 (Huss et al., 2006).

#### 2.4.4. Formation of low-Ca pyroxene rims

Mineralogical zonation is a typical chondrule appearance in ordinary chondrites. We examine three possible hypotheses for the formation of low-Ca pyroxene rims.

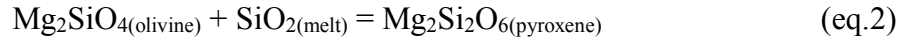
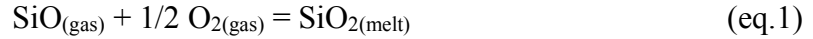
(i) *Crystallisation during chondrule cooling*: Assuming a simple chondrule formation scenario in which molten silicate droplets were surrounded by relatively cool gas, the droplets would have likely cooled from their border to their centre. Olivine, the first mineral to crystallise, should then dominate the chondrule margins. Pyroxene, which crystallises at lower temperatures, should have been concentrated in the centre. However, the opposite is observed: olivine is located in the core and pyroxene at the rim. This simple cooling and crystallisation from a melt, therefore, cannot have produced the observed textures. Experimental attempts to reproduce chondrule textures without gas-melt exchange also have never produced mineralogically zoned chondrules (e.g. Connolly and Hewins, 1996; Hewins et al., 2005).

(ii) *Parent body processes*: All studied chondrules are hosted in unequilibrated meteorites that did not experience extensive metamorphism or alteration on their parent bodies. Nevertheless, chemical equilibration occurred in samples of higher petrologic types (e.g. Suwahib H3.8). The formation of zoned chondrules on the chondrite parent bodies via the metamorphic reaction  $\text{olivine} + \text{SiO}_2 = \text{pyroxene}$  is highly unlikely. It would have required olivine chondrules surrounded by quartz-rich matrix, which is not observed in unequilibrated chondrites. It would also have also required high temperatures and the transport of  $\text{SiO}_2$  to the olivine (Friend et al., 2016). Such conditions were never achieved on the parent bodies of these meteorites. Furthermore, there is no correlation between the abundance of zoned chondrules and increasing petrologic type (up to 3.8). On the contrary, the most pristine sample, NWA8276 (L3.00) with a peak metamorphic temperature below  $200^\circ\text{C}$  (Huss et al., 2006) even has the highest fraction of zoned chondrules (43–52%). Hence, parent body processes can be ruled out.

(iii) *Chondrule melt-gas interactions*: Gas-melt interaction under high  $\text{SiO}_{(\text{g})}$  partial pressures can explain major petrographic, chemical and isotopic characteristics of chondrules (Tissandier et al., 2002; Hezel et al., 2003, 2006; Krot et al., 2004; Libourel et al., 2006; Chaussidon et al., 2008; Harju et al., 2014; Marrocchi and Chaussidon, 2015). In high temperature experiments, Tissandier et al. (2002) exposed partially molten, chondrule-like samples to high  $\text{SiO}_{(\text{g})}$  partial pressures. Their experimental charges reproduced typical zoned chondrule textures: Olivines occur preferentially in the centres of the chondrules and are frequently poikilitically enclosed in pyroxenes. Elevated dust/gas ratios in the solar nebula are invoked by several authors to explain the presence of silicate liquids (e.g. Wood, 1963; Wood and Hashimoto, 1993; Ebel and Grossman, 2000; Tissandier et al., 2002; Cuzzi and Alexander, 2006; Libourel et al., 2006; Johansen et al., 2007; Alexander et al., 2008; Hezel et al., 2010, 2018c; Schrader et al., 2013; Marrocchi and Chaussidon, 2015; Tenner et al., 2015). Evaporation in a dust-rich environment of the solar nebula could have generated elevated gas pressures with  $\text{SiO}$  as a dominant species (Libourel et al., 2006; Javoy et al, 2012). As pointed out by Rubin (2017), gas-melt exchange might even occur in a regime of low  $\text{SiO}_{(\text{g})}$  partial pressures, if chondrules formed during multiple melting and cooling events.

Various authors have proposed that olivine and pyroxene in the same chondrule may have different formation histories (e.g. Tissandier et al., 2002; Hezel et al., 2003; Krot et al., 2004; Libourel et al., 2006; Chaussidon et al., 2008; Jacquet et al., 2012; Harju et al., 2014, Friend et al., 2016). On the basis of in-situ oxygen isotope measurements, Chaussidon et al. (2008) showed that in carbonaceous chondrites, chondrule core olivines and rim pyroxenes are not co-

magmatic and did not crystallise from the same melt. The authors proposed that 2/3 of the oxygen in the low-Ca pyroxene originated from partially dissolved precursor olivine, while 1/3 was added by the reaction with SiO from the surrounding gas via the reaction sequence:



This gas-melt exchange requires chondrules to behave as open systems during their formation (e.g. Chaussidon et al., 2008; Di Rocco and Pack, 2015; Marrocchi and Chaussidon, 2015). Subsequent studies, investigating chondrule trace element patterns and silicon isotopic compositions, agree with this scenario (Jacquet et al., 2012; Harju et al., 2014).

The evidence for gas-melt exchange based on O-isotopic differences between olivine and pyroxene reported by Chaussidon et al. (2008) might, however, only exist in a portion of the zoned chondrules. Subsequent studies on chondrules from all chondrite classes unanimously reported O-isotopic homogeneity of coexisting olivine and pyroxene (Kita et al., 2010; Rudraswami et al., 2011; Weisberg et al., 2011; Ushikubo et al., 2012; Tenner et al., 2013, 2015, 2017; Nagashima et al., 2015; Miller et al., 2017; Schrader et al., 2017; Hertwig et al., 2018; Chaumard et al., 2018). These authors concluded that olivine and pyroxene must be co-magmatic and crystallised from a melt with homogenous oxygen isotopic composition. Nevertheless, these studies collectively argue for open system behaviour during chondrule formation, involving interactions between chondrule melt and ambient gas. In continuation of these results, Marrocchi and Chaussidon (2015) modeled how the oxygen isotopic composition of chondrule minerals might be modified by chondrule melt interaction with the surrounding gas. Their model explains how oxygen isotopic homogeneity in chondrule olivine and rim pyroxene is achieved through gas-melt exchange. Both, homogenous and heterogeneous oxygen isotopic compositions in chondrule silicates can be the result of melt-gas interaction, depending on the degree of dust enrichment in the chondrule forming region and processes of isotopic re-equilibration. In particular, Marrocchi and Chaussidon (2015) estimated that at dust to gas ratios greater than ~10, chondrule olivine and pyroxene should have indistinguishable oxygen isotope ratios.

Chondrules were heated to above liquidus temperatures and rapidly cooled and crystallised afterwards in minutes to hours (e.g. Hewins et al., 2005). Di Rocco and Pack (2015) demonstrated experimentally that considerable exchange between chondrule melt and nebula

gas could have occurred. They calculated that 50 to 70% of the oxygen in a chondrule – depending on chondrule type – could have exchanged with oxygen from the ambient gas. Such a quantity is in good agreement with model predictions of the timescales of chondrule formation (e.g. Hewins and Connolly, 1996; Morris and Desch, 2010).

We propose that the zoned chondrule textures observed in ordinary chondrites result from melt-gas exchange during chondrule formation. Chondrule olivine cores, surrounded by poikilitic low-Ca pyroxene rims, are a common chondrule appearance and directly results from the reactions in eq. 1,2. Melt-gas exchange, furthermore, explains variable (silicate-only) bulk chondrule compositions observed in Figs. 2.5, 2.6. Their spread in the Mg-Si plot reflects varying extents of SiO addition to forsteritic chondrule melts. This scenario is in agreement with aforementioned authors, presenting textural, chemical and isotopic evidence for open system chondrule behaviour.

### *2.4.5. Formation of unzoned chondrules*

The fraction of ~40% zoned chondrules in ordinary chondrites is significantly smaller than the fraction of ~80% zoned chondrules reported in carbonaceous chondrites (Friend et al., 2016; Fig. 2.2). This was not necessarily expected, as bulk ordinary chondrites have higher bulk rock Si/Mg ratios than carbonaceous chondrites. Therefore, we expected more low-Ca pyroxene and more zoned chondrules. Yet, more than half of the OC chondrules are unzoned. These unzoned chondrules must have followed a different formation path than the zoned chondrules.

Some authors report abundant low-Ca pyroxene rims around type I, but not type II chondrules (e.g. Scott and Taylor, 1983). Our study confirms these observations, e.g. ~75% of the type I chondrules in Suwahib and Huacachina are zoned (Fig. 2.3b, Table 2.2). Type II chondrules are also mineralogically zoned, but less frequently. The fractions of type II zoned chondrules determined in this study (up to ~35%) are in good agreement with the fraction of 38% zoned type II chondrules in CC, as reported by Friend et al. (2016). Type II chondrules are significantly more abundant in OC compared to CC, consistent with the total fractions of zoned chondrules in OC being lower.

In the previous section, we explained the formation of zoned chondrules by gas-melt interaction between olivine and SiO-rich gas (eqs. 1, 2). As apparently unzoned chondrules have no pyroxene rims, it seems obvious to assume that unzoned chondrules escaped any gas-melt interaction. However, this is unlikely for various reasons: (i) the straightforward explanation

for preventing gas-melt interaction would be a limited supply of  $\text{SiO}_{(g)}$ , allowing only a fraction of the molten chondrules to exchange material with the gas. In this scenario, unzoned chondrules would form at a time when  $\text{SiO}_{(g)}$  was almost entirely consumed. At this point in time, the gas might be generally depleted in condensable elements, including volatile elements such as Na. Such low concentrations of volatiles in the gas might entail evaporation of e.g. Na at the time when unzoned chondrules form. However, the observed alkali contents in the mesostasis of zoned and unzoned chondrules are identical. This does not support the idea that unzoned chondrules formed in a gas with low partial pressures of SiO, Na, and so on. Hence,  $\text{SiO}_{(g)}$  was most likely present in the gas when unzoned chondrules formed, which might then also have been added to the unzoned chondrules. (ii) Secondly, unzoned chondrules probably also interacted with the gas and did not behave as closed systems. We explained above the variable (silicate-only) bulk compositions of zoned chondrules resulting from the addition of SiO from the surrounding gas. If this did not happen to unzoned chondrules, they should have retained their initial bulk compositions and their compositional variability would have to be explained differently. In the Mg vs. Si plot (Fig. 2.6), unzoned chondrules cover the same space as zoned chondrules. Therefore, it seems unlikely that separate explanations for bulk compositional variations in zoned and unzoned chondrules are required. Rather, chondrules that appear to be unzoned also received SiO from the surrounding gas. We suggest two processes to explain the absence of pyroxene rims around unzoned chondrules, and, at the same time, explain the formation of both zoned and unzoned chondrules.

Type I and II chondrules likely formed in close spatial proximity (e.g. Berlin, 2009; Villeneuve et al., 2015), but at different times as demonstrated by Kurahashi et al. (2008) in CO chondrites. They found a formation gap of up to 1 Ma between type I and type II chondrules. If this is true, and also applies to OC chondrules, we suggest the following scenario: Type I chondrules formed early from ol-rich material in a reducing environment and interacted substantially with the surrounding gas, thereby becoming more  $\text{SiO}_2$ -rich and producing low-Ca pyroxene rims. Chondrule formation and gas-melt exchange continued for 1 Ma in a progressively more oxidising reservoir, now mostly forming ol-rich type II chondrules. These chondrules also interacted with the gas, becoming more  $\text{SiO}_2$ -rich and likely developing pyroxene rims. Then, a portion of the chondrules remelted during subsequent heating events, thereby losing their initial zonation. The much more  $\text{SiO}_2$ -rich chondrule melt compositions crystallised olivine and pyroxene throughout the chondrules and prevented further formation of low-Ca pyroxene rims around these chondrules. Zoned and unzoned chondrules are then indistinguishable in

their bulk compositions and cover similar spaces in the Mg-Si plot (Fig. 2.6). As Fe-rich silicates melt at lower temperatures (e.g. forsterite:  $\sim 1900^{\circ}\text{C}$ , fayalite:  $\sim 1200^{\circ}\text{C}$ ; at atmospheric pressure), remelting might have primarily affected type II chondrules, explaining the large fraction of unzoned type II chondrules. This model is consistent with numerous studies presenting evidence for multiple melting events of chondrules (e.g. Wasson, 1993; Alexander, 1994; Rubin and Krot, 1996; Jones et al., 1996b, 2005; Hezel et al., 2003; Wasson and Rubin, 2003; Rubin, 2006, 2010; Ebel et al., 2008), as well as the conclusions of Hezel and Palme (2007) that chondrules were reheated no more than 2–3 times.

### 2.5. Conclusions

Mineralogical zonation (olivine-rich cores, Ca-poor pyroxene-rich rims) is a typical chondrule texture in ordinary chondrites. Previous work has found even more abundant mineralogically zoned chondrules in carbonaceous and Rumuruti chondrites. However, zoned chondrules are significantly less abundant in ordinary ( $\sim 40\%$  of all chondrules) than in carbonaceous chondrites ( $\sim 80\%$ , Friend et al., 2016). The occurrence of two dominant chondrule textures in OC, i.e., zoned and unzoned (i.e. lacking a pyroxene-rich rim) chondrules, is, therefore, a distinctive characteristic of ordinary chondrites. The majority of type I chondrules in OC are zoned, while type II chondrules are largely unzoned. The significantly higher fraction of type II chondrules in OC compared to CC explains their lower total fraction of zoned chondrules.

The abundant occurrence of zoned chondrules in all types of chondrites must represent a dominant process during chondrule formation. We propose the following scenario: Chondrule precursor aggregates were comparatively rich in forsteritic olivine. Chondrule formation started when the precursor aggregates melted during brief high-temperature events. Olivine formed the chondrule cores. This olivine reacted with the SiO from the surrounding gas to form Ca-poor pyroxene. Only minimal amounts of silica diffused deep into the chondrule melts, as Si is a network-forming element in silicate melts (Libourel et al., 2006). The reaction stopped, i.e. was no longer possible as soon as the low-Ca pyroxene rim completely enclosed the chondrule preventing further gas-melt interaction. This scenario is consistent with numerous related studies on chondrules from various groups, as well as experiments on open system interaction between chondrules and gas (e.g. Tissandier et al., 2002; Grossman et al., 2002; Hezel et al., 2003; Krot et al., 2004; Libourel et al., 2006; Chaussidon et al., 2008; Hezel and Palme, 2010; Jacquet et al., 2012; Harju et al., 2014; Di Rocco and Pack, 2015; Marrocchi and Chaussidon, 2015; Friend et al., 2016; Soulié et al., 2017). This open system scenario is,

furthermore, in agreement with the findings of complementarity in major and minor element distributions between chondrules and matrix in carbonaceous and Rumuruti chondrites (e.g., Hezel and Palme, 2010; Palme et al., 2015; Becker et al., 2015; Ebel et al., 2016; Friend et al., 2017; Hezel et al., 2018b). Chondrule-matrix complementarities have not yet been unequivocally identified in ordinary chondrites.

All (silicate-only) bulk chondrule compositions plot between forsteritic olivine and enstatitic pyroxene in a Mg-Si plot (Fig. 2.6), which likely reflects varying extents of SiO addition to initially olivine-rich chondrules (cf. Libourel et al., 2006; Hezel et al., 2006). Zoned and unzoned chondrules cannot be discriminated based on their bulk compositions, i.e., they overlap in their bulk compositional ranges. It seems, therefore, likely that gaseous SiO was added to almost all chondrule melts and the majority of chondrules might have initially formed low-Ca pyroxene rims. The unzoned chondrules might then have formed when a portion of the initially zoned chondrules were remelted, thereby also melting and homogenising their low-Ca pyroxene rims into the bulk chondrule. As Fe-bearing silicates melt at lower temperatures, remelting might have primarily affected type II chondrules. This would imply that unzoned chondrules formed after zoned chondrules. A systematic study of chondrule ages that extends the results of Kurahashi et al. (2008) to zoned and unzoned chondrules could, therefore, prove or disprove this scenario.

## **Acknowledgements**

We thank Hanna Cieszynski for her assistance in operating the SEM. We are grateful for the loan of the thin sections Huacachina, Parnallee, Suwahib and Willard (b) from the Natural History Museum, London. Two students, Sara-Jane Lindlahr and Tim Krause, contributed to this work. We gratefully acknowledge the funding of this study by the Deutsche Forschungsgemeinschaft (DFG) grants HE 5352/10-1 and PA 346/50-1, as well as NASA Emerging Worlds grant NNX16AD37G (DE). We thank R. H. Hewins, G. Libourel and T. J. Tenner for their thorough and helpful reviews and GCA associate editor R. H. Jones for her work.

## **Supplementary Material**

Supplementary data to this article can be found at the end of this chapter or online at <https://doi.org/10.1016/j.gca.2019.01.018>

## References

- Alexander C. M. O'D. (1994) Chondrules from chondrules? An ion probe trace element study. *Lunar Planet. Sci.* **25**, 7–8.
- Alexander C. M. O'D., Grossman J. N., Ebel D. S. and Ciesla F. J. (2008) The formation conditions of chondrules and chondrites. *Science* **320**, 1617–1619.
- Becker M., Hezel D.C., Schulz T., Elfers B-M. and Münker C. (2015) The age of CV chondrites from component specific Hf-W systematics. *Earth Planet. Sci. Lett.* **432**, 472–482.
- Bence A. E. and Albee A. L. (1968) Empirical correction factors for the electron micro-analysis of silicates and oxides. *J. Geol.* **76**, 382–403.
- Berlin J., Jones R. H. and Brearley A. J. (2006) Determining the bulk chemical composition of chondrules by electron microprobe. *Lunar Planet. Sci. Conf.* **37**, #2370 (abstr.).
- Berlin J. (2009) Mineralogy and bulk chemistry of chondrules and matrix in petrologic type 3 chondrites: implications for early solar system processes. PhD thesis, University of New Mexico.
- Bouvier A., Gattacceca J., Agee C., Grossman J. and Metzler K. (2017) The Meteoritical Bulletin, No. 104. *Meteorit. Planet. Sci.* **1**.
- Burkhardt C., Gerber S., Budde G., Metzler K. and Kleine T. (2017) Mixing and transport of solids in the circumsolar disk as inferred from Ti isotope anomalies in planetary materials. GeoBremen 2017, #A357, (abstr.).
- Chaumard N., Defouilloy C. and Kita N. T. (2018) Oxygen isotope systematics of chondrules in the Murchison CM2 chondrite and implications for the CO-CM relationship. *Geochim. Cosmochim. Acta* **228**, 220–242.
- Chaussidon M., Libourel G. and Krot A. N. (2008) Oxygen isotopic constraints on the origin of magnesian chondrules and on the gaseous reservoirs in the early Solar System. *Geochim. Cosmochim. Acta* **72**, 1924–1938.
- Clayton R. N. (2005) Oxygen isotopes in meteorites. In *Chondrites and the Protoplanetary Disk*, vol. 341 (eds. A. N. Krot, E. R. D. Scott and B. Reipurth), 129–142.
- Connolly Jr. H. C. and Hewins, R. H. (1996) Constraints on chondrule precursors from experimental data. In *Chondrules and the Protoplanetary Disk* (eds. R. H. Hewins, R. H. Jones and E. R. D. Scott), 129–135.
- Cuzzi J. N. and Alexander C. M. O'D. (2006) Chondrule formation in particle-rich nebular regions at least hundreds of kilometres across. *Nature* **441**, 483–485.

- Desch S. J. and Connolly Jr. H. C. (2002) A model of the thermal processing of particles in solar nebula shocks: Application to the cooling rates of chondrules. *Meteorit. Planet. Sci.* **37**, 183–207.
- Di Rocco T. D. and Pack A. (2015) Triple oxygen isotope exchange between chondrule melt and water vapor: an experimental study. *Geochim. Cosmochim. Acta* **164**, 17–34.
- Ebel D. S. and Grossman L. (2000) Condensation in dust-enriched systems. *Geochim. Cosmochim. Acta* **64**, 339–366.
- Ebel D. S., Weisberg M. K., Hertz J. and Campbell A. J. (2008) Shape, metal abundance, chemistry, and origin of chondrules in the Renazzo (CR) chondrite. *Meteorit. Planet. Sci.* **43**, 1725–1740.
- Ebel D. S., Leftwich K., Brunner C. E. and Weisberg M. K. (2009) Abundance and size distribution of inclusions in CV3 chondrites by X-ray image analysis. *40th Lunar Planet. Sci. Conf.*, #2065, (abstr.).
- Ebel D. S., Brunner C., Konrad K., Leftwich K., Erb I., Lu M., Rodriguez H., Crapster-Pregont E. J., Friedrich J. M. and Weisberg M. K. (2016) Abundance, major element composition and size of components and matrix in CV, CO and Acfer 094 chondrites. *Geochim. et Cosmochim. Acta* **172**, 322–356.
- Friend P., Hezel D. C. and Mucerschi D. (2016) The conditions of chondrule formation, Part II: Open system. *Geochim. Cosmochim. Acta* **173**, 198–209.
- Friend P., Hezel D. C., Palme H., Bischoff A. and Gellissen M. (2017) Complementary element relationships between chondrules and matrix in Rumuruti chondrites. *Earth Planet. Sci. Lett.* **480**, 87–96.
- Grossman J. N. (1996) Zoning of mesostasis in FeO-poor Semarkona chondrules. *31th Meteorite Planet. Sci. Conf.*, A55, (abstr.).
- Grossman J. N., Alexander C. M. Ó'D., Wang J. and Brearley A. J. (2002) Zoned chondrules in Semarkona: Evidence for high- and low-temperature processing. *Meteorite Planet. Sci.* **37**, 49–73.
- Grossman J. N. and Brearley A. J. (2005) The onset of metamorphism in ordinary and carbonaceous chondrites. *Meteorit. Planet. Sci.* **40**, 87–122.
- Harju E. R., Kohl I. E., Rubin A. E. and Young E. D. (2014) Evaluating silicon condensation in type 1AB chondrules using in-situ silicon isotopes. *37th Lunar Planet. Sci. Conf.*, #2370, (abstr.).

- Hertwig A. T., Defouilloy C. and Kita N. T. (2018) Formation of chondrules in a moderately high dust enriched disk: Evidence from oxygen isotopes of chondrules from the Kaba CV3 chondrite. *Geochim. Cosmochim. Acta* **224**, 116–131.
- Hewins R. H. and Connolly Jr. H. C. (1996) Peak temperatures of flash melted chondrules. In *Chondrules and the Protoplanetary Disk* (eds. R. H. Hewins, R. H. Jones and E. R. D. Scott), 197–204.
- Hewins R. H., Connolly Jr. H. C., Lofgren G. E. and Libourel G. (2005) Experimental constraints on chondrule formation. In *Chondrites and the Protoplanetary Disk*, vol. 341 (eds. A. N. Krot, E. R. D. Scott and B. Reipurth), 286–316.
- Hewins R. H. and Zanda B. (2012) Chondrules: precursors and interactions with the nebular gas. *Meteorit. Planet. Sci.* **47**, 1120–1138.
- Hezel D. C., Palme H., Brenker F. E. and Nasdala L. (2003) Evidence for fractional condensation and reprocessing at high temperatures in CH-chondrites. *Meteorit. Planet. Sci.* **38**, 1199–1216.
- Hezel D. C., Palme H., Nasdala L. and Brenker F. E. (2006) Origin of SiO<sub>2</sub>-rich components in ordinary chondrites. *Geochim. Cosmochim. Acta* **70**, 1548–1564.
- Hezel D. C. (2007) A model for calculating the errors of 2D bulk analysis relative to the true 3D bulk composition of an object, with application to chondrules. *Comput. Geosci.* **33**, 1162–1175.
- Hezel D. C. and Palme H. (2007) The conditions of chondrule formation, Part I: closed system. *Geochim. Cosmochim. Acta* **71**, 4092–4107.
- Hezel D. C. (2010) A mathematica code to produce phase maps from two element maps. *Comput. Geosci.* **36**, 1097–1099.
- Hezel D. C., Needham A. W., Armytage R., Georg B., Abel R., Kurahashi E., Coles B. J., Rehkämper M. and Russell S. S. (2010) A nebula setting as the origin for bulk chondrule Fe isotope variations in CV chondrites. *Earth Planet. Sci. Lett.* **296**, 423–433.
- Hezel D. C. and Kießwetter R. (2010) Quantifying the error of 2D bulk chondrule analyses using a computer model to simulate chondrules (SIMCHON). *Meteorit. Planet. Sci.* **45**, 555–571.
- Hezel D. C. and Palme H. (2010) The chemical relationship between chondrules and matrix and the chondrule matrix complementarity. *Earth Planet. Sci. Lett.* **294**, 85–93.
- Hezel D. C., Harak M. and Libourel G. (2018a) What we know about elemental bulk chondrule and matrix compositions: Presenting the ChondriteDB Database. *Chemie der Erde* **78**, 1–14.

- Hezel D. C., Bland P. A., Palme H., Jacquet E. and Bigolski J. (2018b) Composition of chondrules and matrix and their complementary relationship in chondrites. In: *Chondrules: Records of Protoplanetary Disk Processes* (Cambridge Planetary Science). Eds: S. S. Russell, H. C. Connolly Jr. and A. N. Krot. Cambridge University Press, Cambridge UK, pp. 457.
- Hezel D. C., Wilden J. S., Becker D., Steinbach S., Wombacher F. and Harak M. (2018c) Fe isotope composition of bulk chondrules from Murchison (CM2): Constraints for parent body alteration, nebula processes and chondrule-matrix complementarity. *Earth Planet. Sc. Lett.* **490**, 31–39.
- Huss G. R., Rubin, A. E. and Grossman J. N. (2006) Thermal metamorphism in chondrites. In *Meteorites and the Early Solar System II*, vol. 1 (eds. D. S. Lauretta and H. Y. McSween), 567–586.
- Jacquet E., Alard O. and Gounelle M. (2012) Chondrule trace element geochemistry at the mineral scale. *Meteorit. Planet. Sci.* **47**, 1695–1714.
- Jacquet E. and Marrocchi Y. (2017) Chondrule heritage and thermal histories from trace element and oxygen isotope analyses of chondrules and amoeboid olivine aggregates. *Meteorit. Planet. Sci.* **52**, 2672–2694.
- Javoy M., Balan E., Méheut M., Blanchard M. and Lazzeri M. (2012) First-principles investigation of equilibrium isotopic fractionation of O- and Si-isotopes between refractory solids and gases in the solar nebula. *Earth Planet. Sc. Lett.* **319**, 118–127.
- Johansen A., Oishi J. S., Low M-M. M., Klahr H., Henning T. and Youdin A. (2007) Rapid planetesimal formation in turbulent circumstellar disks. *Nature* **448**, 1022–1025.
- Jones R. H. (1996a) FeO-rich, porphyritic pyroxene chondrules in unequilibrated ordinary chondrites. *Geochim. Cosmochim. Acta* **60**, 3115–3138.
- Jones R. H. (1996b) Relict grains in chondrules: Evidence for chondrule recycling. In *Chondrules and the Protoplanetary Disk* (eds. R. H. Hewins, R. H. Jones and E. R. D. Scott), 163–172.
- Jones R. H., Grossman J. N. and Rubin A. E. (2005) Chemical, mineralogical and isotopic properties of chondrules: clues to their origin. In *Chondrites and the Protoplanetary Disk*, vol. 341 (eds. Krot A. N., Scott E. R. D. and Reipurth B.), 251–285.
- Jones R. H. (2012) Petrographic constraints on the diversity of chondrule reservoirs in the protoplanetary disk. *Meteorit. Planet. Sci.* **47**, 1176–1190.
- Kita N. T., Nagahara H., Tachibana S., Tomomura S., Spicuzza M. J., Fournelle J. H. and Valley J. W. (2010) High precision SIMS oxygen isotope study of chondrules in LL3

- chondrites: Role of ambient gas during chondrule formation. *Geochim. Cosmochim. Acta* **74**, 6610–6635.
- Krot A. N., Libourel G., Goodrich C. and Petaev M. I. (2004) Silica-igneous rims around magnesian chondrules in CR carbonaceous chondrites: evidence for fractional condensation during chondrule formation. *Meteorit. Planet. Sci.* **39**, 1931–1955.
- Kurahashi E., Kita N. T., Nagahara H. and Morishita Y. (2008)  $^{26}\text{Al}$ – $^{26}\text{Mg}$  systematics of chondrules in a primitive CO chondrite. *Geochim. Cosmochim. Acta* **72**, 3865–3882.
- Lauretta D. S., Nagahara H. and Alexander C. M. O'D. (2006) Petrology and origin of ferromagnesian silicate chondrules. In *Meteorites and the Early Solar System II*, vol. 1 (eds. D. S. Lauretta and H. Y. McSween), 431–459.
- Libourel G., Krot A. N. and Tissandier L. (2006) Role of gas–melt interaction during chondrule formation. *Earth Planet. Sci. Lett.* **251**, 232–240.
- Lobo A., Wallace S. W. and Ebel D. S. (2014) Modal abundances, chemistry and sizes of clasts in the Semarkona (LL3.0) chondrite by X-ray map analysis. *45th Lunar Planet. Sci. Conf.*, #1423, (abstr.).
- Marrocchi Y. and Chaussidon M. (2015) A systematic for oxygen isotopic variations in meteoritic chondrules. *Earth Planet. Sci. Lett.* **430**, 308–315.
- McCoy T. J., Scott E. R. D., Jones R. H., Keil K. and Tylor J. G. (1991) Composition of chondrule silicates in LL3–5 chondrites and implications for their nebular history and parent body metamorphism. *Geochim. Cosmochim. Acta* **55**, 601–619.
- Miller K. E., Lauretta D. S., Connolly Jr. H. C., Berger E. L., Nagashima K. and Domanik K. (2017) Formation of unequilibrated R chondrite chondrules and opaque phases. *Geochim. Cosmochim. Acta* **209**, 24–50.
- Morris M. A. and Desch S. J. (2010) Thermal history of chondrules in solar nebula shocks. *Astrophys. J.* **722**, 1474–1494.
- Nagashima K., Krot A. N. and Huss G. R. (2015) Oxygen-isotope compositions of chondrule phenocrysts and matrix grains in Kakangari K-grouplet chondrite: Implication to a chondrule-matrix genetic relationship. *Geochim. Cosmochim. Acta* **151**, 49–67.
- Palme H., Hezel D. C. and Ebel D. S. (2015) The origin of chondrules: Constraints from matrix composition and matrix-chondrule complementarity. *Earth Planet. Sci. Lett.* **411**, 11–19.
- Rubin A. E. and Krot A. N. (1996) Multiple heating of chondrules. In *Chondrules and the Protoplanetary Disk* (eds. R. H. Hewins, R. H. Jones and E. R. D. Scott), Cambridge University Press, 173–180.

- Rubin A. E. (2006) A relict-grain-bearing porphyritic olivine compound chondrule from LL3.0 Semarkona that experienced limited remelting. *Meteorit. Planet. Sci.* **41**, 1027–1038.
- Rubin A. E. (2010) Physical properties of chondrules in different chondrite groups: Implications for multiple melting events in dusty environments. *Geochim. Cosmochim. Acta* **74**, 4807–4828.
- Rubin A. E. (2017) Type-1AB chondrules in LL3.0 Semarkona: No need for high partial pressures of SiO(g) in the solar nebula. *48th Lunar Planet. Sci. Conf.*, #2700, (abstr.).
- Rudraswami N. G., Ushikubo T., Nakashima D. and Kita N. T. (2011) Oxygen isotope systematics of chondrules in the Allende CV3 chondrite: High precision ion microprobe studies. *Geochim. Cosmochim. Acta* **75**, 7596–7611.
- Schrader D. L., Connolly Jr. H. C., Lauretta D. S., Nagashima K., Huss G. R., Davidson J. and Domanik K. J. (2013) The formation and alteration of the Renazzo-like carbonaceous chondrites II: Linking O-isotope composition and oxidation state of chondrule olivine. *Geochim. Cosmochim. Acta* **101**, 302–327.
- Schrader D. L., Nagashima K., Krot A. N., Oglione R. C., Yin Q. Z., Amelin Y., Stirling C. H. and Kaltenbach A. (2017) Distribution of <sup>26</sup>Al in the CR chondrite chondrule-forming region of the protoplanetary disk. *Geochim. Cosmochim. Acta* **201**, 275–302.
- Scott E. R. D. and Taylor G. J. (1983) Chondrules and other components in C, O, and E chondrites: Similarities in their properties and origins. *Journal of Geophysical Research: Solid Earth* **88**, B275–B286.
- Scott E. R. D., Love S. G. and Krot A. N. (1996) Formation of chondrules and chondrites in the protoplanetary nebula. In *Chondrules and the Protoplanetary Disk* (eds. R. H. Hewins, J. Jones and E. R. D. Scott), 45–55.
- Scott E. R. D. and Krot A. N. (2014) Chondrites and their components. In *Treatise on Geochemistry* 2<sup>nd</sup> ed. (eds. H. Holland and K. Turekian), 65–137.
- Sears D. W. G., Huang S. and Benoit P. H. (1996) Open-system behavior during chondrule formation. In *Chondrules and the Protoplanetary Disk* (eds. R. H. Hewins, J. Jones and E. R. D. Scott), 221–232.
- Soulié C., Libourel G. and Tissandier L. (2017) Olivine dissolution in molten silicates: An experimental study with application to chondrule formation. *Meteorit. Planet. Sci.* **52**, 225–250.
- Tenner T. J., Ushikubo T., Kurahashi E., Kita N. T. and Nagahara H. (2013) Oxygen isotope systematics of chondrule phenocrysts from the CO3.0 chondrite Yamato 81020:

- Evidence for two distinct oxygen isotope reservoirs. *Geochim. Cosmochim. Acta* **102**, 226–245.
- Tenner T. J., Nakashima D., Ushikubo T., Kita N. T. and Weisberg M. K. (2015) Oxygen isotope ratios of FeO-poor chondrules in CR3 chondrites: Influence of dust enrichment and H<sub>2</sub>O during chondrule formation. *Geochim. Cosmochim. Acta* **148**, 228–250.
- Tenner T. J., Kimura M. and Kita N. T. (2017) Oxygen isotope characteristics of chondrules from the Yamato-82094 ungrouped carbonaceous chondrite: Further evidence for common O-isotope environments samples among carbonaceous chondrites. *Meteorit. Planet. Sci.* **52**, 268–294.
- Tissandier L., Libourel G. and Robert F. (2002) Gas-melt interactions and their bearing on chondrule formation. *Meteorit. Planet. Sci.* **37**, 1377–1389.
- Ushikubo T., Kimura M., Kita N. T. and Valley J. W. (2012) Primordial oxygen isotope reservoirs of the solar nebula recorded in chondrules in Acfer 094 carbonaceous chondrite. *Geochim. Cosmochim. Acta* **90**, 242–264.
- Villeneuve J., Libourel G. and Soulié C. (2015) Relationships between type I and type II chondrules: Implications on chondrule formation processes. *Geochim. Cosmochim. Acta* **160**, 277–305.
- Walsh K. J., Morbidelli A., Raymond S. N., O'Brien D. P. and Mandell A. M. (2011) A low mass for Mars from Jupiter's early gas-driven migration. *Nature* **475**, 206–209.
- Warren P. H. (2011) Stable-isotope anomalies and the accretionary assemblage of the Earth and Mars: A subordinate role for carbonaceous chondrites. *Earth Planet. Sci. Lett.* **311**, 93–100.
- Wasson J. T. (1993) Constraints on chondrule origins. *Meteoritics* **28**, 14–28.
- Wasson J. T. and Rubin A. E. (2003) Ubiquitous low-FeO relict grains in type II chondrules and limited overgrowth on phenocrysts following the final melting event. *Geochim. Cosmochim. Acta* **67**, 2239–2250.
- Weisberg M. K., Ebel D. S., Connolly Jr. H. C., Kita N. T. and Ushikubo T. (2011) Petrology and oxygen isotope compositions of chondrules in E3 chondrites. *Geochim. Cosmochim. Acta* **75**, 6556–6569.
- Wood J. A. (1963) On the origin of chondrules and chondrites. *Icarus* **2**, 152–180.
- Wood J. A. and Hashimoto A. (1993) Mineral equilibrium in fractionated nebular systems. *Geochim. Cosmochim. Acta*, **57**, 2377–2388.

Zanda B., Hewins R. H., Bourot-Denise M., Bland P. A. and Albarède F. (2006) Formation of solar nebula reservoirs by mixing chondritic components. *Earth Planet. Sci. Lett.* **248**, 650–660.

## **Appendix**

(subsequent pages)

**Suwahib (Buwah) (H), BM.1931,428 (P.4030)**

Details				Texture										Bulk composition (wt.%)									
Chondrule	zoned	rim section	Type I*	Type II	Poikilitic	PO	PP	POP	other**	SiO2	TiO2	Al2O3	Cr2O3	FeO	MnO	NiO	MgO	CaO	Na2O	Sum			
Chd 01																							
Chd 02	x		x		medium			x															
Chd 03				x				x		52.71	0.11	3.33	0.37	8.74	0.43	0.00	32.50	1.85	1.75	101.79			
Chd 04				x				x															
Chd 05		x							RP														
Chd 06	x			x	medium			x															
Chd 07				x		x																	
Chd 08	x		x		medium			x															
Chd 09	x		x		weak			x															
Chd 10		x					x																
Chd 11				x		x																	
Chd 12			x				x																
Chd 13	x		x		medium			x															
Chd 14	x			x	weak			x		49.54	0.06	1.63	0.14	10.51	0.32	0.18	37.47	0.38	0.53	100.75			
Chd 15	x				medium			x	BO	53.42	0.09	1.79	0.35	9.72	0.50	0.04	31.86	1.85	0.83	100.44			
Chd 16	x			x	strong			x		50.93	0.08	1.11	0.38	11.39	0.52	0.15	34.19	1.47	0.55	100.78			
Chd 17	x		x		weak	x			C	45.20	0.12	1.71	0.22	8.85	0.28	0.04	42.63	1.22	0.40	100.66			
Chd 18		x																					
Chd 19			x					x															
Chd 20									BO														
Chd 21																							
Chd 22	x		x		medium		x																
Chd 23	x		x		weak	x																	
Chd 24				x				x															
Chd 25									C														
Chd 26								x															
Chd 27		x	x				x			57.75	0.18	2.81	0.61	5.43	0.45	0.05	30.59	2.82	0.80	101.47			
Chd 28		x	x				x			57.86	0.11	3.06	0.46	5.26	0.44	0.06	29.39	2.71	1.09	100.44			
Chd 29									RP														
Chd 30	x		x		strong			x		53.81	0.17	3.04	0.51	6.22	0.29	0.01	33.49	1.61	1.39	100.55			
Chd 31									BO														
Chd 32	x			x	medium			x															
Chd 33	x			x	weak			x		53.34	0.07	2.06	0.37	11.94	0.54	0.02	30.83	0.74	1.06	100.97			
Chd 34								x															
Chd 35				x				x		54.22	0.13	2.91	0.41	8.43	0.49	0.04	30.13	2.59	1.72	101.06			
Chd 36				x				x															
Chd 37	x		x		weak		x			56.70	0.08	2.80	0.27	5.32	0.28	0.02	32.88	0.50	1.22	100.08			
Chd 38	x		x		strong	x																	
Chd 39							x			54.27	0.08	2.47	0.28	9.06	0.42	0.07	31.17	1.47	1.12	100.41			
Chd 40				x				x		49.12	0.09	2.14	0.35	9.94	0.45	0.01	35.62	1.81	0.89	100.42			
Chd 42	x		x		weak			x		52.32	0.06	1.36	0.35	6.63	0.36	0.03	37.92	1.19	0.35	100.57			
Chd 43			x				x																
Chd 44									BO														
Chd 45	x		x		medium	x				51.95	0.10	1.80	0.56	12.93	0.61	0.05	29.57	2.63	1.07	101.27			
Chd 46				x				x															

continued Chondrule	Details		Texture				Bulk composition (wt.%)										Sum				
	zoned	rim section	Type I*	Type II	Poikilitic	PO	PP	POP	other**	SiO2	TiO2	Al2O3	Cr2O3	FeO	MnO	NiO		MgO	CaO	Na2O	
Chd 48	x		x		medium			x		54.92	0.12	2.84	0.58	7.37	0.40	0.11	32.62	1.24	1.21	101.41	
Chd 49	x		x		medium					58.52	0.14	2.81	0.46	4.27	0.30	0.06	31.01	2.44	1.12	101.12	
Chd 50	x			x	weak			x		53.54	0.09	1.95	0.35	9.69	0.45	0.03	32.02	1.38	1.00	100.51	
Chd 47				x				x													

**Willard (b) (H), BM. 1995, M5 (P15971)**

Chd 01									BO												
Chd 02	x				strong			x													
Chd 05	x				strong			x													
Chd 06	x				weak																
Chd 07								x													
Chd 08		x																			
Chd 09																					
Chd 10				x				x		51.87	0.09	5.63	0.17	10.15	0.33	0.02	25.60	3.54	2.67	100.06	
Chd 11	x		x		weak																
Chd 12	x		x		medium			x		54.09	0.09	1.62	0.56	6.06	0.36	0.02	34.85	1.50	0.60	99.75	
Chd 13				x						49.45	0.12	2.33	0.41	8.66	0.51	0.01	34.55	2.21	0.71	98.96	
Chd 14			x					x													
Chd 15	x		x		medium			x													
Chd 16									BO	39.93	0.11	0.53	0.22	17.14	0.47	0.02	41.82	0.05	0.18	100.49	
Chd 17				x						47.66	0.07	1.08	0.35	14.38	0.44	0.02	32.73	2.66	0.68	100.08	
Chd 18	x			x	weak			x													
Chd 19				x						56.80	0.11	1.70	0.18	10.18	0.41	0.07	28.81	1.77	0.61	100.64	
Chd 20				x						54.29	0.26	3.38	0.25	10.61	0.39	0.01	25.77	2.83	1.57	99.36	
Chd 21				x						46.94	0.12	3.57	0.28	12.76	0.36	0.03	31.18	2.96	2.20	100.40	
Chd 22									BO	48.59	0.15	2.23	0.23	12.99	0.40	0.03	29.77	4.77	1.09	100.24	
Chd 23									RP												
Chd 24				x				x		47.01	0.10	1.61	0.33	13.04	0.44	0.08	35.07	2.32	0.95	100.95	
Chd 25	x			x	strong			x													
Chd 26			x					x		50.42	0.15	2.97	0.48	9.87	0.37	0.01	32.65	2.16	0.89	99.95	
Chd 27			x					x		49.99	0.12	2.31	0.48	8.13	0.44	0.03	34.37	2.47	1.13	99.49	
Chd 28				x				x		49.68	0.18	3.36	0.48	11.31	0.37	0.01	27.76	4.19	1.62	98.95	
Chd 29				x						54.07	0.17	2.31	0.52	9.36	0.39	0.00	29.14	2.44	0.81	99.23	
Chd 30	x		x		medium			x													
Chd 32				x				x		44.92	0.13	2.53	0.19	13.74	0.42	0.05	34.49	1.40	1.18	99.04	
Chd 33																					
Chd 34																					
Chd 35	x			x	medium			x													
Chd 36			x							57.31	0.15	2.83	0.52	4.24	0.51	0.02	29.15	2.71	1.43	98.86	
Chd 37	x		x		weak			x													
Chd 38			x					x		55.94	0.14	2.25	0.72	5.48	0.56	0.02	30.51	3.14	1.01	99.75	
Chd 39		x																			
Chd 40		x																			
Chd 41				x																	
Chd 42	x			x	weak			x													

**NWA 8276 (L), Dominik Hezel**

Details				Texture				Bulk composition (wt.%)													
Chondrule	zoned	rims section	Type I*	Type II	Poikilitic	PO	PP	POP	other**	SiO2	TiO2	Al2O3	Cr2O3	FeO	MnO	NiO	MgO	CaO	Na2O	Sum	
Chd 01	x				weak				BO	50.10	0.30	5.21	0.49	0.70	0.12	0.01	37.95	4.44	0.31	99.63	
Chd 02	x		x		weak	x				46.09	0.28	4.33	0.32	0.83	0.08	0.07	44.11	3.93	0.45	100.49	
Chd 03	x		x		medium			x		48.21	0.11	0.47	0.42	1.47	0.11	0.04	49.01	0.79	0.03	100.66	
Chd 04	x		x		medium			x		48.21	0.11	0.47	0.42	1.47	0.11	0.04	49.01	0.79	0.03	100.66	
Chd 05	x		x		medium			x		50.70	0.13	1.62	0.43	0.88	0.13	0.02	45.52	1.23	0.12	100.77	
Chd 06			x					x		53.59	0.17	2.06	0.84	5.60	0.61	0.01	33.43	3.72	0.47	100.50	
Chd 07			x							43.21	0.06	0.65	0.30	1.67	0.09	0.02	53.76	0.62	0.09	100.46	
Chd 08			x			x				43.31	0.14	1.47	0.46	2.52	0.04	0.04	50.71	2.25	0.03	100.96	
Chd 09	x		x		weak	x				46.87	0.20	2.26	0.32	1.34	0.12	0.02	46.83	2.70	0.32	100.99	
Chd 10	x				no				BO	45.91	0.24	8.97	0.17	0.70	0.04	0.07	39.02	5.04	0.51	100.69	
Chd 11	x		x		no	x				45.97	0.09	1.61	0.30	0.91	0.06	0.02	50.03	1.42	0.18	100.59	
Chd 12				x			x														
Chd 13			x			x				45.14	0.12	2.03	0.46	1.89	0.10	0.03	47.06	1.75	0.64	99.21	
Chd 14	x		x		medium			x		47.33	0.13	2.09	0.62	4.23	0.23	0.13	42.58	2.27	0.48	100.09	
Chd 15	x			x	medium			x		46.00	0.06	1.14	0.82	8.97	0.13	0.06	42.17	1.25	0.02	100.62	
Chd 16	x		x		strong			x		53.34	0.12	2.40	0.72	2.61	0.43	0.01	37.91	2.82	0.29	100.67	
Chd 17	x		x		medium	x				46.99	0.11	3.29	0.33	0.87	0.08	0.04	46.44	2.03	0.17	100.35	
Chd 18				x						48.96	0.17	0.87	0.50	12.73	0.22	0.02	35.59	1.53	0.04	100.64	
Chd 19	x		x		medium	x															
Chd 20	x		x		strong			x		50.35	0.13	2.76	0.68	5.08	0.34	0.04	38.53	2.34	0.57	100.82	
Chd 21	x		x		weak	x				46.19	0.22	4.19	0.27	0.64	0.08	0.04	46.03	3.17	0.40	101.24	
Chd 22	x		x		no	x				45.36	0.14	2.19	0.35	2.67	0.10	0.06	47.75	1.99	0.11	100.72	
Chd 23				x						47.39	0.08	0.64	0.48	17.41	0.31	0.01	33.47	1.06	0.06	100.90	
Chd 24			x			x				41.27	0.04	0.14	0.29	9.07	0.22	0.05	49.79	0.30	0.06	101.23	
Chd 25		x					x			57.32	0.10	0.93	0.68	4.23	0.49	0.02	32.47	2.70	0.21	99.16	
Chd 26	x		x		no		x			57.41	0.13	1.16	0.83	2.31	0.46	0.04	35.98	1.94	0.17	100.41	
Chd 27		x	x				x			57.72	0.07	0.87	0.53	1.49	0.21	0.02	37.96	0.41	0.19	99.46	
Chd 28	x		x		strong			x		51.46	0.10	2.74	0.59	4.46	0.26	0.07	39.55	1.59	0.67	101.49	
Chd 29									BO	46.51	0.06	0.75	0.57	17.81	0.39	0.03	33.30	0.99	0.03	100.43	
Chd 30	x		x		strong			x		54.50	0.16	2.33	0.60	1.29	0.20	0.04	38.37	2.67	0.17	100.33	
Chd 31				x		x				47.99	0.13	1.74	0.60	10.74	0.44	0.01	35.36	2.90	0.69	100.59	
Chd 32			x					x													
Chd 33	x		x		strong			x		54.84	0.18	2.88	0.86	2.75	0.45	0.04	35.91	2.73	0.54	101.18	
Chd 34	x		x		medium			x													
Chd 35			x					x		53.76	0.12	1.68	0.77	4.80	0.47	0.09	36.52	2.34	0.48	101.02	
Chd 36	x		x		strong			x		53.94	0.14	2.05	0.58	1.94	0.28	0.10	38.95	1.98	0.28	100.23	
Chd 37	x		x		medium			x		53.68	0.08	1.19	0.64	2.69	0.37	0.03	40.24	1.41	0.21	100.54	
Chd 38			x					x													
Chd 40	x		x		strong			x													
Chd 41				x		x				43.30	0.10	2.23	0.37	16.45	0.32	0.02	34.96	1.38	0.79	99.92	
Chd 42	x				weak				BO	44.81	0.30	5.99	0.26	0.91	0.03	0.05	42.76	5.12	0.05	100.28	
Chd 43	x		x		medium			x		47.70	0.13	1.57	0.50	2.15	0.11	0.07	46.85	1.44	0.19	100.71	
Chd 44		x							FP	58.61	0.12	1.77	0.71	2.66	0.30	0.02	32.90	2.40	0.61	100.10	
Chd 45			x					x		52.66	0.15	2.35	0.77	5.34	0.63	0.09	35.02	2.72	0.71	100.43	

continued	Details			Texture				Bulk composition (wt.%)													
	zoned	rim section	Type I*	Type II	Poikilitic	PO	PP	POP	other**	SiO2	TiO2	Al2O3	Cr2O3	FeO	MnO	NiO	MgO	CaO	Na2O	Sum	
Chd 46	x		x		medium	x				44.34	0.04	0.35	0.46	7.14	0.33	0.07	47.47	0.52	0.07	100.79	
Chd 47	x		x		strong			x													
Chd 48			x					x		52.69	0.14	2.20	0.65	6.05	0.49	0.03	34.97	2.29	0.59	100.08	
Chd 49		x	x				x														
Chd 50				x																	
Chd 51	x		x		strong			x													
Chd 52	x		x		strong			x	BO	54.80	0.13	1.52	0.63	2.54	0.23	0.06	38.41	1.84	0.16	100.32	
Chd 53																					
Chd 54			x					x													
Chd 55	x		x		medium		x														
Chd 56			x				x			57.78	0.11	1.58	0.64	2.06	0.31	0.04	36.14	1.34	0.28	100.28	
Chd 57			x						RP	57.06	0.09	1.21	0.70	5.06	0.60	0.02	34.63	1.16	0.26	100.79	
Chd 58	x		x		medium			x		52.67	0.06	0.99	0.58	4.09	0.32	0.02	41.41	0.43	0.22	100.78	
Chd 59				x		x				44.31	0.10	1.91	0.43	12.19	0.31	0.02	37.69	1.70	0.67	99.33	
Chd 60		x							RP	54.81	0.04	0.52	0.75	16.98	0.77	0.01	25.12	0.95	0.15	100.10	
Chd 61			x					x		47.86	0.13	1.12	0.87	7.84	0.33	0.09	41.08	1.14	0.05	100.52	
Chd 62			x					x		50.66	0.09	2.05	0.54	3.62	0.31	0.05	42.72	1.16	0.53	101.73	
Chd 63				x				x		49.36	0.09	1.38	0.56	11.22	0.44	0.06	36.79	0.43	0.80	101.12	
Chd 64	x			x	strong			x		53.64	0.09	1.23	0.67	10.08	0.19	0.01	33.37	1.78	0.02	101.08	
Chd 65		x	x				x														
Chd 66	x		x		medium			x		53.95	0.15	1.90	0.59	2.31	0.21	0.06	39.01	2.23	0.25	100.67	

**Parnallee (38) (LL), BM.34792 (P.6397)**

Chd 01	x		x		medium																	
Chd 02			x																			
Chd 03				x		x				47.60	0.15	2.76	0.48	12.98	0.42	0.01	28.68	4.54	1.17	98.80		
Chd 04			x																			
Chd 05		x							C													
Chd 06			x					x		50.01	0.08	1.95	0.32	10.39	0.41	0.04	34.44	0.99	0.92	99.54		
Chd 07				x				x														
Chd 08	x			x	medium			x		52.80	0.11	2.17	0.30	8.81	0.50	0.01	30.73	2.06	1.23	98.72		
Chd 09	x			x	medium	x																
Chd 10									BO	52.81	0.04	5.88	0.22	13.37	0.33	0.01	22.66	0.51	3.38	99.22		
Chd 11	x			x	medium		x			55.75	0.07	2.99	0.71	7.33	0.51	0.01	29.29	1.69	0.71	99.07		
Chd 12	x		x		strong			x														
Chd 13	x			x	medium			x														
Chd 14	x			x	medium		x			55.69	0.18	2.71	0.67	5.59	0.33	0.01	30.53	2.01	0.97	98.69		
Chd 15		x		x			x			57.37	0.02	0.34	0.42	5.67	0.29	0.00	34.23	0.19	0.13	98.66		
Chd 16				x				x		44.64	0.12	1.60	0.25	16.10	0.28	0.08	34.71	0.86	0.66	99.30		
Chd 17				x				x		49.72	0.11	1.97	0.43	12.11	0.46	0.01	30.87	3.00	0.88	99.57		
Chd 18	x			x	strong			x		52.13	0.15	2.31	0.43	6.81	0.18	0.05	35.15	1.55	0.75	99.49		
Chd 19				x			x			55.29	0.06	1.36	0.44	7.28	0.39	0.03	32.15	1.41	0.38	98.80		
Chd 20	x		x		medium		x			54.82	0.08	1.31	0.55	5.94	0.47	0.03	33.54	2.00	0.54	99.27		
Chd 21		x		x			x			56.02	0.16	3.19	0.61	4.68	0.40	0.03	29.28	3.14	0.78	98.29		
Chd 22				x			x			57.24	0.09	1.61	0.45	6.54	0.52	0.01	31.10	1.72	0.82	100.10		

continued	Details			Texture				Bulk composition (wt.%)												
	zoned	rim section	Type I*	Type II	Poikilitic	PO	PP	POP	other**	SiO2	TiO2	Al2O3	Cr2O3	FeO	MnO	NiO	MgO	CaO	Na2O	Sum
Chd 23				x				x		52.91	0.05	0.99	0.31	9.08	0.33	0.01	34.65	1.04	0.41	99.78
Chd 24				x				x		46.22	0.05	1.20	0.18	18.58	0.45	0.04	31.74	0.57	0.59	99.61
Chd 25	x			x	strong		x													
Chd 26				x		x				44.74	0.12	2.24	0.20	13.71	0.22	0.01	36.91	0.61	0.65	99.42
Chd 27				x				x		52.70	0.11	2.47	0.55	11.67	0.56	0.01	29.44	1.98	0.96	100.46
Chd 28				x			x			56.26	0.15	3.05	0.66	4.73	0.59	0.05	28.75	4.19	0.87	99.31
Chd 29				x				x		51.44	0.05	2.04	0.51	13.48	0.40	0.01	28.93	1.84	0.72	99.42
Chd 30	x			x	medium			x		52.47	0.12	2.60	0.61	7.97	0.43	0.01	31.07	2.81	0.65	98.75
Chd 31				x				x		53.35	0.11	3.27	0.37	13.39	0.40	0.05	25.64	1.23	1.88	99.70
Chd 32				x		x														
Chd 33	x			x	medium		x			57.46	0.07	1.44	0.45	4.32	0.33	0.01	33.68	1.23	0.61	99.59
Chd 34				x		x														
Chd 35	x			x	strong			x		50.76	0.08	1.49	0.64	13.91	0.58	0.01	29.91	1.33	0.68	99.40
Chd 36								x												
Chd 37	x			x	medium			x		45.65	0.07	1.00	0.28	13.57	0.43	0.06	35.54	1.95	0.57	99.13
Chd 39								x												
Chd 40				x				x		53.23	0.26	4.33	0.38	5.42	0.17	0.03	31.44	1.98	1.70	98.96

**Huacachina (LL) BM.2015,M1 (P20129)**

Chd 01																					
Chd 02		x							GP												
Chd 03	x			x	no	x				43.84	0.07	1.12	0.20	8.14	0.11	0.10	46.11	0.41	0.34	100.45	
Chd 04		x							RP												
Chd 05				x	medium		x			53.87	0.10	0.95	0.54	8.04	0.30	0.06	35.07	1.43	0.24	100.61	
Chd 06	x			x						44.99	0.16	3.27	0.20	13.46	0.21	0.09	35.98	1.34	0.91	100.61	
Chd 07							x														
Chd 08									C												
Chd 09				x				x		51.18	0.07	1.69	0.53	11.70	0.37	0.18	34.84	0.40	0.69	101.64	
Chd 10									BO												
Chd 11	x			x	strong			x		46.12	0.15	1.14	0.10	13.12	0.24	0.07	39.19	1.02	0.16	101.31	
Chd 12									RP												
Chd 13																					
Chd 14	x			x	medium	x															
Chd 15	x			x	strong			x		48.26	0.10	1.87	0.23	9.98	0.16	0.08	39.22	0.90	0.50	101.30	
Chd 16							x			55.48	0.48	9.86	0.37	2.83	0.07	0.25	23.28	7.09	1.33	101.04	
Chd 17									BO	48.05	0.13	1.85	0.51	14.54	0.44	0.13	32.41	2.77	0.75	101.58	
Chd 18	x			x	strong			x													
Chd 19				x				x		48.81	0.13	2.98	0.44	11.11	0.39	0.05	33.73	1.80	1.47	100.90	
Chd 20	x			x	medium			x													
Chd 21	x			x	medium			x		50.55	0.08	1.74	0.39	12.98	0.40	0.02	32.40	1.33	1.02	100.92	
Chd 22	x			x	medium			x													
Chd 23	x				weak				BO	46.13	0.24	4.50	0.14	7.72	0.12	0.29	37.91	2.22	1.20	100.48	
Chd 24				x			x														
Chd 25																					
Chd 26	x				strong			x													

continued Chondrule	Details		Texture					Bulk composition (wt.%)													
	zoned	rim section	Type I*	Type II	Poikilitic	PO	PP	POP	other**	SiO2	TiO2	Al2O3	Cr2O3	FeO	MnO	NiO	MgO	CaO	Na2O	Sum	
Chd 27				x				x													
Chd 28	x			x	strong	x				50.27	0.14	2.32	0.47	8.46	0.59	0.11	33.58	3.47	1.04	100.46	
Chd 29				x				x		56.57	0.08	0.98	0.59	3.76	0.24	0.08	37.22	1.08	0.25	100.83	
Chd 30				x						56.61	0.11	1.53	0.55	5.23	0.33	0.12	34.55	1.71	0.41	101.17	
Chd 31				x				x		45.02	0.11	2.02	0.21	14.09	0.35	0.08	34.83	2.61	0.94	100.27	
Chd 32				x	medium																
Chd 33	x							x													
Chd 34				x				x		55.62	0.09	2.19	0.65	6.26	0.44	0.03	31.89	2.26	0.54	99.97	

\*\*

Fo > 90, olivine cores only

Fs < 10 in samples of petrol. type 3.6 and higher

\*

POP

PO

PP

BO

RP

C

GP

porphyritic olivine-pyroxene

porphyritic olivine

porphyritic pyroxene

barred olivine

radial pyroxene

cryptocrystalline

granular pyroxene

# Chapter 3

## Sectioning effects of porphyritic chondrules: Implications for the PP/POP/PO classification and correcting modal abundances of mineralogically zoned chondrules

Jens Barosch, Dominik C. Hezel, Lena Sawatzki, Lucia Halbauer, Yves Marrocchi

Meteoritics and Planetary Science (2020)

<https://doi.org/10.1111/maps.13476>

### **Abstract**

Mineralogically zoned chondrules are a common chondrule type in chondrites. They consist of olivine cores, surrounded by low-Ca pyroxene rims. By serial sectioning porphyritic chondrules from carbonaceous, ordinary and enstatite chondrites, we demonstrate that the 2D textural appearances of these chondrules largely depend on where they are cut. The same chondrule may appear as a porphyritic pyroxene (PP) chondrule when sectioned through the low-Ca pyroxene rim, and as a porphyritic olivine-pyroxene (POP) or porphyritic olivine (PO) chondrule when sectioned close or through its equator. Chondrules previously classified into PP/POP/PO chondrules might therefore not represent different types, but various sections through mineralogically zoned chondrules. Classifying chondrule textures into PP, POP and PO has therefore no unequivocal genetic meaning, it is merely descriptive. Sectioning effects further introduce a systematic bias when determining mineralogically zoned chondrule fractions from 2D sections. We determined correction factors to estimate 3D mineralogically zoned chondrule fractions when these have been determined in 2D sections: 1.24 for carbonaceous chondrites, 1.29 for ordinary chondrites and 1.62 for enstatite chondrites. Using these factors then show that mineralogically zoned chondrules are the dominant chondrule type in chondrites with estimated 3D fractions of 92% in CC, 52% in OC and 46% in EC.

### 3.1. Introduction

Chondrules and fine-grained matrix are the two major components of chondrites. Chondrules are millimetre-sized igneous droplets mainly composed of silicates (olivine, pyroxene, plagioclase), Fe-Ni metal, sulphide and a glassy or micro-crystalline mesostasis. A series of studies argued that chondrules formed in an open system and interacted with the ambient gas during their molten stage (Ebel et al., 2018, and references therein). Important support for this open system scenario is recorded in chondrules as a mineralogical and/or a compositional zonation (e.g., Tissandier et al., 2002; Hezel et al., 2003; Krot et al., 2004; Libourel et al., 2006; Nagahara et al., 2008; Friend et al., 2016; Marrocchi et al., 2018; Barosch et al., 2019, and references therein). The open system scenario constrains chondrule formation processes and explains various chondrule characteristics, such as the abovementioned chondrule zonations or bulk compositional variations in chondrule populations.

Chondrules are classified either according to their textures and mineralogies, or their chemical compositions (cf. Scott and Krot, 2014, and references therein). Three main classification schemes are commonly used: (i) *textural appearance*- as introduced by Gooding and Keil (1981). The major textural categories are porphyritic olivine (PO), porphyritic pyroxene (PP), porphyritic olivine-pyroxene (POP), barred olivine (BO), and radial pyroxene (RP). Minor textural classifications, partly restricted to individual chondrite classes, are for example skeletal olivine (SO), granular olivine (GO), cryptocrystalline (C), or microporphyritic olivine chondrules (MPO); (ii) *bulk chondrule Si-concentration*- these are the three types A (Si-rich), AB (intermediate) and B (Si-poor). The distinction between Si-rich and -poor is only qualitative, not quantitative, and directly related to the textural types. PO are Si-poor, POP intermediate, and PP Si-rich. (iii) *chondrule olivine FeO-concentration*- chondrules are divided into type I, when the chondrule olivine FeO content is below 10 wt.%, and in type II, when the chondrule olivine FeO content is above 10 wt.%. We note that various authors might, however, use different threshold values. Furthermore, this classification only works for unequilibrated samples with petrologic types below  $\sim 3.5$ . Another, though more rarely used chemical chondrule classification is based on the cathodoluminescence (CL) activity of chondrule minerals (Sears et al., 1995). Lastly, a small number of chondrules are Al-rich with  $>10$  wt.%  $\text{Al}_2\text{O}_3$  (Bischoff and Keil, 1983).

Ideally, a chondrule classification provides genetic information. Chondrules are however mostly classified using 2D sections, which are not necessarily representative of the 3D

chondrules (e.g., Hezel, 2007; Ebel et al., 2009; Hezel and Kießwetter, 2010; Cuzzi and Olson, 2017, and references therein), and thus might skew any potential genetic information. If a sectioning bias is present in the majority of chondrules, the classification becomes meaningless or even incorrect. Mineralogically zoned chondrules might be particularly deceiving with regard to textural classification: they have an olivine core, surrounded by a low-Ca pyroxene rim, and their 2D appearances depend on where they are sectioned. Classification of such mineralogically zoned chondrules in 2D sections could therefore be unreliable, and might easily lead to misclassifications.

Here we study this bias with sectioning experiments on chondrules in carbonaceous (CC; Efremovka CV3), ordinary (OC; Moorabie L3.8-an) and enstatite chondrite samples (EC; Sahara 97096 EH3, see Piani et al., 2012, 2016). In addition, we measured CM, CV and CR chondrites (Table 3.1) with cabinet-sized micro-tomography to test whether this method can be used to study chondrule textures. The study of chondrules in 3D allows us to understand if, and to what extent their 2D classification into PO/POP/PP, as well as A/AB/B depends on sectioning effects.

## 3.2. Methods

### 3.2.1. Microtomography ( $\mu$ -CT)

Micro-CT allows studying the petrography of a sample in 3D (e.g., Ketcham, 2005; Ebel et al., 2009; Beitz et al., 2013; Hezel et al., 2013; Hanna and Ketcham, 2017), largely non-destructive (Sears et al., 2018) and non-invasive, and therefore seems to be the undisputed technique of choice for this study. This technique is nonetheless highly challenging for this kind of study, as  $\mu$ -CT primarily images the density contrast between minerals. Olivine and pyroxene have very similar densities, with a span from 3.27 to 4.39 g/cm<sup>3</sup> for forsterite and fayalite, and a span from 3.20 to 3.95 g/cm<sup>3</sup> for enstatite and ferrosilite. We therefore performed a number of experiments with various measurement settings, as well as the two software-packages ImageJ/Fiji and Avizo, to test whether the low-Ca pyroxene can be reliably discriminated from the olivine based on density contrasts.

Individual meteorite chips of a few mm in diameter were CT scanned in a Zeiss Xradia 520 Versa X-ray microscope at the Natural History Museum in London. Up to 4 chips were stacked upon each other in a plastic tube for a single experiment. Table 3.1 lists the settings used for the various experiments. The chips could only be a few mm in diameter to obtain the resolution

of a few  $\mu\text{m}$  required to identify the often only tens of  $\mu\text{m}$  thick low-Ca pyroxene layers surrounding the olivine core. We therefore chose a chondrite group with many chondrules, but small chondrule sizes: CM, with average chondrules sizes of 145  $\mu\text{m}$  (Friend et al., 2018); and two chondrite groups with large chondrule sizes, but then only few chondrules: CR and CV, with average chondrules sizes of 700 and 900  $\mu\text{m}$ , respectively (Friedrich et al., 2016). All samples studied are listed in Table 3.1.

The resulting image stack was first processed with the Avizo software to correct for ring artefacts and reduce the noise as well as increase the contrast of the images using smoothing-wave and enhancement filtering (cf. Li et al. 2017; Ni et al. 2017; Ferreira et al. 2018). As the olivine is slightly denser than the low-Ca pyroxene, olivine should appear slightly brighter than the pyroxene. Figure 3.1 displays a representative slice through Vigarano (CV3). It is almost impossible to unequivocally discriminate olivine from low-Ca pyroxene based on their respective different brightness. We also hoped to identify pyroxene by their characteristic 110 cleavages, which is principally very distinctive from the homogeneous appearance of olivine. However, the images were insufficiently resolved to unequivocally identify these cleavages.

**Table 3.1:** Measurement conditions for the various  $\mu$ -CT experiments.

Samples*	Experiment	Current ( $\mu\text{A}$ )	Voltage (kV)	Exposure Time (s)	Number of Projections
	1	80.2	50	2	3000
Murchison (CM2)	2	80.2	50	5	6401
NWA801 (CR2)	3	80.2	30	20	6401
Vigarano (CV3)	4	75	40	5	6401
	5	80	40	5	6400
Cold Bokkeveld (CM2)	6	80	50	7	1601
	7	80	40	60	1601
Mokoia (CV3)					
Cold Bokkeveld (CM2)					
Jbilet Winselwan (CM2)	8	80	40	10	3201
Kaba (CV3)					

\*The samples were stacked upon each other and all measured together in each experiment.

In places where large pyroxenes or olivines could be identified, e.g., based on their appearance with and without cleavages, we could measure the grey value changes across individual minerals. Such grey value difference across individual minerals were a few units, e.g., two to five gray value units. However, absolute gray value differences between olivine and pyroxene were also in the range of about three to six gray value units. This means, olivine and pyroxene

gray values overlap already because of their individual gray value spread, resulting from mineral inhomogeneities. This makes it virtually impossible to threshold olivine from pyroxene using their gray values. This unfortunate result is true for all instrument settings we tested. And although in rare cases discriminating olivine from pyroxene may be possible, the density difference of olivine and low-Ca pyroxene in the samples studied and the instrument used was simply not enough for sufficiently reliable phase identification. Hence, reliably studying mineralogically zoned chondrules in 3D with  $\mu$ -CT based on phase density contrasts, and without crystallographic information, is not yet possible. We instead used 3D serial sectioning for this study.

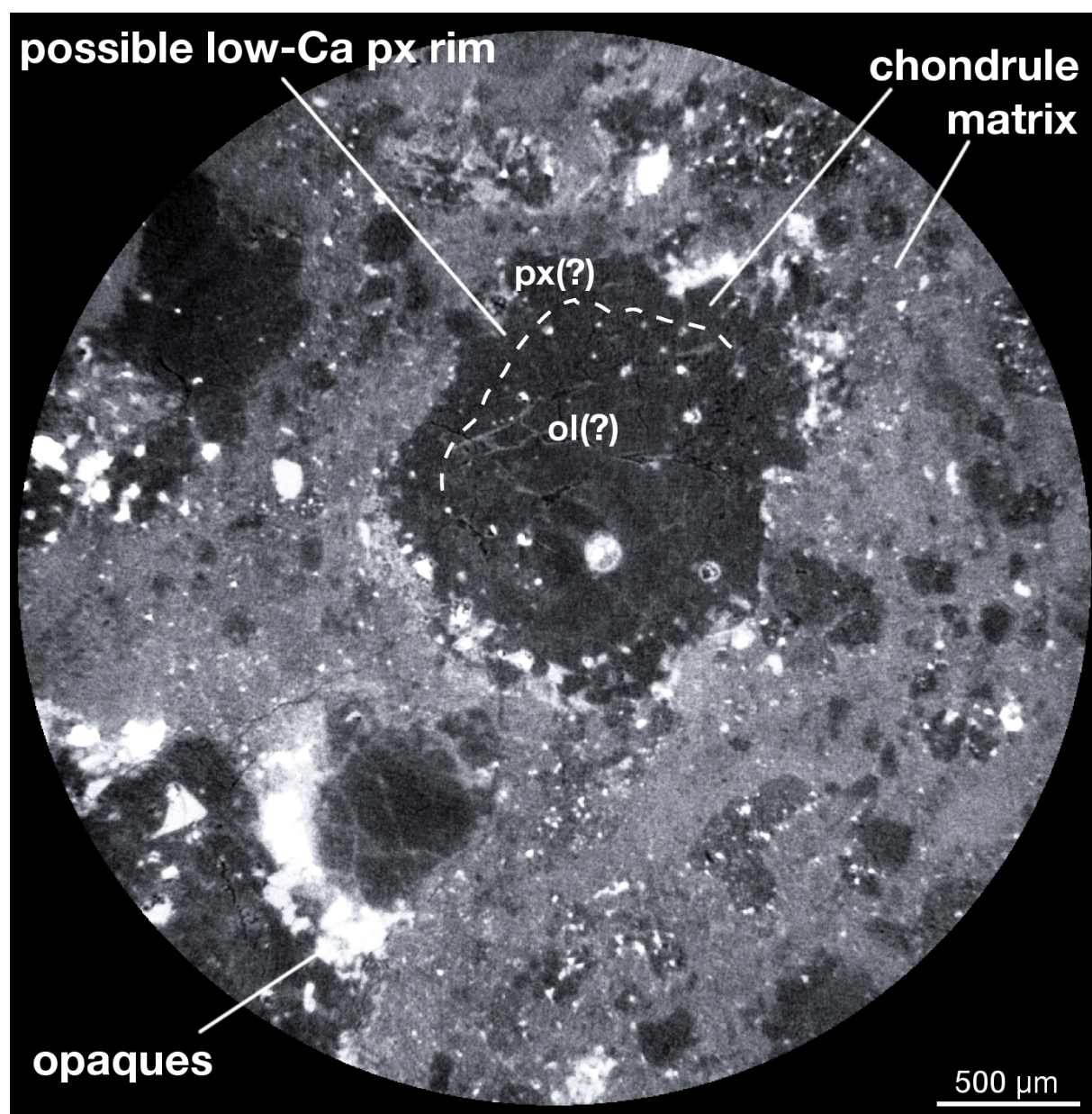


**Fig. 3.1:** A representative slice through the tomography image stack of Vigarano (CV3). The contact between olivine core and low-Ca pyroxene rim might be vaguely guessed, but cannot be determined reliably.

### 3.2.2. 3D serial sectioning

Serial sectioning, combined with scanning electron microscopy (SEM), allows 3D reconstruction of chondrules. At first, a chondrite thick section was prepared by saw-cutting a large (0.5–1 cm-sized) chondrite chip, embedded in epoxy resin. The surface was polished with a diamond polishing compound. Then, the following 3-step procedure was repeatedly carried out: (i) 2D element maps of entire sample surfaces were recorded using an SEM (Zeiss Sigma 300 VP, located at the Institute of Geology and Mineralogy, Cologne). The focused electron beam rastered the stationary sample surface over small areas ( $\sim 500 \times 400 \mu\text{m}$ , pixel size  $\sim 4 \mu\text{m}$ ). The aperture was set to  $60 \mu\text{m}$ , the accelerating voltage to 20 kV and the dwell time to 10 ms, resulting in a count rate of  $\sim 50,000$  cps. The sample was then moved to a new position and the next map was obtained. All individual element maps were stitched together to a large area map (LAM), showing the entire chondrite section. (ii) From the LAM, a phase map was created using the PHAPS program (Hezel, 2010). Every colour in the phase map represents a different mineral phase, allowing instant visual identification of chondrule textures. (iii) Finally, the sample was ground down a few tens of  $\mu\text{m}$  and again polished with a diamond polishing compound.

Each large-area phase map represents a different section perpendicular to the z-axis of the sample and, when stacked on top of each other, the resulting image stack allows 3-dimensional insights into the sample. The amount of grinding in each step was monitored using a slide gauge. In addition, two precise aluminium cones were embedded on opposing sides of every sample thick section. The basal cone diameters were measured at each sectioning step and the difference to the previous section was used to calculate the slice of material removed by grinding. Depending on the sample, typical abrasion thicknesses varied between 20 and 120  $\mu\text{m}$ . In Efremovka and Moorabie, on average  $\sim 80 \mu\text{m}$  were ground down in each step. Grinding step sizes were smaller for Sahara 97096, with on average  $\sim 40 \mu\text{m}$ . This was done for  $\sim 10$  sections for each of the three chondrites. We then obtained 3D chondrule images by tracing the chondrules through the phase maps of the neighbouring sections.

### 3.3. Results

#### 3.3.1. Sectioning effects when classifying chondrules

Three unequilibrated chondrites were serial sectioned – covering all three chondrite classes – and their chondrules studied in 2D and 3D: Efremovka (CV3; 86 chondrules), Moorabie (L3.8-an; 117 chondrules) and Sahara 97096 (EH3; 252 chondrules). Mineralogically zoned chondrules typically consist of an olivine core surrounded by a low-Ca pyroxene rim of variable thickness (cf. examples in Fig. 3.2). We designate chondrules based on their mineral modal abundances as follows: PP (with ol/px  $\leq 0.1$ ), POP and PO (with ol/px  $\geq 0.9$ ).

The apparent 2D textural appearances of mineralogically zoned chondrules vary, depending on where a chondrule is sectioned (Fig. 3.2). A 2D section close to the chondrule border will cut through the low-Ca pyroxene rim, and the chondrule texture appears as PP. Small olivine grains are often poikilitically enclosed in the rim pyroxene crystals, but in some rims, olivine is completely absent. In sections closer to the equator of a chondrule, the olivine- plus mesostasis-rich core is cut, and the apparent 2D texture is POP, due to the commonly still high abundance of pyroxene. A section close or through the chondrule equator is the most likely to appear as a PO texture, depending on the thickness of the pyroxene rim. We found only 3 Efremovka (CV) chondrules that had PP textures in every section through these chondrules. PP chondrules were naturally more common in the enstatite chondrite Sahara 97096, with a 3D fraction of ~60%.

Examples for the sectioning effects are displayed in Figure 3.2: *Row a*– the Efremovka chondrule rim section has an apparent PP 2D texture – i.e., the chondrule is seemingly unzoned –, but then shows an apparent POP texture in sections located in-between border and equator, and finally an apparent PO texture, when sectioned directly through its equator. This example also demonstrates how the mineralogical zonation of this chondrule is disguised in the rim section by the apparent PP texture. We further note that the apparent chondrule diameter increases from PP (smallest diameter), to POP (intermediate) and lastly, to PO (largest). *Row b*– the Moorabie chondrule has an apparent PP 2D texture in the section through its rim, again disguising the zoned nature of this chondrule. The sections closer to and directly through this chondrule's equator then result in apparent POP textures. *Row c*– enstatite chondrite chondrules almost always appear as PP chondrules due to their thick low-Ca pyroxene rims. Tiny olivine cores are however highly abundant in EC chondrules (see also Piani et al., 2016). The example demonstrating this in Fig. 3.2 is a chondrule from Sahara 97096.

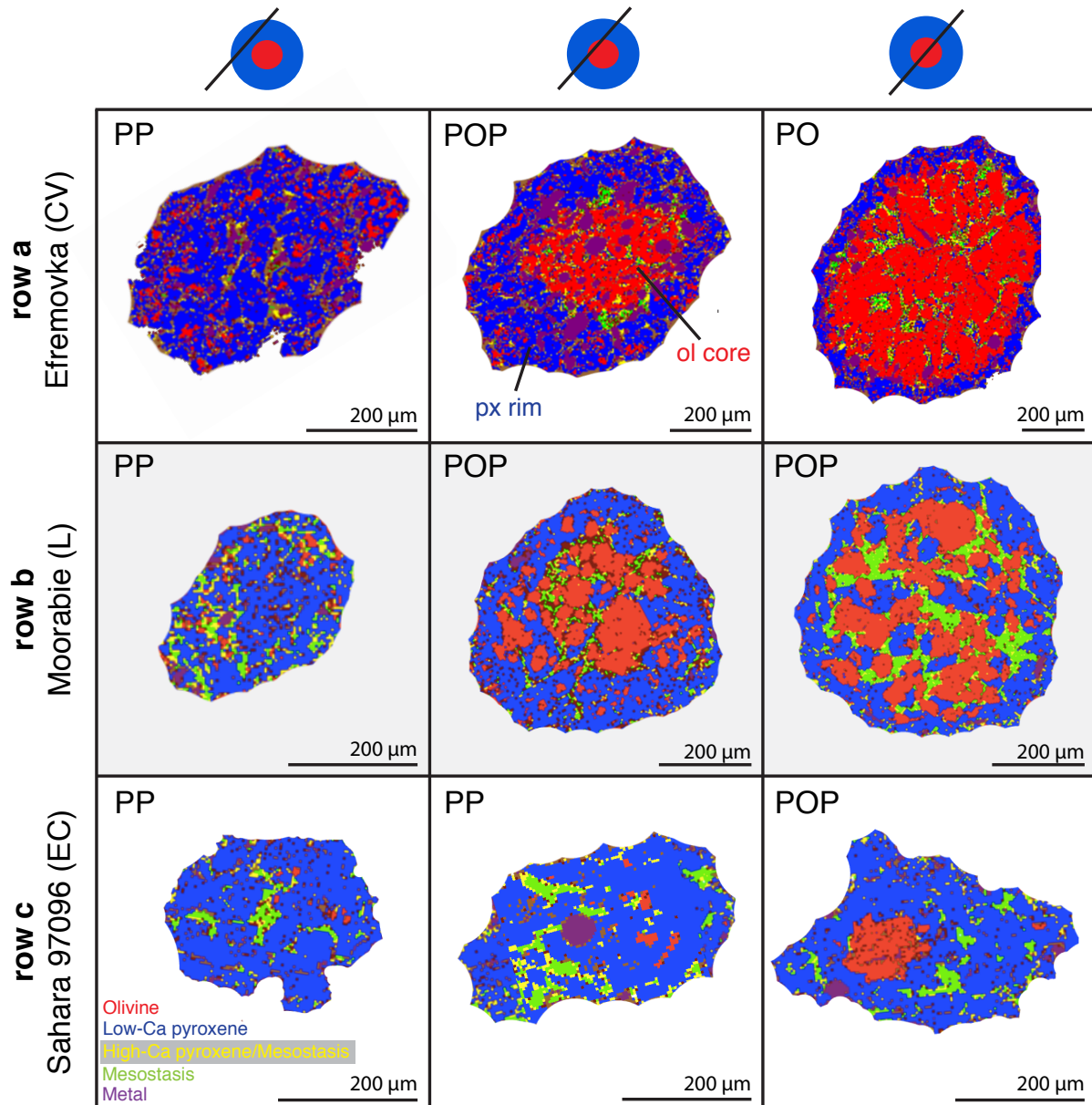


**Fig. 3.2:** Different sections through single chondrules in Efremovka, Moorabie and Sahara 97096 are displayed. The apparent 2D textures and, hence, their classifications into PP, PO or POP depend on where a chondrule is sectioned. Chondrule diameters in row a, and b, apparently increase from PP (smallest) to POP (intermediate) and PO (largest) diameter.

### 3.3.2. Sectioning effects when determining the fraction of mineralogically zoned chondrules

To determine 2D and 3D zoned chondrule fractions in all three samples, we first picked the middle sections of each sample's image stack for 2D evaluations. Every chondrule studied in 2D in these sections was subsequently studied in 3D, by tracing it through the phase maps of the neighbouring sections. The zoned chondrule fractions determined from 2D sections are 64% in Efremovka (86 chondrules studied in total), 42% in Moorabie (117 chondrules studied in total) and 26% in Sahara 97096 (252 chondrules studied in total). The zoned chondrule

fractions of the same chondrules, but determined in 3D, are significantly and systematically higher: 79% in Efremovka, 54% in Moorabie and 43% in Sahara 97096. In relative proportions, the increase from 2D to 3D zoned chondrule fractions are +24% (i.e., by factor 1.24) in Efremovka, +29% (i.e., by factor 1.29) in Moorabie and +62% (i.e., by factor 1.62) in Sahara 97096 (Fig. 3.3).

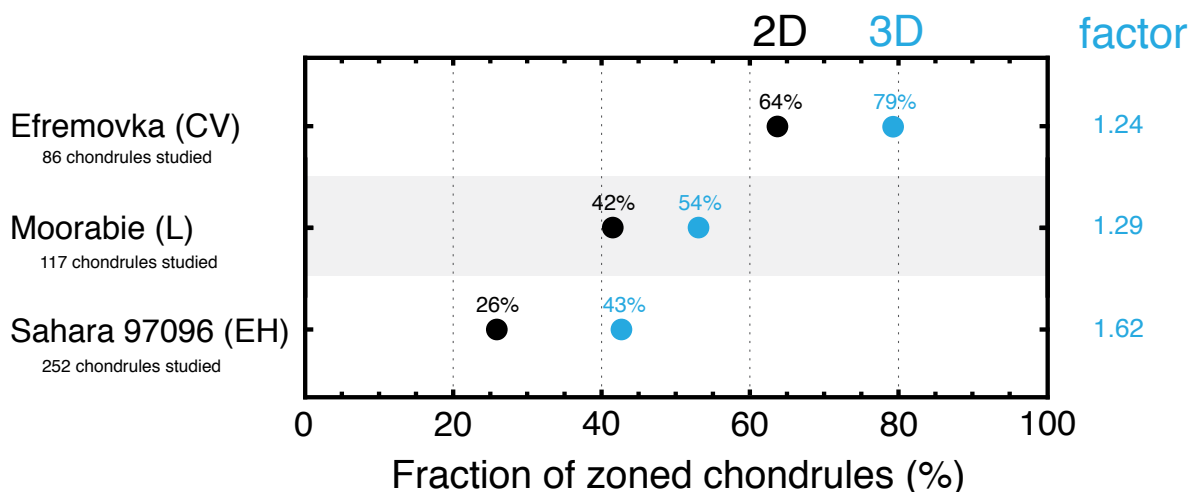


**Fig. 3.3:** Here, 2D and 3D zoned chondrule fractions have been determined in the same samples. The fraction of zoned chondrules is always higher when determined in 3D, demonstrating the systematic bias when the fraction of zoned chondrules is determined in 2D. The 2D-3D differences can be used as approximate correction factors to estimate the true 3D fraction of zoned chondrules from a determined 2D fraction.

### 3.4. Discussion and Summary

A classification scheme for chondrule textures can ideally be used to draw conclusions about their formation processes. It is therefore critical that such a scheme does not provide misleading information. Chondrule textures are first discriminated into porphyritic and non-porphyritic chondrules. Different thermal histories apply to these types: porphyritic chondrules crystallized from melts with abundant nuclei after incomplete melting of precursor materials (Lofgren, 1996; Connolly et al., 1998; Marrocchi et al., 2018, 2019), while non-porphyritic chondrules likely crystallized from superheated melts without nuclei (e.g., Connolly and Hewins, 1995). Porphyritic chondrules are then classified into PP, PO and POP (e.g., Gooding and Keil, 1981). This classification is, however, not always meaningful and can be misleading, as most chondrules are studied in 2D only. We demonstrate in Fig. 3.2 that an individual porphyritic zoned chondrule can be classified as PP, POP and PO, solely based on where it was sectioned. Thus, discriminating between PP, POP and PO chondrules often only indicates where a chondrule was cut, but does not necessarily reveal useful genetic information. This then also applies to the sub-classification of chondrules into A (Si-rich), AB (intermediate) and B (Si-

poor), as this is directly related to the textural types PP, POP, and PO. Therefore, the same argument applies to this classification scheme: It is largely controlled by sectioning effects. However, not all 2D PP chondrules are rim sections: we indeed find entire PP chondrules in 3D. These are very common in the EC sample, rare in the OC sample and very rare in the CC sample. Using a sub-set of our data, we estimate the true (3D) fraction of PP chondrules to ~60% in the EC sample and to ~7% in the CC sample. This is significantly lower than the 2D PP chondrule fractions of ~80% in EC and 30% in CC, thereby further illustrating the sectioning problem. Hence, in CC, where most chondrules are mineralogically zoned, the vast majority of PP chondrules – as observed in 2D sections – are actually rim sections of POP/PO chondrules.

Based on the aforementioned observations, it is clear that the textural classification of porphyritic chondrules needs to be used with caution. Designating chondrules as either *mineralogically zoned* (MZ) chondrules or *mineralogically unzoned* (MU) chondrules might be a useful addition to the PP, POP, PO classification, as it adds currently missing textural information. However, reliably identifying zoned chondrules in 2D sections is as well problematic. Therefore, deciding which classification scheme is used might depend on what specific problem is studied. All we need to do here is to clearly point out and quantify the sectioning effects with regard to mineralogically zoned chondrules. This is of great importance, as these are – as demonstrated below – the dominant chondrule type in most chondrites.

Mineralogically zoned chondrules sectioned through their low-Ca pyroxene rims usually appear as unzoned. Consequently, the fractions of mineralogically zoned chondrules in chondrites are underestimated in 2D studies (e.g., Friend et al., 2016; Barosch et al., 2019). Determining true zoned chondrule fractions requires 3D textural analysis, e.g., serial sectioning. With this technique, we studied chondrules in 3D, excluding all sectioning effects. We determined the following correction factors for estimating true 3D fractions from measured 2D fractions: 1.24 for CC, 1.29 for OC and 1.62 for EC (Fig. 3.3).

The weighted average 2D zoned chondrule fractions reported in previous studies, and including the new 2D data reported in this study, are ~74% in CC (Friend et al., 2016), ~40% in OC (Barosch et al., 2019) and ~29% in EC (unpublished). The 3D corrected, i.e., estimated true average zoned chondrule fractions are then: 92% in CC, 52% in OC and 46% in EC. This makes mineralogically zoned chondrules the dominant chondrule type in chondrites.

## Acknowledgements

We thank Hanna Cieszynski for her assistance operating the SEM and Kathrin Jung for sample preparation. DH is grateful for a Europlanet grant to the London Natural History Museum that was essential for this study. Europlanet 2020 RI has received funding from the European Union's Horizon 2020 research and innovation program under grant agreement No. 654208. This study was funded by the Deutsche Forschungsgemeinschaft (DFG) grants HE 5352/10-1 and PA 346/50-1. We thank G. Libourel and A. N. Krot for their thorough and helpful reviews, as well as associate editor K. Righter for handling the manuscript.

## References

- Barosch J., Hezel D. C., Ebel D. S. and Friend P. 2019. Mineralogically zoned chondrules in ordinary chondrites as evidence for chondrule open system behaviour. *Geochimica et Cosmochimica Acta* 249:1–16.
- Beitz E., Blum J., Mathieu R., Pack A. and Hezel D. C. 2013. Experimental investigation of the nebular formation of chondrule rims and the formation of chondrite parent bodies. *Geochimica et Cosmochimica Acta* 116:41–51.
- Bischoff A. and Keil K. 1983. Al-rich objects in ordinary chondrites: related origin of carbonaceous and ordinary chondrites and their constituents. *Geochimica et Cosmochimica Acta* 48:693–709.
- Connolly H. C. Jr. and Hewins R. 1995. Chondrules as products of dust collisions with totally molten droplets within a dust-rich nebular environment: An experimental investigation. *Geochimica et Cosmochimica Acta* 59:3231–3246.
- Connolly H. C. Jr., Jones B. D. and Hewins R. H. 1998. The flash melting of chondrules: an experimental investigation into the melting history and physical nature of chondrule precursors. *Geochimica et Cosmochimica Acta* 62:2725–2735.
- Cuzzi J. N. and Olson D. M. 2017. Recovering 3D particle size distributions from 2D sections. *Meteoritics & Planetary Science* 52:532–545.
- Ebel D. S., Leftwich K., Brunner C. E. and Weisberg M. K. 2009. Abundance and size distribution of inclusions in CV3 chondrites by X-ray image analysis. In *40th Lunar and Planetary Science Conference*, #2065 (abstr.).
- Ebel D. S., Alexander C. M. O'D. and Libourel G. 2018. Vapor-melt exchange. In: *Chondrules: Records of Protoplanetary Disk Processes* (Cambridge Planetary Science).

- Eds: S. S. Russell, H. C. Connolly Jr. and A. N. Krot. Cambridge University Press, Cambridge UK, pp. 457.
- Gooding J. L. and Keil K. 1981. Relative abundances of chondrule primary textural types in ordinary chondrites and their bearing on conditions of chondrule formation. *Meteoritics*, 16:17–43.
- Ferreira T. R., Pires L. F., Wildenschild D., Heck R. J. and Antonino A. C. 2018. X-ray microtomography analysis of lime application effects on soil porous system. *Geoderma* 324:119–130.
- Friedrich J. M., Weisberg M. K., Ebel D. S., Biltz A. E., Corbett B. M., Iotzov I. V., Khan W. S. and Wolman M. D. 2015. Chondrule size and related physical properties: A compilation and evaluation of current data across all meteorite groups. *Geochemistry* 75:419–443.
- Friend P., Hezel D. C. and Mucerschi D. 2016. The conditions of chondrule formation, Part II: Open system. *Geochimica et Cosmochimica Acta* 173:198–209.
- Friend P., Hezel D. C., Barrat J. A., Zipfel J., Palme H. and Metzler K. 2018. Composition, petrology and chondrule-matrix complementarity of the recently discovered Jbilet Winselwan CM2 chondrite. *Meteoritics & Planetary Science* 53:2470–2491.
- Hanna R. D. and Ketcham R. A. 2017. X-ray computed tomography of planetary materials: A primer and review of recent studies. *Geochemistry* 77:547–572.
- Hezel D. C., Palme H., Brenker F. E. and Nasdala L. 2003. Evidence for fractional condensation and reprocessing at high temperatures in CH-chondrites. *Meteoritics & Planetary Science* 38:1199–1216.
- Hezel D. C. 2007. A model for calculating the errors of 2D bulk analysis relative to the true 3D bulk composition of an object, with application to chondrules. *Computers & Geosciences* 33:1162–1175.
- Hezel D. C. 2010. A mathematica code to produce phase maps from two element maps. *Computers & Geosciences* 36:1097–1099.
- Hezel D. C. and Kießwetter R. 2010. Quantifying the error of 2D bulk chondrule analyses using a computer model to simulate chondrules (SIMCHON). *Meteoritics & Planetary Science* 45:555–571.
- Hezel D. C., Elangovan P., Viehmann S., Howard L., Abel R. L. and Armstrong R. 2013. Visualisation and quantification of CV chondrite petrography using micro-tomography. *Geochimica et Cosmochimica Acta* 116:33–40.

- Ketcham R. A. 2005. Computational methods for quantitative analysis of three-dimensional features in geological specimens. *Geosphere* 1:32–41.
- Krot A. N., Libourel G., Goodrich C. A. and Petaev M. I. 2004. Silica-rich igneous rims around magnesian chondrules in CR carbonaceous chondrites: Evidence for condensation origin from fractionated nebular gas. *Meteoritics & Planetary Science* 39:1931–1955.
- Li Z., Liu D., Cai Y., Ranjith P. G. and Yao Y. 2017. Multi-scale quantitative characterization of 3-D pore-fracture networks in bituminous and anthracite coals using FIB-SEM tomography and X-ray  $\mu$ -CT. *Fuel* 209:43–53.
- Libourel G., Krot A. N. and Tissandier L. 2006. Role of gas–melt interaction during chondrule formation. *Earth and Planetary Science Letters* 251:232–240.
- Lofgren G. 1996. A dynamic crystallization model for chondrules melts. In: Hewins R. H., Jones R. H., and Scott E. R. D. (eds.) *Chondrules and the Protoplanetary Disk*, pp. 1887–1896, Cambridge University Press.
- Marrocchi Y., Villeneuve J., Batanova V., Piani L. and Jacquet E. 2018. Oxygen isotopic diversity of chondrule precursors and the nebular origin of chondrules. *Earth and Planetary Science Letters* 496:132–141.
- Marrocchi Y., Euverte R., Villeneuve J., Batanova V., Welsch B., Ferrière L. and Jacquet E. 2019. Formation of CV chondrules by recycling of amoeboid olivine aggregate-like precursors. *Geochimica et Cosmochimica Acta* 247:121–141.
- Nagahara H., Kita N. T., Ozawa K. and Morishita Y. 2008. Condensation of major elements during chondrule formation and its implication to the origin of chondrules. *Geochimica et Cosmochimica Acta* 72:1442–1465.
- Ni X., Miao J., Lv R. and Lin X. 2017. Quantitative 3D spatial characterization and flow simulation of coal macropores based on  $\mu$ CT technology. *Fuel* 200:199–207.
- Piani L., Robert F., Beyssac O., Binet L., Bourot-Denise M., Derenne S., Le Guillou C., Marrocchi Y., Mostefaoui S., Rouzaud J.-N. and Thomen A. 2012. Structure, composition and location of the organic matter found in the Enstatite Chondrite Sahara 97096 (EH3). *Meteoritics & Planetary Science* 47:8–29.
- Piani L., Marrocchi Y., Libourel G. and Tissandier L. 2016. Magmatic sulfides in the porphyritic chondrules of EH enstatite chondrites. *Geochimica et Cosmochimica Acta* 195:84–99.
- Scott E. R. D. and Krot A. N. 2014. Chondrites and their components. In: *Treatise on Geochemistry* 2<sup>nd</sup> ed. (eds. H. Holland and K. Turekian), Oxford: Elsevier, pp. 65–137.

- Sears D. W. G., Morse A. D., Hutchinson R., Guimon R. K., Jie L., Alexander C. M. O'D., Benoit P. H., Wright I., Pillinger C., Xie T. and Lipschutz M. E. 1995. Metamorphism and aqueous alteration in low petrographic type ordinary chondrites. *Meteoritics* 30:169–181.
- Sears D. W. G., Sehlke A., Friedrich J. M., Rivers M. L. and Ebel D. S. 2018. X-ray computed tomography of extraterrestrial rocks eradicates their natural radiation record and the information it contains. *Meteoritics & Planetary Science* 53:2624–2631.
- Tissandier L., Libourel G. and Robert F. 2002. Gas-melt interactions and their bearing on chondrule formation. *Meteoritics & Planetary Science* 37:1377–1389.

# Chapter 4

## An unusual compound object in Yamato 793408 (H3.2-an): The missing link between compound chondrules and macrochondrules?

Jens Barosch, Dominik C. Hezel, Yves Marrocchi, Andrey Gurenko, Christoph Lenting

Meteoritics and Planetary Science (2020)

<https://doi.org/10.1111/maps.13496>

### **Abstract**

We found a large (~2 mm) compound object in the primitive Yamato 793408 (H3.2-an) chondrite. It consists mostly of microcrystalline material, similar to chondrule mesostasis, that hosts an intact barred olivine (BO) chondrule. The object contains euhedral pyroxene and large individual olivine grains. Some olivine cores are indicative of refractory forsterites with very low Fe- and high Ca, Al-concentrations, although no  $^{16}\text{O}$  enrichment. The entire object is most likely a new and unique type, as no similar compound object has been described so far. We propose that it represents an intermediate stage between compound chondrules and macrochondrules, and formed from the collision between chondrules at low velocities (below 1 m/s) at high temperatures (around 1550°C). The macrochondrule also trapped and preserved a smaller BO chondrule. This object appears to be the first direct evidence for a genetic link between compound chondrules and macrochondrules. In accordance with previous suggestions and studies, compound chondrules and macrochondrules likely formed by the same mechanism of chondrule collisions, and each represents different formation conditions, such as ambient temperature and collision speed.

## 4.1. Introduction

Ordinary chondrites (OC) are dominated by up to 80 vol.% chondrules. The mafic chondrules typically consist of olivine, pyroxene and opaque phases such as metal, sulphide and spinel. These phases are set in a glassy or fine-crystalline, so-called mesostasis. Chondrules have a complex formation history: in the canonical view of chondrule formation, a chondrule precursor aggregate was briefly heated to up to >2000 K, melted, and solidified subsequently in minutes to hours (Hewins et al., 2005).

Chondrules were open systems during their molten stage and interacted with their surrounding nebular gas (e.g., Tissandier et al., 2002; Libourel et al., 2006; Marrocchi and Chaussidon, 2015; Friend et al., 2016; Piani et al., 2016; Soulié et al., 2017; Ebel et al., 2018; Barosch et al., 2019). The open system scenario is further supported by Marrocchi et al. (2018, 2019) and Libourel and Portail (2018), who suggested that refractory forsterites (RF) – olivines with high Ca,Al- and very low Fe-concentrations – formed from crystallisation and interaction with the surrounding gas. The latter, however, is in conflict with the interpretation of Pack et al. (2004), who suggested that these refractory olivines originated from a common reservoir, i.e., RF are basically xenolithic in chondrites.

Compound chondrules formed when a chondrule collided and fused together with another chondrule, fragment or other object (Wasson et al., 1995; Arakawa and Nakamoto, 2016, 2019). Such chondrule collisions might have also led to macrochondrule formation (e.g., Weyrauch and Bischoff, 2012). Macrochondrules are similar in texture and composition to regular chondrules, only significantly larger (i.e., > 5 mm in maximum dimension; Weisberg et al., 1988). They typically contain abundant coarse-grained olivines, while low-Ca pyroxene is often only a minor constituent – a difference to regular chondrules. The mesostases of chondrules as well as macrochondrules are mostly feldspathic. Bridges and Hutchison (1997) report identical oxygen isotope compositions for macrochondrules and normal chondrules in the same meteorite. The O-isotope compositions of OC chondrules are usually  $^{16}\text{O}$ -poor and range from approx. +2 to +5‰ in  $\delta^{17}\text{O}$  and +4 to +7‰ in  $\delta^{18}\text{O}$  (Scott and Krot, 2014). It has been proposed that compound chondrules and macrochondrules represent various stages and/or ambient conditions of chondrule collisions, e.g., macrochondrules possibly formed through collisions between molten chondrules that fully merged and grew into the exceptionally large macrochondrules (Weyrauch and Bischoff, 2012; Bischoff et al., 2017; Bogdan et al., 2019).

However, no unequivocal evidence for this relationship between compound and macrochondrules has so far been reported.

Ordinary chondrites occasionally contain another group of large objects with diameters above 5 mm. These *clasts* (Bridges and Hutchison, 1997), represent a highly diverse group: they range from clearly xenolithic, chondritic fragments (e.g., impact melt clasts) to chemically fractionated objects with mineralogies and bulk compositions different from most chondrules. Therefore, these are often related to planetary differentiation processes (Hutchison et al., 1988; Bischoff et al., 1993; Ruzicka et al., 1995; Bridges et al., 1995; Bridges and Hutchison, 1997; Sokol et al., 2007; Terada and Bischoff, 2009; Rubin et al., 2017; Yokoyama et al., 2017; Crowther et al., 2018). Impact melt clasts represent a large sub-group of clasts, and likely formed when objects from as small as chondrules up to as large as planetesimals collided. They commonly represent a different chondrite group than their host chondrites. For example, Herd et al. (2013) described an impact melt clast in the Peace River L6 chondrite that formed from LL-group chondritic material. A similar object was described in NWA 5764 – a brecciated LL6 chondrite – that contains L4 clasts (Gattacceca et al., 2017). H chondrite melt clasts were detected in L (Hutchison et al., 1988), and LL chondrite hosts (Corrigan et al., 2015). Bischoff et al. (2006, and references therein) list melt clasts of various origins and formation histories. Impact melt clasts typically have microporphyritic textures, dominated by euhedral to subhedral olivine phenocrysts (e.g., Lunning et al., 2016). Pyroxenes are only observed as admixed relict grains (Metzler et al., 2011), although Fe-rich glasses of plagioclase and pyroxene-normative compositions occur frequently (e.g. Lunning et al., 2016). Many impact melt clasts completely lack any metal and sulphides (Metzler et al., 2011; Corrigan et al., 2015; Crowther et al., 2018).

Atypical objects in chondrites that are either xenolithic, rare and/or otherwise different from the common chondritic assemblage can provide unique, and in cases even pivotal clues to understand processes in the protoplanetary disk, such as chondrule formation. Here we study a large, 2 mm-sized fragment in the H3.2-an chondrite Yamato 793408, which has been described as being among the least equilibrated H chondrites by Kimura et al. (2002). This fragment has a peculiar texture and mineralogy and contains a well-preserved barred olivine (BO) chondrule.

## 4.2. Methods

### *Electron microprobe*

Mineral analyses were obtained with the electron microprobe (EMP) JEOL 8900RL at the Institute of Geology and Mineralogy, University of Cologne. The accelerating voltage was set to 15 kV and the beam current to 20 nA. The ZAF-algorithm was used for correction (Bence and Albee, 1968). Cathodoluminescence images were taken with a black and white detector mounted on the EMP. Back scattered electron (BSE) images were also taken with the EMP.

### *Oxygen isotope analyses using secondary ion mass spectrometry*

We measured the oxygen isotope compositions with a CAMECA IMS 1280 at CRPG-CNRS (Nancy, France).  $^{16}\text{O}^-$ ,  $^{17}\text{O}^-$ , and  $^{18}\text{O}^-$  ions produced by a  $\text{Cs}^+$  primary ion beam ( $\sim 15$  mm,  $\sim 4$  nA) were measured in multi-collection mode with two off-axis Faraday cups (FC) for  $^{16,18}\text{O}^-$  and the axial FC for  $^{17}\text{O}^-$ . To remove  $^{16}\text{OH}^-$  interference on the  $^{17}\text{O}^-$  peak and to maximize flatness atop the  $^{16}\text{O}^-$  and  $^{18}\text{O}^-$  peaks, the entrance and exit slits of the central FC were adjusted to obtain mass resolution power of  $\sim 7000$  for  $^{17}\text{O}^-$ . A slit #1 (MRP = 2500) was used with the multicollection FC detectors. The total measurement times were 240 s (180 s measurement + 60 s pre-sputtering). We used five terrestrial standard materials (San Carlos olivine, magnetite, glass, clinopyroxene and diopside) to define the instrumental mass fractionation line for the 3 oxygen isotopes and correct the instrumental mass fractionation (IMF) due to the matrix effect for the olivine, clinopyroxene and glass. Typical count rates obtained on the San Carlos olivine standards were  $2.5 \times 10^9$  cps for  $^{16}\text{O}$ ,  $1.0 \times 10^6$  cps for  $^{17}\text{O}$ , and  $5.4 \times 10^6$  cps for  $^{18}\text{O}$ . The  $2\sigma$  errors were  $\approx 0.2\text{‰}$  for  $\delta^{18}\text{O}$ ,  $\approx 0.4\text{‰}$  for  $\Delta^{17}\text{O}$ , and  $\approx 0.8\text{‰}$  for  $\delta^{17}\text{O}$  ( $\Delta^{17}\text{O}$  representing the deviation from the TFL,  $\Delta^{17}\text{O} = \delta^{17}\text{O} - 0.52 \times \delta^{18}\text{O}$ ).

### *$\mu$ -Raman spectroscopy*

Raman spectra were obtained with a confocal Horiba HR800 Raman spectrometer equipped with an Olympus BX41 microscope in  $180^\circ$  backscatter geometry and an EM-CCD detector at the Institute of Geoscience at the University of Bonn, Germany. Analyses were performed with a He-Ne laser (632.81 nm) with about 100 mW laser output power, a 100x objective, a 600 grooves/mm grating, a confocal hole of 500–1000  $\mu\text{m}$  and a spectrometer entrance slit width of 100  $\mu\text{m}$ , yielding a spectral resolution of approx.  $3.5 \text{ cm}^{-1}$ . Prior to analysis, the spectrometer

was calibrated with a Si standard. Spectra of samples were then measured for 3 x 10 s, their relative intensities were corrected with a white light source, and a 5<sup>th</sup> order polynomial was fitted for background subtraction.

## 4.3. Results

### 4.3.1. Petrography

Figure 4.1 displays the Y-793408 section. The unusual compound object is the largest object (~2 mm) in the section. It is metal-free and hosts a barred olivine chondrule of about 1 mm in diameter (Fig. 4.2). In the following, we discriminate between the *BO chondrule* inclusion and the surrounding *host object*. The mesostasis of the BO chondrule and the mesostasis of the host object appear to be identical. Both are fine grained (nm to ~10  $\mu\text{m}$ -sized), eutectic intergrowths of feldspar, pyroxene, silica and a few tiny spinels (Fig. 4.3). Some BO chondrule olivines have inclusions of mesostasis-like material that sometimes even show the same mineral intergrowths as the mesostases (inset b in Fig. 4.2). All olivines are fractured and have subhedral to rounded shapes. The olivines in the host object are up to ~500  $\mu\text{m}$  long, ~200  $\mu\text{m}$  wide and seem to free-float in its mesostasis. Most clinopyroxenes occur along the border of the host object and some are free-floating in its mesostasis. They sometimes also grew onto the olivines as well as onto the border of the BO chondrule. The pyroxenes are euhedral to subhedral and often show sector zoning and the typical pyroxene cleavage along [110] (Fig. 4.2). The mesostasis in the host object appears to have domains, in which the tiny minerals are oriented in the same direction. The center of the host object and the center of the BO chondrule have visible and highly localized porosities (Fig. 4.2).

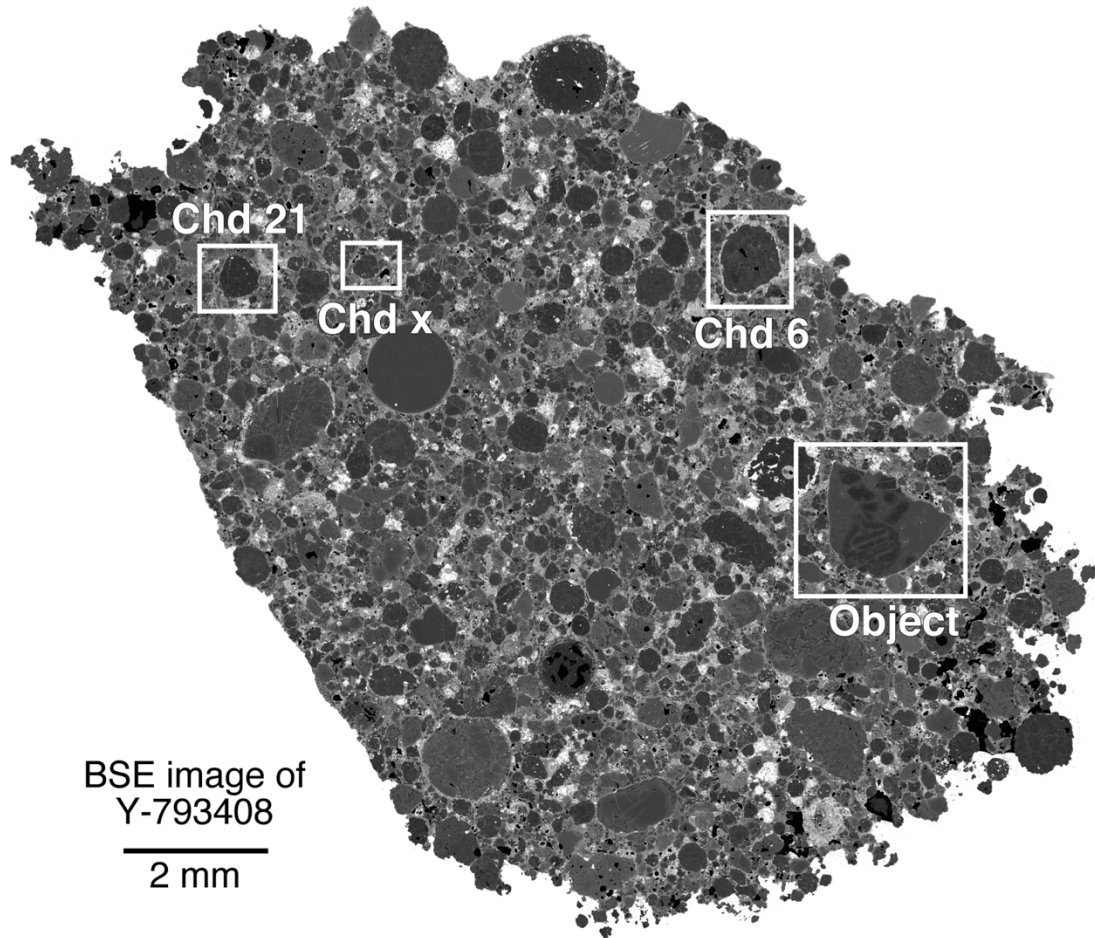


**Fig. 4.1:** BSE image overview of the Y-793408 thin section studied. The unusual compound object and three additional chondrules are shown in the boxes. We analysed the O-isotope compositions of their mineral phases.

#### 4.3.2. Element compositions of the minerals in the compound object

Table 4.1 lists representative major and minor elements of all minerals in the compound object. All olivines – no matter whether these occur in the host object or are part of the BO chondrule – are zoned with respect to several elements: FeO has the most prominent zonation from as low as 0.8 wt.% in the olivine cores to up to 8.3 wt.% at their rims. Some of the individual olivines have CaO (~0.9 wt.%) and Al<sub>2</sub>O<sub>3</sub> (~0.2 wt.%) concentrations typical of refractory forsterites (RF; Steele et al., 1986; Pack et al., 2004). Some of these olivines are CL-active – also typical of RF –, e.g., the two forsterites shown in inset a. of Fig. 4.2. Unlike the other olivines, these forsterites are unzoned and have very low FeO concentrations of 0.2 wt.%.

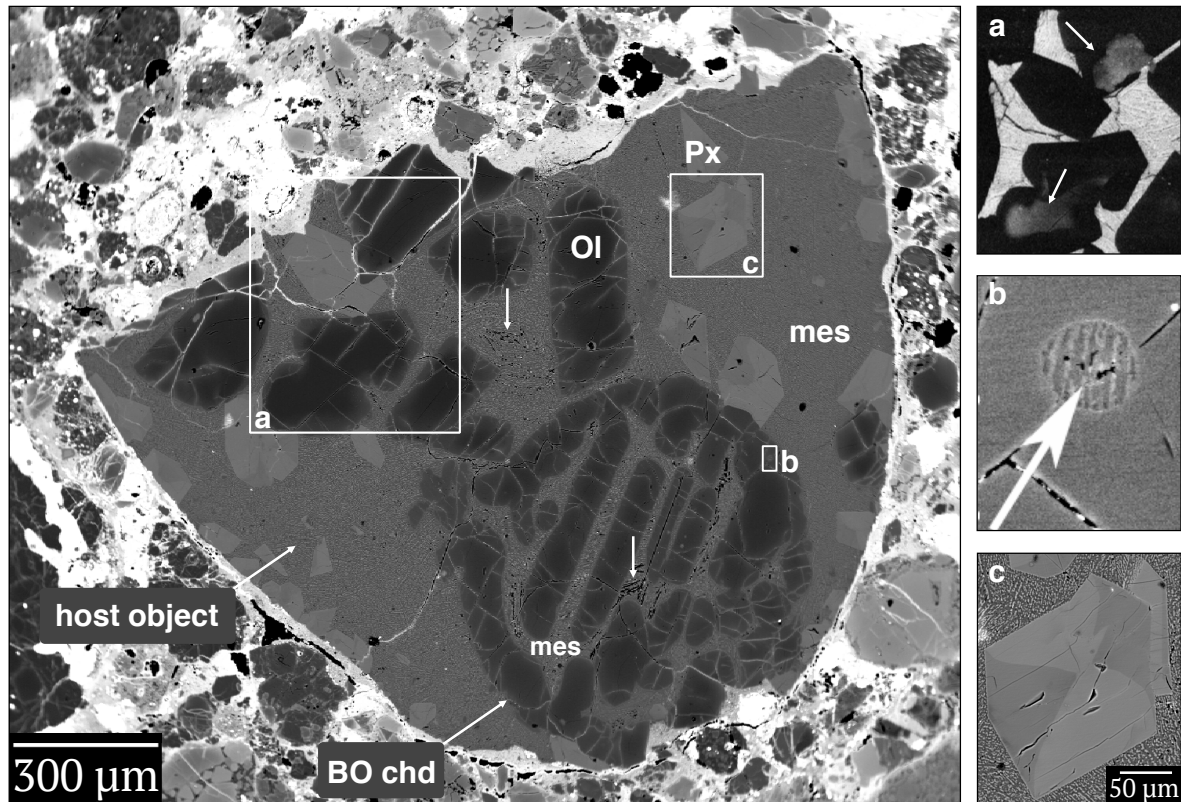


**Fig. 4.2:** BSE image of the compound object. Inset a. is a CL image. The white cores in two olivines (white arrows) are indicative of refractory forsterites with very low Fe- and high Ca, Al-concentrations. The mesostasis (mes) in the CL-image is very bright due to the abundant presence of feldspar. Inset b. shows the inclusion in a BO chondrule olivine. The texture and composition of this inclusion is identical to the mesostasis. Clinopyroxene shows sector zoning and [110]-cleavage (see close-up in inset c). White arrows in the center of the host object as well as the BO chondrule point at porosities.

The pyroxenes are clinopyroxenes and are always zoned, with sometimes textbook-like developed sector zoning (Fig. 4.2). The oxides  $\text{SiO}_2$  and  $\text{MgO}$  have higher concentrations in the pyroxene cores and lower concentrations at the rims ( $\text{SiO}_2$ -core-rim: 53.5–48.1 wt.%;  $\text{MgO}$ -core-rim: 21.1–16.3 wt.%). Inverse to this zonation,  $\text{Al}_2\text{O}_3$ ,  $\text{CaO}$ ,  $\text{Cr}_2\text{O}_3$  and  $\text{TiO}_2$  are depleted in the cores and enriched at the rims ( $\text{Al}_2\text{O}_3$ -core-rim: 3.2–10.2 wt.%;  $\text{CaO}$ -core-rim: 19.0–20.5 wt.%;  $\text{Cr}_2\text{O}_3$ -core-rim: 1.0–1.6 wt.%;  $\text{TiO}_2$ -core-rim: 0.4–1.4 wt.%).  $\text{FeO}$  (~1.9 wt.%) and  $\text{MnO}$  (~0.2 wt.%) do not show any zonation. The chemical compositions of other pyroxenes with less developed zonations range between the two extremes of the pyroxene. All pyroxenes have a fassaite component with  $\text{Al}_2\text{O}_3$  ranging between 2.9 and 10.2 wt.%. The  $\text{FeO}$ -concentration in these is low, between 1.8 and 2.0 wt.%.

The fine-crystalline material in the host object's mesostasis and the mesostasis of the BO chondrule are compositionally identical: both are high in  $\text{SiO}_2$  (51 wt.%),  $\text{Al}_2\text{O}_3$  (22 wt.%),  $\text{CaO}$  (14 wt.%), and low in  $\text{MgO}$  (7 wt.%) and  $\text{FeO}$  (2 wt.%).

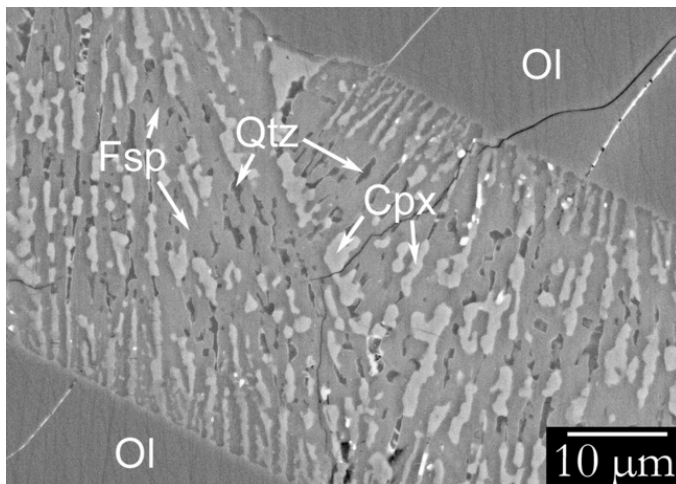
**Table 4.1:** Representative mineral element compositions.

Host Object	Ol-1	Ol-1 inc in Ol-1	Ol	Ol	Ol rim	Ol core	CL-OL	CL-OL	por Px	por Px	por Px rim or Px core	fc Px	fc Fsp	mesA	mesA <sup>3</sup>		
SiO <sub>2</sub>	41.23	41.94	38.90	41.60	42.16	41.26	42.61	41.97	42.10	50.26	48.42	48.14	53.45	54.10	49.58	51.58	51.32
TiO <sub>2</sub>	<d.l.	0.05	1.72	<d.l.	<d.l.	0.03	<d.l.	<d.l.	<d.l.	0.98	1.05	1.37	0.44	1.14	0.24	1.64	0.74
Al <sub>2</sub> O <sub>3</sub>	0.04	0.17	24.77	0.10	0.05	0.05	0.04	0.17	0.20	7.68	8.84	10.22	3.19	6.17	30.42	20.55	22.57
Cr <sub>2</sub> O <sub>3</sub>	0.07	0.14	0.47	0.13	0.12	0.30	0.16	0.05	0.08	1.58	1.72	1.63	1.00	0.67	<d.l.	0.37	0.27
FeO	6.62	1.05	0.36	3.38	0.87	8.27	0.81	0.19	0.19	1.77	1.85	1.86	1.91	7.37	0.47	3.28	2.60
MnO	0.05	<d.l.	<d.l.	0.03	0.03	<d.l.	<d.l.	<d.l.	0.04	0.10	0.21	0.22	0.14	0.41	<d.l.	0.20	0.17
MgO	51.72	56.00	8.83	54.05	56.12	49.85	56.62	56.68	56.50	17.01	16.78	16.32	21.10	21.62	1.00	7.08	6.30
CaO	0.11	0.65	25.07	0.49	0.56	0.30	0.41	0.88	0.76	20.60	20.85	20.47	18.99	9.79	16.40	13.63	14.27
Na <sub>2</sub> O	<d.l.	<d.l.	<d.l.	<d.l.	<d.l.	<d.l.	<d.l.	<d.l.	<d.l.	<d.l.	<d.l.	<d.l.	<d.l.	0.15	2.02	0.63	1.49
K <sub>2</sub> O	0.04	<d.l.	<d.l.	<d.l.	<d.l.	<d.l.	<d.l.	<d.l.	<d.l.	<d.l.	<d.l.	<d.l.	<d.l.	<d.l.	0.05	<d.l.	<d.l.
Total	99.93	100.05	100.16	99.83	99.94	100.27	100.68	99.97	99.94	100.02	99.75	100.28	100.26	101.43	100.20	98.97	99.74

Barred Olivine Chondrule	Ol	Ol	Ol rim	Ol core	Ol rim	Ol core	inc in Ol	inc in Ol	Spl	fc Px	fc Fsp	fc Silica	mesB <sup>2</sup>	mesB <sup>4</sup>
SiO <sub>2</sub>	41.23	41.39	41.09	41.11	41.26	41.92	50.44	50.18	1.13	52.47	49.15	92.05	51.65	53.58
TiO <sub>2</sub>	<d.l.	0.05	0.03	<d.l.	<d.l.	<d.l.	1.16	0.48	0.49	2.24	0.37	0.50	0.91	0.53
Al <sub>2</sub> O <sub>3</sub>	0.10	0.03	0.09	0.07	0.07	0.08	21.41	20.86	51.16	3.53	29.81	2.89	21.11	23.08
Cr <sub>2</sub> O <sub>3</sub>	0.26	0.14	0.18	0.21	0.08	0.19	0.50	0.38	14.09	1.54	0.12	<d.l.	0.35	0.20
FeO	4.33	7.34	4.48	3.08	5.45	2.70	0.74	2.22	13.96	5.12	0.49	0.43	2.20	1.11
MnO	0.11	0.15	0.09	0.05	0.16	0.08	<d.l.	0.09	0.13	0.37	0.05	<d.l.	0.10	0.05
MgO	53.24	51.42	53.08	54.18	52.33	54.63	3.96	10.01	17.21	17.42	1.18	0.74	7.16	5.65
CaO	0.33	0.29	0.27	0.43	0.20	0.41	15.20	12.28	0.30	18.47	16.30	2.57	14.82	13.91
Na <sub>2</sub> O	<d.l.	<d.l.	<d.l.	<d.l.	<d.l.	<d.l.	5.67	2.06	<d.l.	0.08	2.57	0.32	0.81	1.77
K <sub>2</sub> O	<d.l.	<d.l.	<d.l.	<d.l.	<d.l.	<d.l.	<d.l.	<d.l.	<d.l.	<d.l.	<d.l.	<d.l.	<d.l.	<d.l.
Total	99.60	100.79	99.30	99.13	99.57	100.03	99.09	98.62	98.50	101.24	100.06	99.54	99.13	99.91

‘Host object’ is the object surrounding the barred olivine chondrule. Ol: olivine; inc: inclusion; CL-OL: cathodoluminescence active olivine; por Px: porphyritic pyroxene crystals in the host object; mesA: mesostasis in the host object; mesA<sup>3</sup>: mean from 55 points; fc Px: fine-crystalline pyroxene in mesA; fc Fsp: fine-crystalline feldspar in mesB; Spl: spinel; mesB: BO mesostasis; mesB<sup>2</sup>: mean from 29 points; mesB<sup>4</sup>: mean from 17 points



**Fig. 4.3:** BSE image enlargement of BO chondrule mesostasis. Mesostases in BO chondrule and host object appear to be petrographically and chemically identical.

#### 4.3.3. Silica is quartz in the BO mesostasis and cristobalite in the host object’s mesostasis

The silica polymorphs in the fine-crystalline mesostases of BO chondrule and host object are different – despite otherwise almost identical petrographic and petrologic characteristics of both mesostases. The silica in the BO chondrule is quartz, while the silica in the host object is cristobalite. Representative  $\mu$ -Raman spectra of the silica polymorphs in the respective mesostases are displayed in Fig. 4.4.

## 4.3.4. Mineral O-isotope compositions

We measured the O-isotope compositions of the mineral phases in the compound object and three additional chondrules (Table 4.2; cf. Fig. 4.1). Figure 4.5a displays the results from the compound object. The  $\delta^{17}\text{O}$  compositions of the BO chondrule olivines are systematically shifted to lighter values by – on average – 0.8 ‰, and compared to the individual olivine grains in the host object. The porphyritic pyroxenes in the host object are lighter than all olivines in the host object, in both  $\delta^{17}\text{O}$  and  $\delta^{18}\text{O}$ , and by – on average – about 1 ‰. Both mesostases span a surprisingly large range, although most analyses fall roughly in between the olivine and pyroxene compositions of the host object.

The O-isotope compositions of all minerals in the compound object are similar or slightly shifted to lighter compositions when compared to ordinary chondrite bulk O-isotope compositions. The opposite is observed for the O-isotope compositions of all minerals in the three other chondrules studied: all of these are shifted to slightly heavier compositions when compared to ordinary chondrite bulk O-isotope compositions. However, within the error these are almost identical. The olivines in the three other chondrules are always lighter by a few permil than the pyroxenes, while the mesostasis has a roughly similar composition as pyroxene. This is a similar pattern as in the compound object. One olivine grain in chondrule 6 has a very light composition of -6.49 ‰ in  $\delta^{17}\text{O}$  and -6.71 ‰ in  $\delta^{18}\text{O}$  (inset in Fig. 4.5b).

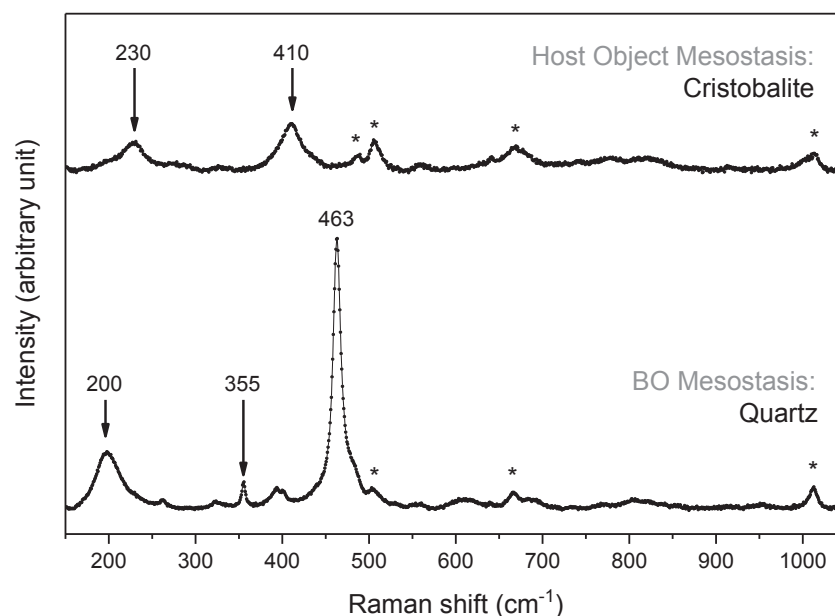


**Fig. 4.5:** Representative Raman spectra of  $\text{SiO}_2$  phases in the host object's mesostasis and the BO mesostasis, identified as cristobalite and quartz, respectively. For reference spectra of alpha-quartz, the reader is referred to Scott and Porto (1967), Etchepare et al. (1974), and Nasdala et al. (2004) and for cristobalite to Etchepare et al. (1978). Asterisks mark Raman bands originating from laser scattering of adjacent feldspar and clinopyroxene grains.

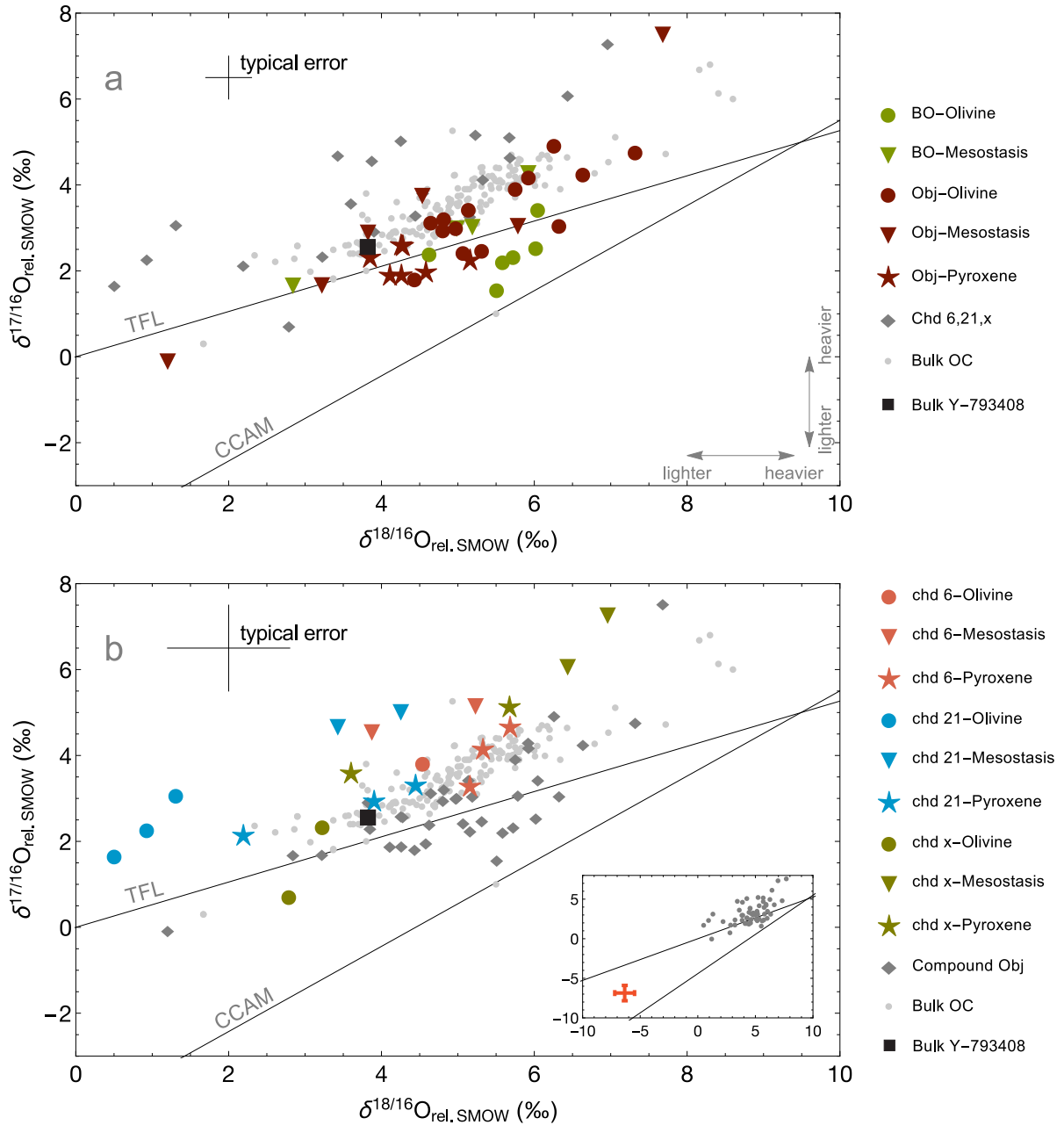


**Fig. 4.6:** a. Mineral O-isotope compositions of the compound object. b. Mineral O-isotope compositions of the 3 other chondrules (cf. Fig. 4.1). The blue dot in the inset represents one olivine grain in chondrule 6, with significantly lighter O-isotope composition than all other studied mineral grains. Grey dots in the inset represent all measured chondrule mineral values. Grey dots in a. are the data from the 3 other chondrules, and grey dots in b. are the data from the compound object. Black dots represent a selection of ordinary chondrite bulk O-isotope compositions taken from MetBase (2017). Bulk Y-793408 (2.52‰ in  $\delta^{17}\text{O}$  and 3.87‰ in  $\delta^{18}\text{O}$ ) was taken from Kimura et al. (2002). TFL: terrestrial fractionation line; CCAM: carbonaceous chondrite anhydrous mixing line (cf. Young and Russell, 1998; Kita et al., 2008)

**Table 4.2:** O-isotope composition of chondrule and host object minerals.

Phase	Location	Point	$\delta^{18}\text{O}$	2 s.e.	$\delta^{17}\text{O}$	2 s.e.
olivine	Host-obj	1	6.26	0.29	4.93	0.39
olivine	Host-obj	2	4.64	0.29	3.14	0.43
olivine	Host-obj	3	4.97	0.29	3.01	0.40
olivine	Host-obj	4	5.92	0.29	4.19	0.39
olivine	Host-obj	5	6.63	0.29	4.26	0.41
olivine	Host-obj	6	5.14	0.29	3.44	0.41
olivine	Host-obj	7	4.65	0.29	3.06	0.46
olivine	Host-obj	8	5.31	0.29	2.49	0.45
olivine	Host-obj	9	6.32	0.29	3.07	0.44
olivine	Host-obj	10	4.43	0.29	1.82	0.53
olivine	Host-obj	11	7.32	0.29	4.78	0.39
olivine	Host-obj	12	4.81	0.29	3.23	0.45
olivine	Host-obj	13	4.80	0.29	2.96	0.43
olivine	Host-obj	14	5.07	0.29	2.44	0.45
olivine	Host-obj	15	5.75	0.29	3.93	0.39
olivine	Host-obj	16	3.84	0.29	2.78	0.47
pyroxene	Host-obj	17	3.85	0.54	2.31	0.90
pyroxene	Host-obj	18	4.25	0.54	2.60	0.89
pyroxene	Host-obj	19	4.32	0.54	4.43	0.86
pyroxene	Host-obj	20	4.26	0.54	1.90	0.97
pyroxene	Host-obj	21	4.58	0.54	1.97	0.97
pyroxene	Host-obj	22	5.77	0.54	3.09	0.89
pyroxene	Host-obj	23	5.16	0.54	2.25	0.94
pyroxene	Host-obj	24	4.11	0.54	1.89	0.94
pyroxene	Host-obj	25	4.28	0.54	2.58	0.93
pyroxene	Host-obj	26	4.09	0.54	3.51	0.88
pyroxene	Host-obj	27	5.77	0.54	3.93	0.88
mesostasis	Host-obj	39	1.20	0.48	-0.07	2.13
mesostasis	Host-obj	40	3.22	0.29	1.70	0.58
mesostasis	Host-obj	46	5.04	0.11	3.03	0.68
mesostasis	Host-obj	47	4.53	0.11	3.79	0.59
mesostasis	Host-obj	48	3.82	0.11	2.93	0.66
mesostasis	Host-obj	49	5.78	0.10	3.08	0.67
mesostasis	Host-obj	50	7.68	0.09	7.54	0.58
olivine	BO	28	5.51	0.29	1.57	0.56
olivine	BO	29	4.87	0.29	2.79	0.48
olivine	BO	30	5.72	0.29	2.34	0.47
olivine	BO	31	5.58	0.29	2.22	0.49
olivine	BO	32	6.04	0.29	3.44	0.42
olivine	BO	33	6.02	0.29	2.55	0.44
olivine	BO	34	4.62	0.29	2.41	0.43
olivine	BO	35	5.19	0.29	3.06	0.41
mesostasis	BO	36	2.84	0.29	1.70	0.64
mesostasis	BO	37	4.98	0.28	3.03	0.44
mesostasis	BO	38	5.92	0.28	4.31	0.40
pyroxene	chd 6	51	5.32	0.83	4.14	0.98
pyroxene	chd 6	52	5.15	0.83	3.28	1.08
olivine	chd 6	53	-6.49	0.81	-6.71	0.92
olivine	chd 6	54	4.54	0.81	3.83	0.95
pyroxene	chd 6	55	5.68	0.82	4.66	0.97
mesostasis	chd 6	56	5.23	0.81	5.19	0.93
mesostasis	chd 6	57	3.87	0.82	4.58	0.95
olivine	chd 21	58	0.50	1.81	1.67	1.11
olivine	chd 21	59	1.31	0.87	3.08	0.96
olivine	chd 21	60	0.93	0.95	2.28	0.99
pyroxene	chd 21	61	4.44	0.85	3.31	1.10
pyroxene	chd 21	62	3.90	1.16	2.93	1.33
pyroxene	chd 21	63	2.19	0.84	2.14	1.20
mesostasis	chd 21	64	3.43	0.82	4.70	0.94
mesostasis	chd 21	65	4.25	0.82	5.05	0.94
olivine	chd x	66	2.79	0.82	0.72	3.89
olivine	chd x	67	3.22	0.82	2.35	1.00
pyroxene	chd x	68	3.60	6.75	3.59	1.00
pyroxene	chd x	69	5.67	0.82	5.13	0.95
mesostasis	chd x	70	6.96	0.81	7.30	0.93
mesostasis	chd x	71	6.43	0.81	6.10	0.93

All data given in ‰ and relative to the SMOW standard.

## 4.4. Discussion

Unusual objects, such as xenolithic clasts are rare and highly diverse constituents of ordinary chondrites (e.g., Bischoff et al., 2006, 2019). Their unusual and, in cases, unique properties often prohibit assigning these to known formation processes and places of origin. This means, studying these objects allows insights to processes and mechanisms in the early solar system that are otherwise concealed. The compound object we studied here is particularly interesting, as it appears to be of a new type. To our knowledge, no similar large, mesostasis- and refractory-rich object, hosting an intact BO inclusion, has been described before. In the following, we discuss the characteristics, origin and evolution of the Y-793408 compound object, and compare it to other rare and unusual objects in chondrites, in particular to macrochondrules and impact melt clasts.

### *4.4.1. Mineralogy, structure and petrography of the Y-793408 compound object*

The compound object is a fragment and must have originally been significantly larger. Based on its shape, it was likely round and up to twice its current size, with an original diameter of ~5 mm. As both, macrochondrules (Weyrauch and Bischoff, 2012) and xenolithic clasts (Bridges and Hutchison, 1997) are frequently fragmented, the broken nature of the compound object is no indication of its origin.

The occurrence of an intact barred olivine chondrule found inside the compound object is particularly remarkable and distinctive. An equally rare clast hosting a barred olivine chondrule was found in the Y-793241 (L6) chondrite (Prinz et al., 1984). However, this clast has a Brachina-like, Ca,Al-poor mineralogy with no individual, large pyroxene or olivine grains and is therefore very different from the compound object studied here. Sokol et al. (2007) reported large (3 mm) clasts in the very primitive Adrar 003 LL(L)3 chondrite, with some of them containing intact BO chondrules. In contrast to their host meteorite, these clasts are strongly metamorphosed and therefore clearly xenolithic. The original textures and compositions of the fragments were largely homogenised during thermal metamorphism on their parent body. To our knowledge, these are the only other clasts hosting BO chondrules reported in the literature. However, these are otherwise very different from the compound object studied here, making the compound object so far unique.

To retain its original BO texture, the chondrule in the compound object must have been in a solid state when it was incorporated into its molten host. We suggest two different formation

scenarios: (i) the compound object formed in the solar nebula, when the molten host object collided with a BO chondrule. This scenario then constrains the relative particle velocities and particle temperatures, i.e., the collision velocity could not have been high, as otherwise the BO chondrule would not have gotten stuck inside the host object (cf. Arakawa and Nakamoto, 2016, 2019; Bogdan et al., 2019). Bogdan et al. (2019) found experimentally that colliding particles at low velocities ( $<1$  m/s) can fully merge and homogenise, thereby forming macrochondrules. We suggest that the compound object studied here could then represent an intermediate stage between compound and macrochondrule formation. According to the findings of Bogdan et al. (2019), the host object and BO chondrule might have collided with an approximate relative velocity below 1 m/s and at a temperature above 1200°C.

Alternatively, (ii) the host object could represent an impact melt that incorporated variable amounts of clastic debris, produced during the impact or collision. The BO chondrule would then represent a piece of such unmelted debris. This scenario is supported by chondrules that occasionally occur as relicts in impact melts, and which were incorporated together with other clasts of the target rock (see Fig. 7a of Bischoff et al., 2019 or Fig. 4b in Morlok et al., 2017 from the Chelyabinsk melt lithology). However, the large sizes of the individual free-floating olivine grains are atypical when compared to impact melt clast textures described in the literature, which are usually microporphyritic (e.g., Lunning et al., 2016). It is rather likely that the free-floating olivine grains in the host object are remnants of one or more other chondrules that were added to the host object with which the BO chondrule collided.

Therefore, the first scenario seems more likely, and we suggest that the initial host object was a rare, but not unusual large (macro)chondrule, dominated by significant amounts of mesostasis-like material. We then suggest that the molten host object (mesostasis melting point:  $\sim 1100$ – $1200$ °C at 1 atm; Anderson, 1915) collided with other chondrules at ambient temperatures slightly below the olivine melting point (forsterite: 1800°C at 1 atm; Kirkpatrick et al., 1983). Chondrules trapped in the host object would then dissolve and their olivines would be scattered throughout the host object. The solid olivine shell surrounding the BO chondrule could have protected this chondrule from dissolving. However, openings in this shell would have allowed exchange of mesostasis material between the host object and the BO chondrule. The identical compositions of mesostasis in the BO chondrule and the host object support material exchange between both mesostases. Alternatively, the homogeneity of BO and host object mesostases is a primary feature. In this case, both mesostases formed at the same time,

from the same precursor material and in the same location, thus resulting in the observed chemical similarity.

The free-floating, large, euhedral pyroxene crystals are located at the borders of the host object, and, to a smaller extent, also on the surfaces of the free-floating olivines and the BO chondrule. These sites likely acted as nucleation points of the pyroxenes. The unusually high Al and Ti concentrations in the pyroxenes support in-situ crystallisation from the Al-, Ti-rich host chondrule melt (see Table 4.1). Pyroxenes have crystallisation temperatures in between olivine and mesostasis, around 1550°C (at 1 atm; Kirkpatrick et al., 1983). Their large sizes indicate that the compound object was exposed to this temperature for a prolonged time, before it was quenched and the mesostasis formed. This would perfectly agree with the aforementioned scenario in which chondrules were added to, or in combination constituted the initial host object. The chondrules were incorporated and dissolved slightly below the olivine melting point, i.e., at temperatures around 1550°C. This temperature pertained for some time after or during ongoing collisions to allow pyroxene crystallisation and, possibly, material exchange between the host object and BO chondrule mesostases. This temperature is also in good agreement with the minimum temperature required to form such objects in experiments (i.e., > 1200°C for macrochondrule formation; Bogdan et al., 2019).

The mesostases in the host object and the BO chondrule have different silica polymorphs: alpha-quartz in the BO chondrule and cristobalite in the host object. Silica is a common, albeit not a frequent constituent of OC chondrules and clasts in OC (e.g. Krot and Wasson, 1994; Hezel et al. 2006, and references therein). It usually occurs as tridymite and cristobalite, whereas quartz is rare. The presence of the high-temperature SiO<sub>2</sub> polymorphs in chondrules is typically interpreted to reflect fast cooling (e.g., Hezel et al., 2006,2003). The cristobalite in the host object might therefore represent fast cooling. The fast temperature drop requires a sudden cool surrounding, as is typical for the fast temperature drop after the chondrule high-T formation event. Alternatively, the host object's mesostasis might have been quenched by the BO chondrule, if the BO chondrule was significantly cooler than the host object during their collision. In this case, the mesostases could not have exchanged material between host object and BO chondrule, nor could the pyroxenes have crystallised on the BO olivine surfaces (cf. Fig. 4.2). We therefore propose that the host object and the BO chondrule had similar temperatures when they collided, i.e., around 1550°C, as indicates above. The cristobalite in the host object likely formed during the sudden and typical temperature drop shortly after

chondrule formation. The olivine shell of the BO chondrule might have slowed cooling of the BO chondrule mesostasis, in which then silica was transformed into alpha-quartz.

#### 4.4.2. O-isotope composition of the compound object

The oxygen isotope compositions of the phases in the compound object plot mostly in the field of ordinary chondrites and their chondrules (Fig. 4.5a; e.g., Clayton et al., 1991; Scott and Krot, 2014). A rough estimate of the bulk O-isotope composition of the compound object (using modal recombination) is  $\sim 4.9$  in  $\delta^{18}\text{O}$  and  $\sim 2.9$  in  $\delta^{17}\text{O}$ . This is consistent with an OC origin of the compound object, while a xenolithic origin is unlikely.

The compound object's olivines are  $^{18}\text{O}$ -enriched compared to olivines in three additional chondrules measured in Y-793408. The same is true for all phases in the compound object, when comparing these to the whole rock O-isotope composition of Y-793408 (black square in Fig. 4.5): the  $\delta^{18}\text{O}$  of all phases in the compound object are shifted towards heavier compositions by up to  $\sim 3\%$ . However, their  $\delta^{17}\text{O}$  are – within error – mostly identical to bulk Y-793408, thereby indicating some mass-independent O-isotope fractionation of the phases in the compound object.

The mesostases in the BO chondrule and host object are compositionally identical and rich in refractory elements (Al, Ca, Ti). Refractory material was obviously a major part of the precursor objects that formed the host chondrule. However, only small amounts of CAI material could have been added to the compound object as the oxygen isotope composition of the mesostases plot mostly in the field of OC, and not towards  $^{16}\text{O}$ -rich compositions, indicative of CAIs (e.g., Scott and Krot, 2014, and references therein). The large amounts of refractory material contributing to the mesostasis likely originated from the same source as all of the material that formed the object studied. However, as some data plot below the terrestrial fractionation line, minor contributions of  $^{16}\text{O}$ -rich (e.g., CAI) material cannot be excluded.

The O-isotope composition of the host object mesostasis has a large scatter, bracketed by the lightest and heaviest O-isotope compositions of all the phases. As these compositions plot on a non-mass-dependent trend, these likely reflect some exchange of material with the surrounding gas (e.g., Tissandier et al., 2002; Hezel et al., 2003; Krot et al., 2004; Libourel et al., 2006; Jacquet et al., 2012; Di Rocco and Pack, 2015; Friend et al., 2016; Metzler and Pack, 2016; Soulié et al., 2017; Ebel et al., 2018; Barosch et al., 2019), i.e., an initially lighter material

exchanged O-isotopes with a heavier gas, e.g., heavy water as found in cosmic symplectites (Sakamoto et al., 2007).

#### 4.4.3. Origin of Ca,Al-rich olivine cores

The Ca,Al-, and Fe-concentration of a few forsteritic olivine cores in the compound object are typical for RF and occur as free-floating grains next to other individual, but apparently non-refractory olivines. The O-isotope composition of these refractory olivines are, however, similar to typical OC chondrule olivines, and thereby unlike the  $^{16}\text{O}$ -enriched isotope compositions of RF ( $\Delta^{17}\text{O}$  between -4 and -10‰; Weinbruch et al., 2000; Pack et al., 2004, 2005). It has been proposed that RF formed by fractional crystallisation of refractory condensed melts that experienced gas-melt interactions (Pack et al., 2005). It is since then generally assumed that RF represent  $^{16}\text{O}$ -rich relict olivine that crystallised early in the thermal history of chondrules (Pack et al., 2004) or were inherited from chondrule precursors (Jones et al., 2004). However, it has been shown recently that  $^{16}\text{O}$ -rich relict chondrule olivine grains are rather Ca-Al-Ti poor (Marrocchi et al., 2018), which is inconsistent with the previous idea that refractory-enriched grains are relicts (Pack and Palme, 2003; Pack et al., 2004). Further, Libourel and Portail (2018) and Marrocchi et al. (2018, 2019) suggest that RF formed together with other chondrule olivine grains by epitaxial growth during gas-melt interactions. These RF show constant  $\Delta^{17}\text{O}$  within a single chondrule and between different chondrules, thus reflecting interaction with an  $^{16}\text{O}$ -poor gas in the chondrule-forming region (Marrocchi et al., 2018). In the compound object studied here, the RF do not show  $^{16}\text{O}$ -rich isotope compositions. This supports our suggestion that all free-floating olivines are in fact remnants of one or more chondrules that collided and constituted the macrochondrule with which the BO chondrule collided (cf. Section 4.4.1).

## 4.5. Conclusions

We found a unique compound object in Y-793408 (H3.2-an) that is composed of at least two sub-components: (i) a large *host object*, likely a mesostasis-rich macrochondrule with individual, free floating, large olivine grains in the mesostasis. Some olivines contain  $^{16}\text{O}$ -poor, forsteritic cores. (ii) A *BO chondrule* trapped in the macrochondrule.

We conclude that the compound object is the fragment of a macrochondrule that collided with and preserved a BO chondrule. If correct, the object appears to be the first macrochondrule

with another object still inside it, and thereby provides the first petrographic evidence that compound chondrules and macrochondrules are indeed genetically related, as e.g., suggested by Bogdan et al. (2019). The object studied therefore allows new insights into macrochondrule formation, their temperature evolution and details of their formation process.

We suggest that the compound object formed in a nebular setting as follows: first, the mesostasis-rich host object formed by collisions and subsequent merging of molten chondrules, similar to compound chondrule formation (Weyrauch and Bischoff, 2012; Bogdan et al., 2019). The free-floating, large olivines represent disaggregated remnants of other chondrules that collided and built the macrochondrule. At least one of these initial chondrules must have consisted of large amounts of mesostasis material, in which the other chondrules dissolved and thereby disintegrated, which then dispersed their olivine grains throughout the macrochondrule. One of the colliding objects was a BO chondrule that got trapped inside the host object, i.e., the macrochondrule. The olivines at the BO chondrule's border likely protected the BO chondrule from disintegration. The mesostasis of the BO chondrule possibly exchanged material with the host object, thereby homogenising both mesostases. During and after these low velocity collisions ( $< 1\text{m/s}$ ; Bogdan et al., 2019), the macrochondrule remained in a molten state for some time. The temperatures must have been below the forsterite melting point, i.e., below  $1800^{\circ}\text{C}$ , at around the pyroxene crystallisation point of  $1550^{\circ}\text{C}$  (Kirkpatrick et al., 1983), during which the pyroxenes at the border of the host object and some olivines formed. The mesostasis was then quenched, preserving cristobalite in the host object. The BO chondrule mesostasis might have cooled a little slower, maybe due to thermal insulation from the olivine shell, thereby allowing a reconstructive transformation of cristobalite to quartz.

A few of the free-floating olivine grains are RF and likely formed from gas-melt interaction with an  $^{16}\text{O}$ -poor gas (Marrocchi et al., 2018, 2019; Libourel and Portail, 2018), rather than being relict olivines (e.g., Jones et al., 2004).

### **Acknowledgements**

We would like to thank Addi Bischoff, Natasha Almeida, Claudia Funk and Marc Chaussidon for helpful discussions and support in the early stage of this work. We thank the National Institute of Polar Research, Japan for the loan of Y-793408. This research was supported with a grant to DH through the Europlanet 2020 RI call for Transnational Access of the European Science Foundation. Europlanet 2020 RI has received funding from the European Union's

Horizon 2020 research and innovation programme under grant agreement No. 654208. DH gratefully acknowledges funding of this study by the Deutsche Forschungsgemeinschaft (DFG) grants HE 5352/10-1 and PA 346/50-1. JB gratefully acknowledges funding by Fellowship Grant No. GSGS-2019X-02 of the Graduate School of Geosciences, University of Cologne. We thank K. Metzler and S. S. Russell for their thorough and helpful reviews, as well as associate editor G. Benedix for her work.

## References

- Andersen O. 1915. The system anorthite-forsterite-silica. *American Journal of Science* 232:407–454.
- Arakawa S. and Nakamoto T. 2016. Compound chondrule formation via collision of supercooled droplets. *Icarus* 276:102–106.
- Arakawa S. and Nakamoto T. 2019. Compound chondrule formation in optically thin shock waves. *The Astrophysical Journal* 877:84–100.
- Barosch J., Hezel D. C., Ebel D. S. and Friend P. 2019. Chondrule open system behaviour in ordinary chondrites. *Geochimica et Cosmochimica Acta* 249:1–16.
- Bence A. E. and Albee A. L. 1968. Empirical correction factors for the electron micro-analysis of silicates and oxides. *Journal of Geology* 76:382–403.
- Bischoff A., Geiger T., Palme H., Spettel B., Schultz L., Scherer P., Schlüter J. and Lkhamsuren J. 1993. Mineralogy, chemistry, and noble gas contents of Adzhi-Bogdo – an LL3-6 chondritic breccia with L-chondritic and granitoidal clasts. *Meteoritics* 28:570–578.
- Bischoff A., Scott E. R. D., Metzler K. and Goodrich C. A. 2006. Nature and origins of meteoritic breccias. In: *Meteorites and the early solar system II*, edited by D. S. Lauretta and H. Y. McSween Tucson, AZ: The University of Arizona Press. pp. 679–712.
- Bischoff A., Wurm G., Chaussidon M., Horstmann M., Metzler K., Weyrauch M. and Weinauer J. 2017. The Allende multicomponent chondrule (ACC) – Chondrule formation in a local super-dense region of the early solar system. *Meteoritics & Planetary Science* 52:906–924.
- Bischoff A., Schleiting M. and Patzek M. 2019. Shock stage distribution of 2280 ordinary chondrites – Can bulk chondrites with a shock stage of S6 exist as individual rocks? *Meteoritics & Planetary Science* 54:1–14.

- Bogdan T., Teiser J., Fischer N., Kruss M. and Wurm G. 2019. Constraints on compound chondrule formation from laboratory high-temperature collisions. *Icarus* 319:133–139.
- Bridges J. C., Franchi I. A., Hutchison R., Morse A. D., Long J. V. P. and Pillinger C. T. 1995. Cristobalite- and tridymite-bearing clasts in Parnallee (LL3) and Farmington (L5). *Meteoritics* 30:715–727.
- Bridges J. C. and Hutchison R. 1997. A survey of clasts and large chondrules in ordinary chondrites. *Meteoritics & Planetary Science* 32:389–394.
- Clayton R. N., Mayeda T. K., Goswami J. N. and Olsen E. J. 1991. Oxygen isotope studies of ordinary chondrites. *Geochimica et Cosmochimica Acta* 55:2317–2337.
- Corrigan C. M., Lunning N. G. and Ziegler K. 2015. An H chondrite melt clast in an LL chondrite: Evidence for mixing of ordinary chondrite parent bodies. In *46th Lunar and Planetary Science Conference*, abstract #2678.
- Crowther S. A., Filtner M. J., Jones R. H. and Gilmour J. D. 2018. Old formation ages of igneous clasts on the L chondrite parent body reflect an early generation of planetesimals or chondrule formation. *Earth and Planetary Science Letters* 481:372–386.
- Di Rocco T. D. and Pack A. (2015) Triple oxygen isotope exchange between chondrule melt and water vapor: an experimental study. *Geochimica et Cosmochimica Acta* 164:17–34.
- Ebel D. S., Alexander C. M. O'D and Libourel G. 2018. Vapor-melt exchange – Constraints on chondrite formation conditions and processes. In: *Chondrules: Records of Protoplanetary Disk Processes*, ed. S. S. Russell, H. C. Connolly, Jr., & A. N. Krot (Cambridge: Cambridge Univ. Press).
- Etchepare J., Merian M. and Smetankine L. 1974. Vibrational normal modes of SiO<sub>2</sub>. I. a- and b-quartz. *The Journal of Chemical Physics* 60:1873–1876.
- Etchepare J., Merian M. and Kaplan P. 1978. Vibrational normal modes of SiO<sub>2</sub>. II. cristobalite and tridymite. *The Journal of Chemical Physics* 68:1531–1537.
- Gattacceca J., Krzesinska A., Marrocchi Y., Meier M. M. M., Bourot-Denise M. & Lenssen R. 2017. Asteroid mixing revealed by NWA 5764, a polymict LL breccia with L clasts. *Meteoritics & Planetary Science* 52:2289–2304.
- Friend P., Hezel D. C. and Mucerschi D. 2016. The conditions of chondrule formation, Part II: Open system. *Geochimica et Cosmochimica Acta* 173:198–209.
- Herd C. D., Friedrich J. M., Greenwood R. C. and Franchi I. A. 2013. An igneous-textured clast in the Peace River meteorite: insights into accretion and metamorphism of asteroids in the early solar system. *Canadian Journal of Earth Sciences* 50:14–25.

- Hewins R. H., Connolly Jr. H. C., Lofgren G. E. and Libourel G. 2005. Experimental constraints on chondrule formation. In *Chondrites and the Protoplanetary Disk*, vol. 341 (eds. A. N. Krot, E. R. D. Scott and B. Reipurth):286–316.
- Hezel D. C., Palme H., Brenker F. E. and Nasdala L. 2003. Evidence for fractional condensation and reprocessing at high temperatures in CH-chondrites. *Meteoritics & Planetary Science* 38:1199–1216.
- Hezel D. C., Palme H., Nasdala L. and Brenker F. E. 2006. Origin of SiO<sub>2</sub>-rich components in ordinary chondrites. *Geochimica et Cosmochimica Acta* 70:1548–1564.
- Hutchison R., Williams C. T., Din V. K., Clayton R. N., Kirschbaum C., Paul R. L. and Lipschutz M. E. 1988. A planetary, H-group pebble in the Barwell, L6, unshocked chondritic meteorite. *Earth and Planetary Science Letters* 90:105–118.
- Jacquet E., Alard O. and Gounelle M. 2012. Chondrule trace element geochemistry at the mineral scale. *Meteoritics & Planetary Science* 47:1695–1714.
- Jones R. H., Leshin L. A., Guan Y., Sharp Z. D., Durakiewicz T. and Schilk A. J. 2004. Oxygen isotope heterogeneity in chondrules from the Mokoia CV3 carbonaceous chondrite. *Geochimica et Cosmochimica Acta* 68:3423–3438.
- Kimura M., Hiyagon H., Palme H., Spettel B., Wolf D., Clayton R. N., Mayeda T. K., Sato T., Suzuki A. and Kojima H. 2002. Yamato 792947, 793408 and 82038: The most primitive H chondrites, with abundant refractory inclusions. *Meteoritics & Planetary Sciences* 37:1417–1434.
- Kirkpatrick R. J., Reck B. H., Pelly I. Z. and Kuo L-C. 1983. Programmed cooling experiments in the system MgO-SiO<sub>2</sub>: kinetics of a peritectic reaction. *American Mineralogist* 68:1905–1983.
- Kita N. T., Kimura M., Ushikubo, T., Valley J. W. and Nyquist L. E. 2008. Oxygen isotope systematics of chondrules from the least equilibrated H chondrite. *39th Lunar and Planetary Science Conference*, abstract #2059.
- Krot A. N. and Wasson J. T. 1994. Silica-merrhueite/roedderite-bearing chondrules and clasts in ordinary chondrites: New occurrences and possible origin. *Meteoritics* 29:707–718.
- Krot A. N., Libourel G., Goodrich C. and Petaev M. I. 2004. Silica-igneous rims around magnesian chondrules in CR carbonaceous chondrites: evidence for fractional condensation during chondrule formation. *Meteoritics & Planetary Science* 39:1931–1955.
- Libourel G., Krot A. N. and Tissandier L. 2006. Role of gas–melt interaction during chondrule formation. *Earth and Planetary Science Letters* 251:232–240.

- Libourel G. and Portail M. 2018. Chondrules as direct thermochemical sensors of solar protoplanetary disk gas. *Science Advances* 4:eaar3321.
- Lunning N. G., Corrigan C. M., McSween H. Y., Tenner T. J., Kita N. T. and Bodnar R. J. 2016. CV and CM chondrite impact melts. *Geochimica et Cosmochimica Acta* 189:338–358.
- Marrocchi Y. and Chaussidon M. 2015. A systematic for oxygen isotopic variation in meteoritic chondrules. *Earth and Planetary Science Letters* 430:308–315.
- Marrocchi Y., Villeneuve J., Batanova V., Piani L. and Jacquet E. 2018. Oxygen isotopic diversity of chondrule precursors and the nebular origin of chondrules. *Earth and Planetary Science Letters* 496:132–141.
- Marrocchi Y., Euverte R., Villeneuve J., Batanova V., Welsch B., Ferriere L and Jacquet E. 2019. Formation of CV chondrules by recycling of amoeboid olivine aggregate-like precursors. *Geochimica et Cosmochimica Acta* 247:121–141.
- MetBase: Meteorite Information Database, <http://www.metbase.org>, 1994–2017, GeoPlatform UG, Germany.
- Metzler K., Bischoff A., Greenwood R. C., Palme H., Gellissen M., Hopp J., Franchi I. A. and Trieloff M. 2011. The L3–6 chondritic regolith breccia Northwest Africa (NWA) 869:(I) Petrology, chemistry, oxygen isotopes, and Ar-Ar age determinations. *Meteoritics & Planetary Science* 46:652–680.
- Metzler K. and Pack A. 2016. Chemistry and oxygen isotopic composition of cluster chondrite clasts and their components in LL 3 chondrites. *Meteoritics & Planetary Science* 51: 276–302.
- Morlok A., Bischoff A., Patzek M., Sohn M. and Hiesinger H. 2017. Chelyabinsk – a rock with many different (stony) faces: An infrared study. *Icarus* 284:431–442.
- Nasdala L., Wopenka B. and Lengauer C. L. 2004. Discussion on: transformation of SiO<sub>2</sub> to the amorphous state by shearing at high pressure, by Furuichi et al. (2003, vol. 88:926–928). *American Mineralogist* 89:912–913.
- Pack A. and Palme H. 2003. Partitioning of Ca and Al between forsterite and silicate melt in dynamic systems with implications for the origin of Ca, Al-rich forsterites in primitive meteorites. *Meteoritics & Planetary Science* 38:1263–1281.
- Pack A., Yurimoto H. and Palme H. 2004. Petrographic and oxygen-isotopic study of refractory forsterites from R.-chondrite Dar Al Gani 013 (R3. 5-6), unequilibrated ordinary and carbonaceous chondrites. *Geochimica et Cosmochimica Acta* 68:1135–1157.

- Pack A., Palme H. and Shelley J. M. G. 2005. Origin of chondritic forsterite grains. *Geochimica et Cosmochimica Acta* 69:3159–3182.
- Piani L., Marrocchi Y., Libourel G. and Tissandier L. 2016. Magmatic sulfides in the porphyritic chondrules of EH enstatite chondrites. *Geochimica et Cosmochimica Acta* 195:84–99.
- Prinz M., Nehru C. E., Weisberg M. K., Delaney J. S., Yanai K. and Kojima H. 1984. H chondritic clasts in a Yamato L6 chondrite: Implications for metamorphism. *Meteoritics* 19:292–293, abstract.
- Rubin A. E., Breen J. P., Isa J. and Tutorow S. 2017. NWA 10214 - an LL3 chondrite breccia with an assortment of metamorphosed, shocked, and unique chondrite clasts. *Meteoritics & Planetary Science* 52:372–390.
- Ruzicka A., Kring D. A., Hill D. H., Boynton W. V., Clayton R. N., Mayeda T. K. 1995. Silica-rich orthopyroxenite in the Bovedy chondrite. *Meteoritics* 30:57–70.
- Sakamoto N., Seto Y., Itoh S., Kuramoto K., Fujino K., Nagashima K., Krot A. N. and Yurimoto H. 2007. Remnants of the early solar system water enriched in heavy oxygen isotopes. *Science* 317:231–233.
- Scott J. F. and Porto S. P. S. 1967. Longitudinal and transversal optical lattice vibrations in quartz. *Physical Review* 161:903–910.
- Scott E. R. D. and Krot A. N. 2014. Chondrites and their components. In: *Treatise on Geochemistry* 2<sup>nd</sup> ed. (eds. H. Holland and K. Turekian) Elsevier, Oxford, pp. 65–137.
- Soulié C., Libourel G. and Tissandier L. 2017. Olivine dissolution in molten silicates: an experimental study with application to chondrule formation. *Meteoritics & Planetary Science* 52:225–250.
- Sokol A. K., Bischoff A., Marhas K. K., Mezger K. and Zinner E. 2007. Late accretion and lithification of chondritic parent bodies: Mg isotope studies on fragments from primitive chondrites and chondritic breccias. *Meteoritics & Planetary Science* 42:1291–1308.
- Steele I. M. 1986. Compositions and textures of relic forsterite in carbonaceous and unequilibrated ordinary chondrites. *Geochimica et Cosmochimica Acta* 50:1379–1395.
- Terada K. and Bischoff A. 2009. Asteroidal granite-like magmatism 4.53 Gyr ago. *The Astrophysical Journal* 699:L68–L71.
- Tissandier L., Libourel G. and Robert F. 2002. Gas-melt interactions and their bearing on chondrule formation. *Meteoritics & Planetary Science* 37:1377–1389.
- Wasson J. T., Krot A. N., Lee M. S. and Rubin A. E. 1995. Compound chondrules. *Geochimica et Cosmochimica Acta* 59:1847–1869.

- Weinbruch S., Palme H. and Spettel B. 2000. Refractory forsterite in primitive meteorites: Condensates from the solar nebula? *Meteoritics & Planetary Science* 35:161–171.
- Weisberg M. K., Prinz M. and Nehru C. E. 1988. Macrochondrules in ordinary chondrites: Constraints on chondrule-forming processes. *Meteoritics* 23:309–310, abstract.
- Weyrauch M. and Bischoff A. 2012. Macrochondrules in chondrites-formation by melting of mega-sized dust aggregates and/or by rapid collisions at high temperatures? *Meteoritics & Planetary Science* 47:2237–2250.
- Young E. D. and Russell S. S. 1998. Oxygen reservoirs in the early solar nebula inferred from an Allende CAI. *Science* 282:452–455.
- Yokoyama T., Misawa K., Okano O., Shih C. Y., Nyquist L. E., Simon J. I., Tappa M. J. and Yoneda. S. 2017. Extreme early solar system chemical fractionation recorded by alkali-rich clasts contained in ordinary chondrite breccias. *Earth and Planetary Science Letters* 458:233–240.

# Chapter 5

## Formation of chondrules and matrix in Kakangari chondrites

Jens Barosch, Denton S. Ebel, Dominik C. Hezel, Samuel Alpert, Herbert Palme

Earth and Planetary Science Letters (2020)

<https://doi.org/10.1016/j.epsl.2020.116286>

### **Abstract**

The study of chondritic meteorites and their components allows us to understand processes and conditions in the protoplanetary disk. Chondrites with high and about equal proportions of chondrules and matrix are ideal candidates to not only study the formation conditions of chondrules, but also the relationship between these two major components. An important question is whether these formed in the same or in separate reservoirs in the protoplanetary disk. So far, such studies have been mainly restricted to carbonaceous chondrites. We here expand these studies to the K (Kakangari-like) chondrite grouplet. These have various distinctive properties, but the abundance of major components – chondrules and matrix – is similar to other primitive meteorites. We obtained a comprehensive petrographic and chemical dataset of Kakangari and Lewis Cliff 87232 chondrules and matrix. Chondrules in Kakangari show a large compositional scatter, supporting material addition to chondrules during their formation. Contrary to almost all other chondrite groups, the majority of Kakangari chondrules are not mineralogically zoned. However, Kakangari chondrules were likely initially zoned, but then lost this zonation during chondrule remelting and fragmentation. Average compositions of bulk chondrules, matrix and bulk Kakangari are identical and approximately solar for Mg/Si. This might indicate the formation of chondrules and matrix from a common reservoir and would agree with findings from carbonaceous and Rumuruti chondrites: chondrules and matrix in most chondrite groups were not transported through the protoplanetary disk and then mixed together. Rather, these major components are genetically related to each other and formed in the same reservoir.

## 5.1. Introduction

The K grouplet comprises four chondrites (Kakangari, Lewis Cliff 87232, NWA 10085 and – with minor taxonomic uncertainties; cf. Prinz et al., 1991 – Lea County 002). They are named after Kakangari, the first and largest K chondrite fall. Previous studies identified a combination of properties that define this new grouplet, as Kakangari was so different from any of the other major chondrite classes (Weisberg et al., 1996). Based on its chemical composition, Kakangari was first recognised as a “unique” chondrite by Graham and Hutchison (1974), later confirmed by Davis et al. (1977). With relatively high fractions of matrix (33–77 vol%) and chondrules (19–41 vol%), K chondrites resemble carbonaceous chondrites (CC; Weisberg et al., 1996). The high metal contents (6–10 vol%) are more similar to the metal fractions of H-group ordinary chondrites (OC).

Chondrules are mm-sized silicate spherules that formed during brief high-temperature events. It has only recently been recognised that most chondrules (> 80%) in carbonaceous and Rumuruti (R) chondrites are mineralogically zoned, with olivine in the core and low-Ca pyroxene at the border of these chondrules (Friend et al., 2016; Barosch et al., 2020). The number of mineralogically zoned chondrules is significantly lower in OC and enstatite chondrites (EC; about 30–40%; Barosch et al., 2019, 2020). Mineralogically zoned chondrule textures are attributed to open system behaviour during chondrule formation, when chondrule olivine reacted with gaseous SiO, thereby forming the low-Ca pyroxene rims (e.g., Tissandier et al., 2002; Libourel et al., 2006; Ebel et al., 2018, and references therein). Most of the type I chondrules, defined as porphyritic chondrules with low FeO-olivine ( $Fo > 90$ ), are mineralogically zoned, while mineralogical zoning is less common in type II chondrules ( $Fo < 90$ ). Interestingly, type II chondrules seem to be either entirely absent in Kakangari (Nehru et al., 1986; Weisberg et al., 1996; Genge and Grady, 1998) or could be missing as a consequence of FeO reduction in the nebula, according to Berlin (2009) who studied 20 Kakangari chondrules in detail. Most chondrules have porphyritic textures, are pyroxene and olivine-rich, contain patches of mesostasis, metal beads, troilite, and sometimes silica and/or Cr-spinel.

The abundant fine-grained matrix in Kakangari has been investigated by Brearley (1989) and Berlin (2009). Scott and Krot (2005, and references therein) pointed out that the reduced mineralogy of the Kakangari matrix is unusual compared to other chondrite matrices. Most interestingly, these authors found that the Kakangari matrix composition is surprisingly similar to the average chondrule composition in K chondrites. The fine-grained Kakangari matrix is

dominated by enstatite (~50 vol%) and magnesian olivine (~20 vol%), with lower amounts of high-albite, anorthite, troilite, Fe,Ni-metal, Cr-spinel, as well as secondary ferrihydrite and chlorapatite (Brearley, 1989; Berlin, 2009).

The mechanism of chondrule and matrix formation is not yet understood, although there is no shortage of proposed hypotheses (Russell et al., 2018, and references therein). A key question is whether chondrules and matrix originated from a single common reservoir, or multiple separate reservoirs in the solar nebula. In recent years, the chondrule-matrix complementarity has been recognised as a key characteristic of many CC and R chondrites (e.g., Hezel et al., 2018a, and references therein). A large number of element ratios in these bulk meteorites, but also the few isotope ratios studied so far (Becker et al., 2015; Budde et al., 2016a, b), are close to the respective CI chondrite ratios, while their ratios in chondrules and matrix are different. The most likely – but not universally accepted (cf. Zanda et al., 2018) – interpretation of these complementarities is that chondrules and matrix in these meteorites formed from single reservoirs of near-solar composition. This interpretation, or its falsification, is an important constraint for models of chondrule formation and parent body accretion. Chondrule-matrix complementarities have not yet been demonstrated for classes other than CC and R chondrites (Hezel et al., 2018a). Ordinary chondrites present difficulties for demonstrating complementary chemical compositions of matrix and chondrules, as the fraction of matrix is small and important element ratios (e.g., Mg/Si) are non-solar in bulk OC.

Various authors have proposed that Kakangari chondrules and matrix formed in close spatial proximity in the protoplanetary disk, e.g., based on compositional similarities between both components (Brearley, 1989; Scott and Krot, 2005; Berlin, 2009). This is supported by Nagashima et al. (2015), who observed O-isotope homogeneity between chondrules and most parts of matrix, and proposed that both sampled a common O-isotope reservoir. Kakangari therefore seems to be an interesting candidate to study chondrule-matrix complementarity. Both components are abundant and bulk Kakangari is close to solar for some element ratios (e.g., CI-normalised  $\text{Mg/Si} = \text{Mg/Si/CI} = 0.964$ , Mason and Wiik, 1966; Palme et al., 2014).

Kakangari was described as a ‘pristine’ meteorite by various authors (e.g., Brearley, 1989; Nuth et al., 2005; Scott and Krot, 2005). However, recent evidence presented by Berlin (2009) indicates that Kakangari experienced secondary alteration and metamorphism on its parent body. Large apatite grains, Ni-zoning profiles in olivine and narrow ranges of olivine compositions, as well as narrow ranges of MnO contents in olivines point towards a petrologic subtype between 3.4 and 3.8 (Berlin, 2009).

Only a few K chondrite bulk chondrule compositions and matrix analyses have been reported in the literature (ChondriteDB, Hezel et al., 2018b). Also, the abundance of mineralogically zoned chondrules in K chondrites is so far unmeasured. Here, we study chondrules and matrix in Kakangari (K3) and Lewis Cliff (LEW) 87232 (K) sections. We present a comprehensive dataset that contains petrographic and chemical data of components in these meteorites. We use this dataset to study the origin and formation of chondrule textures, bulk chondrule and matrix compositions and chondrule-matrix complementarities in K grouplet meteorites.

### 5.2. Methods

All samples were prepared with diamond polishing compounds and then analysed with an electron probe microanalyzer (EPMA) using element mapping and spot analyses. Element maps of four Kakangari sections and one LEW 87232 section were produced with the CAMECA SX-100 at the American Museum of Natural History (AMNH), New York. BSE images (Fig. 5.1) and element maps were obtained by rastering the stage under a stationary electron beam in 512x512 pixel frames with a resolution of 4  $\mu\text{m}/\text{px}$ . We used a 1  $\mu\text{m}$  focussed beam with a 40 nA beam current at 15 kV accelerating voltage. The dwell time was set to 15 ms. Contiguous X-ray frames were stitched together, creating single element maps of entire chondrite sections for Al, Ca, Fe, Mg, Na, Ni, P, S, Si and Ti. In addition, we created phase maps of all samples using the PHAPS program (Hezel, 2010). A phase map shows every mineral phase in false-colour. This was used for visual identification of chondrule textures and mineral distributions throughout the samples.

Quantitative data of chondrule phases and matrix minerals were collected with the EPMA at AMNH (Kakangari) and the JEOL JXA-8900 RL Superprobe at the Institute of Geology and Mineralogy, University of Cologne, Germany (LEW 87232). For chondrule phases, we used a 1  $\mu\text{m}$  focussed beam and a 20 nA beam current at 15 kV accelerating voltage for Kakangari, and at 20 kV for LEW 87232. Well-characterised reference materials were used for calibration and ZAF corrections were applied (Bence and Albee, 1968). Matrix material was analysed in two Kakangari sections (3956-t1-ps1A, and -ps2A) with the same settings (15 kV, 20 nA), but with a 20  $\mu\text{m}$  defocused beam. Spot analyses were randomly placed and opaque phases (metals, sulphides) were not avoided. We excluded analyses with totals below 80 wt.% and above 105 wt.%. Low totals likely result from holes and cracks in the thin sections, while high totals are usually due to abundant Fe, Ni-rich opaque phases, for which element contents were

recalculated as oxides. Bulk chondrule compositions were obtained from mineral spot analyses with modal recombination, using the equation:

$$bulk = \frac{\sum \chi \rho c}{\sum \chi \rho} \quad \text{eq. 1}$$

$\chi$  = phase abundance;  $\rho$  = phase density;  $c$  = element concentration

Following the protocol of Ebel et al. (2016), all samples were segmented for statistical evaluation (Fig. 5.2). Element maps, RGB composite maps and phase maps were used to identify all components in the samples. These were then outlined and categorised, i.e., classified into one of several categories: porphyritic chondrules, nonporphyritic chondrules, chondrule and silicate fragments, opaques (metals & sulphides), CAI-like material, AOAs, chlorapatite and matrix (Table 5.1). The components of each category were subsequently characterised for statistical evaluation, e.g., object abundances, sizes and average compositions. As segmentation was done by hand, outlining extremely small particles proved challenging. Silicate particles sized  $\sim 15 \times 15 \mu\text{m}$  and below were therefore collectively categorised as matrix. While we were also unable to outline opaque phases of the aforementioned size, these particles were easily identified in the RGB composite- and phase maps. They were initially categorised as matrix. In an additional step, the abundance of these opaque particles in the matrix was determined, subtracted from the total matrix abundance and then reclassified into the correct category.

We use bulk K chondrite compositions reported in the literature, however, little data exists. For example, Kakangari bulk chemistry was determined by neutron activation analysis (INAA; Weisberg et al., 1996), hence, no Si and Ti concentrations were reported. We therefore use the wet chemistry data from Mason and Wiik (1966) for Kakangari. However, only INAA bulk data are available for LEW 87232 (Weisberg et al., 1996). K chondrite material is highly limited, which is why we approximated bulk chondrite compositions using modal recombination (eq. 1; using data from Tables 5.1 & 5.4; see appendix). All calculated element ratios in Kakangari are within  $\sim 10$  rel% when compared to the data from Mason and Wiik (1966), except for element ratios involving Ti, which might be concentrated in small matrix phases such as perovskite that might have been missed. Fe and Ni are also challenging: (i) chondrule metal and sulphide contents cannot be determined reliably in 2D sections, as demonstrated by e.g., Hezel (2007), Ebel et al. (2009), Hezel and Kießwetter (2010). Therefore, all chondrule bulk data reported in this study are silicate-only. However, if only chondrule silicates are considered, then we clearly underestimate bulk chondrule Fe-metal contents. This

is especially the case for chondrules with opaque rims. (ii) Fe,Ni-rich opaque phases are recalculated as oxides in EPMA matrix analyses, leading to artificially high FeO concentrations (~10 rel%). These difficulties illustrate the general uncertainties of modal recombination, which cannot replace accurate bulk chondrite measurements.

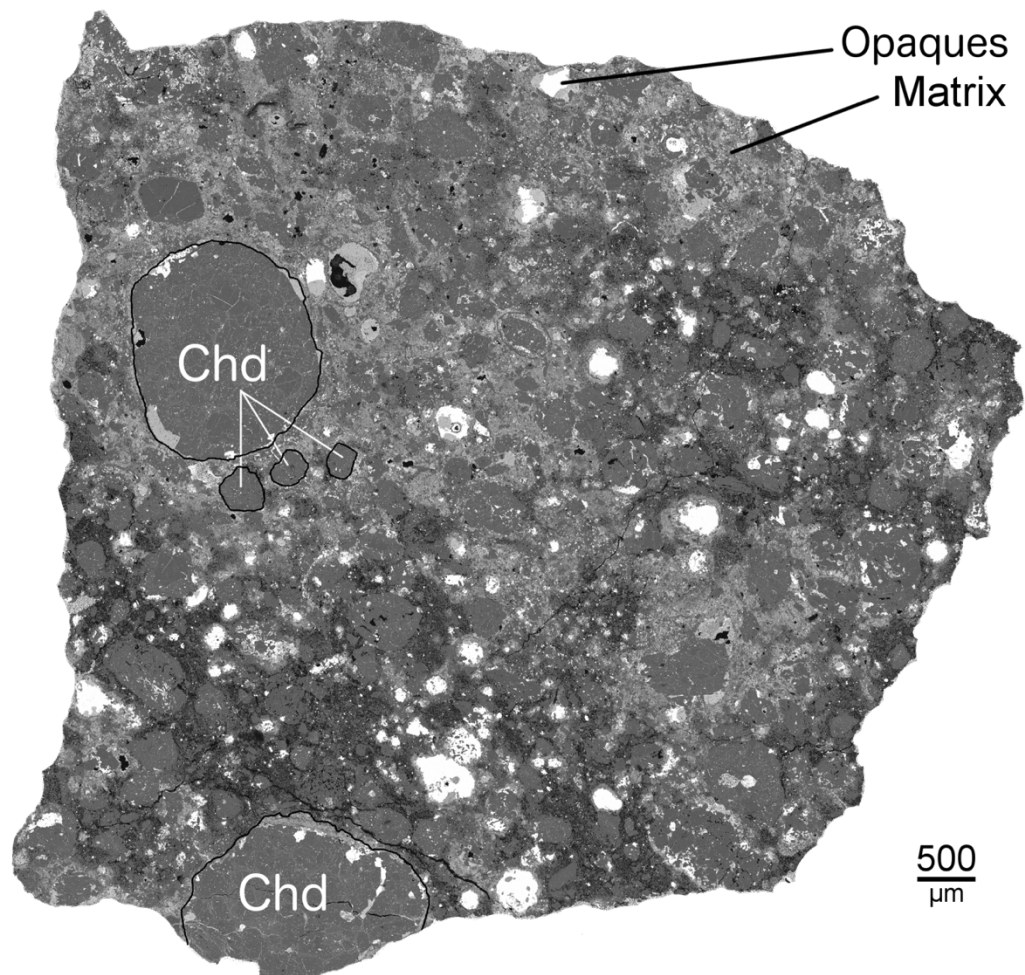


**Fig 5.1:** BSE image of LEW 87232.

**Table 5.1:** Modal abundances of Kakangari and LEW 87232 components (area%).

	<b>Kakangari</b>	<b>LEW87232</b>
area studied (mm <sup>2</sup> )	237.50	54.96
matrix	66.78	53.36
chondrules + fragments (silicates)	22.71	33.68
opaques in matrix	5.43	10.92
opaques in chondrules	4.16	2.05
CAI-like material	0.19	<0.1
AOA	0.16	<0.1
Chlorapatite	0.58	<0.1
Total	100.00	100.00

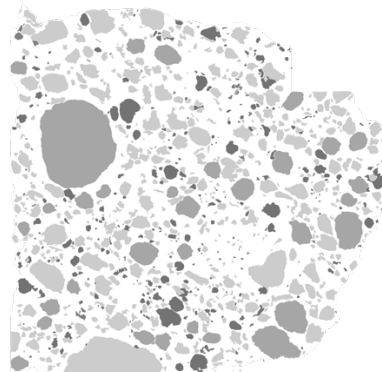


**Fig. 5.2** (previous page, right): Components in LEW 87232 after the entire section was mapped and segmented by outlining every object and particle (cf. Fig. 5.1). Each grayscale represents an object of a different category. Component modal abundances are listed in Table 5.1.

## 5.3. Results

### 5.3.1. Abundances and characteristics of components in K chondrites

We mapped and studied a total area of 238 mm<sup>2</sup> in four Kakangari sections: AMNH 3956-1, -2 and 3956-t1-ps1A, -ps2A. Additionally, we received LEW 87232.14 from the Meteorite Working Group with a total area of 55 mm<sup>2</sup> (Fig. 5.1, 5.2). Component modal abundances are listed in Table 5.1. Matrix is dominant in both samples, with ~67 area% in Kakangari and 53 area% in LEW 87232. Complete chondrules, fragments and silicate aggregates – often interpreted as debris derived from shattered chondrules (cf. Brearley, 1989) – of various sizes have significantly lower abundances in Kakangari (23 area%) and LEW 87232 (34 area%). Opaque phases in Kakangari are equally abundant in chondrules (4 area%; including chondrule opaque rims) and matrix (5 area%), which is less than the reported 16% opaques by Weisberg et al. (1996). In LEW 87232, opaques mostly occur in the matrix (11 area%) and to a smaller extent in chondrules (2 area%). AOAs (0.16 area%) and fragmented CAI-like material (0.19 area%; cf. Bischoff and Keil, 1983) were observed in Kakangari, but not in LEW 87232. Additionally, the abundance of chlorapatite (0.58 area%) was determined in Kakangari.

In the following we briefly describe the characteristics of chondrules and potential chondrule fragments in K chondrites. Bulk chondrule and matrix compositions will be described separately in Section 5.3.2. We refer to Brearley (1989) and Berlin (2009) for a detailed description of matrix in Kakangari.

#### *Chondrules*

Many chondrules seem to be incomplete and heavily fragmented. Here, we only describe chondrules which are apparently complete, i.e., without major holes and fractures. Potential chondrule fragments were excluded from textural analysis and will be described separately. The average Kakangari chondrule has an apparent diameter of ~700 μm. Individual chondrule diameters range from 200 μm up to ~2.6 mm. LEW 87232 chondrules are generally smaller with ~400 μm average diameter.

We used chondrule phase maps to determine the textural types of 119 Kakangari chondrules and 47 LEW 87232 chondrules (Table 5.2). A total of 102 Kakangari chondrules are taken

from this study, complemented by 17 intact chondrules from Berlin (2009). Porphyritic textures are most common among K chondrite chondrules (Figs. 5.3a, b, 5.4). Kakangari has a high portion of porphyritic olivine-pyroxene chondrules (POP, 43%) and about equal amounts of porphyritic olivine (PO; with  $ol/px \geq 0.9$ ) and porphyritic pyroxene (PP; with  $ol/px \leq 0.1$ ) chondrules (each 21–22%). Radial pyroxene chondrules (RP; 9%) and agglomeratic chondrules (AC) – consisting of fine-grained silicates and abundant metal and sulphide beads – are less frequent (5%). The dominant chondrule texture in LEW 87232 is PP (57%), with intermediate amounts of POP (30%) and a low fraction of PO textures (9%). A few chondrules are AC (4%). Other chondrule textures (e.g., barred olivine, BO chondrules) seem to be absent in both meteorites.

We classify chondrules as mineralogically zoned if olivine is largely concentrated in the chondrule cores, while simultaneously these are surrounded by, or poikilitically enclosed in low-Ca pyroxene crystals. In Kakangari, 9 out of 119 chondrules (7.5%) meet these criteria (Table 5.2, Fig. 5.3c). In contrast, LEW 87232 has a much higher abundance of mineralogically zoned chondrules (30%, 14 of 47 chondrules; Fig. 5.3d). Most zoned chondrule cores consist of either a single or few large (up to 300  $\mu\text{m}$ -sized), or abundant small (often  $< 50 \mu\text{m}$ -sized) olivine crystals. The pyroxene rim fractions vary strongly, but often occupy large portions ( $> 50 \text{ vol}\%$ ) of zoned chondrules. Large pyroxene crystals frequently poikilitically enclose olivine crystals. This can, however, also be observed in unzoned chondrules.

The average compositions of major chondrule phases, i.e., olivine, low-Ca pyroxene, high-Ca pyroxene and mesostasis, are given in Table 5.3. Olivine and low-Ca pyroxene are the dominant chondrule minerals in both samples. LEW 87232 chondrules, in particular, are dominated by enstatite. The total surface olivine/enstatite ratio is 0.77 for Kakangari chondrules, but much lower (0.32) for LEW 87232 chondrules. All porphyritic chondrules in both samples are type I ( $Fo > 90$ ), with average Mg numbers of 93.8 in Kakangari and 97.3 in LEW 87232. Olivines are forsteritic with average  $Fo_{96.3}$  in Kakangari and  $Fo_{98.8}$  in LEW 87232, while enstatite is on average  $En_{93.0}$  and  $En_{97.0}$ , respectively.

Some chondrules are surrounded by rims with igneous textures. These rims have variable thicknesses and are dominated by fine-grained silicates, and frequently contain opaque phases (cf. Genge and Grady, 1998). Other chondrules are surrounded by massive or porous opaque rims. Igneous textured rims and porous opaque rims often completely enclose chondrules, but massive opaque rims only occur as partial rims. Opaque phases are not restricted to the chondrule borders, but often also appear as beads inside chondrules. Most chondrules contain

at least a few opaque beads. The abundance of opaque phases can be as high as 30 area%. Approximately one-third of the Kakangari chondrules are metal-free in 2D sections.

**Table 5.2:** Frequency of chondrule textural types and zoned chondrules in K chondrites (PP: porphyritic pyroxene, PO: porphyritic olivine, POP: porphyritic olivine-pyroxene, RP: radial pyroxene, AC: agglomeratic chondrules).

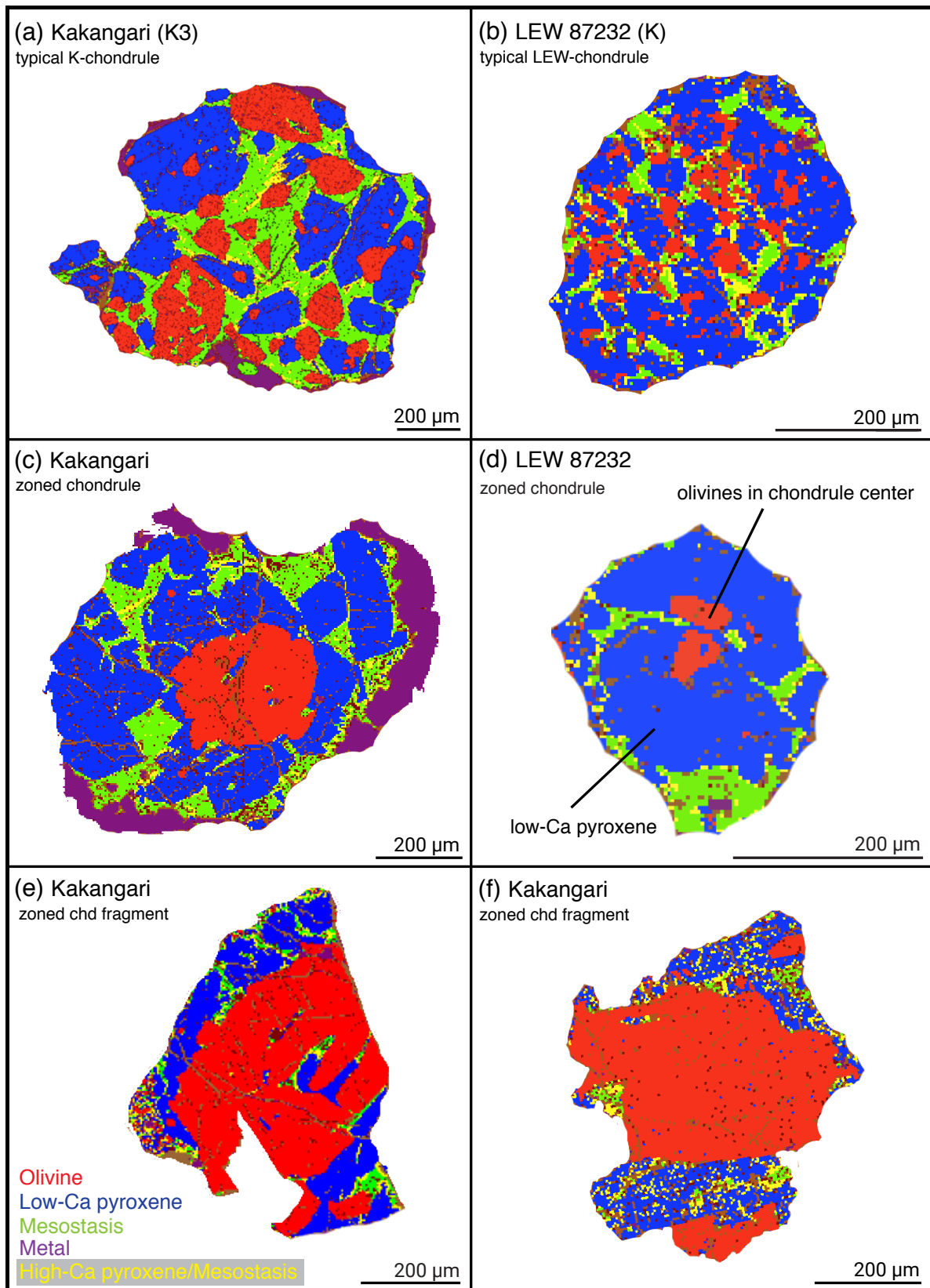
	<b>Kakangari</b>		<b>LEW87232</b>	
	No. of chd*	%	No. of chd	%
PP	26	21.85	27	57.45
PO	25	21.01	4	8.51
POP	51	42.86	14	29.79
RP	11	9.24	0	0.00
AC	6	5.04	2	4.26
Total	119		47	
intact zoned chondrules	9	7.56	14	29.79
zoned chd fragments**	21		4	

\*17 chondrules were taken from Berlin (2009).

\*\*fragments potentially derived from zoned chondrules (see phase maps in Fig. 5.3e, f).

### *Inferred chondrule fragments*

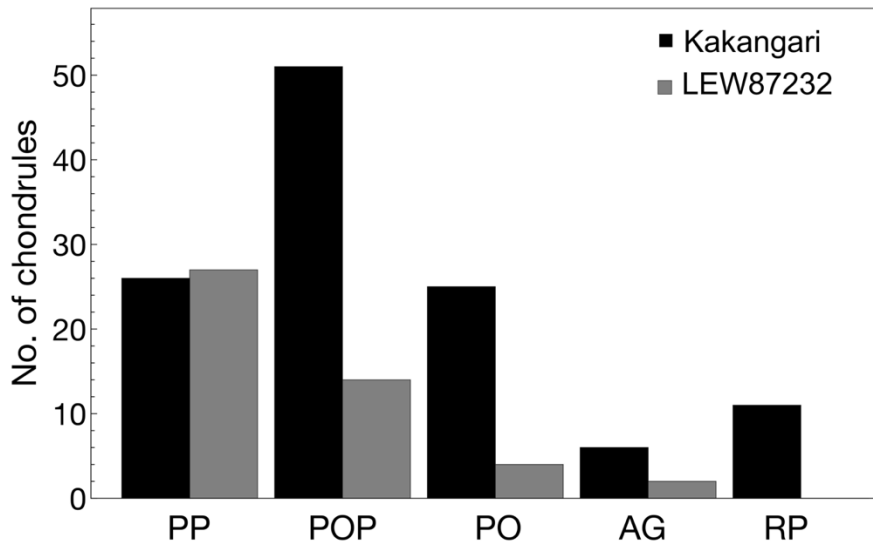
Kakangari contains a large number (~1100) of fragments, i.e., fragmented chondrules with angular outlines and mineral fragments. Fragment sizes vary greatly: some are larger than 1000  $\mu\text{m}$  in diameter, but most have diameters of less than 400  $\mu\text{m}$ . Relatively small silicate mineral fragments with diameters ranging from ~30–200  $\mu\text{m}$  are abundant. These occur either as isolated grains or mineral aggregates composed of typical chondrule phases, e.g., enstatite and/or olivine crystals and sometimes chunks of mesostasis-like material. Mineral assemblages and chemical compositions of fragments, silicate aggregates and intact chondrules are very similar to each other. No fragments of barred olivine chondrules were identified. A number of inferred chondrule fragments in Kakangari consist of olivines that are partially surrounded by low-Ca pyroxene at their margins. The crystals are truncated by fracture surfaces at their edges. They look like pieces of shattered, formerly mineralogically zoned chondrules. Two representative fragments are displayed in Fig. 5.3e, f. Kakangari sections contain a total of 21 of these fragments. Four similar-looking fragments were found in LEW 87232.



**Fig. 5.3:** Chondrule phase maps using the PHAPS program (Hezel, 2010) show: (a, b) typical chondrules in K chondrites, (c, d) representative appearances of mineralogically zoned chondrules in K chondrites, and (e, f) potential fragments of mineralogically zoned chondrules in Kakangari.

**Table 5.3:** Average composition of major chondrule phases in K chondrites (wt%).

Analyses	Kakangari				LEW87232			
	219	258	111	209	135	168	70	139
Mineral	olivine	low-Ca px	high-Ca px	mesostasis	olivine	low-Ca px	high-Ca px	mesostasis
SiO <sub>2</sub>	42.19	58.08	54.44	64.37	42.11	58.73	54.63	60.69
TiO <sub>2</sub>	0.02	0.05	0.42	0.42	0.03	0.08	0.57	0.19
Al <sub>2</sub> O <sub>3</sub>	0.10	0.41	2.99	17.27	0.08	0.41	3.94	20.31
Cr <sub>2</sub> O <sub>3</sub>	0.05	0.53	1.53	0.27	0.08	0.26	1.15	0.12
FeO	3.71	4.63	4.83	2.58	1.24	2.11	1.62	0.93
MnO	0.43	0.47	0.84	0.18	0.21	0.29	0.46	0.07
NiO	0.02	0.03	0.03	0.09	0.01	0.02	0.07	0.05
MgO	53.89	35.31	20.71	3.67	56.20	37.75	20.26	3.54
CaO	0.10	0.87	13.86	4.68	0.03	0.40	17.02	6.06
Na <sub>2</sub> O	0.03	0.09	0.70	5.53	0.03	0.14	1.12	8.54
Total	100.54	100.47	100.36	99.06	100.02	100.19	100.83	100.51

**Fig. 5.4:** Textural types of chondrules in Kakangari and LEW 87232.

### 5.3.2. Bulk chondrule and matrix compositions

We determined the bulk compositions of 57 chondrules in Kakangari and 22 chondrules in LEW 87232 by modal recombination (eq. 1). We further included 20 Kakangari bulk chondrule compositions obtained by Berlin (2009) in the University of New Mexico (UNM) sections 559 and 585. All chondrule bulk compositions are silicate-only. The average Kakangari bulk chondrule compositions from this study and from Berlin (2009) – both listed in Table 5.4 – are similar. Significant differences (> 10 rel%) are only observed in average Al<sub>2</sub>O<sub>3</sub> contents with 2.5 (this study) vs. 2.0 wt% (Berlin, 2009) and average CaO contents with 1.8 (this study) vs. 2.2 wt% (Berlin, 2009). The average composition of LEW 87232 chondrules differs slightly from Kakangari. For example, LEW 87232 chondrules have lower average FeO contents in their silicate portion (1.8 wt%) compared to Kakangari (4.2 wt%). Simultaneously, LEW 87232

chondrules have ~3 wt% higher average SiO<sub>2</sub> contents than Kakangari chondrules, indicating lower olivine/pyroxene ratios.

Bulk chondrule compositional variations of major (Mg, Si) and refractory elements (Al, Ca) in Kakangari are shown in Fig. 5.5. All element distributions, and in particular the distribution of Mg, are unimodal. Chondrules from the study of Berlin (2009) plot in the same, large compositional range between 13–31 wt% in Mg and 20–30 wt% in Si, as the present study.

**Table 5.4:** Average bulk chondrule and matrix compositions in K chondrites (wt%).

Sample Analyses	bulk chondrules*				matrix				Berlin 2009	
	Kakangari		LEW87232		Kakangari**		LEW87232		chondrules*	matrix
	57 bulks	SE	22 bulks	SE	245 spots	SE	342 spots	SE	20 bulks	125 spots
SiO <sub>2</sub>	53.38	0.52	56.22	0.49	34.97	0.28	34.31	0.52	54.10	36.39
TiO <sub>2</sub>	0.11	0.01	0.10	0.01	0.11	0.01	0.07	0.00	0.10	0.10
Al <sub>2</sub> O <sub>3</sub>	2.49	0.14	2.76	0.24	2.60	0.07	2.98	0.13	1.96	3.00
Cr <sub>2</sub> O <sub>3</sub>	0.39	0.03	0.26	0.02	0.50	0.13	0.08	0.00	0.43	0.53
FeO	4.21	0.17	1.79	0.08	24.63	0.60	26.80	0.61	4.64	20.49
MnO	0.43	0.01	0.25	0.01	0.33	0.01	0.13	0.00	0.48	0.32
NiO	0.04	0.00	0.02	0.00	1.23	0.05	2.28	0.07	0.02	1.01
MgO	36.67	0.68	35.91	0.72	24.61	0.28	21.80	0.37	35.47	25.80
CaO	1.78	0.11	1.74	0.13	1.24	0.05	0.58	0.05	2.17	1.50
Na <sub>2</sub> O	0.75	0.06	1.15	0.14	1.22	0.03	1.50	0.04	0.71	1.29
Total	100.25		100.22		91.45		90.54		100.07	90.44

SE = standard error

\*silicates only

\*\*Data from 3956-t1-ps1A, and -ps2A sections.

The average Kakangari matrix compositions from 3956-t1-ps1A, and -ps2A sections are displayed in Table 5.4. We compare our results to the mean of 125 matrix analyses from Kakangari UNM sections 559 and 585 (Table 5.4, Berlin, 2009). The average contents of most oxides are similar (MgO, SiO<sub>2</sub>, Al<sub>2</sub>O<sub>3</sub>, NiO, CaO, Na<sub>2</sub>O, TiO<sub>2</sub>, Cr<sub>2</sub>O<sub>3</sub>, MnO) in both studies. FeO contents are ~4 wt% higher in our study. LEW 87232 matrix has higher FeO, NiO, and lower MgO, CaO and Cr<sub>2</sub>O<sub>3</sub> contents than Kakangari.

Kakangari and LEW 87232 bulk chondrule and matrix compositions of the two major elements Mg and Si are displayed in Fig. 5.6. The plot shows comparatively large variations in Si and Mg concentrations of bulk chondrule and matrix analyses. The average Mg/Si ratio of all chondrules in Kakangari is close to CI-chondritic (Mg/Si/CI = 0.98). The same is true for the average Mg/Si ratio of the matrix (Mg/Si/CI = 1.03). The Kakangari bulk meteorite composition was taken from Mason and Wiik (1966, wet chemistry) and CI data are from Palme et al. (2014).

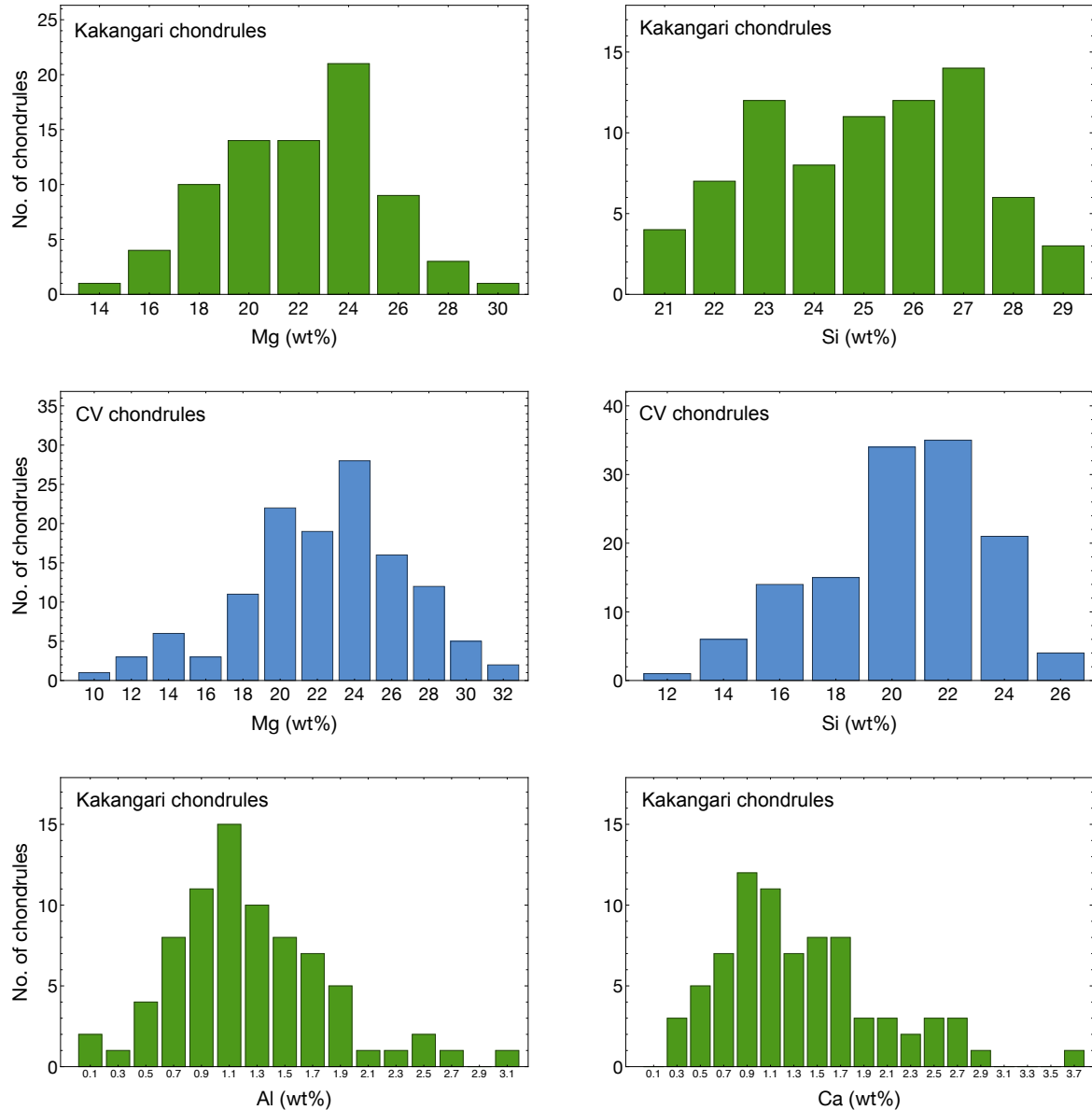


**Fig. 5.5:** Kakangari bulk chondrule compositional variations in major (Mg, Si) and refractory elements (Al, Ca). Bulk CV chondrules also show a unimodal distribution and large compositional variations in Mg and Si. CV chondrule bulks were taken from the ChondriteDB (129 chondrules, Hezel et al., 2018b).

## 5.4. Discussion

### 5.4.1. Why are zoned chondrules rare in Kakangari, but not in LEW 87232?

The very low abundance of mineralogically zoned chondrules in Kakangari (7.5%) is surprising: (i) zoned chondrule textures are abundant in all chondrites, with previously reported >80% zoned chondrules in CC, >40% in OC, and >30% in EC (Friend et al., 2016; Barosch et al., 2019, 2020). These studies (and references therein) also showed that mineralogical zonation is very common in type I and less frequent in type II chondrules. All Kakangari chondrules

seem to be type I, but mostly without zonation. Thus, Kakangari is the first and so far only meteorite with a very low zoned chondrules abundance. (ii) Kakangari chondrules show similar bulk compositional variations as chondrules in other chondrites (Fig. 5.5). The bulk chondrule Mg and Si variations are best explained by chondrule open system behaviour, i.e., the reaction of chondrule melts with ambient SiO-enriched gas during chondrule crystallisation (e.g., Tissandier et al., 2002; Libourel et al., 2006; Ebel et al., 2018, and references therein). Zoned chondrules providing textural evidence for this open system interaction are, however, largely absent in Kakangari. (iii) Finally, in contrast to Kakangari, LEW 87232 has a significantly higher fraction of zoned chondrules (30%).

Barosch et al. (2020) discuss sectioning effects and their consequences for the fraction of mineralogically zoned chondrules. For example, chondrules sectioned through their low-Ca pyroxene rims typically appear unzoned in 2D sections. When studied in 3D, zoned chondrule fractions are significantly higher in all chondrites. Many chondrules in LEW 87232 are relatively small and pyroxene-rich. The most abundant textural type is PP (57%; Table 5.2, Fig. 5.4). Similar to EC chondrules, zoned LEW 87232 chondrules have small olivine cores and thick low-Ca pyroxene rims (Fig. 5.3d). They might be especially susceptible to sectioning effects as there is a high probability that these chondrules are frequently sectioned through their thick pyroxene rims. The true 3D abundance of mineralogically zoned chondrules in LEW 87232 could therefore be significantly higher. We estimate that the 3D zoned chondrule fraction in LEW 87232 could be as high as 50% (cf. Barosch et al., 2020). This does, however, not necessarily apply to Kakangari chondrules, which are larger and have a lower fraction of PP chondrules (20%; Table 5.2, Fig. 5.4). It is therefore unlikely that 3D studies would reveal significantly higher fractions of zoned chondrules in Kakangari.

It might be hypothesised that the absence of mineralogically zoned chondrules is related to the high inferred abundance of chondrule fragments in Kakangari, which may result from widespread chondrule fragmentation. We observed a total of 102 complete chondrules in Kakangari and more than 1000 fragments of various sizes that are commonly interpreted as fragments of shattered chondrules (based on similar compositions, cf. Brearley, 1989). An average complete chondrule covers an area of 0.38 mm<sup>2</sup>, and all fragments in our dataset sum up to a combined area of ~30 mm<sup>2</sup>. Roughly estimating, all fragments could then be derived from ~80 average-sized chondrules. This means, that from the initial chondrule population about 56% remained intact, while 44% were fragmented.

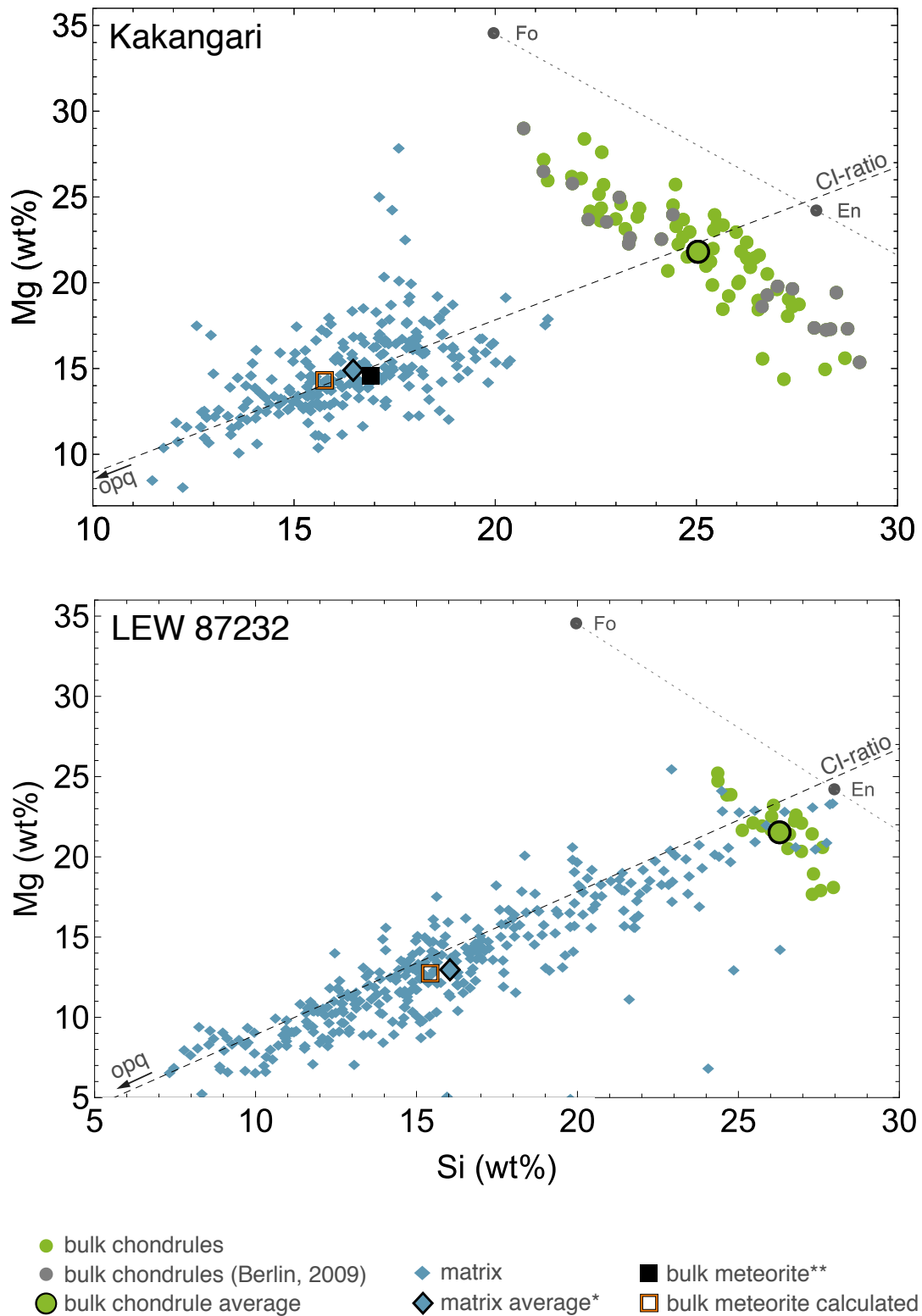


**Fig. 5.6:** Mg/Si plot showing Kakangari and LEW 87232 bulk chondrule, matrix and bulk meteorite compositions. The standard errors of average chondrules and matrix are smaller than the respective symbols (Table 5.4). Bulk meteorite mass balance calculations are listed in the appendix. The calculated bulk Mg/Si does not plot in-between chondrule and matrix compositions as opaque phases are included in this calculation. We further note that calculated bulk compositions likely have large uncertainties and cannot replace bulk meteorite measurements. CI data are from Palme et al. (2014). \*Kakangari matrix weighted average (see appendix), calculated from McSween and Richardson (1977, 20 spot analyses), Berlin (2009, 125 spots), 3956-t1-ps1A (51 spots), and -ps2A (194 spots). \*\*bulk Kakangari data is from Mason and Wiik (1966, wet chemistry).

This estimate is in accordance with that of Genge and Grady (1998), who reported the same fractions of chondrules and inferred chondrule fragments (50% out of 154 chondrules studied). In Section 5.3.1., we reported fragments that were likely derived from shattered mineralogically zoned chondrules (e.g., Fig. 5.3e, f). Widespread chondrule fragmentation could therefore have either destroyed initially zoned chondrules, or abraded large portions of the pyroxene rims from zoned chondrules. However, as almost all intact chondrules are unzoned, this hypothesis would require selective fragmentation of zoned chondrules. Nelson and Rubin (2001) pointed out that some types of chondrules are indeed more easily destroyed than others. For example, broken chunks of porphyritic chondrules are more often observed than remnants of non-porphyritic chondrules. Such selectivity can, however, be excluded for mineralogically zoned and unzoned chondrules, as these appear in a large variety of chondrule textural types (e.g., Friend et al., 2016; Barosch et al., 2019).

Genge and Grady (1998) observed igneous rims around Kakangari chondrule fragments and single crystals. They interpret these fragments and crystals as remnants of shattered, former chondrules and suggest that the igneous rims around them formed during one or more subsequent reheating events in the nebula. Berlin (2009) also suggested reheating of a portion of Kakangari chondrules to explain what she believes was solid-state reduction of type II to type I chondrules. Reheating of chondrules has also been suggested for chondrules in other chondrites (e.g., Jones, 1996; Jones et al., 2005; Genge and Grady 1998, Hezel et al., 2003; Wasson and Rubin, 2003; Rubin, 2006, 2010; Ebel et al., 2008).

The aforementioned arguments indicate a complex formation history of Kakangari chondrules prior to parent body accretion, including at least two heating events and chondrule fragmentation. This complex history could explain the absence of mineralogically zoned chondrules in Kakangari: if the first generation of chondrules was mineralogically zoned, subsequent remelting and fragmentation could have destroyed or removed their initial zonation. The main evidence for this hypothesis are bulk chondrule compositional variations in CC, OC and Kakangari chondrites (Fig. 5.5), which most likely resulted from open system gas-melt interaction (e.g., Tissandier et al., 2002; Libourel et al., 2006; Ebel et al., 2018, and references therein). Barosch et al. (2019) found that the ranges of bulk compositions of zoned and unzoned chondrules in OC are indistinguishable from each other. They then argued that initially the majority of chondrules received SiO from the ambient gas, thereby forming zoned chondrules. Some chondrules then lost their initial zonation during the subsequent remelting events. If correct, the same scenario might apply to Kakangari chondrules. Open system exchange,

fragmentation and remelting of Kakangari chondrules might then explain the absence of mineralogically zoned chondrules.

#### *5.4.2. The likely origin and formation of agglomeratic chondrules in Kakangari*

Berlin (2009) found a considerable abundance of agglomeratic chondrules (AC) in Kakangari (14% of all chondrules) and interpreted these as evidence for partial melting of fine-grained chondrule precursor material at ~1200°C (see also Weisberg and Prinz, 1996). We measured a lower abundance of AC of about 5%. Berlin (2009) noticed that AC chondrules and silicate-dominated rims with igneous textures (i.e., igneous rims) around chondrules (cf. Genge and Grady, 1998) have similar textures and compositions, which we can confirm. Agglomeratic textures might therefore simply represent sections through thick igneous rims, even though Berlin (2009) dismissed this idea for larger ACs (e.g., one AC at 1500 µm diameter). The largest AC in our study has a diameter of 1700 µm. We also observed at least one AC with a diameter of >1000 µm and containing a ~300 µm compact, coarse-grained, enstatite-rich core. This texture likely resulted from sectioning a chondrule mostly through its igneous rim. This is similar to the sectioning effects observed in mineralogically zoned chondrules by Barosch et al. (2020) and discussed above (Section 5.4.1.). It is apparent that igneous rims around some Kakangari chondrules can be very thick and therefore chondrule sizes are not a sufficient criterion to reliably distinguish AC chondrules from sections through chondrule igneous rims. We therefore suggest that perhaps all AC in Kakangari are sections through igneous rims. Studies in 3D would be required to test this hypothesis and/or determine how many AC chondrules exist, or if these are better explained by the processes suggested by Berlin (2009).

#### *5.4.3. Mg/Si ratios of Kakangari chondrules and matrix*

The chondrule-matrix complementarity is based on two essential criteria outlined in Hezel et al. (2018a): (i) the bulk meteorite has a close to CI-chondritic ratio of an element or isotope pair, and (ii) average chondrules and matrix differ in this element or isotope ratio. This is then best explained by chondrule and matrix formation from a single solar reservoir. A prominent example for complementarity in CC is the Mg/Si ratio, as reported by various authors (e.g., Klerner, 2001; Hezel and Palme, 2010; Palme et al., 2015; Ebel et al., 2016; Friend et al., 2018; Hezel et al., 2018a, and references therein). Mg and Si are major elements in all chondrites – and chondrules and matrix are by far the largest reservoirs of these two elements. In CC with

Mg/Si complementarities, chondrules generally have higher Mg/Si ratios than CI chondrites. This is compensated by a lower than CI Mg/Si ratio in the matrix.

Kakangari appears to be an intriguing exception with respect to Mg/Si complementarity (Fig. 5.6): first, the Mg/Si/CI ratio of bulk Kakangari is 0.964 (Mason and Wiik, 1966; Palme et al., 2014), which is close to CI-chondritic, thereby meeting one of the two criteria for complementarity. Chondrules and matrix plot in distinct areas in the Mg-Si space, which are similar to where chondrules and matrix from chondrites with complementary Mg/Si ratios plot, i.e., Mg- and Si- concentrations in chondrules are about a factor of 1.6 higher than in the matrix (Table 5.4). However, the Mg/Si ratios of average chondrules and matrix in Kakangari are indistinguishable from each other (Mg/Si/CI matrix: 1.03, chondrules: 0.98), which are then also close to CI-chondritic. Kakangari therefore does not meet the second criterion for complementarity.

Ebel et al. (2016) found for CO chondrites that initially different chondrule and matrix element ratios – i.e., the second criterion for complementarity – can be entirely equalised by parent body processes: the Mg/Si ratios in chondrules and matrix in CO chondrites of petrologic type 3.0 are significantly different, but become progressively more uniform and CI-chondritic with increasing petrologic type (cf. Fig. 10 in Ebel et al., 2016). The Mg/Si ratios of chondrules and matrix in Warrenton (CO3.7) are about CI-chondritic. This is attributed to Fe-Mg exchange between chondrules and matrix during a mild thermal event on the parent body of the various CO chondrites. Hence, chondrules and matrix in Warrenton are interpreted to initially also have had different and complementary Mg/Si ratios, but parent body alteration equalised this difference. Warrenton chondrule and matrix Mg/Si ratios now no longer fulfil the second criterion of complementarity (Ebel et al., 2016).

As stated in Section 5.1, Berlin (2009) classified Kakangari as petrologic type  $\geq 3.5$  and  $\leq 3.8$  based on a large set of criteria. Therefore, Kakangari has a similar petrologic type as the CO3.7 chondrite Warrenton. The Mg/Si ratios of chondrules and matrix in Kakangari might therefore represent the result of a similar process as observed in Warrenton: chondrules and matrix initially had significantly different and complementary Mg/Si ratios. This initial difference equilibrated during parent body metamorphism, and towards the bulk Kakangari, CI-chondritic Mg/Si ratio. If true, Kakangari had an initial Mg/Si complementarity which would support formation of chondrules and matrix from a common reservoir. Alternatively, chondrules and matrix could have also formed from spatially separated reservoirs, but with identical, solar compositions. They were then transported and mixed together.

There are multiple arguments supporting a common origin of chondrules and matrix in Kakangari: (i) chondrule populations typically show large variations in their bulk compositions and a close to normal distribution (Hezel et al., 2006, 2018a; Hezel and Parteli, 2018; Barosch et al., 2019). As demonstrated in Fig. 5.5, this is also the case for Kakangari chondrules. Hezel and Parteli (2018) modelled whether such distributions could be explained by mixing of chondrules from multiple reservoirs. They concluded that transport and mixing of chondrules from different reservoirs in the protoplanetary disk seems unlikely. Rather, all chondrules of individual chondrites originated from the same reservoir. It is remarkable that the very diverse chondrule population (Fig. 5.6) has an average Mg/Si equal to that of the matrix. It is therefore unlikely that Kakangari chondrules originated from multiple parental reservoirs.

(ii) Many previous studies argued that the mineralogy and chemical characteristics of chondrules and matrix are very similar and both therefore formed in the same reservoir and location. Apparently, this similarity is a unique feature of the Kakangari chondrite and led Nehru et al. (1983) to propose that Kakangari consists of only one major component, instead of two. Based on chondrule and matrix similarities, Brearley (1989) suggested that both could have formed from identical precursor material during the same thermal event, but at different temperatures. Scott and Krot (2005) supported this statement, pointing out that matrix particles must have formed in close spatial proximity to the chondrules. However, these aforementioned authors assumed a low petrologic type for Kakangari, while recent arguments by Berlin (2009) instead indicate a relatively high petrologic type, i.e.,  $\geq 3.5$ . Berlin (2009) presented a model for Kakangari formation, taking into account a complex history of secondary overprints, e.g., metamorphism, reduction and secondary alteration. Nevertheless, Berlin (2009) fully agrees with the aforementioned authors: chondrules and matrix formed from similar precursor material in close spatial proximity and potentially by the same heating mechanism.

(iii) Prinz et al. (1989) and Weisberg et al. (1996) reported O-isotope differences between Kakangari chondrules and matrix, with an  $^{16}\text{O}$ -enriched bulk matrix when compared to chondrules. These results suggest that both components sampled separate O-isotope reservoirs, implying that there is no genetic relation. Similar results were reported by Nagashima et al. (2015), however, these authors argued that the matrix has a bimodal O-isotope composition. For the most part, the matrix is identical to the chondrules, but  $\sim 10\%$   $^{16}\text{O}$ -rich material was added to the Kakangari reservoir and incorporated into the matrix and chondrule rims. If this admixed  $^{16}\text{O}$ -rich material had a CI-chondritic composition, it would not disturb a complementary relationship, but only dilute the effect seen in the matrix (cf. Jacquet et al.,

2016; Braukmüller et al., 2018). O-isotope characteristics may therefore also support a common reservoir for Kakangari chondrules and most of the matrix.

(iv) Lastly, an additional argument for a single reservoir applies the criteria of Jones (2012), who argued that chondrule populations from different chondrite groups show characteristic properties. In Kakangari we observe a unique population of chondrules, and complete lack of whole or fragmental barred olivine chondrules.

In accordance with the aforementioned arguments from the literature, we propose that Kakangari chondrules and matrix were most likely initially complementary in Mg/Si and formed from a common reservoir. The different initial compositions were then equalised during parent body metamorphism, similar to CO chondrites (Ebel et al., 2016).

#### *5.4.4. Chondrule and matrix relationships in LEW 87232*

If we strictly apply the complementarity criteria as outlined at the beginning of Section 5.4.3., no element pair studied is complementary in either LEW 87232 or Kakangari. This makes K chondrites the first chondrite group in which no direct evidence for complementarities has been found. Due to analytical difficulties and an incomplete record of literature bulk chondrite data (cf. Section 5.2), only a limited number of elements was available to test complementary relationships: Al, Ca as major refractory, and Mg, Si, Cr as major elements in chondrules and matrix. In the following, we discuss potential reasons why chondrule-matrix complementarities are not observed in LEW 87232 for these elements.

LEW 87232 has been significantly altered during terrestrial weathering and was classified into weathering category B, referring to moderate rustiness (Mason, 1992). Weisberg et al. (1996) observed brownish staining covering the friable sample. Kallemeyn (1994) and Weisberg (1996) reported depletion of lithophile and siderophile elements as a result of Antarctic weathering, e.g., Fe is depleted in bulk LEW 87232 relative to Kakangari. A number of elements that are typically interesting for complementarity – foremost Ca – have also been affected by this weathering. The bulk Al/Ca/CI ratio in LEW 87232 is 2.27. This requires a significant fractionation, which is unknown from nebular processes, but can easily be achieved by terrestrial weathering, strongly indicating Ca loss in bulk LEW 87232 while resting in the ice.

Bulk LEW 87232 Mg/Si has not yet been determined. As Kakangari and LEW 87232 are both classified as K group meteorites (Weisberg et al., 1996), we assumed that their bulk Mg/Si

ratios are the same. This is in conflict with our calculated bulk Mg/Si/CI ratio of 0.92 for LEW 87232, which is well below the CI-chondritic ratio. Interestingly, the average Mg/Si ratio of chondrules and matrix in LEW 87232 are sub-chondritic and virtually identical, with Mg/Si/CI = 0.92. This would mean that bulk LEW 87232 is also sub-chondritic and – contrary to our assumption – different from Kakangari.

In comparison to Kakangari, LEW 87232 contains highly abundant low-Ca pyroxene in chondrules and matrix. Most chondrules have a PP textural type, while olivine-rich PO chondrules are rare (Table 5.2, Fig. 5.4). The olivine/pyroxene ratio in all intact LEW 87232 chondrules is 0.32, whereas it is much higher in intact Kakangari chondrules (0.77). The ratios are similar if fragments are included. This means that the main carrier phase of Mg – forsterite – is significantly underrepresented in LEW 87232 compared to Kakangari, resulting in sub-chondritic Mg/Si ratios for LEW 87232 main components. Mg/Si ratios are also sub-chondritic in OC and R chondrites, and could be explained by removal of early formed forsterites (Mg-loss; Petaev and Wood, 1998; Dauphas et al., 2015). Alternatively, these ratios could result from Si-addition to the reservoir. The latter is invoked by Friend et al. (2017) to explain sub-chondritic Mg/Si in R chondrites. Both scenarios could explain why LEW 87232, in contrast to Kakangari, does not have a bulk CI-chondritic Mg/Si ratio.

## 5.5. Conclusions

K group meteorites have unique petrographic, chemical and isotopic characteristics (Graham and Hutchison, 1974; Davis et al., 1977; Weisberg et al., 1996; Scott and Krot, 2005). Our study emphasises and expands on these unique properties: (i) almost no mineralogically zoned chondrules are present in Kakangari (7%), although these are abundant chondrule textures in virtually all other chondrites (Friend et al., 2016; Barosch et al., 2019, 2020). The other K chondrite studied, LEW 87232, contains 30% zoned chondrules. (ii) Bulk Kakangari is approximately CI-chondritic in various major (e.g., Mg/Si) and refractory element ratios (e.g., Al/Ca), and average chondrules and matrix also have CI-chondritic ratios for, at least, Mg/Si. Chondrules, matrix and likely also bulk LEW 87232 are identical and sub-chondritic in Mg/Si. The conditions and processes forming K chondrites appear to have been similar to other chondrites: the bulk chondrule compositional variation in K chondrites is close to a normal distribution and with a large compositional spread, similar to chondrules in OC and CC (Fig. 5.5). This is best explained if Kakangari and LEW 87232 chondrules were open systems and

received material (i.e., SiO) from the ambient gas during their formation (Tissandier et al., 2002; Libourel et al., 2006; Ebel et al. 2018, and references therein). SiO-addition to chondrules typically produces mineralogically zoned chondrules as observed in many other chondrites (Friend et al., 2016; Barosch et al., 2019, 2020, and references therein). Zoned chondrules are only occasionally seen in Kakangari, likely because nebular processes such as chondrule fragmentation and remelting of chondrules abraded and overprinted most of the initial mineralogical zoning.

SiO-addition further explains how chondrules with initially super-chondritic Mg/Si developed towards chondritic Mg/Si ratios. This process has been suggested for chondrules in CC, in which cases the average chondrule Mg/Si ratio remained super-chondritic to variable degrees (Hezel and Palme, 2010). The result in CC is a complementary relationship of chondrules with CC matrices, as bulk CC Mg/Si ratios are close to CI-chondritic (Hezel et al., 2018, and references therein). The same process likely happened in Kakangari, and initially, chondrules had super-chondritic Mg/Si ratios, and matrix had complementary, sub-chondritic Mg/Si ratios. Subsequent thermal overprint on the Kakangari parent body equilibrated this initial difference, similar to what has been reported in CO chondrites (Ebel et al., 2016). We therefore conclude that Kakangari chondrules and matrix initially had complementary Mg/Si ratios. Therefore, matrix most likely formed together with chondrules in the same reservoir. This conclusion is also supported by various arguments from previous studies (e.g., Brearley, 1989; Scott and Krot, 2005; Berlin, 2009; Nagashima et al., 2015).

LEW 87232 has distinct petrographic, mineralogical and bulk chemical characteristics compared to Kakangari. Chondrules are more abundant and generally smaller in LEW 87232, mostly intact and not fragmented. They are frequently mineralogically zoned and more pyroxene-rich. Bulk LEW 87232 Mg/Si is probably sub-chondritic. LEW 87232 is also less pristine than Kakangari. To better understand the relationship between LEW 87232 and Kakangari it would be beneficial to determine bulk Si concentrations for LEW 87232.

### **Acknowledgements**

JB is grateful for the support provided by AMNH museum staff, with special thanks to M. Rios, B. Green, K. Hammond, N. Nicholson and A. Fiege. The authors thank the Meteorite Working Group for the generous loan of LEW 87232.14 and M. Weisberg for helpful discussions. This work was supported by the Annette Kade Graduate Student Fellowship

Program of the RGGS at the American Museum of Natural History, through generous contributions of the Annette Kade Charitable Trust. DH gratefully acknowledges funding of this study by the Deutsche Forschungsgemeinschaft (DFG) grants HE 5352/10-1 and PA 346/50-1. JB gratefully acknowledges funding by Fellowship Grant No. GSGS-2019X-02 of the Graduate School of Geosciences, University of Cologne. This material is based upon work partially supported by the National Aeronautics and Space Administration under Grant No. NNX16AD37G issued through the Emerging Worlds program (DE). We thank A. Krot and three anonymous referees for their comments, as well as associate editor F. Moynier for handling the manuscript.

## Supplementary Material

Supplementary data can be found or online at <https://doi.org/10.1016/j.epsl.2020.116286> or at the end of this chapter. An extended digital supplement containing x-ray maps, derived data, and software, is available through the AMNH Library at <https://dx.doi.org/10.5531/sd.eps.6>

## References

- Barosch, J., Hezel, D.C., Ebel, D.S., Friend, P., 2019. Mineralogically zoned chondrules in ordinary chondrites as evidence for chondrule open system behaviour. *Geochim. Cosmochim. Acta* 249, 1–16.
- Barosch, J., Hezel, D.C., Sawatzki, L., Halbauer, L., Marrocchi Y., 2020. Sectioning effects of porphyritic chondrules: implications for the PP/POP/PO classification and correcting modal abundances of mineralogically zoned chondrules. *Meteorit. Planet. Sci.* (in press). <https://doi.org/10.1111/maps.13476>
- Becker, M., Hezel, D.C., Schulz, T., Elfers, B.-M., Münker, C., 2015. Formation timescales of CV chondrites from component specific Hf-W systematics. *Earth Planet. Sci. Lett.* 432, 472–482.
- Bence, A.E., Albee, A.L., 1968. Empirical correction factors for the electron micro-analysis of silicates and oxides. *J. Geol.* 76, 382–403.
- Berlin, J. 2009. Mineralogy and bulk chemistry of chondrules and matrix in petrologic type 3 chondrites: implications for early solar system processes. PhD thesis, University of New Mexico.

- Bischoff, A., Keil, K., 1983. Catalog of Al-rich chondrules, inclusions and fragments in ordinary chondrites. UNM, Institute of Meteoritics, Albuquerque, Spec. Publ. No. 22, 1–33.
- Braukmüller, N., Wombacher, F., Hezel, D.C., Escoube, R., Münker, C., 2018. The chemical composition of carbonaceous chondrites: Implications for volatile element depletion, complementarity and alteration. *Geochim. Cosmochim. Acta* 239, 17–48.
- Brearley, A.J., 1989. Nature and origin of matrix in the unique type 3 chondrite, Kakangari. *Geochim. Cosmochim. Acta* 53, 2395–2411.
- Budde, G., Kleine, T., Kruijer, T.S., Burkhardt, C., Metzler, K., 2016a. Tungsten isotopic constraints on the age and origin of chondrules. *Proc. Natl. Acad. Sci.* 113, 2886–2891.
- Budde, G., Burkhardt, C., Brennecka, G.A., Fischer-Gödde, M., Kruijer, T.S., Kleine, T., 2016b. Molybdenum isotopic evidence for the origin of chondrules and a distinct genetic heritage of carbonaceous and non-carbonaceous meteorites. *Earth Planet. Sci. Lett.* 454, 293–303.
- Dauphas, N., Poitrasson, F., Burkhardt, C., Kobayashi, H., Kurosawa, K., 2015. Planetary and meteoritic Mg/Si and  $\delta^{30}\text{Si}$  variations inherited from solar nebula chemistry. *Earth Planet. Sci. Lett.* 427, 236–248.
- Davis, A.M., Grossman, L., Ganapathy, R., 1977. Yes, Kakangari is a unique chondrite. *Nature* 265, 230–232.
- Ebel, D.S., Weisberg, M.K., Hertz, J., Campbell, A.J., 2008. Shape, metal abundance, chemistry, and origin of chondrules in the Renazzo (CR) chondrite. *Meteorit. Planet. Sci.* 43, 1725–1740.
- Ebel, D.S., Leftwich, K., Brunner, C.E., Weisberg, M.K., 2009. Abundance and size distribution of inclusions in CV3 chondrites by X-ray image analysis. 40th Lunar Planet. Sci. Conf., #2065, abstract.
- Ebel, D.S., Brunner, C., Konrad, K., Leftwich, K., Erb, I., Lu, M., Rodriguez, H., Crapster-Pregont, E.J., Friedrich, J.M., Weisberg M.K., 2016. Abundance, major element composition and size of components and matrix in CV, CO and Acfer 094 chondrites. *Geochim. Cosmochim. Acta* 172, 322–356.
- Ebel, D.S., Alexander, C.M.O'D., Libourel, G., 2018. Vapor-melt exchange: constraints on chondrite formation conditions and processes. In: *Chondrules: Records of Protoplanetary Disk Processes (Cambridge Planetary Science)* (eds. S.S. Russell, H.C. Connolly Jr. and A.N. Krot). Cambridge University Press, Cambridge UK. pp. 457.

- Friend, P., Hezel, D.C., Mucerschi, D., 2016. The conditions of chondrule formation, Part II: Open system. *Geochim. Cosmochim. Acta* 173, 198–209.
- Friend, P., Hezel, D.C., Palme, H., Bischoff, A., Gellissen, M., 2017. Complementary element relationships between chondrules and matrix in Rumuruti chondrites. *Earth Planet. Sci. Lett.* 480, 87–96.
- Friend, P., Hezel, D.C., Barrat, J.A., Zipfel, J., Palme, H., Metzler, K., 2018. Composition, petrology, and chondrule-matrix complementarity of the recently discovered Jbilet Winselwan CM2 chondrite. *Meteorit. Planet. Sci.* 53, 2470–2491.
- Genge, M.J., Grady, M.M., 1998. The textures and abundances of chondrules in the Kakangari chondrite. *Lunar and Planetary Science Conference Vol. 29*, abstract.
- Graham, A.L., Hutchison, R., 1974. Is Kakangari a unique chondrite? *Nature* 251, 128–129.
- Hezel, D.C., Palme, H., Brenker, F.E., Nasdala, L., 2003. Evidence for fractional condensation and reprocessing at high temperatures in CH-chondrites. *Meteorit. Planet. Sci.* 38, 1199–1216.
- Hezel, D.C., Palme, H., Nasdala, L., Brenker, F.E., 2006. Origin of SiO<sub>2</sub>-rich components in ordinary chondrites. *Geochim. Cosmochim. Acta* 70, 1548–1564.
- Hezel, D.C., 2007. A model for calculating the errors of 2D bulk analysis relative to the true 3D bulk composition of an object, with application to chondrules. *Comput. Geosci.* 33, 1162–1175.
- Hezel, D.C., 2010. A mathematica code to produce phase maps from two element maps. *Comput. Geosci.* 36, 1097–1099.
- Hezel, D.C., Kießwetter, R., 2010. Quantifying the error of 2D bulk chondrule analyses using a computer model to simulate chondrules (SIMCHON). *Meteorit. Planet. Sci.* 45, 555–571.
- Hezel, D.C., Palme, H., 2010. The chemical relationship between chondrules and matrix and the chondrule matrix complementarity. *Earth Planet. Sci. Lett.* 294, 85–93.
- Hezel, D.C., Bland, P.A., Palme, H., Jacquet, E., Bigolski, J., 2018a. Composition of chondrules and matrix and their complementary relationship in chondrites. In *Chondrules: Records of Protoplanetary Disk Processes (Cambridge Planetary Science)* (eds. S. S. Russell, H. C. Connolly Jr. and A. N. Krot). Cambridge University Press, Cambridge UK. pp. 457.
- Hezel, D.C., Harak, M., Libourel, G., 2018b. What we know about elemental bulk chondrule and matrix compositions: Presenting the ChondriteDB Database. *Chemie der Erde* 78, 1–14.

- Hezel, D.C., Parteli, E.J.R., 2018. The spatial origin of chondrules in individual chondrites: constraints from modeling chondrule mixing. *The Astrophysical Journal* 863, 54.
- Jacquet, E., Barrat, J.A., Beck, P., Caste, F., Gattacceca, J., Sonzogni, C., Gounelle, M., 2016. Northwest Africa 5958: a weakly altered CM-related ungrouped chondrite, not a CI3. *Meteorit. Planet. Sci.* 51, 851–869.
- Jones, R.H., 1996. Relict grains in chondrules: Evidence for chondrule recycling. In *Chondrules and the Protoplanetary Disk* (eds. R. H. Hewins, R.H. Jones and E.R.D. Scott), 163–172.
- Jones, R.H., Grossman, J.N., Rubin, A.E., 2005. Chemical, mineralogical and isotopic properties of chondrules: clues to their origin. In *Chondrites and the Protoplanetary Disk*, vol. 341 (eds. Krot A. N., Scott E. R. D. and Reipurth B.), 251–285.
- Jones, R.H., 2012. Petrographic constraints on the diversity of chondrule reservoirs in the protoplanetary disk. *Meteor. Planet. Sci.* 47, 1176–1190.
- Kallemeyn, G.W., 1994. Compositional study of Kakangari and LEW 87232. *Meteoritics* 29, 479–480.
- Klerner, S., 2001. *Materie im frühen Sonnensystem: Die Entstehung von Chondren, Matrix und refraktären Forsteriten*. PhD thesis, University of Cologne.
- Libourel, G., Krot, A.N., Tissandier, L., 2006. Role of gas-melt interaction during chondrule formation. *Earth Planet. Sci. Lett.* 251, 232–240.
- Mason, B.H., Wiik, H.B., 1966. The composition of the Bath, Frankfort, Kakangari, Rose City, and Tadjera meteorites. *American Museum Novitates* 2272, 1–24.
- Mason, B., 1992. Thin section description of LEW 87232. *Antarctic Meteorite Newsletter* 15, 24.
- McSween, Jr. H.Y., Richardson, S.M., 1977. The composition of carbonaceous chondrite matrix. *Geochim. Cosmochim. Acta* 60, 1145–1161.
- Nagashima, K., Krot, A.N., Huss, G.R., 2015. Oxygen-isotope compositions of chondrule phenocrysts and matrix grains in Kakangari K-grouplet chondrite: Implication to a chondrule-matrix genetic relationship. *Geochim. Cosmochim. Acta* 151, 49–67.
- Nehru, C.E., Prinz, M., Weisberg, M.K., Delaney, J.S., 1983. The Kakangari chondrite and its relationship to carbonaceous chondrite. *Meteoritics* 18, 361.
- Nehru, C.E., Weisberg, M.K., Prinz, M., 1986. Chondrules in the Kakangari chondrite. 49th Annual Meeting of the Meteoritical Society Vol. 600, p. 207, abstract.

- Nelson, V.E., Rubin, A.E., 2001. Size-frequency distributions of chondrules and chondrule fragments in LL3 chondrites: Implications for parent-body fragmentation of chondrules. *Meteorit. Plant. Sci.* 37, 1361–1376.
- Nuth, J.A. III., Brearley, A.J., Scott, E.R.D., 2005. Microcrystals and amorphous material in comets and primitive meteorites: Keys to understanding processes in the early solar system. In *Chondrites and the protoplanetary disk*, edited by Krot A.N., Scott E.R.D., and Reipurth B. San Francisco: Astronomical Society of the Pacific, 675–700.
- Palme, H., Lodders, K., Jones, A., 2014. Solar system abundances of elements. In *Treatise on Geochemistry* 2nd ed. (eds. H. Holland and K. Turekian), 15–34.
- Palme, H., Hezel, D.C., Ebel, D.S., 2015. The origin of chondrules: Constraints from matrix composition and matrix-chondrule complementarity. *Earth Planet. Sci. Lett.* 411, 11–19.
- Petaev, M.I., Wood, J.A., 1998. The condensation with partial isolation (CWPI) model of condensation in the solar nebula. *Meteorit. Planet. Sci.* 33, 1123–1137.
- Prinz, M., Weisberg, M.K., Nehru, C.E., MacPherson, G.J., Clayton, R.N., Mayeda, T.K., 1989. Petrologic and stable isotope study of the Kakangari (K-group) chondrite: chondrules, matrix, CAI's. *Lunar and Planetary Science Conference* vol. 20, abstract.
- Prinz, M., Weisberg, M.K., Clayton R.N., Mayeda T.K., 1991. Lea Co. 002: A second Kakangari-type chondrite. *Lunar and Planetary Science Conference* vol. 22, abstract.
- Rubin, A.E., 2006. A relict-grain-bearing porphyritic olivine compound chondrule from LL3.0 Semarkona that experienced limited remelting. *Meteorit. Plant. Sci.* 41, 1027–1038.
- Rubin, A.E., 2010. Physical properties of chondrules in different chondrite groups: implications for multiple melting events in dusty environments. *Geochim. Cosmochim. Acta* 74, 4807–4828.
- Russell, S.S., Connolly, Jr. H.C., Krot, A.N., 2018. Chondrules – records of protoplanetary disk processes. Part II – possible chondrule forming mechanisms. Cambridge University Press, Cambridge UK. pp. 457.
- Scott, E.R.D., Krot, A.N., 2005. Thermal processing of silicate dust in the solar nebula: clues from primitive chondrite matrices. *The Astrophysical Journal* 623, 571–578.
- Tissandier, L., Libourel, G., Robert, F., 2002. Gas-melt interactions and their bearing on chondrule formation. *Meteorit. Planet. Sci.* 37, 1377–1389.
- Wasson, J.T., Rubin, A.E., 2003. Ubiquitous low-FeO relict grains in type II chondrules and limited overgrowth on phenocrysts following the final melting event. *Geochim. Cosmochim. Acta* 67, 2239–2250.

- Weisberg, M.K., Prinz, M., Clayton, R.N., Mayeda, T.K., Grady, M.M., Franchi, I., Pillinger, C.T., Kallemeyn, G. W., 1996. The K (Kakangari) chondrite grouplet. *Geochim. Cosmochim. Acta* 60, 4253–4263.
- Weisberg, M.K., Prinz, M., 1996. Agglomeratic chondrules, chondrule precursors, and incomplete melting. In *Chondrules and the protoplanetary disk*, edited by Hewins R. H., Jones R. H., and Scott E. R. D. Cambridge: Cambridge University Press, 119–127.
- Zanda, B., Lewin, E., Humayun, M., 2018. The chondritic assemblage: complementarity is not a required hypothesis. In *Chondrules: Records of Protoplanetary Disk Processes* (Cambridge Planetary Science) (eds. S.S. Russell, H.C. Connolly Jr. and A.N. Krot). Cambridge University Press, Cambridge UK, pp. 457.

## Appendix

### Element ratios (CI normalised)

Meteorite	Mg/Al	Mg/Si	Mg/Ca	Mg/Ti	Mg/Fe	Al/Si	Al/Ca	Al/Ti	Al/Fe	Si/Ca	Si/Ti	Si/Fe	Ca/Ti	Ca/Fe	Ti/Fe
Kakangari A (literature)	1.08	0.96	1.18	0.95	1.26	0.89	1.08	0.87	1.17	1.22	0.98	1.31	0.80	1.08	1.34
Kakangari B (literature)	1.09		1.10		1.09		1.01		0.99					0.99	
Kakangari (calculated)	1.07	1.01	1.28	1.11	1.24	0.95	1.19	1.03	1.15	1.26	1.09	1.22	0.86	0.97	1.12
LEW87232 (literature)	1.04		2.36		1.61		2.27		1.55					0.68	
LEW87232 (calculated)	0.90	0.92	2.25	1.49	0.98	1.02	2.50	1.66	1.09	2.44	1.62	1.07	0.66	0.44	0.66

Kak A: Mason and Wiik (1966); wet chemistry

Kak B: Weisberg et al. (1996); INAA

LEW: Weisberg et al. (1996); INAA

CI normalised element ratios >0.9, <1.1

CI normalised element ratios <0.9, >1.1

### Bulk meteorite element concentrations (wt%)

Meteorite	Mg	Al	Si	Ca	Ti	Fe	
CI	9.54	0.84	10.70	0.91	0.04	18.66	Palme et al. (2014)
Kakangari A (literature)	14.53	1.18	16.90	1.18	0.07	22.47	Mason and Wiik (1966)
Kakangari B (literature)	14.40	1.16	-	1.25	-	25.90	Weisberg et al. (1996)
Kakangari (calculated)	14.25	1.17	15.76	1.06	0.06	22.56	
LEW87232 (literature)	16.30	1.38	-	0.66	-	19.80	Weisberg et al. (1996)
LEW87232 (calculated)	12.68	1.24	15.43	0.54	0.04	25.25	

### Calculated bulk compositions (wt%)

Kakangari	Chd + Fragments	Matrix	Sulphide	Metal*	CAI	AOA	Chlorapatite	calculated bulk
Abundance (%)	22.78	66.98	3.46	6.43	0.19	0.16	0.58	100
Density (g/cm <sup>3</sup> )	3.2	4.6	4.6	7.9	3.2	3.2	3.2	-
Si	25.04	16.47	0.00	0.00	11.75	39.83	0.00	15.76
Ti	0.06	0.07	0.00	0.00	1.07	0.37	0.00	0.06
Al	1.24	1.33	0.00	0.00	18.06	8.15	0.00	1.17
Cr	0.28	0.42	0.00	0.00	0.00	0.29	0.00	0.34
Fe	3.36	18.61	63.52	77.67	0.39	5.80	0.00	22.56
Mn	0.35	0.24	0.00	0.00	0.00	0.10	0.00	0.23
Ni	0.02	1.02	0.00	21.90	0.00	0.00	0.00	2.16
Mg	21.92	15.07	0.00	0.00	6.10	39.41	0.00	14.25
Ca	1.35	0.92	0.00	0.00	20.09	5.47	38.48	1.06
Na	0.55	0.81	0.00	0.00	0.08	0.11	0.00	0.66

LEW87232	Chd + Fragments	Matrix	Sulphide	Metal	CAI	AOA	Chlorapatite	calculated bulk
Abundance (%)	33.68	53.36	5.19	7.78	0	0	0	100
Density (g/cm <sup>3</sup> )	3.2	4.6	4.6	7.9	3.2	3.2	3.2	-
Si	26.28	16.04	0.00	0.00				15.43
Ti	0.06	0.04	0.00	0.00				0.04
Al	1.46	1.58	0.00	0.00				1.24
Cr	0.18	0.06	0.00	0.00				0.08
Fe	1.39	20.83	63.52	79.70				25.25
Mn	0.20	0.10	0.00	0.00				0.10
Ni	0.02	1.79	0.00	19.63				2.08
Mg	21.65	13.15	0.00	0.00				12.68
Ca	1.25	0.41	0.00	0.00				0.54
Na	0.85	1.11	0.00	0.00				0.83

\*average metal composition from Berlin (2009) and Weisberg et al. (1996)

## 5. Chondrules and matrix in Kakangari

Kakangari		Chondrule texture*					Bulk composition (wt%)											
Sample	Chondrule	PO	PP	POP	RP	AC	SiO <sub>2</sub>	TiO <sub>2</sub>	Al <sub>2</sub> O <sub>3</sub>	Cr <sub>2</sub> O <sub>3</sub>	FeO	MnO	NiO	MgO	CaO	Na <sub>2</sub> O	Sum	
3956-1	Chd01	x					53.00	0.12	3.32	0.38	4.33	0.49	0.02	35.79	1.81	1.66	100.92	
3956-1	Chd02		x				60.32	0.16	3.23	0.67	6.11	0.55	0.04	24.92	3.78	1.44	101.22	
3956-1	Chd03			x			55.86	0.07	3.05	0.25	2.80	0.32	0.04	36.32	1.52	0.85	101.08	
3956-1	Chd04	x					48.38	0.15	3.54	0.23	3.91	0.36	0.04	39.29	2.28	1.96	100.14	
3956-1	Chd05			x			55.76	0.11	3.87	0.29	3.45	0.33	0.02	33.41	1.42	1.69	100.36	
3956-1	Chd06	x					50.34	0.10	1.97	0.34	5.58	0.52	0.03	39.67	1.72	0.76	101.03	
3956-1	Chd07			x			55.70	0.10	2.72	0.44	4.63	0.45	0.05	33.23	1.30	1.21	99.83	
3956-1	Chd08		x				57.77	0.05	1.58	0.51	5.74	0.70	0.06	32.65	1.39	0.74	101.19	
3956-1	Chd09		x				61.38	0.17	4.52	0.46	3.42	0.46	0.02	26.00	2.31	2.13	100.86	
3956-1	Chd10				x		58.33	0.12	1.87	0.75	5.23	0.52	0.03	30.06	2.48	0.79	100.17	
3956-1	Chd11			x			56.35	0.08	2.54	0.60	3.36	0.46	0.02	34.79	1.28	0.89	100.37	
3956-1	Chd12			x			54.60	0.07	1.22	0.41	3.26	0.37	0.04	38.99	1.46	0.23	100.65	
3956-1	Chd13	x					49.70	0.13	3.60	0.38	3.80	0.42	0.01	38.50	2.42	1.61	100.58	
3956-1	Chd14			x			56.60	0.06	2.52	0.29	3.12	0.34	0.03	35.71	1.03	0.95	100.65	
3956-1	Chd15			x			56.16	0.07	2.00	0.30	3.31	0.38	0.02	37.21	0.53	0.83	100.80	
3956-1	Chd16			x			54.41	0.07	2.64	0.24	3.03	0.36	0.02	38.38	0.74	1.26	101.15	
3956-1	Chd17	x					48.55	0.09	2.00	0.19	3.79	0.42	0.01	42.76	1.68	1.01	100.51	
3956-1	Chd18			x			52.41	0.05	2.03	0.29	5.01	0.44	0.02	38.74	1.02	0.87	100.89	
3956-1	Chd19			x			55.60	0.08	3.43	0.06	1.46	0.21	0.02	38.19	0.75	1.29	101.08	
3956-1	Chd20			x			47.53	0.04	0.85	0.18	3.71	0.42	0.02	47.20	0.62	0.41	100.98	
3956-1	Chd21			x			54.36	0.10	3.21	0.31	3.26	0.40	0.01	36.59	1.40	1.45	101.08	
3956-1	Chd22			x			52.24	0.05	2.07	0.63	3.27	0.42	0.01	40.79	1.25	0.48	101.21	
3956-1	Chd23			x			54.90	0.05	1.63	0.32	3.07	0.43	0.04	38.86	1.17	0.30	100.78	
3956-2	Chd01			x			56.81	0.12	2.52	0.37	3.27	0.39	0.02	35.95	1.36	0.43	101.25	
3956-2	Chd02			x			54.45	0.07	1.09	0.33	3.52	0.41	0.02	39.85	1.32	0.25	101.33	
3956-2	Chd03		x				56.76	0.06	1.62	0.65	6.15	0.53	0.02	31.58	1.32	0.24	98.94	
3956-2	Chd04	x					49.47	0.10	1.79	0.28	4.84	0.48	0.01	40.89	2.42	0.33	100.64	
3956-2	Chd05			x			56.16	0.08	2.07	0.43	3.55	0.38	0.02	35.67	1.60	0.42	100.38	
3956-2	Chd06			x			58.39	0.11	1.94	0.51	4.61	0.60	0.01	31.70	1.63	0.39	99.89	
3956-2	Chd07	x					48.30	0.12	2.61	0.20	3.79	0.37	0.02	41.85	2.18	0.90	100.35	
3956-2	Chd08	x					48.42	0.13	2.79	0.26	4.07	0.39	0.05	40.50	2.94	0.76	100.31	
3956-2	Chd09	x					50.46	0.10	2.73	0.17	4.43	0.36	0.07	40.48	1.15	0.48	100.44	
3956-2	Chd10			x			57.25	0.13	2.68	0.44	2.96	0.40	0.02	34.14	1.91	0.66	100.58	
3956-2	Chd11			x			51.96	0.38	4.56	0.28	4.63	0.44	0.02	34.44	1.99	1.31	99.99	
3956-2	Chd12	x					47.98	0.15	2.60	0.36	4.98	0.42	0.04	40.05	3.46	0.68	100.72	
3956-2	Chd13			x			52.78	0.04	1.51	0.26	4.08	0.38	0.13	39.40	0.97	0.24	99.79	
3956-2	Chd14			x			48.45	0.04	0.45	0.22	4.16	0.47	0.02	45.91	1.08	0.17	100.97	
3956-2	Chd15	x					49.19	0.14	3.17	0.33	3.49	0.39	0.03	39.45	3.36	0.78	100.34	
3956-2	Chd16			x			54.23	0.13	2.09	0.42	4.77	0.54	0.03	35.33	2.06	0.44	100.03	
t1-ps1A	Chd01		x				58.93	0.09	1.60	0.51	5.82	0.42	0.01	31.20	0.95	0.33	99.86	
t1-ps1A	Chd02			x			52.76	0.09	1.46	0.46	4.51	0.38	0.02	37.69	2.00	0.33	99.71	
t1-ps1A	Chd03			x			46.86	0.06	1.39	0.26	5.54	0.49	0.03	43.55	0.74	0.41	99.33	
t1-ps1A	Chd04			x			54.33	0.14	4.67	0.28	3.23	0.38	0.24	33.07	2.10	1.33	99.76	
t1-ps1A	Chd05			x			54.88	0.23	5.09	0.29	3.16	0.47	0.02	30.74	3.43	1.08	99.39	
t1-ps1A	Chd06			x			53.12	0.04	1.61	0.34	4.76	0.49	0.02	38.20	0.94	0.40	99.92	
t1-ps1A	Chd07		x				58.14	0.24	5.95	0.80	3.59	0.61	0.04	23.97	3.66	1.02	98.01	
t1-ps1A	Chd08				x		58.59	0.12	2.22	0.70	4.48	0.61	0.01	30.99	1.98	0.59	100.30	
t1-ps2A	Chd01					x	45.36	0.11	2.00	0.17	3.34	0.38	0.04	45.19	2.54	0.47	99.59	
t1-ps2A	Chd03			x			52.37	0.03	0.83	0.03	1.84	0.24	0.02	42.79	0.53	0.24	98.94	
t1-ps2A	Chd04			x			54.00	0.19	2.55	1.00	3.27	0.51	0.04	34.91	3.17	0.39	100.04	
t1-ps2A	Chd05	x					47.35	0.09	1.78	0.27	4.01	0.42	0.02	43.38	1.47	0.24	99.03	
t1-ps2A	Chd06			x			47.83	0.12	2.43	0.32	5.54	0.43	0.12	40.19	1.86	0.64	99.49	
t1-ps2A	Chd09			x			55.20	0.12	2.60	0.68	5.47	0.44	0.03	32.01	2.43	0.44	99.41	
t1-ps2A	Chd10			x			56.77	0.10	3.66	0.47	4.36	0.50	0.12	30.70	2.79	0.87	100.33	
t1-ps2A	Chd11			x			52.52	0.07	1.44	0.45	4.14	0.41	0.05	37.01	1.43	0.45	97.98	
t1-ps2A	Chd12			x			57.00	0.19	3.33	0.62	9.07	0.39	0.09	25.94	1.97	0.38	98.98	
t1-ps2A	Chd13					x	45.58	0.22	1.48	0.75	7.79	0.46	0.02	43.17	1.28	0.06	100.81	

**Matrix, weighted average composition** 35.23 0.11 2.51 0.61 23.94 0.32 1.30 24.98 1.29 1.09 91.38  
calculated from McSween and Richardson (1977; 20 spot analyses), Berlin (2009; 125 spots), and this study: Kak-t1-ps1A (51 spots),  
and -ps2A (194 spots)

LEW87232		Chondrule texture*						Bulk composition (wt%)									
Sample	Chondrule	PO	PP	POP	RP	AC	SiO <sub>2</sub>	TiO <sub>2</sub>	Al <sub>2</sub> O <sub>3</sub>	Cr <sub>2</sub> O <sub>3</sub>	FeO	MnO	NiO	MgO	CaO	Na <sub>2</sub> O	Sum
LEW87232	Chd 01			x			55.69	0.10	2.16	0.42	1.94	0.32	0.02	37.48	2.23	0.44	100.80
LEW87232	Chd 02		x				59.07	0.07	2.85	0.30	1.68	0.25	0.01	34.28	1.20	1.28	100.99
LEW87232	Chd 03			x			55.82	0.09	1.86	0.28	1.79	0.28	0.04	38.62	1.44	0.60	100.81
LEW87232	Chd 04			x			57.31	0.06	1.47	0.28	2.38	0.24	0.02	37.62	1.10	0.41	100.87
LEW87232	Chd 05			x			52.12	0.09	2.39	0.13	1.30	0.21	0.02	41.13	1.71	1.07	100.18
LEW87232	Chd 06			x			55.06	0.15	2.93	0.35	1.52	0.28	0.01	36.49	2.92	0.59	100.29
LEW87232	Chd 07		x				58.40	0.12	4.91	0.28	1.70	0.20	0.02	29.43	2.46	2.67	100.18
LEW87232	Chd 08		x				58.95	0.11	4.34	0.27	1.86	0.30	0.01	29.82	2.27	2.21	100.13
LEW87232	Chd 09	x					58.47	0.18	4.80	0.12	1.49	0.25	0.03	31.54	1.46	1.67	100.01
LEW87232	Chd 10			x			53.74	0.12	4.22	0.18	1.26	0.21	0.02	36.04	1.96	1.97	99.72
LEW87232	Chd 11			x			54.45	0.12	2.76	0.26	1.82	0.23	0.02	36.81	1.99	1.19	99.65
LEW87232	Chd 12		x				57.68	0.07	0.89	0.30	2.05	0.26	0.01	36.78	0.89	0.44	99.37
LEW87232	Chd 13			x			52.11	0.07	2.24	0.11	1.30	0.21	0.02	41.95	0.56	1.09	99.66
LEW87232	Chd 14			x			52.98	0.18	2.10	0.22	1.69	0.26	0.04	39.73	1.82	1.11	100.13
LEW87232	Chd 15			x			56.77	0.13	2.48	0.37	2.21	0.34	0.02	34.17	2.70	0.69	99.88
LEW87232	Chd 16			x			55.65	0.15	3.02	0.33	1.36	0.28	0.02	36.08	2.36	0.96	100.21
LEW87232	Chd 17		x				57.67	0.08	3.43	0.20	1.79	0.28	0.02	33.86	1.10	1.54	99.97
LEW87232	Chd 18		x				59.80	0.07	4.43	0.20	1.58	0.20	0.01	30.14	1.93	2.23	100.59
LEW87232	Chd 19						58.38	0.07	1.25	0.39	2.52	0.27	0.02	35.67	2.28	0.40	101.26
LEW87232	Chd 21			x			52.72	0.08	2.66	0.19	1.72	0.24	0.03	39.70	1.54	1.27	100.17
LEW87232	Chd 22		x				56.88	0.08	2.14	0.21	2.43	0.22	0.05	35.63	1.19	0.97	99.81
LEW87232	Chd 23		x				57.22	0.12	1.46	0.27	1.92	0.24	0.03	37.01	1.24	0.54	100.05
<b>Matrix, average composition (this study)</b>							34.31	0.07	2.98	0.08	26.80	0.13	2.28	21.80	0.58	1.50	90.54

\*

POP porphyritic olivine-pyroxene  
 PO porphyritic olivine  
 PP porphyritic pyroxene  
 RP radial pyroxene  
 AC agglomeratic chondrule

# Chapter 6

## Discussion

The publications presented in this thesis address in detail the extent of chondrule-gas interaction in different chondrites (Chapter 2, 3 and 5), the interaction among chondrules during their formation (Chapter 4), and the genetic relationship of chondrules and matrix in Kakangari chondrites (Chapter 5). These results provide pivotal constraints for chondrule formation conditions, which will be summarised and discussed. Ultimately, these constraints help to identify the chondrule forming mechanism.

### 6.1. Constraints for chondrule formation conditions

#### 6.1.1. Chondrules behaved as open systems

An important constraint for chondrule formation is whether chondrules interacted with their environment or not. This is essential to explain the various petrographic and petrologic observations of chondrules. The results of this thesis strongly support open system behaviour of chondrules, based on textural and compositional evidence.

The first systematic study of mineralogically zoned chondrules in CC and R chondrites was presented by Friend et al. (2016; 256 chondrules in 16 meteorites). Zoned chondrules have olivine cores surrounded by pyroxene (and/or silica) rims. In this present thesis, the textures of ~1800 chondrules from 17 different meteorites were analysed (8xOC, 6xEC, 1xCC, 2xK; Table 6.1), thereby completing the study of mineralogically zoned chondrules in all chondrites. Most EC data in Table 6.1 will be published in a forthcoming paper. The fractions of zoned chondrules as determined in 2D sections and in the different chondrite groups are displayed in Table 6.1 and Fig. 6.1. Fractions are high in CC (78%), intermediate in R (41%) and OC (39%), and comparatively low in EC (28%) and K chondrites (19%).

A total of 455 chondrules from CC, OC and EC samples were studied in 3D. Their 3D fractions of mineralogically zoned chondrules are systematically and significantly higher compared to their respective 2D fractions. 3D fractions are higher by factor 1.24 in CC, by factor 1.29 in OC and by factor 1.62 in EC (Fig. 6.2). These differences result from sectioning effects, which also skew the widely-used textural classification of porphyritic chondrules (cf. Chapter 3). The

apparently distinct textural types (PP, PO, POP) often simply represent 2D sections through the same mineralogically zoned chondrule, i.e., sections through pyroxene rims (PP) or olivine cores (PO).

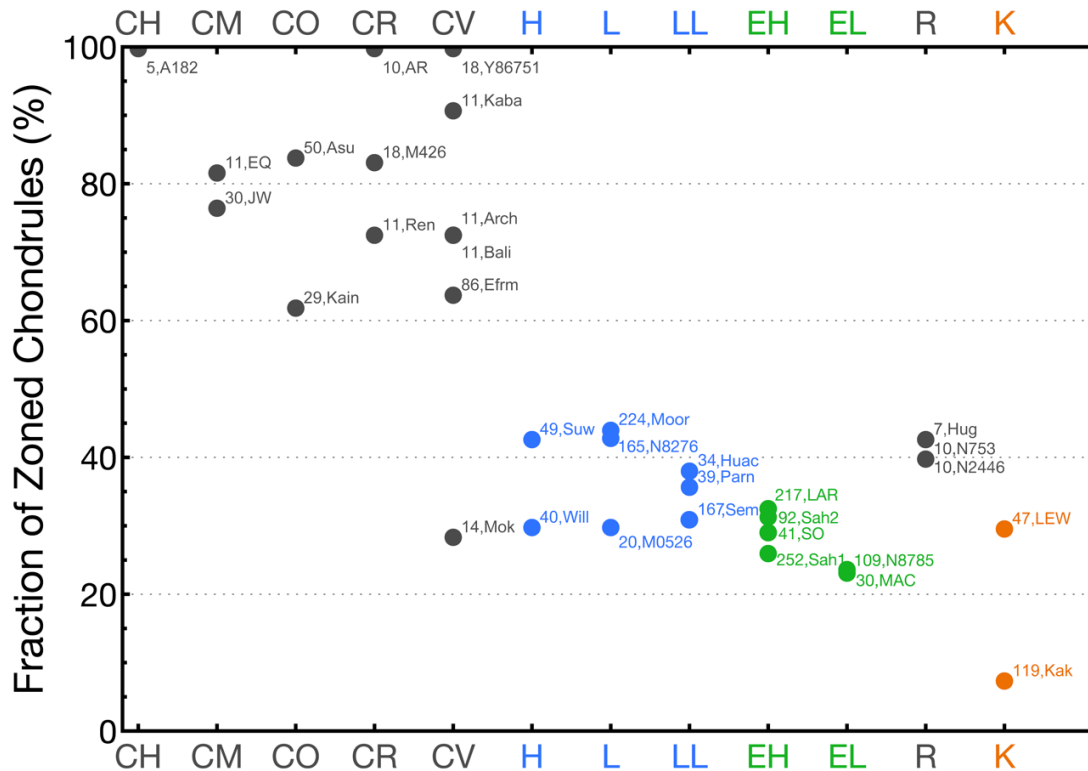


**Fig. 6.1:** 2D fractions of mineralogically zoned chondrules in all chondrite groups. Data and meteorite abbreviations are taken from Table 6.1. The numbers indicate the total amount of chondrules studied. Black: carbonaceous chondrites and Rumuruti (Friend et al., 2016, modified), blue: ordinary chondrites, green: enstatite chondrites, orange: Kakangari.

The formation of mineralogically zoned chondrules is attributed to open system behaviour of chondrules (cf. Chapter 2; Tissandier et al., 2002; Libourel et al., 2006; Ebel et al., 2018, and references therein). Low-Ca pyroxene rims result from the reaction of chondrule olivine with an SiO-rich surrounding gas. Mineralogically zoned chondrules therefore provide direct textural evidence for chondrule open system behaviour.

The aforementioned high fractions of mineralogically zoned chondrules (Fig. 6.1, 6.2, Table 6.1) clearly indicate that zoned chondrules represent a large, and in cases even the dominant sub-population of chondrules in chondrites. Non-mineralogically zoned chondrules constitute the second sub-population. If zoned chondrules are explained by open system gas-melt interaction, then unzoned chondrules could indicate the absence of this process, i.e., they might have been closed systems during their formation. To test this, the bulk compositions of 274 chondrules in OC, EC and K chondrites were studied. Bulk chondrule compositions in these

meteorites are highly variable, spreading along the forsterite-enstatite mixing line. This represents an increasing molar fraction of  $\text{SiO}_2$ , as indicated in Fig. 6.3.

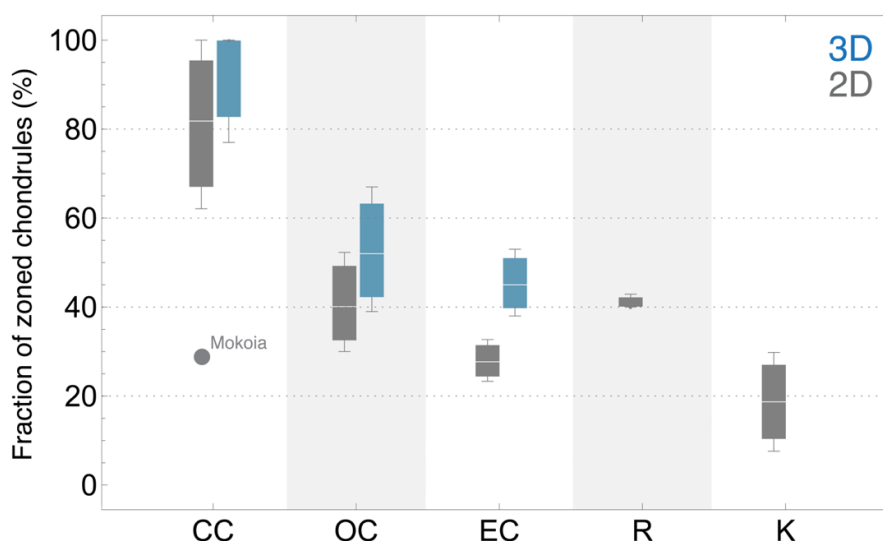


**Fig. 6.2:** 2D and 3D fractions of mineralogically zoned chondrules in different chondrite groups. 3D fractions were calculated from the 2D data (Table 6.1) by using the approximate correction factors as determined from real 3D data in Chapter 3: 1.24 for carbonaceous chondrites, 1.29 for ordinary chondrites and 1.62 for enstatite chondrites.

The variability of chondrule bulk compositions is best explained by open system behaviour: chondrules were initially forsterite-rich but received various amounts of gaseous  $\text{SiO}$  during cooling, thus altering their bulk compositions (cf. Chapter 2; Tissandier et al., 2002; Libourel et al., 2006; Hezel et al., 2006; Ebel et al., 2018, and references therein). The relative addition of material to each chondrule likely depended on various factors, such as the surface/volume ratio, the ambient  $\text{SiO}$ -gas pressure, chondrule peak temperatures, cooling rates, timing, and so on. Zoned and unzoned chondrules have the same range of bulk compositions (Fig. 6.3). This requires  $\text{SiO}$  addition to both chondrule sub-populations and, therefore, it is likely that all chondrules were open systems.

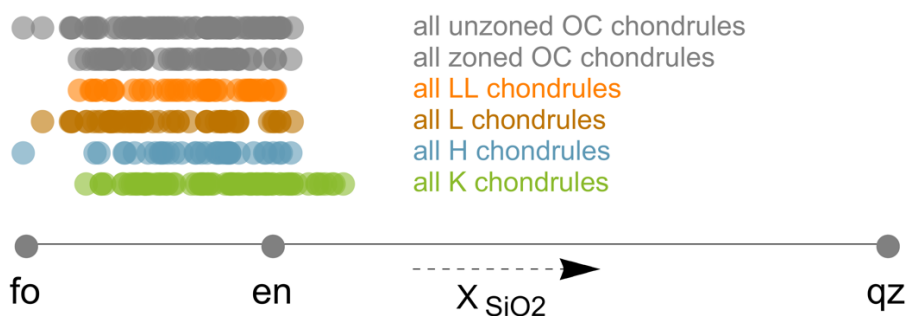


**Fig. 6.3:** Highly variable  $\text{SiO}_2$  molar fractions ( $X$ ) of bulk chondrules in ordinary (H, L, LL) and Kakangari chondrites. These likely result from  $\text{SiO}$  addition to initially fo-rich chondrules. Zoned and unzoned OC chondrules have the same range of bulk compositions. fo: forsterite, en: enstatite, qz: quartz.

**Table 6.1:** Fractions of mineralogically zoned chondrules in chondrites

Class	Group	Meteorite Name	Abbreviation	Petr. type	Method*	Chd studied	Zoned 2D	Zoned 3D	
CC	CH	Aefer 182	A182	3	IM	5	5 = 100 %	-	
	CM	El-Quss Abu Said	EQ	2	IM	11	9 = 82 %	-	
	CM	Jbilet Winselwan	JW	2	IM	30	23 = 77 %	-	
	CO	Asuka 881632	Asu	3	IM	50	42 = 84 %	-	
	CO	Kainsaz	Kain	3.2	IM	29	18 = 62 %	-	
	CR	Al Rais	AR	2-an	IM	10	10 = 100 %	-	
	CR	Meteorite Hills 00426	M426	2	IM	18	15 = 83 %	-	
	CR	Renazzo	Ren	2	IM	11	8 = 73 %	-	
	CV	Arch	Arch	3	IM	11	8 = 73 %	-	
	CV	Bali	Bali	3	IM	11	8 = 73 %	-	
	CV	Kaba	Kaba	3	IM	11	10 = 91 %	-	
	CV	Mokoia	Mok	3	IM	14	4 = 29 %	-	
	CV	Yamato 86751	Y86751	3	IM	18	18 = 100 %	-	
	CV	Efremovka	Efrm	3	LAM + 3D	86	55 = 64 %	68 = 79%	
	OC	LL	Huacachina	Hua	3	IM	34	13 = 38 %	-
		LL	Parnallee	Parn	3.6	IM	39	14 = 36 %	-
LL		Semarkona	Sem	3.00	LAM	167	52 = 31 %	-	
L		NWA 8276	N8276	3.00	IM	65	34 = 52 %	-	
L		Moorable	Moor	3.8-an	LAM	165	71 = 43 %	-	
L		Moorable	Moor	3.8-an	LAM	107	50 = 47 %	-	
H		Suwahib (Buwah)	Suw	3.8-an	LAM + 3D	117	49 = 42 %	63 = 53%	
H		Willard (b)	Will	3.6	IM	49	21 = 43 %	-	
L(LL)		Meteorite Hills 00526	M0526	3.05	IM	40	12 = 30 %	-	
L(LL)		Meteorite Hills 00526	M0526	3.05	IM	20	6 = 30 %	-	
FC	EH	Sahara 97096	Sah1	3	LAM + 3D	252	66 = 26 %	107 = 43%	
	EH	Sahara 97127	Sah2	3	LAM	92	29 = 32 %	-	
	EH	Larkman Nunatak 12252	LAR	3	LAM	217	71 = 33 %	-	
	EH	South Oman	SO	4/5	LAM	41	12 = 29 %	-	
	EL	NWA 8785	N8785	3	LAM	109	26 = 24 %	-	
	EL	MacAlpine Hills 02837	MAC	3	LAM	30	7 = 23 %	-	
FC	R	Hughes 030	Hug	3-6	IM	7	3 = 43 %	-	
	R	NWA 753	N753	3.9	IM	10	4 = 40 %	-	
	R	NWA 2446	N2446	3	IM	10	4 = 40 %	-	
FC	K	Kakangari	Kak	3	LAM	119	9 = 8 %	-	
	K	LEW87232	LEW	3	LAM	47	14 = 30 %	-	
						Total:	2052	800	
								238	

Chd: chondrules, CC: carbonaceous chondrites, OC: ordinary chondrites, EC: enstatite chondrites, R: Rumuruti, K: Kakangari

\*IM: Analysis of individual chondrule maps, LAM: Large area maps - analysis of entire chondrite sections, 3D: Large area maps analysed in 2D and 3D (serial sectioning)

\*\*revised after Barosch, unpubl.

If both chondrule sub-populations received gaseous SiO, it is unexpected that some chondrules formed pyroxene rims (zoned chondrules), and others did not (unzoned chondrules). It is, however, possible that unzoned chondrules initially formed pyroxene rims, which they subsequently lost. Several secondary processes are capable of removing pyroxene rims around chondrules. An example is Mokoia, a CV chondrite that was affected by secondary processes on its parent body. For a CC chondrite, Mokoia has an atypically low fraction of zoned chondrules (29%, Fig. 6.1, 6.2; Friend et al., 2016). The outermost layers of Mokoia chondrules (i.e., pyroxene rims of zoned chondrules) were replaced by secondary minerals during parent body aqueous alteration (Tomeoka and Onishi, 2015). Therefore, the original fraction of zoned chondrules in this meteorite was most likely significantly higher. Another example is Kakangari, the chondrite with the lowest fraction of zoned chondrules (~8%, Table 6.1; Chapter 5). Interestingly, this meteorite has the largest spread of bulk chondrule compositions in Fig. 6.3, despite an almost complete absence of zoned chondrules. This might indicate that Kakangari chondrules also received gaseous SiO to various extents. Further, Kakangari chondrules experienced wide-spread fragmentation. This process shattered mineralogically zoned chondrules (cf. Fig. 5.3) and possibly also abraded portions of chondrule pyroxene rims. However, this process cannot be solely responsible for the absence of zoned chondrules in Kakangari as almost all intact chondrules are also unzoned.

Chondrules could have also lost their initial pyroxene rims when they were reheated and subsequently remelted (cf. Chapter 2). This scenario is in line with various previous studies suggesting multiple heating of chondrules (e.g., Wasson, 1993; Wasson et al., 1995; Rubin and Krot, 1996; Rubin, 2000, 2006, 2010; Hezel et al., 2003, 2006; Jones et al., 2005; Ebel et al., 2008), as well as chondrule age constraints (e.g., Kurahashi et al., 2008, Becker et al., 2015; Budde et al., 2016a). Chondrule reheating and remelting is likely true for all chondrites studied in this thesis and would mean that the chondrule population of a meteorite formed during more than one heating event. This has important implications: proposed chondrule forming mechanisms that cannot heat chondrules more than once must be discarded. Excluded heating mechanisms are, for example, jetting during particle collisions, exothermic chemical reactions, supernova shock waves and gamma-ray bursts (cf. Rubin, 2000).

### *6.1.2. Chondrules interacted with each other through collisions*

Important details about chondrule formation might be derived from atypical chondrules and unusual objects in chondrites. An interesting example are macrochondrules (cf. Chapter 4,

Weisberg et al., 1988). These are petrologically similar to average chondrules but significantly larger (i.e., 10 times or more). Weyrauch and Bischoff (2012) suggested that macrochondrules could have formed from chondrule collisions. It is widely accepted that chondrule collisions can fuse two or more chondrules together, forming compound chondrules (e.g., Gooding and Keil, 1981; Ciesla, 2006; Arakawa and Nakamoto, 2016, 2019; Bogdan et al., 2019). However, macrochondrule formation – contrary to compound chondrule formation – would require chondrules to fully merge and homogenise after colliding, thereby destroying any petrographic evidence for the preceding collisions.

In laboratory experiments, Bogdan et al. (2019) determined possible outcomes of chondrule collisions at constant velocities ( $\sim 1$  m/s) but variable temperatures (Fig. 6.4; cf. Arakawa and Nakamoto, 2016, 2019, for high velocity collisions). Their results suggest that collisions at low temperatures lead to chondrule fragmentation or plastic deformation. At intermediate temperatures, partially molten chondrules may stick-, and subsequently fuse together to form compound chondrules. At high temperatures, largely molten chondrules could fully merge after colliding, forming macrochondrules. However, this model of compound and macrochondrule formation is not universally accepted (e.g., Hubbard, 2015) and might be challenging to verify without petrographic evidence.

The unusual compound object presented in Chapter 4 could be the first object genetically linking compound chondrules to macrochondrules. It appears to be a macrochondrule that collided with a solid BO chondrule, and afterwards failed to homogenise. The object thereby provides first petrographic support for the model of Bogdan et al. (2019). Interestingly, the phase map displayed in Fig. 6.4 shows a mineralogically zoned compound chondrule. The displayed compound chondrule must have been partially molten during/after the collision, which then allowed open system gas-melt interaction and thereby pyroxene rim formation during cooling. This scenario would be in conflict with compound chondrule formation from the collision of solid and/or supercooled droplets (Arakawa and Nakamoto, 2016, 2019).

According to Ciesla (2006) and Arakawa and Nakamoto (2016, 2019), the nebular shock wave model (Wood, 1996; Desch and Connolly, 2002; Morris et al., 2012; Morris and Boley, 2018) best explains compound chondrule formation and, therefore, also macrochondrule formation. High abundances of macrochondrules and/or compound chondrules in chondrites (e.g., OC) might, furthermore, indicate that these chondrites formed in dust-rich regions of the solar nebula, allowing frequent chondrule collisions. Nebular regions with elevated dust/gas ratios are invoked by many authors (e.g., Wood, 1963; Ebel and Grossman, 2000; Tissandier et al.,

2002; Libourel et al., 2006; Alexander et al., 2008; Marrocchi and Chaussidon, 2015), but their existence is not undisputed (e.g., Rubin et al., 2018).

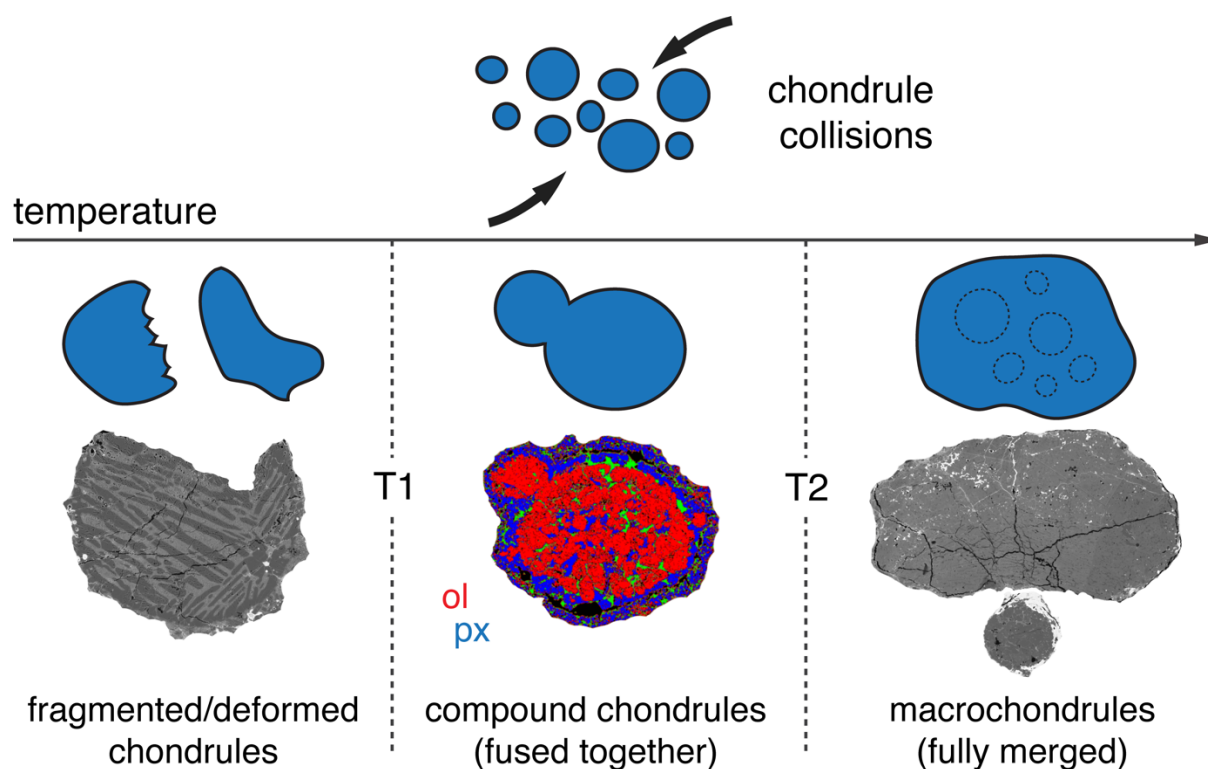


**Fig. 6.4:** Schematic image and examples illustrating the consequences of chondrule collisions at different temperatures. If solid chondrules collide, they are fragmented or deformed. If the colliding chondrules were partially molten ( $T > T_1$ ), they were fused together to form compound chondrules. If the colliding chondrules were largely or completely molten ( $T > T_2$ ), they merged completely to form macrochondrules. The displayed examples show: left: fragmented chondrule, centre: phase map of two chondrules fused together (compound chondrule), right: a macrochondrule in comparison to an average-sized chondrule of  $\sim 700 \mu\text{m}$  diameter.

### 6.1.3. Chondrules and matrix likely formed in common reservoirs

Most chondrule formation models can be categorised into one of two groups: those that propose a common reservoir for chondrules and matrix formation and those that suggest spatially separated origins and subsequent mixing of both components (cf. Hezel et al., 2018b). If a genetic relationship between chondrules and matrix could be proven or refuted, one of these groups must be discarded. As outlined in detail by Hezel et al. (2018b, and references therein) the chondrule-matrix complementarity in CC and R chondrites could be a decisive argument for a common reservoir for both components (see also Section 1.4.2, Section 5.4.3). The study of complementarity was expanded to K chondrites in this thesis. Prior to parent body metamorphism, Kakangari chondrules and matrix were likely complementary in Mg and Si, the two major elements in chondrites (cf. Chapter 5). The results suggest that chondrule open

---

system behaviour has been essential to establish not only bulk chondrule compositional variations (Fig. 6.3), but also Mg/Si complementarity. Together, complementarity and open system interaction provide a coherent picture of chondrule formation.

All chondrites with complementarities formed from reservoirs with solar initial ratios for their complementary element pair(s). In case of Mg/Si, forsterite-rich aggregates condensed at high-temperatures from the cooling nebular gas, thereby preferentially extracting Mg from and progressively enriching SiO in the gas. The forsterite-rich solids served as chondrule precursors and melted during the chondrule forming heating event(s). During cooling, the chondrules received variable amounts of gaseous SiO, thus altering their bulk compositions (Fig. 6.3). Bulk chondrule compositions thereby spread out along the forsterite-enstatite mixing line, reflecting SiO-addition. The displacement of chondrule bulks from the ideal fo-en line in the Mg/Si plot depends on the FeO contents of chondrules. The average bulk chondrule composition gradually approached the solar ratio with progressing SiO-addition to chondrules. In CC, chondrule gas-melt interaction stopped while the average chondrule composition was still at a superchondritic Mg/Si ratio. In Kakangari, these initially different compositions likely equilibrated during parent body metamorphism, similar to what has been observed in CO chondrites by Ebel et al. (2016). Complementarity then requires that matrix formed in the same reservoir, but timing and details are not yet fully understood. Matrix might represent a mixture of un-melted precursor material, added CI-like material, and material that condensed during/after chondrule formation (Alexander, 2005; Hezel and Palme, 2010; Brearley, 2014; Friend et al., 2016; Braukmüller et al., 2018; Hezel et al., 2018b, and references therein). The matrix was subsequently altered during parent body processes.

This proposed scenario is fully consistent with all aforementioned constraints for chondrule formation and is further supported by various authors studying complementarities (cf. references in Hezel et al., 2018b).

## 6.2. Formation of chondrites and their components

In the following, I will review the properties of different chondrite groups as reported in the literature and in this thesis. These might translate to approximate nebular locations of chondrite forming reservoirs and, furthermore, allow valuable insight into the processes and conditions in these reservoirs.

### 6.2.1. Characteristics of chondrite forming reservoirs

The properties of chondrites and their components represent the conditions and processes in their respective formation reservoirs. Many authors proposed a bimodality of chondrite forming reservoirs, in which non-carbonaceous chondrites (EC, OC) formed in heliocentric distances closer to the Sun than carbonaceous chondrites (CC; Fig. 6.5; e.g., Wasson, 1977; Rubin and Wasson, 1995; Weisberg et al., 1996; Warren, 2011; Walsh et al., 2011; Budde et al., 2016a; Gerber et al., 2017; Burkhardt et al., 2019, and references therein). These two major reservoirs might have been isolated from each other when Jupiter formed in-between them (e.g., Walsh et al, 2011; Gerber et al., 2017), and broadly divided the solar system into an inner and an outer region. The following paragraphs will point out some general petrologic, chemical and isotopic differences in inner (non-carbonaceous) and outer (carbonaceous) solar system reservoirs.

*Component abundances:* the main component modal abundances in carbonaceous and non-carbonaceous chondrites are strikingly different: chondrule to matrix proportions are approximately 40:60 in many carbonaceous chondrites, but 80:20 in non-carbonaceous chondrites (Scott and Krot, 2014). The abundances of minor (CAI) and unusual components (e.g., macrochondrules) are also different. CAIs are relatively common in CC but mostly absent in non-carbonaceous chondrites. Macrochondrules are frequently observed in OC, but not as often in CC (Weyrauch and Bischoff, 2012).

*Oxidation states:* Rubin and Wasson (1995) correlated the oxidation states of nebular reservoirs with ambient temperatures. As nebular temperature decreased with heliocentric distance, the inner regions of the solar nebula had lower oxidation states than distant regions. The oxidation states of meteorites then indicate their approximate heliocentric formation distances. Non-carbonaceous meteorites are more reduced and, therefore, formed closer to the sun than CC.

*Bulk chemistries:* there are various differences in the bulk compositions of inner and outer solar system chondrites. Relative to CI, refractory elements (Ca, Al) are slightly enriched in CC, and

slightly depleted in non-CC. Main elements (Si, Mg, Fe) are essentially unfractionated from the solar ratio in most CC, but enriched and/or depleted in non-CC. Bulk CC have approximately solar Mg/Si ratios but OC and EC have Mg/Si/CI ratios of  $\leq 0.9$  (Wasson and Kallemeyn, 1988; Palme et al., 2014; Hezel et al., 2018a), which requires Si enrichment and/or Mg depletion in these meteorites. Volatile elements (e.g., Mn, Na, Rb, Zn, S) are depleted in all chondrites relative to CI, however, CC are slightly more depleted than the other chondrites (Braukmüller et al., 2018).

*Isotope characteristics:* nucleosynthetic isotope anomalies for a large number of elements, e.g., Ti, Mo, Cr, support distinct CC and non-CC reservoirs (e.g., Budde et al., 2016b; Gerber et al., 2017; Burkhardt et al., 2019, and references therein). For example, Gerber et al. (2017) showed that CC contain  $^{50}\text{Ti}$  enriched chondrules, whereas OC and EC do not. The authors argued that these compositions result from the addition of CAI-like material (i.e.,  $^{50}\text{Ti}$ -rich nuggets) to CC chondrule precursors, thereby supporting spatially separated and isolated reservoirs of CC and non-CC chondrites. The trend towards lighter O isotope compositions observed in CC also reflects increasing heliocentric formation distances (Rubin and Wasson, 1995).

*Chondrule characteristics:* The chondrule populations of chondrites exhibit various differences and similarities. Mineralogically zoned chondrules can be found in every chondrite (Fig. 6.1 and 6.5). However, they are more abundant in outer solar system chondrites ( $> 80\%$ , on average). Non-CC have significantly lower fractions of zoned chondrule ( $\leq 50\%$ , on average). All chondrule populations in CC and non-CC show large ranges of bulk compositions and close to normal bulk compositional distributions (Fig. 6.5). Chondrule-matrix complementarities were reported in CC, R (Hezel et al., 2018b, and references therein) and possibly K chondrites (cf. Chapter 4), but not yet in OC and EC.

### 6.2.2. Origin of K chondrites

Weisberg et al. (1996) argued that the properties of K chondrites do not clearly fit into the inner or outer solar system (Fig. 6.5). New insights from recent studies (e.g., Berlin, 2009) and this thesis (Chapter 5) allow an attempt to assign K-grouplet meteorites to an approximate location in the protoplanetary disk.

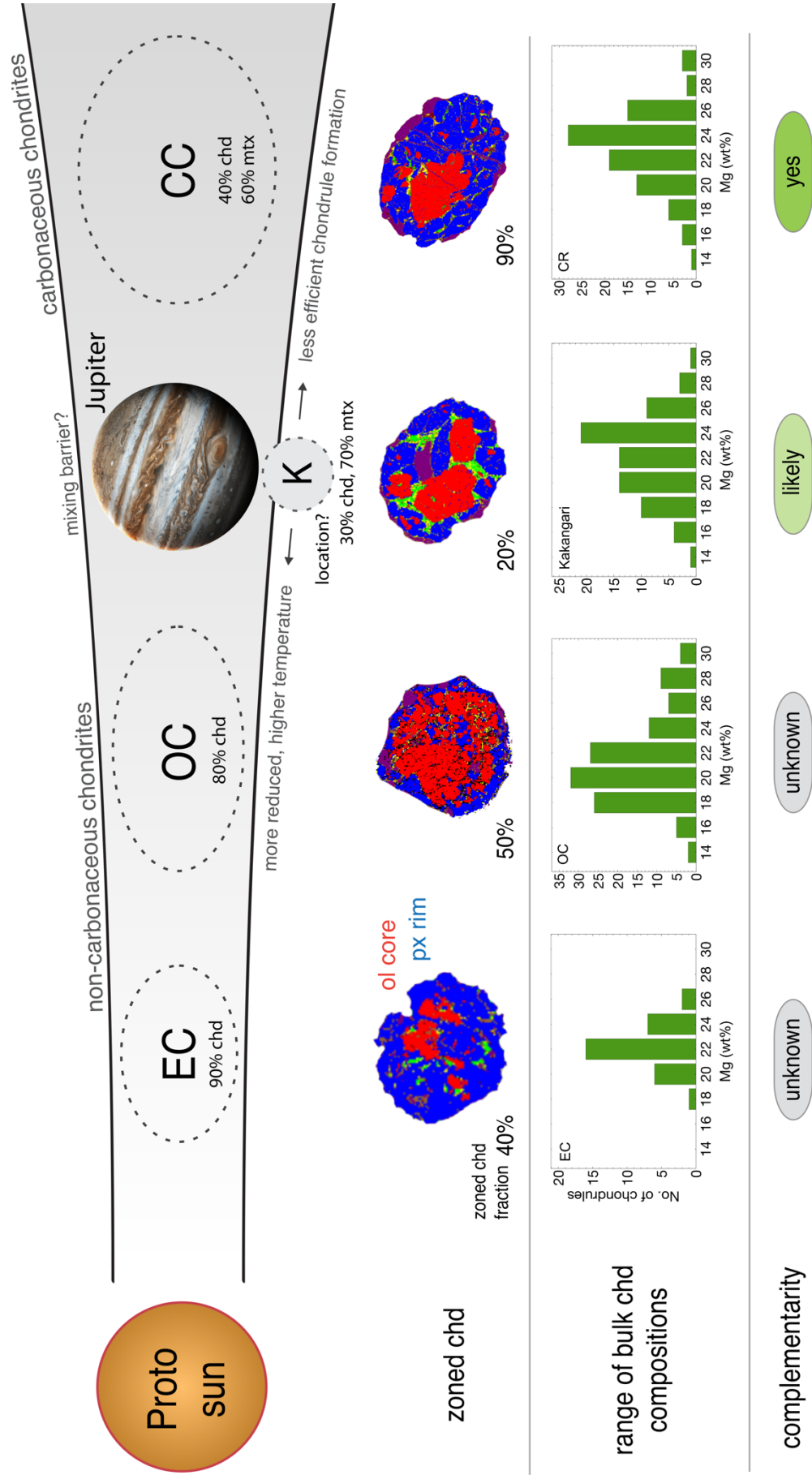


**Fig. 6.5** (previous page): Schematic image of the protoplanetary disk showing likely locations of chondrite forming reservoirs. The results of this thesis show that mineralogically zoned chondrules formed in every reservoir and that chondrule populations in all reservoirs have a normal distribution of bulk compositions. Complementarity was observed in CC (Hezel et al., 2018b) and possibly K chondrites, but not yet in OC and EC.

Kakangari has a high abundance of matrix (70%), which suggests that heating during chondrule formation was inefficient. This is further supported by the degree of chondrule melting, inferred from their textures: barred olivine chondrules – often associated with higher degrees of melting than porphyritic chondrules (Wasson et al., 1995) – are absent in Kakangari. Furthermore, O-isotope compositions of Kakangari (average  $\Delta^{17}\text{O}$  of -1.6‰; Weisberg et al., 1996) imply relatively low nebular temperatures according to Rubin and Wasson (1995). These characteristics support an outer solar system origin of K chondrites.

The main argument for an inner solar system origin of K chondrites is their highly reduced mineralogy. Chondrule silicates and matrix are FeO-poor and indicate an oxidation state intermediate of OC and EC (Weisberg et al., 1996). However, evidence presented by Berlin (2009) suggests that Kakangari might have experienced widespread reduction. It is possible that the conditions in the K chondrite reservoir were more oxidising than previously assumed. Therefore, an outer solar system origin cannot be excluded solely based on the oxidation state of K chondrites.

Weisberg et al. (1996) further refers to the abundances of refractory and main elements to support an inner solar system origin. It is true that refractory elements, relative to CI, are slightly enriched in CC and slightly depleted in OC, EC and K. However, as shown in Chapter 5, bulk main element ratios are close to solar in Kakangari (i.e., Mg/Si/CI is 0.96; Mason and Wiik, 1966; Palme et al., 2014) and, therefore, clearly different from non-carbonaceous chondrites. Kakangari chondrules and matrix, furthermore, were likely complementary in Mg/Si prior to parent body metamorphism. Unfractionated main element ratios and complementarities are key characteristics of many CC (e.g., Hezel et al., 2018b, and references therein).

Zoned chondrule fractions are relatively low in chondrites from inner solar system reservoirs. Of all chondrites studied, Kakangari has the lowest fraction of zoned chondrules. However, this does not necessarily indicate a specific nebular location, but rather highlights the complex history of secondary processing observed in Kakangari chondrules (cf. Chapter 5; Berlin, 2009). Similar to chondrule populations of other chondrites, Kakangari shows a close to normal distribution of bulk chondrule compositions. Thus, these characteristics of Kakangari chondrules do not clearly indicate an inner or outer solar system origin.

The aforementioned arguments show that Kakangari might be more closely associated with CC than OC and EC. This would promote an outer solar system origin of K chondrites. Nucleosynthetic isotope studies (e.g.,  $^{50}\text{Ti}$ ) of Kakangari chondrules would help to more accurately link this meteorite to a nebular location. So far,  $^{50}\text{Ti}$  has only been measured in a single Kakangari chondrule (Niemeyer, 1988). This chondrule does not have a  $^{50}\text{Ti}$  deficit and is, therefore, neither indicative of CC, nor non-CC reservoirs (Gerber et al., 2017).

### *6.2.3. Processes during chondrite component formation*

The distinct properties of the individual chondrite groups (Section 6.2.1.) may be attributed to the conditions in the respective reservoirs and/or the processes that formed chondrites. It is important to determine whether chondrites and their components formed from different processes or if they experienced the same processes throughout the protoplanetary disk. Here, I want to discuss if the constraints reported in this thesis (cf. Section 6.1) result from localised or ubiquitous processes in the disk.

The concept of complementarity – in coalescence with gas-melt interaction (cf. Section 6.1.3) – is theoretically applicable to all chondrites. However, complementarities have not yet been identified in OC and EC and it is still controversial if they exist in these meteorites. Chondrules are the dominant component in most non-carbonaceous chondrites, i.e., these often have up to 80 vol% chondrules and typically only 10–15 vol% matrix (Scott and Krot, 2014). Thus, bulk OC and EC compositions are mainly defined by their chondrules, which causes difficulties for demonstrating complementarities. Unlike CC, there is definitely no main element (i.e., Mg/Si) complementarity in OC and EC as these do not have solar main element ratios (cf. Section 6.2.1). Future work could, instead, focus on refractory lithophile and siderophile elements in these chondrites (e.g., Al, Ca, Ti, Zr, W, Hf, REE). Refractory element ratios are often unfractionated from the respective solar ratios. As demonstrated by Becker et al. (2015), Hf/W behaves complementary in CV chondrules and matrix. Lithophile Hf was mostly incorporated in chondrule silicates, and siderophile W in matrix opaques. This shows that complementarities do not necessarily require comparable chemical behaviour of element pairs. If chondrules and matrix were formed by the same process in all chondrites, then, eventually, complementarities will be detected in non-CC. However, so far, complementarities can only be confirmed for outer solar system reservoirs.

The results of this thesis clearly demonstrate that zoned chondrules are abundant in all chondrites studied (Fig. 6.1, 6.2, 6.5). Thus, the process that formed zoned chondrules – open

system interaction – must have operated ubiquitously in protoplanetary disk reservoirs. This conclusion is challenged by authors who proposed that chondrules from inner and outer solar system reservoirs were transported and mixed together (Olson et al., 2016). In this case, zoned chondrules might have formed in the outer solar system as CC have up to 90% zoned chondrules, and were then mixed into inner solar system chondrites with lower zoned chondrule fractions. This scenario can be ruled out for several reasons: (i) complementarity excludes separate origins and mixing of components for CC (and likely K), however, not yet for OC and EC. (ii) Jupiter likely prevented large scale mixing of components from inner and outer solar system reservoirs (Fig. 6.5; Walsh et al, 2011; Gerber et al., 2017). (iii) All chondrule bulk compositions show close to normal distributions (Fig 6.5). Hezel and Parteli (2018) argued that such distributions can only be explained by a common origin of the chondrule population in a chondrite. Separate origins and disk-wide transport of chondrules would instead produce multimodal distributions. Lastly, (iv) Jones (2012) argued that the distinct properties of chondrule populations in chondrites (i.e., average chondrules sizes, petrographies, bulk chemical and isotope compositions) require common origins. Individual chondrite groups then sampled unique chondrule-forming reservoirs.

### 6.3. Conclusions

The results of this thesis – i.e., fractions of zoned chondrules in chondrites, range and distribution of bulk chondrule compositions, and complementarity – show that the processes during chondrule formation were most likely rather similar in the carbonaceous and non-carbonaceous reservoirs, despite all the aforementioned differences among the groups (Section 6.2). The distinct properties of individual chondrite groups then largely reflect various, and, importantly, local ambient conditions in the distinct reservoirs. For example, as temperatures were higher in the inner solar system, the chondrule heating mechanism might have been more energetic compared to outer regions (e.g., Ciesla, 2005). Thus, more chondrules were produced in inner solar system reservoirs, while less efficient heating resulted in the high matrix fractions observed in outer solar system chondrites.

Based on the results of this thesis and their implications discussed above, I suggest to discard chondrule formation models that (i) require separate origins of chondrules and matrix, or mixing of chondrules from multiple reservoirs (ii) prohibit open system interaction, and (iii) cannot heat chondrules more than once. In principle, the following models would satisfy the constraints presented in this thesis: chondrule formation by nebular shock waves (Wood, 1996;

Desch and Connolly, 2002; Morris et al., 2012; Morris and Boley, 2018, and references therein), current sheet heating from magneto-rotational instabilities (McNally et al., 2013), and the layered disk model introduced by Mac Low et al. (2017). These models provide disk-wide mechanisms for chondrule formation that would also allow localised heating events and cogenetic formation of chondrules and matrix. They are, thus, compatible with complementarity, open system interaction, remelting of chondrules and macrochondrule formation.

# References for Chapters 1 and 6

- Alexander C. M. O'D. (1994) Trace element distributions within ordinary chondrite chondrules: implications for chondrule formation conditions and precursors. *Geochimica et Cosmochimica Acta* **58**, 3451–3467.
- Alexander C. M. O'D. (2005) Re-examining the role of chondrules in producing the elemental fractionations in chondrites. *Meteoritics and Planetary Science* **40**, 943–965.
- Alexander C. M. O'D., Grossman J. N., Ebel D. S. and Ciesla F. J. (2008) The formation conditions of chondrules and chondrites. *Science* **320**, 1617–1619.
- Amelin Y., Krot A. N., Hutcheon I. D. and Ulyanov A. A. (2002) Lead isotopic ages of chondrules and calcium-aluminium-rich inclusions. *Science* **297**, 1678–1683.
- Andrews S. M., Wilner D. J., Zhu Z., Birnstiel T., Carpenter J. M., Pérez L. M., Bai X-N., Öberg K. I., Hughes A. M., Isella A. and Ricci L. (2016) Ringed substructure and a gap at 1 au in the nearest protoplanetary disk. *The Astrophysical Journal Letters* **820**, L40 5pp.
- Arakawa S. and Nakamoto T. (2016) Compound chondrule formation via collision of supercooled droplets. *Icarus* **276**, 102–106.
- Arakawa S. and Nakamoto T. (2019) Compound chondrule formation via high-speed collision of supercooled droplets in optically thin shock waves. *82nd Annual Meteoritical Society Meeting*, abstract #6113.
- Asphaug E., Jutzi M. and Movshovitz N. (2011) Chondrule formation during planetesimal accretion. *Earth and Planetary Science Letters* **308**, 369–379.
- Becker M., Hezel D. C., Schulz T., Elfers B. M. and Münker C. (2015) Formation timescales of CV chondrites from component specific Hf-W systematics. *Earth and Planetary Science Letters* **432**, 472–482.
- Berlin J. (2009) Mineralogy and bulk chemistry of chondrules and matrix in petrologic type 3 chondrites: implications for early solar system processes. *PhD thesis*, University of New Mexico.
- Bizzarro M., Baker J. A. and Haack H. (2004) Mg isotope evidence for contemporaneous formation of chondrules and refractory inclusions. *Nature* **431**, 275–278.

- Bland P. A., Alard O., Benedix G. K., Kearsley A. T., Menzies O. N., Watt L. E. and Rogers N. W. (2005) Volatile fractionation in the early solar system and chondrule-matrix complementarity. *Proceedings of the National Academy of Science* **102**, 13755–13760.
- Bogdan T., Teiser J., Fischer N., Kruss M. and Wurm G. (2019) Constraints on compound chondrule formation from laboratory high-temperature collisions. *Icarus* **319**, 133–139.
- Bouvier A. and Wadhwa M. (2010) The age of the Solar System redefined by the oldest Pb-Pb age of a meteoritic inclusion. *Nature Geoscience* **3**, 637–641.
- Brearley A. J. (2014) Nebular versus parent body processing. In: *Treatise on Geochemistry 2<sup>nd</sup> ed.* (eds. H. Holland and K. Turekian), 309–334.
- Braukmüller N., Wombacher F., Hezel D. C., Escoube R. and Münker C. (2018) The chemical composition of carbonaceous chondrites: Implications for volatile element depletion, complementarity and alteration. *Geochimica et Cosmochimica Acta* **239**, 17–48.
- Budde G., Kleine T., Kruijjer T. S., Burkhardt C. and Metzler K. (2016a) Tungsten isotopic constraints on the age and origin of chondrules. *Proceedings of the National Academy of Science* **113**, 2886–2891.
- Budde G., Burkhardt C., Brennecka G. A., Fischer-Gödde M., Kruijjer T. S. and Kleine T. (2016b) Molybdenum isotopic evidence for the origin of chondrules and a distinct genetic heritage of carbonaceous and non-carbonaceous meteorites. *Earth and Planetary Science Letters* **454**, 293–303.
- Burkhardt C., Dauphas N., Hans U., Bourdon B. and Kleine T. (2019) Elemental and isotopic variability in solar system materials by mixing and processing of primordial disk reservoirs. *Geochimica et Cosmochimica Acta* **261**, 145–170.
- Ciesla F. J. (2005) Chondrule-forming processes – an overview. In *Chondrites and the Protoplanetary Disk*, vol. 341 (eds. Krot A. N., Scott E. R. D. and Reipurth B.), 811–820.
- Ciesla F. J. (2006) Chondrule collisions in shock waves. *Meteoritics and Planetary Science* **41**, 1347–1359.
- Clayton R. N. (1993) Oxygen isotopes in meteorites. *Annual Review of Earth and Planetary Sciences* **21**, 115–149.
- Desch S. J. and Connolly Jr. H. C. (2002) A model of the thermal processing of particles in solar nebula shocks: Application to the cooling rates of chondrules. *Meteoritics and Planetary Science* **37**, 183–207.
- Ebel D. S. and Grossman L. (2000) Condensation in dust-enriched systems. *Geochimica et Cosmochimica Acta* **64**, 339–366.

- Ebel D. S., Weisberg M. K., Hertz J. and Campbell A. J. (2008) Shape, metal abundance, chemistry, and origin of chondrules in the Renazzo (CR) chondrite. *Meteoritics and Planetary Science* **43**, 1725–1740.
- Ebel D. S., Brunner C., Konrad K., Leftwich K., Erb I., Lu M., Rodriguez H., Crapster-Pregont E. J., Friedrich J. M. and Weisberg M. K. (2016) Abundance, major element composition and size of components and matrix in CV, CO and Acfer 094 chondrites. *Geochimica et Cosmochimica Acta* **172**, 322–356.
- Ebel D. S., Alexander C. M. O'D. and Libourel G. (2018) Vapor-melt exchange – constraints on chondrite formation conditions and processes. In: *Chondrules: Records of Protoplanetary Disk Processes* (Cambridge Planetary Science). Eds: S. S. Russell, H. C. Connolly Jr. and A. N. Krot. Cambridge University Press, Cambridge UK, pp. 457.
- Friend P., Hezel D. C. and Mucerschi D. (2016) The conditions of chondrule formation, Part II: Open system. *Geochimica et Cosmochimica Acta* **173**, 198–209.
- Friend P., Hezel D. C., Palme H., Bischoff A. and Gellissen M. (2017) Complementary element relationships between chondrules and matrix in Rumuruti chondrites. *Earth and Planetary Science Letters* **480**, 87–96.
- Friend P., Hezel D. C., Barrat J. A., Zipfel J., Palme H. and Metzler K. (2018) Composition, petrology, and chondrule-matrix complementarity of the recently discovered Jbilet Winselwan CM2 chondrite. *Meteoritics and Planetary Science* **53**, 2470–2491.
- Gerber S., Burkhardt C., Budde G., Metzler K. and Kleine T. (2017) Mixing and transport of dust in the early solar nebula as inferred from titanium isotope variations among chondrules. *The Astrophysical Journal Letters* **841**, 1–7.
- Gooding J. L. and Keil K. (1981) Relative abundances of chondrule primary textural types in ordinary chondrites and their bearing on conditions of chondrule formation. *Meteoritics* **16**, 17–43.
- Grossman J. N. and Wasson J. T. (1983) The compositions of chondrules in unequilibrated chondrites: an evaluation of models for the formation of chondrules and their precursor materials. In: *Chondrules and their Origins*. Eds: E. A. King, Lunar and Planetary Institute, Houston, 88–121.
- Harju E. R., Kohl I. E., Rubin A. E. and Young E. D. (2014) Evaluating silicon condensation in type 1AB chondrules using in-situ silicon isotopes. *37th Lunar Planetary Science Conference*, #2370, (abstract).

- Hertwig A. T., Defouilloy C. and Kita N. T. (2018) Formation of chondrules in a moderately high dust enriched disk: Evidence from oxygen isotopes of chondrules from the Kaba CV3 chondrite. *Geochimica et Cosmochimica Acta* **224**, 116–131.
- Hezel D. C., Palme H., Brenker F. E. and Nasdala L. (2003) Evidence for fractional condensation and reprocessing at high temperatures in CH-chondrites. *Meteoritics and Planetary Science* **38**, 1199–1216.
- Hezel D. C., Palme H., Nasdala L. and Brenker F. E. (2006) Origin of SiO<sub>2</sub>-rich components in ordinary chondrites. *Geochimica et Cosmochimica Acta* **70**, 1548–1564.
- Hezel D. C. and Palme H. (2007) The conditions of chondrule formation, Part I: closed system. *Geochimica et Cosmochimica Acta* **71**, 4092–4107.
- Hezel D. C. and Palme H. (2008) Constraints for chondrule formation from Ca–Al distribution in carbonaceous chondrites. *Earth and Planetary Science Letters* **265**, 716–725.
- Hezel D. C., Russell S. S., Ross A. J. and Kearsley A. T. (2008) Modal abundances of CAIs: implications for bulk chondrite element abundances and fractionations. *Meteoritics and Planetary Science* **43**, 1879–1894.
- Hezel D. C. (2010) A mathematica code to produce phase maps from two element maps. *Computers & Geosciences* **36**, 1097–1099.
- Hezel D. C. and Palme H. (2010) The chemical relationship between chondrules and matrix and the chondrule matrix complementarity. *Earth and Planetary Science Letters* **294**, 85–94.
- Hezel D. C., Harak M. and Libourel G. (2018a) What we know about elemental bulk chondrule and matrix compositions: Presenting the ChondriteDB Database. *Chemie der Erde* **78**, 1–14.
- Hezel D. C., Bland P. A., Palme H., Jacquet E. and Bigolski J. (2018b) Composition of chondrules and matrix and their complementary relationship in chondrites. In: *Chondrules: Records of Protoplanetary Disk Processes* (Cambridge Planetary Science). Eds: S. S. Russell, H. C. Connolly Jr. and A. N. Krot. Cambridge University Press, Cambridge UK, pp. 457.
- Hezel D. C. and Parteli E. J. R. (2018) The spatial origin of chondrules in individual chondrites: constraints from modeling chondrule mixing. *The Astrophysical Journal* **863**, pp. 17.
- Hubbard A. (2015) Compound chondrules fused cold. *Icarus* **254**, 56–61.
- Huss G. R., Rubin, A. E. and Grossman J. N. (2006) Thermal metamorphism in chondrites. In: *Meteorites and the Early Solar System II*, vol. 1 (eds. D. S. Lauretta and H. Y. McSween), 567–586.

- Jacquet E., Alard O. and Gounelle M. (2012) Chondrule trace element geochemistry at the mineral scale. *Meteoritics and Planetary Science* **47**, 1695–1714.
- Johnson B. C., Minton D. A., Melosh H. J. and Zuber M.T. (2015) Impact jetting as the origin of chondrules. *Nature* **517**, 339–341.
- Johnson B. C., Ciesla F. J., Dullemond C. P. and Melosh H. J. (2018) Formation of chondrules by planetesimal collisions. In: *Chondrules: Records of Protoplanetary Disk Processes* (Cambridge Planetary Science). Eds: S. S. Russell, H. C. Connolly Jr. and A. N. Krot. Cambridge University Press, Cambridge UK, pp. 457.
- Jones R. H., Grossman J. N. and Rubin A. E. (2005) Chemical, mineralogical and isotopic properties of chondrules: clues to their origin. In: *Chondrites and the Protoplanetary Disk*, vol. 341 (eds. Krot A. N., Scott E. R. D. and Reipurth B.), 251–285.
- Jones R. H. and Schilk A. J. (2009) Chemistry, petrology and bulk oxygen isotope compositions of chondrules from the Mokoia CV3 carbonaceous chondrite. *Geochimica et Cosmochimica Acta* **73**, 5854–5883.
- Jones R. H. (2012) Petrographic constraints on the diversity of chondrule reservoirs in the protoplanetary disk. *Meteoritics and Planetary Science* **47**, 1176–1190.
- Kita N. T., Nagahara H., Tachibana S., Tomomura S., Spicuzza M. J., Fournelle J. H. and Valley J. W. (2010) High precision SIMS oxygen isotope study of chondrules in LL3 chondrites: Role of ambient gas during chondrule formation. *Geochimica et Cosmochimica Acta* **74**, 6610–6635.
- Klerner S. (2001) Materie im frühen Sonnensystem: die entstehung von chondren, matrix, und refraktären forsteriten. *PhD thesis*, Universität zu Köln.
- Krot A. N., Libourel G., Goodrich C. and Petaev M. I. (2004) Silica-igneous rims around magnesian chondrules in CR carbonaceous chondrites: evidence for fractional condensation during chondrule formation. *Meteoritics and Planetary Science* **39**, 1931–1955.
- Kurahashi E., Kita N. T., Nagahara H. and Morishita Y. (2008)  $^{26}\text{Al}$ – $^{26}\text{Mg}$  systematics of chondrules in a primitive CO chondrite. *Geochimica et Cosmochimica Acta* **72**, 3865–3882.
- Libourel G., Krot A. N. and Tissandier L. (2006) Role of gas–melt interaction during chondrule formation. *Earth and Planetary Science Letters* **251**, 232–240.
- Mac Low M.-M., Hubbard A. and Ebel D. S. (2017) Layered disks as a solution to dynamical and cosmochemical constraints on chondrule formation. *Chondrules as Astrophysical Objects*, #1975 (abstract).

- Marrocchi Y. and Chaussidon M. (2015) A systematic for oxygen isotopic variations in meteoritic chondrules. *Earth and Planetary Science Letters* **430**, 308–315.
- Mason B. H. and Wiik H. B. (1962) The Renazzo meteorite. American Museum of Natural History, New York.
- Mason B. H. and Wiik H. B. (1966) The composition of the Bath, Frankfort, Kakangari, Rose City, and Tadjera meteorites. *American Museum Novitates*, no. **2272**.
- McNally C. P., Hubbard A., Mac Low M. M., Ebel D. S. and D'Alessio P. (2013) Mineral processing by short circuits in protoplanetary disks. *The Astrophysical Journal* **767**, L2–L7.
- Morris M. A., Boley A. C., Desch S. J. and Athanassiadou T. (2012) Chondrule formation in bow shocks around eccentric planetary embryos. *The Astrophysical Journal* **752**, 27–44.
- Morris M. A. and Boley A. C. (2018) Formation of chondrules by shock waves. In: *Chondrules: Records of Protoplanetary Disk Processes* (Cambridge Planetary Science). Eds: S. S. Russell, H. C. Connolly Jr. and A. N. Krot. Cambridge University Press, Cambridge UK, pp. 457.
- Nagashima K., Krot A. N. and Huss G. R. (2015) Oxygen-isotope compositions of chondrule phenocrysts and matrix grains in Kakangari K-grouplet chondrite: Implication to a chondrule-matrix genetic relationship. *Geochimica et Cosmochimica Acta* **151**, 49–67.
- NASA (2017) Astronomy picture of the day. Available at: <https://apod.nasa.gov/apod/ap170702.html>. Oct. 10<sup>th</sup>, 2019.
- NASA (2018) Press release 18-114. Available at: <https://www.nasa.gov/press-release/nasa-s-newly-arrived-osiris-rex-spacecraft-already-discovers-water-on-asteroid>. Oct. 10<sup>th</sup>, 2019.
- Niemeyer S. (1988) Titanium isotopic anomalies in chondrules from carbonaceous chondrites. *Geochimica et Cosmochimica Acta* **52**, 309–318.
- Olson M. B., Wielandt D., Schiller M., Van Kooten E. M. M. E. and Bizzarro M. (2016) Magnesium and <sup>54</sup>Cr isotope compositions of carbonaceous chondrite chondrules – Insights into early disk processes. *Geochimica et Cosmochimica Acta* **191**, 118–138.
- Palme H., Lodders K. and Jones A. (2014) Solar system abundances of elements. In: *Treatise on Geochemistry* 2<sup>nd</sup> ed. (eds. H. Holland and K. Turekian), 15–34.
- Palme H., Hezel D. C. and Ebel D. S. (2015) The origin of chondrules: Constraints from matrix composition and matrix-chondrule complementarity. *Earth and Planetary Science Letters* **411**, 11–19.

- Rubin A. E. and Wasson J. T. (1995) Variations of chondritic properties with heliocentric distance. *Meteoritics* **30**, 569.
- Rubin A. E. and Krot A. N. (1996) Multiple heating of chondrules. *Cambridge University Press*, 173–180.
- Rubin A. E. (2000) Petrologic, geochemical and experimental constraints on models of chondrule formation. *Earth-Science Reviews* **50**, 3–27.
- Rubin A. E. (2006) A relict-grain-bearing porphyritic olivine compound chondrule from LL3.0 Semarkona that experienced limited remelting. *Meteoritics and Planetary Science* **41**, 1027–1038.
- Rubin A. E. (2010) Physical properties of chondrules in different chondrite groups: implications for multiple melting events in dusty environments. *Geochimica et Cosmochimica Acta* **74**, 4807–4828.
- Rubin A. E. (2018) Evaluation of petrologic evidence for high partial pressures of SiO<sub>(g)</sub> in the solar nebula. *Meteoritics and Planetary Science* **53**, 2596–2607.
- Rudraswami N. G., Ushikubo T., Nakashima D. and Kita N. T. (2011) Oxygen isotope systematics of chondrules in the Allende CV3 chondrite: High precision ion microprobe studies. *Geochimica et Cosmochimica Acta* **75**, 7596–7611.
- Russell S. S., Connolly Jr. H.C. and Krot A. N. (2018) Chondrules – records of protoplanetary disk processes. Part II – possible chondrule forming mechanisms. Cambridge University Press, Cambridge UK. pp. 457.
- Sanders I. S. and Scott E. R. D. (2012) The origin of chondrules and chondrites: Debris from low-velocity impacts between molten planetesimals? *Meteoritics and Planetary Science* **47**, 2170–2192.
- Sanders I. S. and Scott E. R. D. (2018) Making chondrules by splashing molten planetesimals – the dirty impact plume model. In: *Chondrules: Records of Protoplanetary Disk Processes* (Cambridge Planetary Science). Eds: S. S. Russell, H. C. Connolly Jr. and A. N. Krot. Cambridge University Press, Cambridge UK, pp. 457.
- Schrader D. L., Nagashima K., Krot A. N., Oglione R. C., Yin Q. Z., Amelin Y., Stirling C. H. and Kaltenbach A. (2017) Distribution of <sup>26</sup>Al in the CR chondrite chondrule-forming region of the protoplanetary disk. *Geochimica et Cosmochimica Acta* **201**, 275–302.
- Scott E. R. D. and Krot A. N. (2014) Chondrites and their components. In: *Treatise on Geochemistry* 2<sup>nd</sup> ed. (eds. H. Holland and K. Turekian), 65–137.

- Soulié C., Libourel G. and Tissandier L. (2017) Olivine dissolution in molten silicates: An experimental study with application to chondrule formation. *Meteoritics and Planetary Science* **52**, 225–250.
- Tenner T. J., Ushikubo T., Kurahashi E., Kita N. T. and Nagahara H. (2013) Oxygen isotope systematics of chondrule phenocrysts from the CO3.0 chondrite Yamato 81020: Evidence for two distinct oxygen isotope reservoirs. *Geochimica et Cosmochimica Acta* **102**, 226–245.
- Tenner T. J., Nakashima D., Ushikubo T., Kita N. T. and Weisberg M. K. (2015) Oxygen isotope ratios of FeO-poor chondrules in CR3 chondrites: Influence of dust enrichment and H<sub>2</sub>O during chondrule formation. *Geochimica et Cosmochimica Acta* **148**, 228–250.
- Tenner T. J., Kimura M. and Kita N. T. (2017) Oxygen isotope characteristics of chondrules from the Yamato-82094 ungrouped carbonaceous chondrite: Further evidence for common O-isotope environments samples among carbonaceous chondrites. *Meteoritics and Planetary Science* **52**, 268–294.
- Tissandier L., Libourel G. and Robert F. (2002) Gas-melt interactions and their bearing on chondrule formation. *Meteoritics and Planetary Science* **37**, 1377–1389.
- The Meteoritical Society (2019) Meteoritical bulletin database. International Society for Meteoritics and Planetary Science. [www.lpi.usra.edu/meteor/](http://www.lpi.usra.edu/meteor/)
- Tomeoka K. and Onishi I. (2015) Redistribution of chondrules in a carbonaceous chondrite parent body: a model. *Geochimica et Cosmochimica Acta* **164**, 543–555.
- Walsh K. J., Morbidelli A., Raymond S. N., O’Brien D. P. and Mandell A. M. (2011) A low mass for Mars from Jupiter’s early gas-driven migration. *Nature* **475**, 206–209.
- Warren P. H. (2011) Stable-isotope anomalies and the accretionary assemblage of the Earth and Mars: A subordinate role for carbonaceous chondrites. *Earth and Planetary Science Letters* **311**, 93–100.
- Wasson J. T. (1977) Relationship between the composition of solid solar-system matter and distance from the Sun. International Astronomical Union Colloquium, Univ. Toledo Press, 551–559.
- Wasson J. T. and Kallemeyn G. W. (1988) Compositions of chondrites. Philosophical Transactions of the Royal Society of London. Series A, *Mathematical and Physical Sciences* **325**, 533–544.
- Wasson J. T. (1993) Constraints on chondrule origins. *Meteoritics* **28**, 14–28.
- Wasson J. T., Krot A. N., Lee M. S. and Rubin A. E. (1995) Compound chondrules. *Geochimica et Cosmochimica Acta* **59**, 1847–1869.

- Wasson J. T. (2008) Evaporation of nebular fines during chondrule formation. *Icarus* **195**, 895–907.
- Weisberg M. K., Prinz M. and Nehru C. E. (1988) Macrochondrules in ordinary chondrites: constraints on chondrule-forming processes. *Meteoritics* **23**, 309–310, abstract.
- Weisberg M. K., Prinz M., Clayton R. N., Mayeda T. K., Grady M. M., Franchi I., Pillinger C. T. and Kallemeyn G. W., (1996) The K (Kakangari) chondrite grouplet. *Geochimica et Cosmochimica Acta* **60**, 4253–4263.
- Weisberg M. K., Ebel D. S., Connolly Jr. H. C., Kita N. T. and Ushikubo T. (2011) Petrology and oxygen isotope compositions of chondrules in E3 chondrites. *Geochimica et Cosmochimica Acta* **75**, 6556–6569.
- Weyrauch M. and Bischoff A. (2012) Macrochondrules in chondrites-formation by melting of mega-sized dust aggregates and/or by rapid collisions at high temperatures? *Meteoritics and Planetary Science* **47**, 2237–2250.
- Wood J. A. (1963) On the origin of chondrules and chondrites. *Icarus* **2**, 152–180.
- Wood J. A. (1985) Meteoritic constraints on processes in the solar nebula. D. C. Black, M. S. Matthews (Eds.), *Protostars and Planets II*, Univ. of Arizona Press, Tucson, 687–702
- Wood J. A. (1996) Processing of chondritic and planetary material in spiral density waves in the nebula. *Meteoritics and Planetary Science* **31**, 641–645.
- Van Schmus W. R. and Wood J. A. (1967) A chemical-petrologic classification for the chondritic meteorites. *Geochimica et Cosmochimica Acta* **31**, 747–765.
- Zinner E. (2014) Presolar Grains. In: *Treatise on Geochemistry* 2<sup>nd</sup> ed. (eds. H. Holland and K. Turekian), 181–213.
- Zanda B., Lewin E. and Humayun M. (2018) The chondritic assemblage – complementarity is not a required hypothesis. In: *Chondrules: Records of Protoplanetary Disk Processes* (Cambridge Planetary Science). Eds: S. S. Russell, H. C. Connolly Jr. and A. N. Krot. Cambridge University Press, Cambridge UK, pp. 457.

## Danksagung

Es ist Sonntag der 03.10.2019, 21:17 Uhr. Vor mir liegt eine druckfertige Dissertation. Drei Jahre als Promotionsstudent der Universität zu Köln gehen für mich zu Ende. Mein Dank gilt an dieser Stelle zahlreichen Personen, die mich während dieser Zeit unterstützten.

An erster Stelle ist dies natürlich *Dominik Hezel*, mein Doktorvater und Mentor. Seine Unterstützung bei allen Fragen und Problemen („hast du kurz Zeit?“) haben wesentlich zu dieser Arbeit beigetragen. Danke für all die Korrekturen, Ratschläge, Erklär-Videos und schnellen Email-Antworten. Ich hätte mir keinen besseren Promotionsbetreuer wünschen können.

Ganz besonders möchte ich mich bei meinen Kollegen, Freunden, Mitstreitern und Leidensgenossen (und -innen) bedanken, die mich während meiner Promotionszeit begleitet haben. Sei es durch Unterstützung bei Fragen und Problemen, dem Zusammensitzen beim Coffice, den langen Abenden und Wochenenden im 4. Stock der Black Box, Konferenzen, Exkursionen, Unifit, Mauerbier, TGIF-Kochen, Ascendancy, und und und ... dank euch werde ich mich gerne an meine Promotionszeit zurückerinnern.

## Ich danke

meinen Freunden und Kollegen der Geo/Kosmochemie Arbeitsgruppe:

*Alessandro, Almut, Bo, Carina, Carsten, Chris, Christiane, Christina, Daniela, Eric, Florian, Frank, Ina, Jonas, Josua, Julia, Laura, Markus & Markus, Mario, Max, Meckie, Mike, Ninja, Pia, Ramon, Raúl, Sebb, Selina, Sophie, Victoria,*

meinen Bachelor und Master-Studierenden: *Lena, Lucia, Lahja, Robert, Luca, Jan,*

dem Mikrosonden, REM und Präp-Team: *Marina, Hanna, Kathrin, Reiner,*

meinen Co-Autoren,

meiner Familie.

(und allen die ich vergessen habe)



FORTUNA FAVET FORTIBUS

## Erklärung zum Eigenanteil an den Publikationen

Als Erstautor bin ich für den Inhalt der hier gelisteten Publikationen verantwortlich. Alle Daten wurden von mir persönlich erhoben, ausgewertet und interpretiert, sofern nicht anderweitig gekennzeichnet.

Messungen außerhalb der Universität zu Köln fanden im Rahmen von Kollaborationen statt. Bei diesen Messungen war ich persönlich zugegen und habe diese, wenn möglich, selbständig durchgeführt. Kollaborationspartner sind als Co-Autoren an den entsprechenden Publikationen beteiligt. Dazu zählen:

μ-CT Messungen am Natural History Museum, London (UK; Ansprechpartner: Vincent Fernandez).

SIMS Messungen in Kollaboration mit Yves Marrocchi und Andrey Gurenko am CRPG-CNRS, Université de Lorraine, Nancy (Frankreich).

Raman Spektroskopie in Kollaboration mit Christoph Lenting am Steinmann-Institut für Geologie, Mineralogie und Paläontologie, Universität zu Bonn.

EPMA Messungen am American Museum of Natural History, NYC (USA), in Kollaboration mit Denton Ebel und Samuel Alpert, im Rahmen des Annette Kade Fellowship Exchange Programs.

Beiträge der Masterstudierenden Lena Sawatzki und Lucia Halbauer wurden unter meiner Aufsicht und Betreuung erstellt und ausgewertet. An der entsprechenden Publikation sind beide Studierende als Co-Autoren beteiligt.

## Erklärung gemäß §4, Abs. 9 der Promotionsordnung MNF

Ich versichere, dass ich die von mir vorgelegte Dissertation selbständig angefertigt, die benutzten Quellen und Hilfsmittel vollständig angegeben und die Stellen der Arbeit – einschließlich Tabellen, Karten und Abbildungen –, die anderen Werken im Wortlaut oder dem Sinn nach entnommen sind, in jedem Einzelfall als Entlehnung kenntlich gemacht habe; dass diese Dissertation noch keiner anderen Fakultät oder Universität zur Prüfung vorgelegen hat; dass sie – abgesehen von unten angegebenen Teilpublikationen – noch nicht veröffentlicht worden ist, sowie, dass ich eine solche Veröffentlichung vor Abschluss des Promotionsverfahrens nicht vornehmen werde. Die Bestimmungen der Promotionsordnung sind mir bekannt. Die von mir vorgelegte Dissertation ist von PD. Dr. Dominik C. Hezel betreut worden.

Köln, 04.11.19



### Veröffentlichte Teilpublikationen:

Barosch J., Hezel D. C., Marrocchi Y., Gurenko A. and Lenting C. (2020) An unusual compound object in Y-793408 (H3.2-an): The missing link between compound chondrules and macrochondrules? *Meteorit. Planet. Sci.*  
<https://doi.org/10.1111/maps.13496>

Barosch J., Hezel D. C., Sawatzki L., Halbauer L. and Marrocchi Y. (2020) Sectioning effects of porphyritic chondrules: Implications for the PP/POP/PO classification and correcting modal abundances of mineralogically zoned chondrules. *Meteorit. Planet. Sci.*  
<https://doi.org/10.1111/maps.13476>

Barosch J., Ebel D. S., Hezel D. C., Alpert S., Palme H. (2020) Formation of chondrules and matrix in Kakangari chondrites. *Earth Planet. Sci. Lett.*  
<https://doi.org/10.1016/j.epsl.2020.116286>

Barosch J., Hezel D. C., Ebel D. S. and Friend P. (2019) Mineralogically zoned chondrules in ordinary chondrites as evidence for chondrule open system behaviour. *Geochim. Cosmochim. Acta* **249**, 1–16.  
<https://doi.org/10.1016/j.gca.2019.01.018>